Mitochondria and Protein Homeostasis in Parkinson's Disease:

From quality control pathways to an integrated network

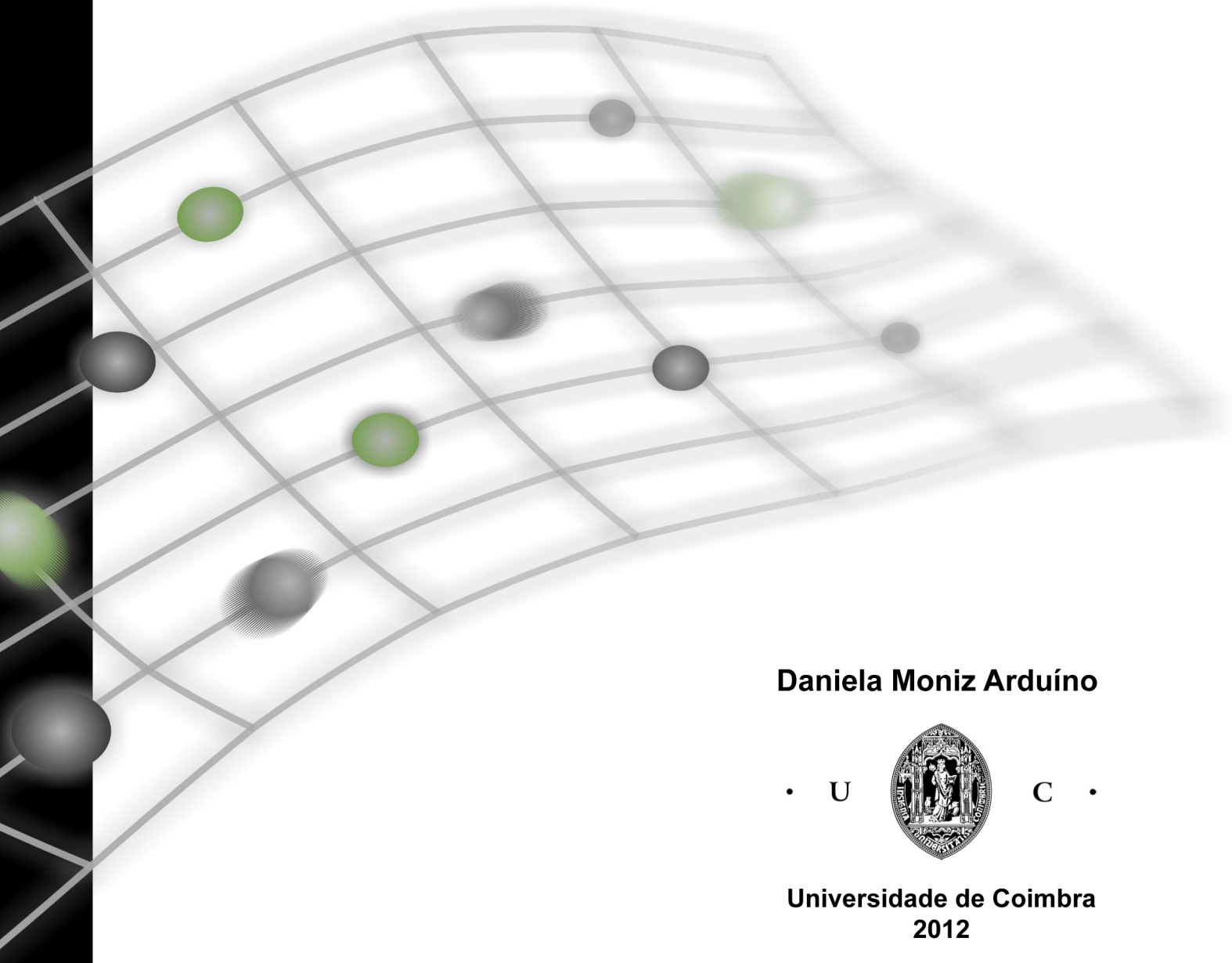

Daniela Moniz Arduíno

· U C ·

Universidade de Coimbra

2012

Mitochondria and Protein Homeostasis in Parkinson's Disease:

From quality control pathways to an integrated network

Daniela Moniz Arduíno

Universidade de Coimbra

2012

Dissertação apresentada à Faculdade de Medicina da Universidade de Coimbra para prestação de provas de Doutoramento em Ciências da Saúde, ramo de Ciências Biomédicas.

Os trabalhos apresentados nesta tese foram realizados no grupo *Molecular Mechanisms of Disease* do Centro de Neurociências e Biologia Celular da Universidade de Coimbra sob a orientação das Professoras Doutoras Catarina Isabel Neno Resende de Oliveira e Sandra Isabel Morais de Almeida Costa Cardoso.

O trabalho apresentado nesta tese foi financiado pelo projecto PTDC/SAU-NEU/102710/2008 concedido à Professora Doutora Sandra Morais Cardoso pela Fundação para a Ciência e Tecnologia (FCT-MEC, Portugal). A autora usufruiu de uma bolsa de Doutoramento (SFRHD/BD/38743/2007) concedida pela FCT-MEC, Portugal.

The work presented in this thesis was supported by the Portuguese Foundation for Science and Technology (FCT-MEC, Portugal), Grant PTDC/SAU-NEU/102710/2008 to Sandra Morais Cardoso. Daniela Moniz Arduíno was supported by a PhD fellowship, SFRHD/BD/38743/2007, from FCT-MEC, Portugal.

Os trabalhos apresentados nesta tese foram integral ou parcialmente publicados ou submetidos para publicação nas seguintes revistas científicas internacionais indexadas:

The work presented in this thesis has been total or partially published in the following papers in international scientific periodicals with referees:

Arduino DM, Esteves AR, Cardoso SM, Oliveira CR (2009) Endoplasmic reticulum and mitochondria interplay mediates apoptotic cell death: relevance to Parkinson's disease. Neurochem Int 55:341-348.

Arduino DM, Esteves AR, Domingues AF, Pereira CM, Cardoso SM, Oliveira CR (2009) ER-mediated stress induces mitochondrial-dependent caspases activation in NT2 neuron-like cells. BMB rep 42:719-724.

Arduino DM, Esteves AR, Oliveira CR, Cardoso SM (2010) Mitochondrial metabolism modulation: a new therapeutic approach for Parkinson's disease. CNS Neurol Disord Drug Targets 9:105-119.

Arduino DM, Esteves AR, Cardoso SM (2011) Mitochondrial fusion/fission, transport and autophagy in Parkinson's disease: when mitochondria get nasty. Parkinsons Dis 2011:767230.

Arduino DM, Esteves AR, Silva DF, Martins-Branco D, Santos D, Pimentel DF, Cardoso SM (2011) Therapeutic Intervention at Cellular Quality Control Systems in Alzheimer's and Parkinson's Diseases. Curr Pharm Des.17(31):3446-59.

Arduino DM, Esteves AR, Cortes L, Silva DF, Grazina M, Swerdlow RH, Oliveira CR, Cardoso SM (2012) Mitochondrial Metabolism in Parkinson’s Disease Impairs Quality Control Autophagy by Hampering Microtubule-Dependent Traffic. Hum Mol Genet. (under second review).

Aos meus Pais

Ao Ricardo

CONTENTS

Agradecimentos

Acknowledgements

Endereço uma palavra de apreço a todos aqueles que contribuíram para que fosse possível alcançar esta importante meta na minha carreira.

Primeiramente gostaria de agradecer às minhas orientadoras de Doutoramento pelo apoio dado na realização dos trabalhos apresentados.
À Professora Catarina Resende de Oliveira agradeço a forma como me recebeu e acolheu no Centro de Neurociências e Biologia Celular, permitindo a minha integração no Grupo *Molecular Mechanisms of Disease*.
À Professora Sandra Morais Cardoso pela orientação, discussões científicas, observações e sugestões pertinentes que sempre são uma mais-valia. Agradeço também a amizade e todo o apoio ao longo destes anos e, em especial, por ter acreditado em mim e me proporcionar todas as oportunidades que estavam ao seu alcance, permitindo o meu enriquecimento científico e profissional.

I would like to express my gratitude to Professor Ana Maria Cuervo for her willingness to receive me as a visiting scientist in her lab. I consider myself really fortunate to have been part of her research group during my training period abroad. I learned and benefited a lot from her research insights, scientific enthusiasm, critical thinking and extraordinary sapience. I would also like to thank all her kindness and support, helpful inputs and persistent encouragements to my research work.

À Raquel Esteves, um obrigada muito especial pela amizade, por todo o apoio quer a nível profissional quer pessoal e pelo contributo e esforço colaborativo para o sucesso deste trabalho.

À Luisa Cortes agradeço a enorme simpatia, disponibilidade incansável e prontidão em ajudar-me. Agradeço também pelo contributo para os trabalhos apresentados.

A todos os colegas do Grupo *Molecular Mechanisms of Disease* pelos momentos de boa disposição e troca de ideias. Uma palavra especial à Diana, Diogo, Daniel, Rosa e Renato pela enorme disponibilidade sempre que necessitei.

I would also like to extend my thanks to all the members of Prof. Cuervo Lab. They really made me feel at home. A special thank to Hiroshi, Esther, Bindi, Jaime, Susmita and Rajat for their generous assistance and scientific discussions during my stay in the lab.

Claro que ter chegado aqui só foi possível graças aos meus Pais que desde sempre deram o seu melhor para tudo me proporcionar. É graças ao seu enorme carinho e apoio incondicional que se deve o meu sucesso.
Do mesmo modo agradeço à minha irmã por estar sempre presente com especial dedicação e prontidão.
Por fim, um agradecimento muito especial para ti Ricardo. Porque o que poderia ser aqui escrito nunca iria traduzir o que eu quero transmitir, Obrigada por tudo o que nós sabemos.

Abbreviations

3-MA	3-methyladenine
6-OHDA	6-hydroxydopamine
ADP	Adenosine diphosphate
ANOVA	Analysis of variance
APAF-1	Apoptosis protease activating factor 1
araC	Cytosine β-D-arabinofuranoside
Atg	Autophagy-related
ATP	Adenosine triphosphate
ATRA	*All-trans* retinoic acid
BcL	B-cell leukemia/lymphoma
BiP	Immunoglobulin binding protein
BSA	Bovine serum albumin
CHAPS	3-[(3-cholamidopropyl)dimethylammonio]-1-propanesulfonate
CMA	Chaperone-mediated autophagy
CNS	Central nervous system
COX IV	Cytochrome c oxidase
DIV	Days in vitro
DMEM	Dulbecco's modified eagle medium
DNAse I	Deoxyribonuclease I
DRP-1	Dynamin-related protein-1
DTT	Dithiothreitol
ECF	Enhanced chemifluorescence
EDTA	Ethylenediamine tetraacetic acid
EGTA	Ethylene glycol tetraacetic acid
ER	Endoplasmic reticulum
ERAD	ER-associated degradation
ETC	Electron transport chain
$FADH_2$	Flavin adenine dinucleotide (reduced form)
FBS	Fetal bovine serum
FCCP	Carbonyl cyanide-p trifluoromethoxyphenylhydrazone
FIP200	Focal adhesion kinase family-interacting protein of 200 kDa
FOXO1	Forkhead box protein O1

FUdR	5-fluoro-2'-deoxyuridine
GAPDH	Glyceraldehyde 3-phosphate dehydrogenase
GFAP	Glial fibrillary acidic protein
GPI	Glycophosphatidylinositol
GRP	Glucose regulated protein
GTP	Guanosine 5'- triphosphate
HBSS	Hanks' balanced salt solution
HDAC6	Histone deacetylase 6
HEPES	4-(2-hydroxyethyl)-1-piperazineethanesulfonic acid
hFis1	Human fission 1
HSC70	Heat shock cognate
Hsp60	Heat shock protein 60
HTRA2	Heat transfer requirement 2
IMS	Intermembrane space
IP_3R	Inositol-1,4,5-triphosphate receptor
KO	Knockout
LAMP-1	Lysosomal-associated membrane protein 1
LAMP-2A	Lysosome-associated membrane protein type 2A
LBs	Lewy bodies
LC3	Microtubule-associated protein light chain 3
LRRK2	Leucine-rich-repeat kinase 2
MAM	Mitochondrial-associated membrane
MAP2	Microtubule-associated protein 2
MEF2D	Myocyte enhancer factor 2D
MFNs	Mitofusins
MIM	Mitochondrial inner membrane
MOM	Mitochondrial outer membrane
MOMP	Mitochondrial outer membrane permeabilization
MPP^+	1-methyl-4-phenylpyridinium
MPTP	1-methyl-4-phenyl-1,2,3,6-tetrahydrodropyridine
MT	Microtubule
mtDNA	Mitochondrial DNA
MTOC	Microtubule-organizing centre
mTOR	Mammalian target of rapamycin
NAc-DEVD-*p*NA	N-Ac-Asp-Glu-Val-Asp-*p*Na
NAc-LEDH-*p*NA	N-Ac-Leu-Glu-His-Asp-*p*Na

NAc-LEVD-*p*NA	N-Ac-Leu-Glu-Val-Asp-*p*Na
NAc-VDVAD-*p*NA	N-Ac-Val-Asp-Val-Ala-Asp-*p*NA
NAD	Nicotinamide adenine dinucleotide
NADH	Nicotinamide adenine dinucleotide (reduced form)
NAD^+	Nicotinamide adenine dinucleotide (oxidized form)
NBR1	Neighbor of Brca1protein
ND	NADH dehydrogenase
NDUFA2	NADH dehydrogenase (ubiquinone) 1 alpha subcomplex, 2
NL	NH_4Cl/leupetin
NURR1	Nuclear receptor related-1
OPA1	Optic atrophy 1
PBMCs	Peripheral blood mononuclear cells
PBS	Phosphate buffered saline
PD	Parkinson's disease
PDI	Protein disulfide isomerase
PEG	Polyethylene glycol
PERK	Protein kinase RNA-like endoplasmic reticulum kinase
PINK1	(PTEN)-induced kinase 1
PMSF	Phenylmethylsulfonyl fluoride
POLG	Polymerase γ
PtdIns(3)P	Phosphatidylinositol 3-phosphate
PtdIns3K	Phosphatidylinositol 3-kinase
PTEN	Phosphatase and tensin homolog
PVDF	Polyvinylidene difluoride
QC	Quality control
RAB1A	Ras-related protein Rab-1A
Rh123	Rhodamine 123
RIPA	Radio-immunoprecipitation assay
ROS	Reactive oxygen species
rRNA	Ribosomal RNA
RyR	Ryanodine receptor
SDS	Sodium dodecyl sulphate
SIRT2	Sirtuin 2
S-MEM	Minimum essential medium
SNpc	Substantia nigra pars compacta
sPD	Sporadic PD

SQSTM1	Sequestosome-1
TBP	TATA-binding protein
TBS	Tris-buffered saline
TCA	Tricarboxylic acid
TOM20	Translocase of outer membrane 20 kDa subunit
tRNA	Transfer RNA
Ubl	Ubiquitin-like
UCH-L1	Ubiquitin carboxy-terminal hydrolase L1
ULK	Uncoordinated 51-like kinase
UPR	Unfolded protein response
UPS	Ubiquitin-proteasome system
Urd	Uridine
VDAC-1	Voltage-dependent anion-selective channel protein 1
Vps	Vacuolar protein sorting
VTA	Ventral tegmental area
$\Delta\psi_m$	Mitochondrial membrane potential

Abstract

Parkinson's disease (PD) is the second most prevalent neurodegenerative disorder affecting almost 2% of people over 65 years of age. The primary neuropathological hallmark of PD is the degeneration of the nigrostriatal dopaminergic pathway which, by depleting dopamine in the brain, initiates abnormal motor symptoms including resting tremor, bradykinesia, postural instability, gait difficulty and rigidity. A second relevant hallmark is the presence of intracellular inclusion bodies, known as Lewy bodies that mainly contain aggregated α-synuclein.

While the etiology involved in the development of PD is unknown, 90-95% of PD cases occurs sporadically and correlates, in part, with mitochondrial dysfunction and oxidative stress. Furthermore, the identification of single genes associated to the familial forms of PD has revolutionized this field of research, providing unique opportunities to pursue novel mechanisms and clues to the pathogenesis of PD. The sustained study of the cellular functions of each PD-related gene indicates that protein misfolding and aggregation, as well as, dysfunction of their quality control systems may play a crucial role in the cascade of deleterious events implicated in the neurodegenerative process of PD. Thus, clear insights into how mitochondrial dysfunction, oxidative stress and protein homeostasis systems interconnect, overlap or converge to produce nigral neuronal degeneration is essential to understand the pathogenesis of sporadic PD (sPD).

In this thesis, we initially addressed the potential implications of an altered structural and functional crosstalk between mitochondria and the endoplasmic reticulum (ER), two important metabolic organelles for the maintenance of cellular protein homeostasis. We reported that mitochondrial dysfunction induced by an acute stimulus of the neurotoxin MPP^+ renders cells more susceptible to develop an ER stress response. We found that MPP^+ was able to evoke a sustained flux of Ca^{2+} from the ER to mitochondria which subsequently triggered ER- and mitochondria-dependent apoptotic pathways. Our findings highlight the inevitable role of ER to mitochondria Ca^{2+} fluxes and their requirement for a mitochondria-dependent cell death induction, enclosing a feedback loop whereas mitochondria signals ER and ER induces further mitochondrial alterations, leading to the activation of cascade of signals that culminates in apoptotic cell death.

Furthermore, we also found that ER stress response strengthens mitochondrial stress-induced abnormalities. We demonstrated that sustained ER stress caused by accumulation of unfolded or misfolded proteins potentiated Ca^{2+} overload and impairment

of mitochondrial function mainly characterized by dissipation of mitochondrial membrane potential and substantial decline in the mitochondrial respiratory chain complex I activity. These cumulative events led to induction of apoptotic cell death.

In addition, we assessed the role of mitochondrial metabolism in the regulation of the autophagy-lysosomal pathway, a major cellular homeostatic process that mediates the degradation of long-lived proteins and dysfunctional or superfluous organelles in eukaryotic cells. We demonstrated that prolonged metabolic failure due to mitochondrial dysfunction, either in cellular models harboring sPD subjects mtDNA (sPD cybrids), cells depleted of all mtDNA (Rho0 cells), or in MPP^+-treated rat cortical neurons causes a functional decline in the activity of the autophagic system. This defect is a consequence of alterations in microtubules (MT) assembly that hamper mitochondria and autophagosome transport along the MT network toward the lysosomal compartment. Consequently, deficient autophagic turnover potentiates the accumulation of α-synuclein oligomers and, ultimately, prompts apoptosis. Our data identify for the first time the PD-associated defects in mitochondrial dysfunction as the basis for the selective transport abnormalities and highly characteristic pattern of neuritic dystrophy associated to the autophagic pathology in PD.

Finally, we dissected the molecular mechanisms by which mitochondrial metabolism in sPD can affect MT-directed autophagic turnover that, in turn, regulates intracellular protein homeostasis. We demonstrated that sirtuin 2 (SIRT2), a NAD^+ dependent protein deacetylase, controls the functional ability of the autophagic system by modulating the acetylation status of the MT cytoskeleton.

The studies presented here provide novel insights into the multiple mechanisms that dictate the association between mitochondria, intracellular metabolism and proteotoxicity in sPD, and contribute with new findings that could have important therapeutic implications to halt or retard the progression of sPD pathology.

Resumo

A doença de Parkinson (DP) é a segunda doença neurodegenerativa mais comum, afectando cerca de 2% dos indivíduos com idade superior a 65 anos. A marca neuropatológica primária desta doença é a disfunção da via dopaminérgica nigroestriatal, da qual resulta a depleção de dopamina no cérebro, conduzindo aos principais sintomas motores que caracterizam a clínica da doença e que incluem tremor de repouso, bradicinesia, instabilidade postural e rigidez muscular. Outra característica neuropatológica da DP é a presença de corpos de inclusão intracelulares, designados de Corpos de Lewy, que são maioritariamente constituídos por α-synucleína na forma agregada.

Embora a etiologia da doença permaneça por esclarecer, sabe-se que 90-95% dos casos de DP ocorrem de uma forma esporádica e pensa-se que, em parte, se correlacionam com a disfunção da mitocôndria e com o stresse oxidativo. A identificação de genes associados às formas familiares da DP revolucionou a forma de pensar dos investigadores da área, proporcionando oportunidades únicas para estudar novos mecanismos envolvidos na etiopatogenia da DP. O estudo continuado das funções celulares de cada um dos genes relacionados com a DP indica que o *misfolding* e a agregação proteica, bem como a disfunção dos sistemas de controlo de qualidade proteica, desempenham um papel crucial na cascata de eventos implicada no processo de neurodegeneração da DP. Assim, uma visão clara de como e quando a disfunção mitocondrial, o stresse oxidativo e os mecanismos de homeostase proteica se entrecruzam, sobrepõem ou convergem para produzir degeneração nigorestriatal é essencial para a compreensão da fisiopatologia da DP do tipo esporádico (sDP).

Nesta tese, abordámos, inicialmente, as potenciais implicações das alterações na interação estrutural e funcional entre a mitocôndria e o retículo endoplasmático (RE), dois organelos importantes envolvidos na manutenção da homeostase proteica celular. Reportamos que a disfunção mitocondrial induzida por um estímulo agudo da neurotoxina MPP^+ aumenta a susceptibilidade das células para o desenvolvimento de uma resposta ao stresse do RE. Verificámos que o MPP^+ foi capaz de evocar um fluxo contínuo de Ca^{2+} entre o RE e a mitocôndria, desencadeando, subsequentemente, a activação de vias apoptóticas dependentes do RE e da mitocôndria. Os resultados obtidos destacam o papel inevitável dos fluxos de Ca^{2+} entre o RE e a mitocôndria, e a sua relevância para a indução de morte celular dependente da mitocôndria, estabelecendo-se um ciclo de retrocontrolo em que a mitocôndria sinaliza o RE e o RE

induz alterações posteriores na mitocôndria, conduzindo à activação de uma cascata de sinalização que culmina na morte celular por apoptose.

Do mesmo modo, observámos que o stresse do RE potencia alterações ao nível da função mitocôndrial. Demonstramos que stresse do RE prolongado devido à acumulação de proteínas mal processadas no seu interior conduz a um fluxo excessivo de Ca^{2+} para o interior mitocôndria e a um comprometimento da função mitocondrial, caracterizada principalmente pela dissipação do potencial de membrana e por um decréscimo substancial da actividade da cadeia respiratória mitocondrial. Cumulativamente, estes eventos desencadeam a indução de morte celular por apoptose.

Por outro lado, avaliámos o papel do metabolismo mitocondrial na regulação da via autofágica-lisossomal, um processo homeostático celular que medeia a degradação de proteínas de longa duração e organelos disfuncionais em células eucarióticas. Demonstramos que uma falência metabólica prolongada devido a disfunção mitocondrial quer em células híbridas portadoras de ADN mitocondrial de doentes de sDP (cíbridos sDP), em células depletadas do seu ADN mitocondrial (células Rho0) ou em culturas primárias de neurónios corticais de rato tratados com MPP^+, provoca um declínio funcional na actividade do sistema autofágico. Este defeito é uma consequência de alterações estruturais na rede microtubular (MT), comprometendo o transporte de mitocôndrias e autofagossomas para o compartimento lisossomal, onde ocorre degradação. Consequentemente, um ineficaz *turnover* autofágico potencia a acumulação de oligómeros de α-sinucleína e, em última análise, desencadeia apoptose. Assim, os dados obtidos identificam pela primeira vez os defeitos na função mitocondrial associados à DP como a base para alterações específicas no transporte intracelular e no padrão característico da distrofia neurítica associado à patologia autofágica na DP.

Por fim, analisámos os mecanismos moleculares através dos quais o metabolismo mitocondrial em sDP pode afectar o *turnover* autofágico dependente da rede MT, o qual, por sua vez, regula a homeostase proteica intracelular. Demonstramos que a sirtuina 2 (SIRT2), uma desacetilase citoplasmática dependente do NAD^+, controla a capacidade funcional do sistema autofágico, modulando o estado de acetilação do MTs.

Os estudos apresentados fornecem novas pistas relativamente aos múltiplos mecanismos que determinam a associação entre mitocôndria, metabolismo intracelular e proteotoxicidade e contribuem com novas perspectivas que poderão ter importantes implicações terapêuticas no sentido impedir ou retardar a progressão da sPD.

CHAPTER I

Introduction

1.1 Parkinson's disease: a single disorder?

Parkinson disease (PD) is a chronically progressive, age-related neurodegenerative disease considered the most common movement disorder that is estimated to affect 1.5% to 2% of the population older than 60 years of age (Lang and Lozano, 1998b, a). This disorder was first described in 1817 by James Parkinson in his seminal monograph "An Essay on the Shaking Palsy" where the core clinical features were presented (Parkinson, 2002). However, after almost two centuries since its description, PD remains an idiopathic disorder without cure and with limited symptomatic treatment. While the etiology of PD is still unknown, remarkable research advances have shed light on what fails in this disorder, and how those failures might be overcome. In addition to the motor symptoms primarily described by Parkinson, one has come to realize that this disorder is much more complex and includes panoply of convergent factors that may concur to the pathophysiology and pathologic biochemistry of PD.

Clinically, PD presents with four cardinal motor manifestations: tremor at rest, rigidity, bradykinesia (or slowing of movement), and postural instability. Many patients also suffer from non-motor symptoms, including disturbances of autonomic functions and deterioration of cognition (Poewe, 2008). These symptoms result from the progressive and selective degeneration of dopaminergic neurons in the substantia nigra pars compacta (SNpc), visible in brain sections as depigmentation of the SNpc in the midbrain, which constitutes a major signature of PD (**Figure I.1**). The loss of inhibitory dopaminergic innervation causes overactivity of the subthalamic nucleus and globus pallidus, which causes the movement symptoms (Hirsch et al., 2000; Obeso et al., 2000). Neuroimageing reveals a typically asymmetric loss of dopamine terminals in the striatum. However, it is now clear that other neurons are also affected, and there are even suggestions that PD may initiate in other brainstem, subcortical and cortical structures or elsewhere in the central nervous system (CNS) and spread to the nigral neurons by, perhaps, noncell autonomous processes (Braak et al., 2003; Ilieva et al., 2009; Bosco et al., 2011). PD surviving neurons exhibit the formation of round eosinophilic intracytoplasmic protein inclusions termed Lewy bodies (LBs), when they are present in cell bodies, and dystrophic neurites (Lewy neurites), when they are present in neuronal processes (Forno, 1996). These LBs comprise a dense core of different proteins, such as α-synuclein, parkin, synphilin-1, tubulin and other cytoskeletal proteins, components of the ubiquitin-proteasome system (UPS) and molecular chaperones, and lipids (Halliday et al., 2005; Uryu et al., 2006; Uversky, 2007) **(Figure I.1)**.

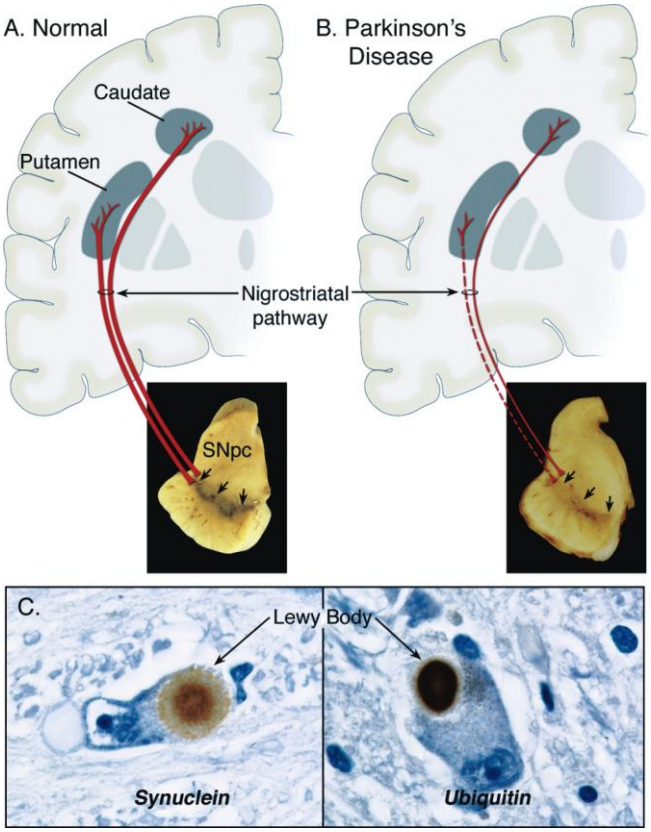

Figure I.1. Neuropathology of Parkinson's disease.
A. Schematic representation of the normal nigrostriatal pathway (in red). It is composed of dopaminergic neurons whose cell bodies are located in the substantia nigra pars compacta (SNpc; see arrows). These neurons project (thick solid red lines) to other basal ganglia and synapse in the striatum (i.e., putamen and caudate nucleus). The photograph demonstrates the normal pigmentation of the SNpc, produced by neuromelanin within the dopaminergic neurons. **B.** Schematic representation of the PD nigrostriatal pathway (in red). In PD, the nigrostriatal pathway degenerates. There is a marked loss of dopaminergic neurons that project to the putamen (dashed line) and a modest loss of those that project to the caudate (thin red solid line). The photograph demonstrates depigmentation (i.e., loss of dark-brown pigment neuromelanin; arrows) of the SNpc due to the marked loss of dopaminergic neurons. **C.** Photographic images of Lewy bodies stained with antibodies against α-synuclein and ubiquitin [Adapted from (Dauer and Przedborski, 2003)].

Although the constituents of LBs have been characterized, few insights into the formation and function of LBs within cells have been achieved. The localization of LBs to regions of the CNS undergoing neuronal cell death further suggests a key role for protein misfolding and aggregation in the PD pathogenesis. For example, the number of LBs-containing neurons was positively correlated with the expression of clinical symptoms (Kovari et al., 2003).

In the outline of the protein misfolding and aggregation hypothesis for midbrain degeneration in PD, a crucial question is: why those proteins are prone to misfold, aggregate and accumulate in these selective brain regions, thereby leading to such specific patterns of neurodegeneration?

Actually, we can speculate about the answer. Local changes in expression or in post-translational modifications of the proteins that are misfolded might explain the selectivity of protein aggregation. Also, local alterations in the concentration or activity of chaperone proteins, or organelles that specifically control the folding of certain proteins, such as the endoplasmic reticulum (ER), might also be involved. Another potential mechanism involves selective alterations in clearance pathways that will remove different misfolded and aggregated proteins, such as the autophagy-lysosomal system. Finally, SNpc dopaminergic neurons might be more vulnerable to toxic stimuli, which in turn contribute to an accumulation of protein aggregates in these cells. But, a basic question arises: Does a unifying event trigger and account for all of these potential alterations?

An emerging concept is that SNpc homeostasis is vulnerable to different genetic, cellular and environmental factors that independently or concomitantly promote neuronal cell death over time (Perier et al., 2007; Sulzer, 2007). However, one factor that most strongly relates to the onset of PD is age or the ageing process. Indeed, epidemiological studies have identified age as the greatest risk factor for PD, and mitochondria through accumulation of mitochondrial DNA (mtDNA) mutations and production of reactive oxygen species (ROS) as the driving force of that process (Thomas, 2009). Accordingly, experimental data indicate that dopaminergic neurons are particularly sensitive to mitochondrial impairment and oxidative damage (Jenner, 2003). This can be due to their reliance on a high metabolic demand and should mean that they age more rapidly than other types of neurons. Consistent with this hypothesis studies on normal ageing-related cell death have suggested that SNpc dopaminergic neurons are lost at a considerably higher rate (5–10% per decade) than many other types of neurons (Stark and Pakkenberg, 2004). Functional measurements have shown that the nigrostriatal system activity is reduced with normal ageing (Backman et al., 2000), although not as rapidly as neuron loss, presumably because of the capacity of the remaining neurons to compensate (Zigmond et al., 1990).

Over the course of a lifetime, the rate of cellular ageing might have a significant effect on the time at which cell loss reaches the threshold necessary for the appearance of the first PD symptoms. Obviously, causative factors may differ among individuals determining different clinical subtypes of the disease or no disease at all. These differences might arise from diverse genetic backgrounds (genetic mutations or polymorphisms) that discreetly change the efficiency of the mitochondrial oxidative

phosphorylation system and the rate of generation of ROS. Indeed, some mutations or polymorphisms in mtDNA have been associated with different incidence of PD (Ghezzi et al., 2005; Huerta et al., 2005; Pyle et al., 2005; Larsson, 2010) and at least nine nuclear genes have been identified as causing or affecting the risk of PD. These include α-synuclein, parkin, ubiquitin carboxy-terminal hydrolase L1 (UCH-L1), DJ-1, phosphatase and tensin homologue (PTEN)-induced kinase 1 (PINK1), leucine-rich-repeat kinase 2 (LRRK2), the nuclear receptor related-1 (NURR1), heat transfer requirement 2 (OMI/HTRA2), and tau. Among the nuclear genes, mutations in α-synuclein, parkin, DJ-1, PINK1, LRRK2, and HTRA2 are either directly or indirectly associated with mitochondrial dysfunction (Thomas and Beal, 2007). However, the genetic burden of actual mutations in PD is small, accounting for only 5–10% of the overall PD population.

The rate of ageing and neuronal cell loss could also be accelerated by secondary factors arising from exposure to environmental toxins that compromise mitochondrial function or that of cellular systems dealing with the consequences of oxidative stress. These factors might per se be fairly inoffensive but, due to their potential to synergise with the intrinsic vulnerabilities of SNpc dopaminergic neurons, might become relevant.

Thus, cumulative “normal” stress over a long period of time, such as the ageing process, or exposure to toxins could further tip the balance from a genetically determined cellular state to programmed cell death culminating in neuronal cell loss. This explains why several distinct molecular mechanisms may converge to a final common pathological and clinical phenotype in different individuals, unifying the molecular pathways implicated in the familial forms of PD into a “puzzling” multifactorial profile for sporadic PD (sPD), making it a “single disorder”.

1.2 Mitochondria: the trigger of Parkinson's disease?

Mitochondria are intracellular membrane enclosed organelles exceptionally primed to play a key role in cell biology. The intrinsic properties of mitochondria make them essential integrators of cellular functions, such as pyruvate oxidation, the citric acid or tricarboxylic acid (TCA) cycle, the metabolism of amino acids, fatty acids, steroids, and most importantly, the generation of energy as adenosine triphosphate (ATP).

Structurally, each mitochondrion comprises a matrix delimited by two membranes, the mitochondrial inner membrane (MIM) and the mitochondrial outer membrane (MOM), which occasionally came together to form junctional complexes or contact sites. The space between the two membranes is referred to as the intermembrane space (IMS), housing some proteins which play major roles in cell physiology, in mitochondrial energetics and in cell death, particularly cytochrome c. The convoluted and invaginated MIM includes multiple enzymes of oxidative phosphorylation system, the cofactor coenzyme Q1 or ubiquinone, the F_0-F_1-ATP synthase and some ion channels and carrier proteins [e.g., the voltage-dependent anion channel (VDAC-1) and the translocase of outer mitochondrial membrane (TOM20)]. In the matrix, surrounded by the MIM, there are many enzymes for different metabolic pathways, including the TCA cycle, fatty acid oxidation and the urea cycle, peptidases and chaperones (e.g., heat shock protein 60, Hsp60).

Mitochondria are the only organelles of the cell besides the nucleus that contain their own DNA (i.e., mtDNA), and their own machinery for synthesizing RNA and proteins. A given mitochondrion contains several copies of its genome (2–15 copies, termed "polyplasmia"), within its matrix, which codes for a small (12S) and large (16S) ribosomal RNA (rRNA), 22 transfer RNAs (tRNA) and 13 polypeptides that are all components of the oxidative phosphorylation system. The majority of proteins required to assemble and regulate mitochondrial function are therefore encoded by nuclear DNA, synthesized in the cytosol, and imported into mitochondria, where they are targeted to one of the four mitochondrial compartments. An example is NDUFA2, a subunit of the hydrophobic protein fraction of the NADH:ubiquinone oxidoreductase (complex I), which is thought to be involved in regulating complex I activity or its assembly via assistance in redox processes.

In addition to their role as ATP suppliers, mitochondria are critical as calcium buffers and as transducers of intracellular signaling pathways which integrate programmed cell death, marking the point of no return in apoptosis. Furthermore, mitochondria are highly dynamic organelles and are actively transported throughout axons and dendrites in neurons to facilitate their recruitment to critical subcellular

compartments distant from the cell body. Therefore, mitochondrial function has a critical role in the brain physiology and, alterations in any of these mitochondrial features can potentially be associated to the pathogenesis of PD.

1.2.1 Mitochondrial metabolism and the oxidative phosphorylation system

Mitochondria are usually considered to be “the powerhouses of the cell” and to be responsible for the aerobic production of ATP, via the combined efforts of the TCA and the respiratory chain/oxidative phosphorylation system.

The mitochondrial respiratory chain is implanted in the MIM and consists of five enzyme complexes and cofactors, arranged functionally according to the electrochemical hierarchy based on their redox potentials: reduced nicotinamide adenine dinucleotide (NADH) dehydrogenase-ubiquinone oxidoreductase (complex I, approximately 46 subunits), succinate dehydrogenase- ubiquinone oxidoreductase (complex II, four subunits), ubiquinone-cytochrome c oxidoreductase (complex III, 11 subunits), cytochrome c oxidase (complex IV, 13 subunits), and ATP synthase (complex V, approximately 16 subunits).

The TCA cycle maintains the coenzymes NADH and flavoproteins in a reduced state to supply reducing equivalents for the electron transport chain (ETC). The transfer of electrons occurs due to the oxidation of NADH (at complex I) or $FADH_2$ (at complex III) by ubiquinone to complex IV where they react with molecular oxygen (O_2) to reduce it to H_2O. The transport of electrons down the ETC releases favorable energy that is used by Complex I, III, and IV to pump protons from the matrix to the mitochondrial IMS, thus creating a proton gradient (basic inside) and an electrochemical gradient (negative inside) across the MIM. The electrochemical gradient (known as mitochondrial membrane potential, $\Delta\psi_m$) is used by the F_1F_0-ATP synthase for running the endoergonic reaction of adenosine diphosphate (ADP) phosphorylation **(Figure I.2)**.

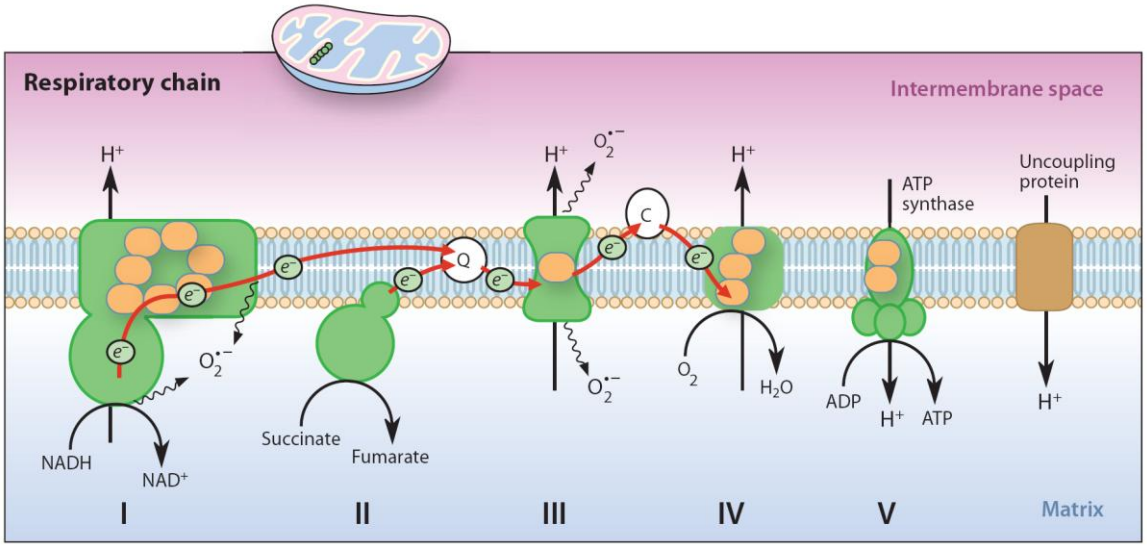

Figure I.2. Mitochondrial compartimentalization and the oxidative phosphorylation system. The mammalian oxidative phosphorylation system consists of five enzyme complexes. Complexes I–IV constitute the respiratory chain, whereas complex V is the ATP synthase. Complex I (NADH dehydrogenase) and complex II (succinate dehydrogenase) receive electrons (*e*−) from intermediary metabolism and translocate them to coenzyme Q, which, in turn, delivers the electrons to complex III (cytochrome *c* reductase). The electron shuttling protein cytochrome *c* then transfers the electrons to complex IV (cytochrome *c* oxidase), which constitutes the final step in the electron transport chain that reduces molecular oxygen (O_2) to water (H_2O). The electron transport is coupled to proton (H^+) pumping across the inner mitochondrial membrane by complexes I, III, and IV. The resulting proton gradient drives ATP synthesis, and there is thus a coupling between electron transport and ATP synthesis. Protons can be translocated from the intermembrane space to the mitochondrial matrix through the activated uncoupling protein or by other uncoupling mechanisms, which leads to a dissociation (uncoupling) of electron transport and ATP synthesis. The mtDNA encodes critical subunits of complexes I, III, IV, and V (*orange dots*). Electrons may also exit the respiratory chain at the level of complex I or III to form the reactive oxygen species superoxide ($O_2^{\cdot-}$) as a result of the one-electron reduction of O_2 [Adapted from (Larsson, 2010)].

Defective mitochondrial function, in particular at the level of complex I, has long been associated with the pathogenesis of PD. Indeed, the first report comes in 1975, when Ahlqvist *et al.* showed ultrastructural abnormalities in mitochondria of muscle biopsies from PD patients (Ahlqvist et al., 1975). However, the most compelling evidence of mitochondrial complex I involvement PD emerged following the human accidental exposure to the synthetic meperidine analogue 1-methyl-4-phenyl-1,2,3,6-tetrahydrodropyridine (MPTP) which induced a parkinsonian syndrome (Langston et al., 1983; Burns et al., 1985). Mitochondrial association with idiopathic PD was first

established when a mitochondrial complex I activity deficit was identified in the SNpc of post mortem PD patients brains (Schapira et al., 1989) and in PD patient platelets (Parker et al., 1989). Further evidences suggested a similar complex I deficiency in PD patients lymphocytes (Yoshino et al., 1992; Barroso et al., 1993) and skeletal muscle (Penn et al., 1995), although some studies failed to demonstrate consistent changes between healthy individuals and idiopathic PD patients (Mann et al., 1992; Taylor et al., 1994; Hanagasi et al., 2005). In addition, cell lines engineered to contain mitochondria derived from platelets of PD patients (cybrids) were also shown to exhibit a stable decrease in complex I activity, increased ROS production, proton leak and decreased maximum respiratory capacity (Swerdlow et al., 1996; Cassarino et al., 1997; Esteves et al., 2008; Esteves et al., 2010c).

Supporting a functional role of complex I dysfunction in PD-related neurodegeneration, the feeding of mitochondrial ETC directly at complex II by infusion of the ketone body D-b-hydroxybutyrate was shown to bypass complex I blockade, enhance oxidative phosphorylation, and confer protection against the structural and functional deleterious effects of MPTP in mice (Tieu et al., 2003). In addition, viral injection of the alternative single polypeptide NADH-quinone oxidoreductase of *Saccharomyces cerevisiae* mitochondria (Ndi1), which is insensitive to complex I inhibitors, has been shown to protect against neurodegeneration and behavioral deficits of acute MPTP and rotenone mouse models of PD (Seo et al., 2006a; Richardson et al., 2007; Marella et al., 2008). Also, methylene blue, an alternative electron carrier which accepts electrons from NADH and transfers them to cytochrome *c* and bypasses complex I/III blockage, was shown to dramatically reduce behavioral, neurochemical, and neuropathological impairments induced by rotenone in a PD rat model (Wen et al., 2011). Reinforcing the involvement of respiratory chain dysfunction in PD, most of the pesticides which have been epidemiologically associated to an increased risk of PD are able to induce complex I dysfunction (Sherer et al., 2002; Schuh et al., 2005; Richardson et al., 2009; Schuh et al., 2009). However, the finding that the knockout (KO) mice for the Ndufs4 gene, encoding a subunit required for the complex I assembly and activity, are not protected from MPTP, rotenone, and paraquat-induced dopaminergic neuron death (Choi et al., 2008) raised the possibility that they can cause parkinsonism by acting also on different targets or that other complex I subunits are involved in toxicity. In fact, Ndufs4-deficient dopaminergic neurons are even more sensitive to rotenone, and complex I-independent mechanisms have been reported to contribute to the toxicity of rotenone, such as microtubule depolymerization (Ren et al., 2005; Choi et al., 2011). However, it was recently shown that complex I activity is only partially decreased but not abolished in Ndufs4 KO mice due to the formation of respiratory supercomplexes with a

stabilizing effect of complex III (Calvaruso et al., 2012; Sterky et al., 2012). This finding can explain why Ndufs4-deficient neurons are still sensitive to MPTP and rotenone toxicity. Dopaminergic neuron-specific conditional Ndufs4 KO mice do not show overt nigrostriatal degeneration, only a mild decrease (7.5%) in tyrosine hydroxylase-positive neurons at 24 months of age (Sterky et al., 2012). Nevertheless, striatal dopamine turnover is increased and dopamine release is decreased in Ndufs4-deficient mice, which may reflect an early consequence of mitochondrial impairment. These findings support the notion that complex I deficiency can contribute to the pathogenesis of PD.

1.2.2 Mitochondrial DNA (mtDNA) and the energetic threshold effect

The human mitochondrial genome (mtDNA) is a circular double-stranded molecule containing 37 genes (16,569 base pairs), 13 of which encode protein subunits of the mitochondrial respiratory apparatus (seven subunits of NADH:ubiquinone oxidoreductase, one subunit of cytochrome c reductase, three subunits of cytochrome c oxidase, and two subunits of ATP synthase) **(Figure I.3)**.

The rules of inheritance of mtDNA differ considerably from Mendelian inheritance. In fact, a peculiar characteristic of mtDNA is that it is inherited almost exclusively through the mother, and may exist in many different copies in the oocyte cytoplasm. This implies that no mtDNA recombination occurs at fertilization and only a sequential accumulation of mutations from the maternal lineage account for mtDNA variations. Moreover, mtDNA is particularly prone to mutations, being estimated as 10 times greater than nuclear DNA, due to the absence of protective proteins (such as histones) and of a high-efficiency repair system, although short and long-patch base excision repair systems are now well documented. Thus, mutant mtDNA can coexist with normal mtDNA, a condition referred to as heteroplasmy, and the levels of mutant mtDNA could vary dramatically during ageing. It was also discovered that pathogenic mtDNA mutations only cause mitochondrial respiratory chain dysfunction if they are present above a certain threshold level, which is >60% for single large mtDNA deletions and >90% for certain point mutations in tRNA genes (“threshold effect”). Single large mtDNA deletions, which always remove one or several tRNA genes, as well as point mutations of tRNA genes, lead to impaired mitochondrial translation and respiratory chain deficiency **(Figure I.3)**.

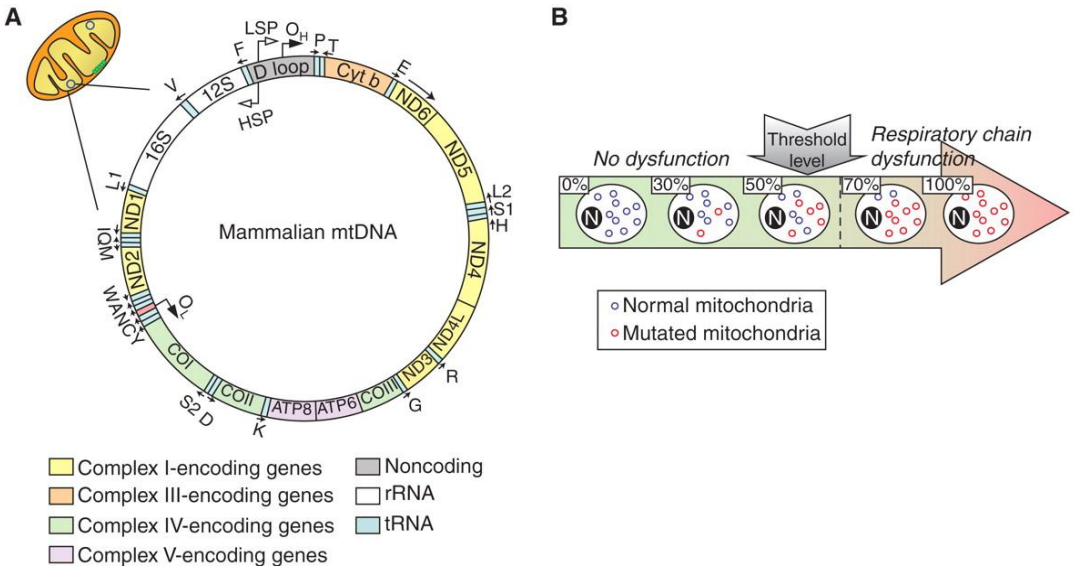

Figure I.3. Mitochondrial DNA (mtDNA) and the energetic threshold effect.

A. Mammalian mtDNA is a double-stranded circular molecule. The two strands are denoted the heavy (H) andlight (L) strand due to different buoyant densities. The only longer noncoding region, the displacement loop (D loop), contains a triplex structure with a nascent H strand. The D loop contains the promoters for transcription of the H and L strand (HSP and LSP) as well as the origin of replication of the leading strand of mtDNA (OH). The origin of replication of the lagging strand (OL) is located in a cluster of tRNA genes.Transcription from HSP produces 2 rRNAs (12S and 16S rRNA), 12 mRNAs (ND1–5, ND4L, Cyt b, COI–III, ATP6, and ATP8), and 14 tRNAs (F, V, L1, I, M, W, D, K, G, R, H, S1, L2, T). Transcription from LSP has a dual function. First, it produces RNA primers needed for initiation of replication at OH. Second, it is needed to produce one mRNA (ND6) and eight tRNAs (P, E, S2, Y, C, N, A, Q). **B.** Clonal expansion of mutated mtDNA molecules. In a normal situation, all mtDNAs within a cell are identical (homoplasmy). In a pathological situation linked to pathogenic mtDNA mutations, cells can harbor both normal and mutant mtDNA (heteroplasmy). Somatic mtDNA mutations tend to undergo clonal expansion and thereby cause focal respiratory chain deficiency and clinical signs (“threshold effect”) [Adapted from (Perier and Vila, 2012)].

The threshold for disease is lower in cells with high energy demands, such as neurons and muscle cells, rendering them particularly vulnerable to the effects of pathogenic mtDNA mutations (Perier and Vila, 2012). SNpc neurons seem to be especially vulnerable to mtDNA mutations, since hippocampal neurons or pyramidal cortical neurons of aged individuals did not contain high levels of mtDNA mutations.

Evidence regarding inherited “damaged” mtDNA that could explain mitochondrial dysfunction observed in PD patient brains and blood peripheral models is still inconsistent, but several studies have suggested an association between mtDNA

mutations and PD (Parker and Parks, 2005; Winkler-Stuck et al., 2005). As mentioned in the section 1.2.1, cybrids generated with mitochondria harvested from PD patient platelets exhibit complex I deficiency similar to patient cells, showing direct inheritance of the biochemical abnormality through mitochondria. Cybrids are produced by fusing cells previously deprived of their endogenous mtDNA (called Rho0 cells) with mitochondria from patient samples, resulting in a hybrid with a constant nuclear background and a transfered mitochondrial gene complement. In this way the influences of the mitochondrial genome on the physiology of a cell can be separated from nuclear factors, and direct comparisons can be made between the functional properties of mtDNA from various sources. Since this complex I deficiency is stable over tens of cell doublings, any protein or membrane components transferred with mtDNA become diluted and removed, leaving only mtDNA as the carrier of information causing complex I dysfunction. In addition to complex I deficiency, PD cybrids exhibit a number of other physiological alterations found in PD patient tissues, including abnormalities of calcium homeostasis (Sheehan et al., 1997; Esteves et al., 2010b), increased antioxidant enzymes, increased ROS production (Cassarino et al., 1997; Esteves et al., 2009), and protein aggregation in the form of LBs, the histopathological hallmarks of PD (Trimmer et al., 2004a; Esteves et al., 2009, 2010a). These observations suggest that PD-derived mtDNA encodes pathogenic information and highlight the possibility that mitochondrial abnormalities in PD may be inherited from mtDNA or related to somatic mtDNA alterations acquired during the ageing process. In fact, Swerdlow *et al.* found that cybrid cell lines prepared using platelet mitochondria from PD-affected kindred members and the young, asymptomatic descendents of PD mothers had lower complex I activity, increased ROS production and more abnormal mitochondrial morphologic features than cybrid cell lines containing mtDNA from paternal descendants (Swerdlow et al., 1998). These results support a precedent for inherited mtDNA as causative of mitochondrial dysfunction in PD sporadic cases. Accordingly, analysis of multiple PD subject databases found sex ratio differences between PD probands and the PD-affected parents of those probands (Swerdlow et al., 2001). While the proband sex ratio showed more men than women, the PD-affected parental generation showed more women than men. This finding is consistent with a maternal inheritance bias [reviewed in (Swerdlow, 2011)]. Also, the existing defect of complex I activity in PD patient platelets, a non-degenerating tissue, represents a systemic dysfunction, which is more compatible with inherited rather than somatic mtDNA alterations.

There is, however, considerable evidence showing that mtDNA acquires mutations during ageing, more prevalent in the brain, composed of long-lived postmitotic neurons, which have a great rate of oxidative metabolism, with increased ROS production

(Terman et al., 2010). Consistent with this observation, a new conditional KO mouse modeling PD was generated by disruption of the gene for mitochondrial transcription factor A (TFAM) in dopaminergic neurons, termed “MitoPark” mouse. This is the first animal model showing slow progressive degeneration of dopaminergic neurons similar to PD patient brains. This mouse show reduced mtDNA expression, reduced respiratory chain function in midbrain dopaminergic neurons which, in turn, lead to a parkinsonian phenotype, with adult onset of slowly progressive impairment of motor function associated to the formation of intraneuronal inclusions and dopamine nerve cell death, suggesting that impaired mtDNA expression may primarily contribute to the pathogenesis of PD (Ekstrand et al., 2007). Similarly, expression of mitochondrially targeted PstI endonuclease in dopaminergic neurons, which induces double-strand breaks in mtDNA, causes progressive neuronal degeneration and striatal dopamine depletion (Pickrell et al., 2011). Moreover, transgenic mice expressing a proofreading-deficient version of the mtDNA polymerase γ (POLG) accumulate mtDNA mutations and display features of premature ageing (Trifunovic et al., 2004; Kujoth et al., 2005). Remarkably, cosegregation of parkinsonism with mutations in the human POLG1 gene has been reported in several families [reviewed in (Orsucci et al., 2011)].

An age-dependent increase in mtDNA deletions have been observed in individual dopaminergic neurons dissected from the SNpc of *post mortem* human brains from normal individuals and idiopathic PD patients (Bender et al., 2006; Kraytsberg et al., 2006). Different types of mtDNA deletions were found in the same individual, but each neuron contained only a single mtDNA mutation, indicating that the mutation was acquired and clonally expanded. In comparison with age-matched controls, the amount of mtDNA mutations was slightly higher in dopaminergic neurons from PD patients (Bender et al., 2006).

Therefore, either by inherited mtDNA mutations or by somatic mutations which initially occurs in a single DNA molecule but can clonally expand, mtDNA mutational burden ultimately might exceed the phenotypic threshold, resulting in focal ETC defects.

1.2.3. Mitochondrial motility: an on track sliding-dependent cellular process

Mitochondria are extremely dynamic organelles that undertake constant changes in shape and distribution into the cell in order to achieve their exact assignment at the suitable time and site. Therefore, mitochondria accumulate in subcellular regions with high metabolic energy demands and/or where calcium buffering is required (Morris and Hollenbeck, 1993) and reallocate in response to changes in the local energy state

(Hollenbeck, 1996). Proper functioning of mitochondria depends on their intracellular location which is decisively governed by aspects of mitochondrial spatial arrangement and motility beyond fusion and fission. Mitochondria apparently maintain their identity as discrete organelles through long travels that involve frequent stops and re-starts and some changes in direction (Fahim et al., 1985). Their movement is, to varying degrees, saltatory and bidirectional, and this sets them apart from small vesicles, endosomes and most other axonally transported organelles (Hollenbeck, 1996; Ligon and Steward, 2000a). These aspects are critically important when we look to neurons (Hollenbeck and Saxton, 2005) which require mitochondria at sites distant from the cell body. Throughout their traffic in the axon, mitochondria can quickly switch between anterograde and retrograde movement, and their net direction has been shown in isolated neurons to result primarily from modulation of the fraction of time spent moving anterogradely (Morris and Hollenbeck, 1993).

Neuronal populations particularly vulnerable to PD, such as SNpc dopaminergic neurons, have common features as they have long and thin axons, which have little or no myelination (Braak et al., 2004). Neurons with these features are more vulnerable to degeneration and require high energy demands and so they are particularly dependent on suitable mitochondrial trafficking. Indeed, the evidence of reduced cytoplasmic mitochondrial mass and size (Liang et al., 2007; Kim-Han et al., 2011) and impaired axonal transport (Kim-Han et al., 2011) in mice SNpc dopaminergic neurons when compared with non-dopaminergic neurons suggests selective vulnerability of dopaminergic neurons as a result of a mitochondrial dysfunction.

The main mechanism to deliver cellular components to their action site is the long-distance microtubule (MT)-based transport. In turn, fast, long distance, axonal transport of mitochondria is accomplished through the MT network. MTs are one of the main constituents of the cytoskeleton, constituting parallel polymers of α- and β-tubulin dimers which have nearly all of their plus ends directed towards the nerve terminal (Heidemann, 1996; Baas, 2002). Essential to the function of MTs is their rapid and time-sensitive growth and shortening dynamics (dynamic instability) and this stochastic switch from growth to shrinking involves the binding and the hydrolysis of guanosine 5'- triphosphate (GTP) by tubulin. Also implicated in mitochondrial transport and distribution are the motor proteins of the kinesin superfamily in anterograde organelle transport and those of the dynein family in retrograde transport (Hollenbeck, 1996). For short range transport, mitochondria can also move along actin filaments which serve as tracks to areas where the MTs do not reach (Kuznetsov et al., 1992; Morris and Hollenbeck, 1995; Ligon and Steward, 2000b; Langford, 2002; Bridgman, 2004). Kinesins and dyneins are typical molecular motors as they convert the energy of ATP in their work. So, it seems that the

ATP/ADP and GTP/GDP recycling and bioavailability through functional active mitochondria control their proper motility and localization into the cell and that distribution is exquisitely regulated. In fact, it has been shown that mitochondrial movements depend on respiration (Katayama et al., 2006) and stop if respiration is inhibited or under extreme energetic conditions, *i.e*., in the presence of high ATP and high ADP concentrations in the cytoplasm. Inhibition of mitochondrial migration by ADP has been considered to be the mechanism by which mitochondria become trapped at sites with high energy demand (Katayama et al., 2006; Riva et al., 2006). Part of the mechanism underlying this trapping could be a lack of ATP for binding and activity of the motor molecules driving the organelles along cytoskeletal structures. Inhibition of motility by high cytoplasmic ATP is supposed to follow similar principles. Motor molecules lose their connection to the cytoskeletal fibrils at increased ATP concentrations, as shown for the dynein-microtubule interaction (Johnson, 1983).

Relevant to PD, MPP^+ (1-methyl-4-phenylpyridinium) and rotenone were shown to affect MT dynamics (Cappelletti et al., 2005; Ren and Feng, 2007). Moreover, MPP^+ was found to impair anterograde and increase retrograde transport of both mitochondria and other vesicles in isolated squid axoplasm (Morfini et al., 2007), and overall axonal motility of mitochondria but not of other moving particles in mouse dopaminergic neurons (Kim-Han et al., 2011). Supporting the concept that mitochondria has a main role on the control of the microtubule dynamics and microtubule-dependent trafficking, cells harboring mitochondrial deficits (PD cybrids) were found to exhibit ATP-dependent cytoskeletal changes (Esteves et al., 2009, 2010a). Accumulation of functionally impaired mitochondria and MT network destabilization can be counteracted by the formation of new mitochondria, degradation of non-functional organelles and/or aggregated proteins within a cell, as will be further discussed in the sections 1.4.2 and 1.4.3.

1.2.4 Mitochondria and cellular signaling

Mitochondria have long been considered as crucial organelles, primarily for their roles in biosynthetic reactions such as ATP synthesis. However, it is becoming increasingly apparent that mitochondria are intimately involved in cell signalling pathways. Mitochondria perform various signalling functions, serving as platforms to initiate cell signalling, as well as acting as transducers and effectors in multiple processes.

1.2.4.1 Mitochondria and calcium homeostasis

The calcium ion (Ca^{2+}) is one of the most important elements in cellular signaling because Ca^{2+} binding is involved in a great number of cellular processes ranging from the modulation of enzyme activity and gene expression to programmed cell death. Particularly in neurons, Ca^{2+} fluxes across the plasma membrane and between intracellular compartments play significant roles, including the regulation of neurite outgrowth and synaptogenesis, synaptic transmission and plasticity, and cell survival (Mattson, 2007). The concentration of cytosolic free Ca^{2+} in resting neurons (100 nM) is 10,000-fold lower than the concentration of Ca^{2+} in the extracellular space (1.2 mM) (Berridge et al., 2000; Rizzuto, 2001). This steep Ca^{2+} concentration gradient creates a huge driving force allowing a rapid increase in intracellular Ca^{2+} when Ca^{2+} channels located in the plasma membrane open. Therefore, it is critical to regulate the mechanisms governing Ca^{2+} entering neurons, as Ca^{2+} can be either a physiological messenger or a very toxic element when its concentration dynamics is deregulated. Ca^{2+} entering neurons is rapidly sequestered in intracellular organelles such as mitochondria or ER, or pumped back out of the cell across plasma membrane after interaction with mobile buffering proteins within the cytosol. These processes require energy stored in ATP or ion gradients that are maintained through ATP-dependent pumps. The major intracellular storage site of Ca^{2+} is the ER, and there is a significant interplay between mitochondria and ER regarding Ca^{2+} homeostasis, which will be further discussed in the section 1.3.3.1.

Ca^{2+} sequestration by mitochondria is based on their ability to uptake Ca^{2+}, through a uniporter located in the MIM, and to accumulate it in the matrix, a process driven by $\Delta\psi_m$. Ca^{2+} accumulation in the mitochondrial matrix starts when extramitochondrial Ca^{2+} concentration exceeds 400 nM and results from the balance between the low-affinity Ca^{2+} uptake and the efficient Ca^{2+} extrusion from the mitochondrial matrix, occurring via Ca^{2+}/Na^{+} or Ca^{2+}/H^{+} antiporters. Intramitochondrial Ca^{2+} concentration within the physiological range leads to the activation of mitochondrial catabolic processes due to stimulation of three mitochondrial dehydrogenases: pyruvate-, NAD+-isocitrate- and 2-oxoglutarate-dehydrogenase (Duszynski et al., 2006). Therefore, mitochondrial metabolism and Ca^{2+} homeostasis are mutually coupled, thus sustaining the energy requirements associated with neuronal activity.

During normal physiological activity, the intracellular Ca^{2+} concentration increases only transiently (seconds to a few minutes) and has no detrimental effects on the neurons. However, unlike most neurons in the brain, SNpc dopaminergic neurons are

autonomously active, generating action potentials at a clock-like 2–4 Hz in the absence of synaptic input (Grace and Bunney, 1983) (**Figure I.4**).

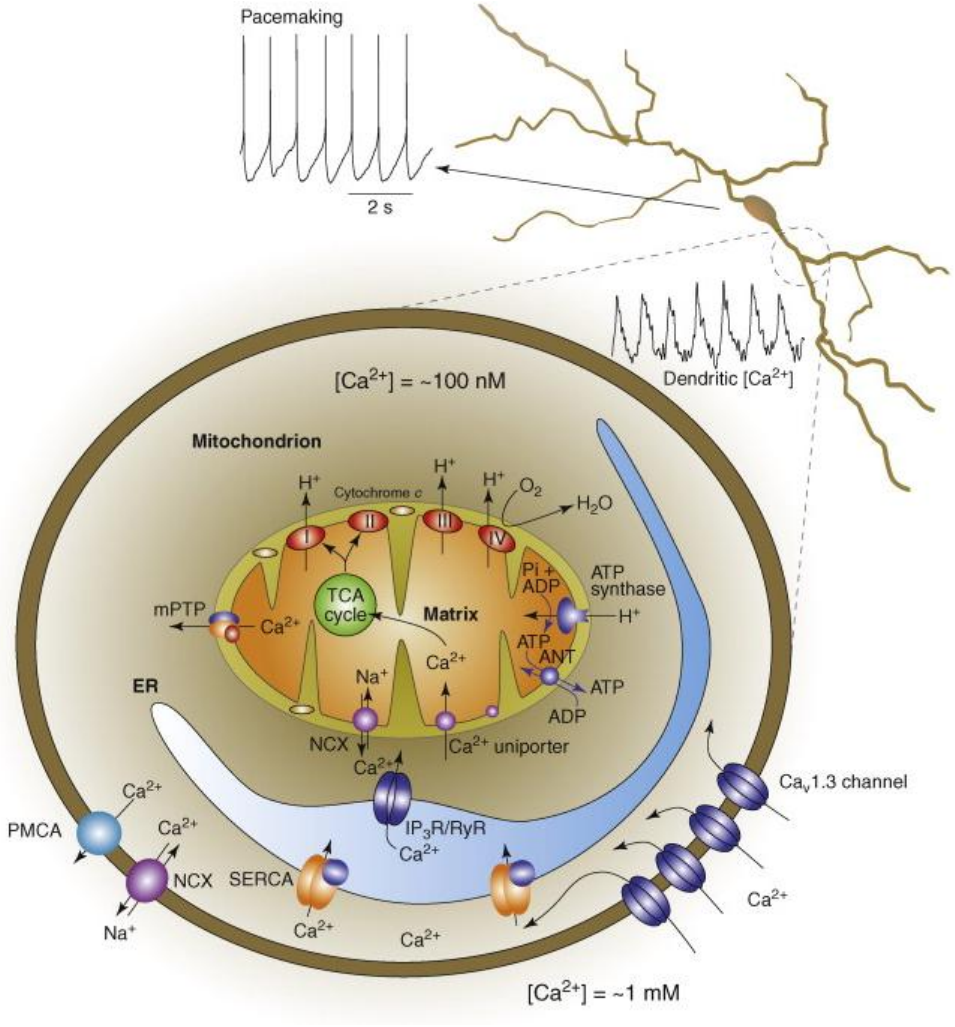

Figure I.4. Mitochondria, ER and Ca^{2+} transport in SNpc dopaminergic neurons.

The steep concentration gradient for Ca^{2+} enables it to cross the plasma membrane readily into cells through open pores such as L-type Ca^{2+} channels. Once inside neurons, it is either transported back across the plasma membrane or sequestered in intracellular organelles. Ca^{2+} is transported across the plasma membrane through either the Ca^{2+}-ATPase or through a Na^{+}/Ca^{2+} exchanger that relies upon the Na^{+} gradient. Ca^{2+} is rapidly sequestered either by ionic interactions with buffering proteins or by transport into cytosolic organelles (i.e. the mitochondria and the ER). The ER uses high-affinity smooth ER Ca^{2+} (SERCA) pumps that depend upon ATP to take Ca^{2+} from the cytoplasm into the ER lumen. Ca^{2+} flows back into the cytoplasm after the opening of inositol trisphosphate receptors (IP_3R) and ryanodine receptors (RyR) studding the ER membrane. Mitochondria are often found in close apposition to the ER and plasma membrane, creating a region of high (but localized) Ca^{2+} concentration that drives Ca^{2+} into the matrix of mitochondria through a Ca^{2+} uniporter [Adapted from (Chan et al., 2009a)].

In this regard, they are much like cardiac pacemakers, relying on a peculiar class of L-type channels, characterized by the presence of Cav1.3 pore forming subunit that confers to this type of Ca^{2+} channels the property to be open at relatively hyperpolarized potentials and thus exposing SNpc dopaminergic neurons to larger Ca^{2+} influxes than other neurons (Wilson and Callaway, 2000). The high magnitude of Ca^{2+}-influx through plasma membrane L-type channels in SNpc dopaminergic neurons ultimately compromises mitochondrial function, resulting in mitochondrial oxidative stress and oscillations in mitochondrial potential, the latter being associated with impaired ATP production (Guzman et al., 2010). Supporting the pathogenic role for Ca^{2+} overload associated to the pacemaking activity in SNpc dopaminergic neurons, the L-type Ca^{2+} channels antagonist iraspidine protects striatal dopaminergic terminals and parent SNpc cell bodies to both acute and chronic challenges with MPTP (Chan et al., 2007) or 6-hydroxydopamine (6-OHDA) (Ilijic et al., 2011). These observations suggest that prolonged Ca^{2+} overload in SNpc dopaminergic neurons may render these cells particularly vulnerable to PD. In accordance with this, dopaminergic neurons in the ventral tegmental area (VTA), which do not rely upon L-type Ca^{2+} channels for pacemaking, are relatively intact in PD patients and in animal models of PD (Kish et al., 1988; Chan et al., 2007). Another supportive observation is the resilience of selected SNpc dopaminergic neuronal populations that express Ca^{2+}-buffering proteins: expression of calbindin, calreticulin or parvalbumin is negatively correlated with degeneration in PD (Yamada et al., 1990; German et al., 1992; Mouatt-Prigent et al., 1994; McMahon et al., 1998).

Other evidences further support a role for alterations in mitochondrial Ca^{2+} homeostasis in PD. A dramatic reduction in calbindin levels has been described in brains of PD patients (Iacopino and Christakos, 1990). In addition, PD cybrid cells exhibit lower mitochondrial Ca^{2+} uptake ability relatively to control cells (Esteves et al., 2010b), even following carbachol-induced Ca^{2+} entering (Sheehan et al., 1997). Similarly, cybrid cell lines expressing mtDNA polymorphisms have alterations in intracellular Ca^{2+} dynamics (Kazuno et al., 2006). In addition, MPP^{+}, 6-OHDA and rotenone were found to stimulate mitochondrial Ca^{2+} release and cause increased cytosolic free Ca^{2+} levels in cultured cell lines (Frei and Richter, 1986; Sousa et al., 2003; Wang and Xu, 2005). Also, some oligomeric forms of α-synuclein exogenously applied to dopaminergic neurons evoked Ca^{2+} influx from the extracellular milieu through a pore-forming mechanism, leading to mitochondrial Ca^{2+} overload and apoptotic cell death (Danzer et al., 2007). Other studies have shown that α-synuclein can be associated to mitochondria and its accumulation is directly related to an increase in mitochondrial Ca^{2+} levels (Parihar et al., 2008), which in turn lead to increased levels of nitric oxide, oxidative stress, and cytochrome c release

(Parihar et al., 2009). However, these observations failed to be consistently reported, as further studies have shown no alterations in cellular Ca^{2+} homeostasis following overexpression of wild-type or mutant α-synuclein (Hettiarachchi et al., 2009). Moreover, evidence has suggested a role for PD-linked protein PINK1 in the regulation of mitochondrial Ca^{2+}, although data is controversial. Initially, it was proposed that PINK1 ablation in dopaminergic neurons causes an impairment of mitochondrial Ca^{2+} efflux, probably by affecting the mitochondrial Na^{+}/Ca^{2+} exchanger activity, resulting in mitochondrial Ca^{2+} overload, increased production of mitochondrial ROS and impaired mitochondrial respiration (Gandhi et al., 2009). Afterward, PINK1 depletion has instead been shown to impair mitochondrial Ca^{2+} uptake, and consequently to affect energy metabolism (Heeman et al., 2011). Coherently, some reports have demonstrated that lack of PINK1 in cells impairs $\Delta\psi_m$ and increases susceptibility to mitochondrial neurotoxins (Wood-Kaczmar et al., 2008) as well as enhances vulnerability to Ca^{2+} (Akundi et al., 2011). Supporting a role for Ca^{2+} overload in PD-related cell death, pharmacological or genetic inhibition of Ca^{2+}-sensitive proteases, such as calpains, has been shown to attenuate caspase-3 dependent cell death in mitochondrial deficient cells (Esteves et al., 2010a) and overall dopaminergic neurodegeneration in a MPTP mouse model of PD (Crocker et al., 2003).

1.2.4.2 Mitochondria and programmed cell death

Programmed cell death, or apoptosis, is a naturally occurring process of cell “suicide” that plays a crucial role in the development and maintenance of all pluricellular organisms by eliminating superfluous or unwanted cells. However, massive or abnormal activation of apoptosis in adulthood can lead to neurodegeneration. Because apoptosis is involved in the maintenance of tissue and organ homeostasis, it is strictly controlled at multiple levels (Green and Kroemer, 2004).

In numerous models, mitochondria represent a central checkpoint of apoptosis control by integrating various signals, including endogenous factors (e.g., cytosolic and organellar concentrations of protons Ca^{2+}, Mg^{2+}, K^{+}, and Na^{+}, metabolites such as ATP, ADP, $NADP^{+}$, glutathione, lipid second messengers, and multiple proteins including kinases and phosphatases) as well as exogenous factors (e.g., specific viral proteins or xenobiotics) (Kroemer et al., 2007). These organelles integrate the sum of death-inducing and life-preserving signals at the level of their membranes and, when the lethal signals predominate over the vital ones, mitochondria proceed with “its intrinsic” or mitochondrial pathway. Here, in response to an apoptotic stimuli, the initiator caspase-9, is activated by multimerization on the adapter molecule apoptosis protease activating

factor 1 (APAF-1) and assemble within a multiprotein complex called apoptosome. The release of cytochrome c (which normally resides only in the IMS) into the cytosol following mitochondrial outer membrane permeabilization (MOMP) is crucial for the generation of the apoptosome and subsequent processing and activation of effector caspases such as caspase-3. Hence, MOMP is the critical event responsible for caspase activation and represents the point of no return in a cell's commitment to die, being regulated by many proteins of the Bcl-2 family which either prevent (e.g., Bcl-2 and Bcl-xL) or promote (e.g., Bax and Bak) the apoptotic cascade of cell death.

Relevant to PD pathology, dopaminergic cell death appears to occur, at least in part, through the activation of mitochondria-dependent apoptotic pathways. Analysis of PD patient *post mortem* brains revealed a great increase in apoptotic neuronal nuclei accompanied of raised immunoreactivity to caspase-3 and Bax (Tatton, 2000). In addition, data from transmitochondrial cybrids have shown that PD mitochondria are more likely than healthy mitochondria to activate the intrinsic apoptotic cascade, when exposed to a mitochondrial toxin, such as MPP^+ (Swerdlow et al., 1996; Esteves et al., 2008). Similarly, MPTP-treated mice were found to develop marked apoptotic features, as caspase-3 and caspase-9 activation (Hartmann et al., 2000), calpain activation (Crocker et al., 2003), downregulation of Bcl-2 levels and strong upregulation of Bax levels in nigrostriatal dopaminergic neurons (Vila et al., 2001). Further supporting the involvement of mitochondria-dependent apoptotic pathway in PD, nigrostriatal degeneration in MPTP-treated mice can also be prevented by targeting some molecules of this pathway, such as caspase-9 or APAF-1 (Mochizuki et al., 2001; Viswanath et al., 2001), or by overexpressing Bcl-2 (Offen et al., 1998; Yang et al., 1998).

In addition, some mutated genes associated with familial forms of PD were found to affect mitochondria-dependent cell death. For instance, overexpression of α-synuclein in vivo and in several cell types triggered apoptosis (Saha et al., 2000; Stefanova et al., 2001; Kim et al., 2004). Several apoptotic markers were also observed in yeast models of α-synuclein toxicity (Flower et al., 2005). α-Synuclein toxicity can be rescued by caspase inhibitors or knock down of caspase-12 (Smith et al., 2005). Activation of caspase-3 has been observed in transgenic mice (Martin et al., 2006) and caspase-9 has been reported in viral models in mice (St Martin et al., 2007) and rats (Yamada et al., 2004). In cell lines, PD-associated mutant LRRK2 led to mitochondria-dependent apoptosis through the release of cytochrome c and caspase-3 activation (Iaccarino et al., 2007). The genetic ablation of Apaf1 abrogated the caspase-3 activation and the neuronal death. In addition, overexpression of wild-type PINK1, but not of mutant PD-linked PINK1, reduced cytochrome c release, caspase activation, and apoptosis induced by mityochondrial neurotoxins in cultured cells (Petit et al., 2005). Likewise,

overexpression of Parkin was shown to prevent ceramide-induced mitochondrial swelling and subsequent cytochrome c release, caspase-3 activation, and apoptotic cell death in vitro (Darios et al., 2003). Together, these data suggest that activation of mitochondria-dependent apoptotic pathways contributes to SNpc dopaminergic neuronal cell death in PD.

1.3 ER, protein folding and misfolding

The ER is a subcellular organelle comprised of a reticular membranous network that extends throughout the cytoplasm and that can be contiguous with the nuclear envelope. In highly elongated and polarized cells such as neurons, ER spreads from the cell body throughout the dendrites and axons (Aridor et al., 2004). The ER organizes its large amount of membrane by folding it into tubular or lamellar structures, generating a complex architecture that varies in response to functional requirements (Borgese et al., 2006). This complex architecture makes ER a primed site for protein folding, and supports a variety of other key activities including Ca^{2+} storage, and steroid, cholesterol and lipid biosynthesis.

Proteins enter the ER as unfolded polypeptide chains and are then correctly folded and assembled prior to transit to the cell surface or to intracellular organelles. The acquisition of the native structure of a protein in vivo takes place within the crowded environment of the ER. In principle, crowding could interfere with folding by favouring the aggregation of unfolded proteins. This effect can be overcome by the action of a complex and dynamic network of protein chaperones, foldases and cofactors that assist the folding and maturation of proteins, preventing their abnormal aggregation or misfolding. Nonetheless, protein folding in the ER is inherently imperfect and errors made at any step on the way to the final product decrease the fraction of proteins that reach their proper conformation. Transient accumulation of unfolded proteins initiates an adaptive coordinated signaling cascade known as the unfolded protein response (UPR). Appropriate adaptation to misfolded protein accumulation within the ER requires regulation at all levels of gene expression including transcription, translation, translocation into the ER lumen or induction of protein degradation in a process termed ER-associated degradation (ERAD) or through autophagy (Malhotra and Kaufman, 2007). Synchronized regulation of these processes is required to restore proper protein folding and ER homeostasis. On the other hand, if protein folding is not repaired, persistent activation of UPR signaling occurs, which eventually induces an apoptotic response.

1.3.1 ER, protein folding and quality control

ER protein folding consists in a complex interplay between a polypeptide primary structural information and associated cellular networks. Folding begins as protein synthesis initiates on ribosomes and ends when native proteins are packaged for ER exit (Brodsky and Skach, 2011).

Relative to cytosol, ER is an oxidizing environment which facilitates several co-translational and post-translational modifications that do not occur in the cytosol [disulfide bond formation, glycosylation and glycophosphatidylinositol (GPI) anchor addition], further stabilizing and conferring specific functionality to proteins (Dorner et al., 1990; Braakman et al., 1992). Thus, secreted and membrane proteins, which transit through the secretory pathway, must first complete their folding in the ER. The ER therefore constitutes a protein folding factory that entails an exquisite quality control (QC) on its products, ensuring that only properly assembled and functional proteins are delivered to their final destinations in the cell (Ellgaard and Helenius, 2003). Consequently, proteins entering the ER immediately encounter a network of chaperone systems that minimize aggregation, facilitate native structure conformation and ensure the fidelity of oligomeric assembly (Jonikas et al., 2009) **(Figure I.5)**.

Chaperones and folding enzymes reside in the ER in high concentrations and participate in all steps of folding and in QC. Key chaperones and folding sensors include the glucose regulated protein GRP78, also known as immunoglobulin binding protein (BiP) and 94 (GRP94), the lectins calnexin and calrecticulin, and the thiol-disulfide oxidoreductases. BiP/GRP78 belongs to the heat shock protein (Hsp)70 family and is one of the molecular chaperones first encountered by most newly synthesized polypeptides **(Figure I.5)**. In mammalian cells, BiP is present at the translocon where it serves to maintain the permeability barrier of the ER during the early stages of targeting nascent chains into the translocon. BiP binds to the hydrophobic patches of unfolded proteins via a substrate-binding domain and facilitates folding through conformational changes evoked by the hydrolysis of ATP by the ATPase domain.

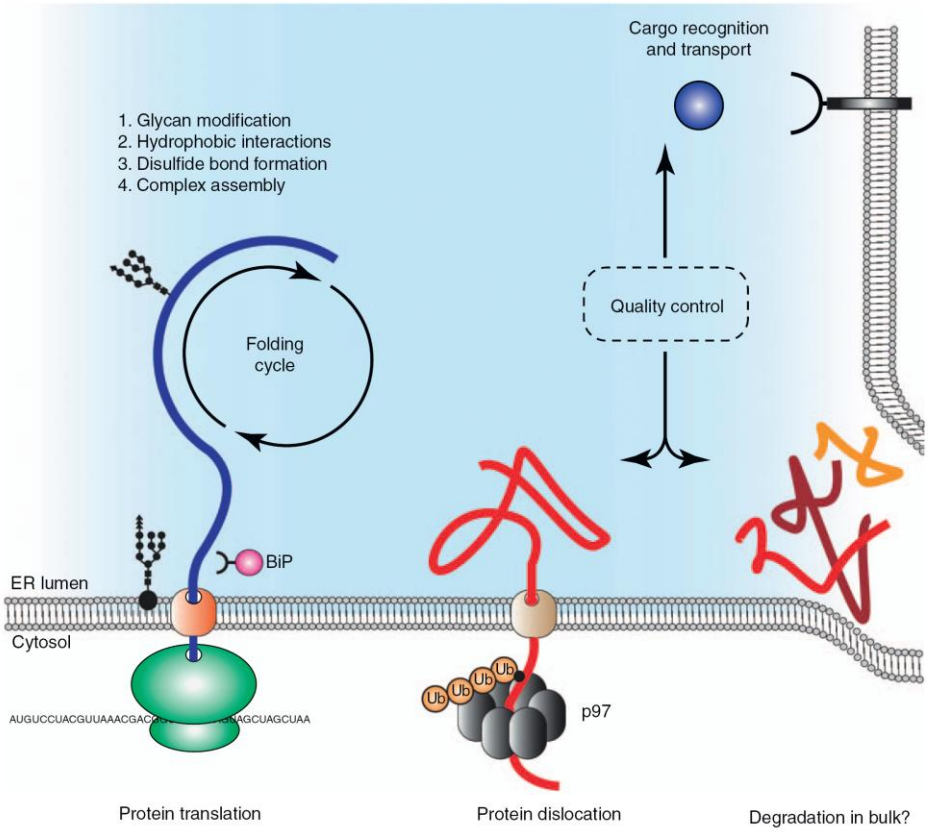

Figure I.5. Protein folding in the ER.

Schematic overview of a nascent polypeptide entering the ER lumen cotranslationally, where it engages folding machinery to obtain its final conformation (folding cycle). Quality control checkpoint(s) establish the folding status of the polypeptide which then either proceeds to its final destination or is selectively degraded, either via the dislocation pathway or via a bulk degradation mechanism (e.g. autophagy) [Adapted from (Claessen et al., 2012)].

1.3.2 Protein misfolding and the ER stress response in Parkinson's disease

As mentioned above, disturbance in the function or loss of integrity of ER therefore disrupts folding and leads to the accumulation of unfolded proteins. Unfolded or misfolded proteins expose amino-acid residues that should be located inside the protein and became prone to form aggregates in the ER as well as in the cytosol. As small aggregates are highly toxic, this potentially leads to ER stress. To alleviate such a stressful condition, cells activate a series of self-defense mechanisms referred collectively to as the ER stress response or UPR (Mori, 2000; Patil and Walter, 2001; Harding et al., 2002; Schroder and Kaufman, 2005).

In mammalian cells, ER stress response consists of four different pathways. The first is attenuation of protein synthesis that prevents any further accumulation of unfolded

proteins. The second is the transcriptional induction of ER chaperone genes to increase folding capacity, and the third is the transcriptional induction of ERAD component genes to increase ERAD ability. The fourth is the induction of apoptosis to safely dispose of cells injured by ER stress to ensure survival of the organisms.

Accumulating evidence strongly suggests the involvement of ER stress in PD. The parkinsonism-inducing neurotoxins 6-OHDA, MPP^+, and rotenone have been shown to induce many genes involved in various aspects of the UPR including ER chaperones such as BiP, protein disulfide-isomerase (PDI) and calreticulin, the inositol requiring enzyme 1 alpha (IRE1-α), and the protein kinase RNA-like endoplasmic reticulum kinase (PERK) in neuronal cells (Ryu et al., 2002; Holtz and O'Malley, 2003). These effects were specific for these PD mimetics but not for other agents (Ryu et al., 2002). In addition, the expression of ER chaperones, such as PDI, was found to be up-regulated in the brain of PD patients and PDI accumulated in LBs (Conn et al., 2004). According with these observations, accumulation of polyubiquitinated proteins and UPR activation have also been observed in the SNpc dopaminergic neurons of post mortem tissue from sporadic PD patients (Hoozemans et al., 2007; Slodzinski et al., 2009), and in Multiple System Atrophy patients, other synucleinopathy (Makioka et al., 2010), indicating that UPR activation may be induced to prevent neurotoxicity associated with ER stress and protein misfolding. Also, PDI inactivation occurs in PD brains through oxidative modifications (Uehara et al., 2006).

More substantial evidence for a role of ER stress in PD pathogenesis comes from the study of juvenile onset forms of genetic PD that is caused by mutation in the Parkin gene, which compromise the ubiquitin ligase function of the protein (Shimura et al., 2000). PD-related mutations in Parkin results in the accumulation of its substrate, Pael-R, in the ER of SNpc dopaminergic neurons, leading to ER stress and cell death (Imai et al., 2001). On the other hand, Parkin expression has a prosurvival activity against ER stress due to modulation of ERAD/proteasome pathway (Imai et al., 2000; Wang et al., 2007). In addition, overexpression of wild-type (Shimazawa et al., 2010) or mutant (Smith et al., 2005) α-synuclein induces chronic ER stress activation, inducing cell death. Reports in the complementary model of yeast demonstrated that the earliest effect following α-synuclein expression is a block in the ER to Golgi vesicular trafficking. Notably, the inhibition of the ER-Golgi trafficking by α-synuclein expression triggers ER stress (Cooper et al., 2006; Gitler et al., 2008) possibly due to the accumulation of cargo vesicles, triggering the accumulation of immature proteins at the ER (Ding and Yin, 2008). α-Synuclein phosphorylation at serine 129 was found to be responsible for UPR-mediated cell death in neuroblastoma cells even before any detectable mitochondrial dysfunction is observed (Sugeno et al., 2008). Similarly, downregulation and mutations in

DJ-1 have been shown to trigger ER-stress, thus suggesting that loss of DJ-1 protein activity makes neurons more vulnerable to ER-stress (Yokota et al., 2003). Furthermore, mutations in the P5 ATPase (ATP13A2, PARK9), responsible for an autosomal recessive form of early onset parkinsonism, were associated with its retention in the ER, where it may exert neurotoxicity (Ramirez et al., 2006). Finally, LRRK2 deficiency in C.elegans triggers hypersensitivity to ER stress (Samann et al., 2009).

1.3.3 ER-mitochondria interorganelle crosstalk

The ER and mitochondria are endowed with several functionalities, and among them is a recently emerged concept of a direct line of communication between these two organelles. Interestingly, mitochondria and the ER are physically and functionally interconnected, as the MOM can associate with the ER membrane, in a structure called mitochondrial-associated membrane (MAM), allowing some important cellular functions (Giorgi et al., 2009). For example, the exchange of metabolites between mitochondria and the ER that occur continuously during the life span of the cell is crucial for cellular functions. Here, ATP produced by oxidative phosphorylation is used by ATPases located in the ER (i.e. Ca^{2+} ATPases); in the opposite direction, products of ER metabolic pathways, such as phospholipids, are transferred continuously to the mitochondrial membranes. However, the best characterized aspect of functional interconnection between these organelles is undoubtedly the regulation of intracellular Ca^{2+} homeostasis. This is because Ca^{2+} exchange between ER and mitochondria not only has a role in regulating physical interactions between the two organelles, but also regulates different fundamental biological processes, including cell survival and apoptosis.

1.3.3.1 The ER and mitochondria partnership in Ca^{2+} homeostasis

The ER has taken a center stage in the machinery responsible for Ca^{2+} homeostasis (Berridge, 2002). As in other neurons, the ER network in SNpc dopaminergic neurons extends throughout the somatodendritic tree (Choi et al., 2006). High-affinity ATP-dependent transporters move Ca^{2+} from the cytoplasm into the ER lumen and pump it back to the cytoplasm. The absence of high-affinity, anchored intraluminal Ca^{2+} buffers and the physical continuity of the lumen within the cell (Mogami et al., 1997; Park et al., 2000) enables the ER to rapidly (~30 μm/s) redistribute Ca^{2+} between intracellular compartments, thus avoiding pro-apoptotic accumulations in the cytosol (Choi et al., 2006). Thus, Ca^{2+} sequestered in the ER by sarco(endo)plasmic reticulum Ca^{2+}ATPase

(SERCA) is further released at sites where it can be pumped back across the plasma membrane or where it can be used to modulate cellular functions (Rose and Konnerth, 2001; Verkhratsky, 2005; Park et al., 2008).

However, the storage capacity of the ER is limited. Ca^{2+} released from the ER through inositol-1,4,5-triphosphate receptor (IP_3R) or ryanodine receptors (RyR) can enter mitochondria at points of close apposition between the organelles which form functional Ca^{2+} microdomains (Csordas et al., 2006; Rizzuto and Pozzan, 2006). Therefore, mitochondria play an important role in shaping the Ca^{2+} fluxes released from the ER. Mitochondria assist with the recovery phase by rapidly sequestering Ca^{2+} and then later returning it to the ER. During normal signaling, there is a continuous ebb and flow of Ca^{2+} between these two organelles. The normal situation is for most of the Ca^{2+} to reside within the ER lumen, except during Ca^{2+} signaling when a small part is periodically released to the cytoplasm and is then recaptured by mitochondria. Because the channels through which Ca^{2+} enters mitochondria are of low affinity, it has been proposed that regions of close proximity between mitochondria and the ER are necessary for Ca^{2+} entry into the mitochondrial matrix (Rizzuto et al., 1998). Thus, a major determinant of the ER-mitochondria interface is the distance between their surfaces, controlled by the movement of these organelles along the cytoskeleton (Hollenbeck and Saxton, 2005; Boldogh and Pon, 2006). Ca^{2+} modulates this distance, as its release from ER channels is a signal that locally arrests mitochondrial motility and promotes their docking at the ER surface, enhancing Ca^{2+} transfer (Yi et al., 2004). Mitochondria respond promptly to physiological rises in Ca^{2+} with very rapid and large increases in their matrix Ca^{2+}, as shown clearly in different cell types [reviewed in (Rizzuto and Pozzan, 2006)]. Thus, no kinetic limitations are apparent in the capacity of mitochondria to uptake and release Ca^{2+} rapidly. The uptake of Ca^{2+} released from the ER into the mitochondrial matrix has important regulatory roles, such as the modulation of the spatio-temporal pattern of Ca^{2+} signaling within the cell and therefore many Ca^{2+}-dependent cellular processes, matching aerobic metabolism to energy demand. In addition, by buffering local Ca^{2+} and/or by returning it back to the cytosol after sequestration, mitochondria have a fundamental role in enabling the maintenance of cytosolic Ca^{2+} oscillations (Ishii et al., 2006; Vay et al., 2007). Also, by functioning as high-capacity Ca^{2+}-sinks, mitochondria modulate the propagation of Ca^{2+} waves and act in restricted microenvironments influencing the allosteric modulation by Ca^{2+} of the ER-release channels, such as the IP_3R and the RyR (Rizzuto and Pozzan, 2006)

1.3.3.2 The ER-mitochondria coupling in apoptosis

Numerous studies point to the ER as a third subcellular compartment implicated in apoptotic execution (Rao et al., 2004). Indeed, several molecules either present on the ER surface or in the soluble compartment have been implicated as effectors that cause cell death in response to prolonged ER stress. Caspase-12 (a murine caspase unequivocally identified in human tissue as caspase-4), which is associated with the ER, was implicated in apoptosis triggered by ER stress (Nakagawa et al., 2000; Rao et al., 2001; Rao et al., 2002). However, further studies demonstrated that caspase-12/capase-4 are not required for ER-stress induced apoptosis and that caspase-4-like activity is not always associated with an initiating event (Obeng and Boise, 2005). Caspase 2, which appears to be partially in the ER, has been proposed to have an important role in the initiation of ER-induced apoptosis, integrating the ER and the Golgi complex with the apoptotic pathway, acting as an upstream trigger to permeabilize the MOM (Cheung et al., 2006).

Similar to mitochondria, the ER is also a repository of apoptotic and antiapoptotic molecules. The known antiapoptotic molecules include GRP78, calreticulin, PDI and the 150-kDa oxygen-regulated protein (ORP-150) (Liu et al., 1997; Ozawa et al., 1999; Tanaka et al., 2000). Also, a significant fraction of endogenous Bcl-2 family members including Bcl-2, Bcl-xL, Bax, Bak and Bik have been shown to be associated with the ER, suggesting that Bcl-2 family proteins operate at the ER (at least in part) to regulate Ca^{2+} homeostasis and apoptotic cell death (Wei et al., 2001; Germain et al., 2002; Germain and Shore, 2003; Scorrano et al., 2003). For example, Bcl-2 overexpression results in a decrease of ER luminal Ca^{2+} content and this effect has been attributed to an increase in the Ca^{2+} leak from the organelle (Foyouzi-Youssefi et al., 2000; Pinton et al., 2000; Palmer et al., 2004; White et al., 2005). Moreover, knockdown of Bax and Bak increases the interaction of Bcl-2 with the type-1 IP_3Rs and promotes both the phosphorylation of the IP_3R and a constitutive Ca^{2+} leak through the IP_3Rs under basal conditions (Scorrano et al., 2003; Oakes et al., 2005). A reduced ER Ca^{2+} content, as in the case of Bcl-2 overexpression or knockdown of Bax/Bak, reduces the amount of Ca^{2+} that can be released from the ER owing to an apoptotic stimulus and thus decreases the probability of a Ca^{2+}-dependent MPTP opening (reviewed in (Oakes et al., 2006; Pinton and Rizzuto, 2006; Giacomello et al., 2007). In addition, released Ca^{2+} from the ER, acting on mitochondria fusion/fission proteins [dynamin-related protein 1 (DRP-1), hFis1, optic atrophy 1 (OPA1) and mitofusins (MFNs)], can also influence mitochondrial cristae remodeling and thus the amount of cytochrome c that can be released in the cytosol (Breckenridge et al., 2003a).

The ER–mitochondria crosstalk therefore amplifies ER-initiated apoptotic pathways or other pathways. In any case, the balance between these various Bcl-2 family members determines an “apoptotic rheostat” that modulates ER-mitochondria-dependent cell survival *versus* death (Korsmeyer et al., 1993).

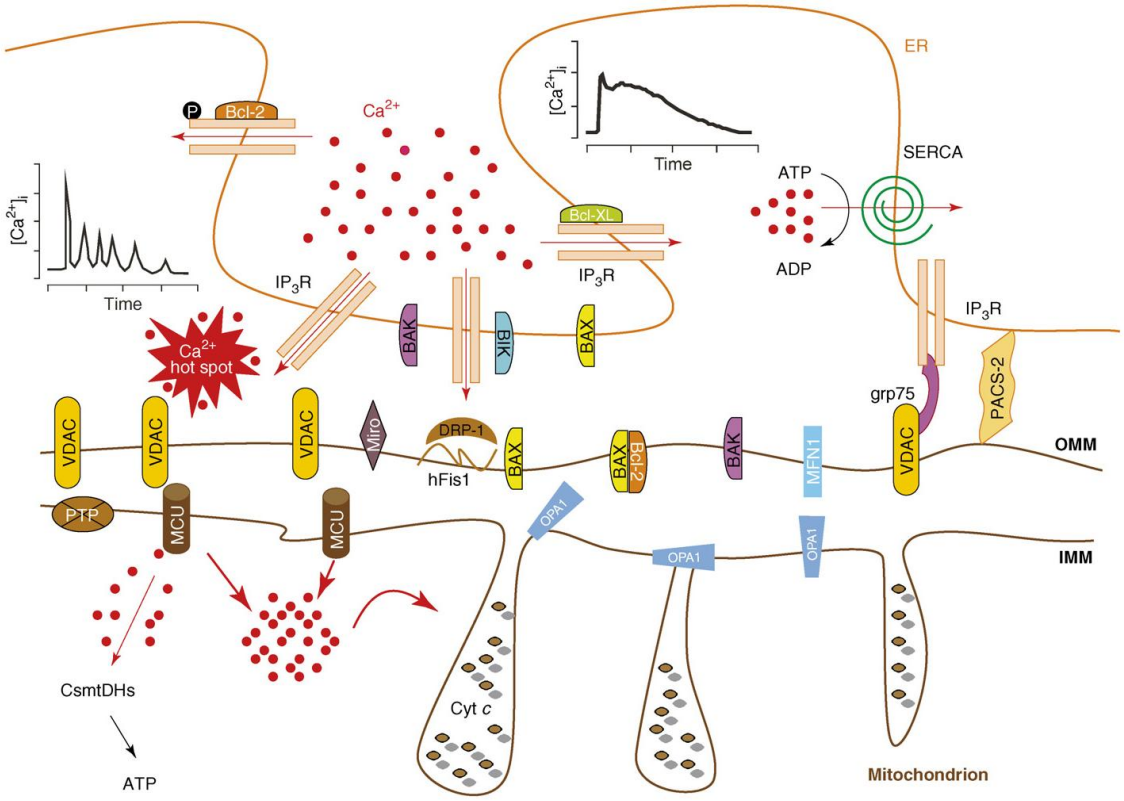

Figure I.6. Local ER–mitochondria interactions and apoptotic signalling at the ER–mitochondria interface.

A representation is depicted of ER–mitochondria relationships and of some of the proteins involved in the crosstalk between the organelles. Ca^{2+} released from the ER through IP_3Rs is taken up by mitochondria through the mitochondria Ca^{2+} uniporter (MCU). Within mitochondria, Ca^{2+} modulates mitochondrial dehydrogenase activity and thus ATP production. Moreover, mitochondrial Ca^{2+} uptake regulates the spatio-temporal pattern of the cytosolic Ca^{2+} signal and, therefore, many Ca^{2+}-dependent cellular processes. Massive and/or a prolonged accumulation of Ca^{2+} in the mitochondria can lead to the opening of the permeability transition pore (PTP) in the MIM and swelling of the organelle or, acting on mitochondria-shaping proteins [DRP-1, hFis1, OPA1, mitofusins (MFNs)], to mitochondrial cristae remodeling and modulation of apoptosis. The concerted action of the two organelles in cell death is further supported by the presence on both the ER membrane and the MOM of different components of the Bcl-2 family that have either a pro- (BIK, BAX, BAK) or an anti-apoptotic role (Bcl-2, Bcl-XL) [Adapted from (Pizzo and Pozzan, 2007)].

1.4 Autophagy and protein homeostasis: more than just a cellular cleaning mechanism in Parkinson's disease

Autophagy refers to a set of evolutionarily conserved and strictly regulated process whereby intracytoplasmic material of any kind is delivered to lysosomes (Mizushima et al., 2008; Yang and Klionsky, 2010). This pathway was first described by Christian De Duve in the 1960's as a simple cellular process in which a double-membrane vesicle, the autophagosome, delivers cytoplasmic constituents to lysosomes for degradation and recycling (De Duve, 1963). A substantial progress on the molecular dissection of autophagy has taken place during only the past 15 years, uncovering the main components that are involved in the different autophagic processes, their regulation and contribution to different cellular functions. Autophagy is induced by different adverse conditions such as limited nutrients, low oxygen levels, and decreased energy supply, and its action results in the release of degradation products, especially amino acids, back into the cytoplasm to be used in essential biosynthetic pathways. According to the different pathways by which cargo is delivered to the lysosome, autophagy can be divided into three major distinct types in mammalian cells: macroautophagy, microautophagy, and chaperone-mediated autophagy (CMA) **(Figure I.7)**.

Macroautophagy involves the sequestration of a complete region of the cytosol, including whole organelles, by a double-membrane vesicle known as the autophagosome. The latter acquires the enzymes required for the degradation of its content after fusion with a lysosome. Macroautophagy is activated in response to nutrient deprivation, where degradation of intracellular components by this pathway provides cells with the amino acids no longer obtained by the diet, but required for the synthesis of proteins essential for survival (Mizushima et al., 2004). Physical and chemical stressors, as well as infectious agents, have also been shown to activate macroautophagy (Levine and Klionsky, 2004). Activation of autophagy under these conditions is aimed at the removal of the aggressor itself (i.e., invading microorganisms) or of the intracellular components that were damaged during exposure to stress. However, some level of basal macroautophagy is detected in almost all cells, and this basal activity plays an important role in the continuous turnover of organelles and clearance of misfolded and damaged proteins (Komatsu et al., 2005; Hara et al., 2006; Komatsu et al., 2006).

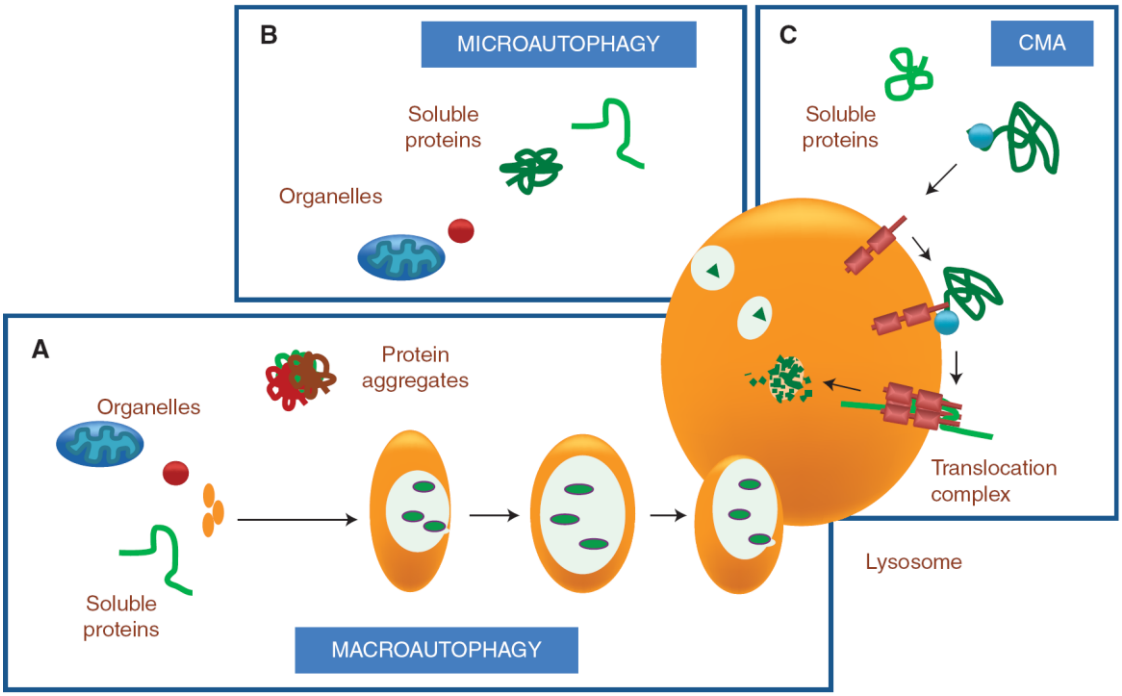

Figure I.7. Autophagic pathways.

Cytosolic proteins can reach the lysosomal lumen for degradation via autophagy through three different mechanisms. **A.** In macroautophagy, a whole region of the cytosol is sequestered into a double membrane vesicle that fuses with lysosomes for cargo delivery. **B.** In microautophagy, the lysosomal membrane invaginates to trap regions of the cytosol that are internalized into the lysosomal lumen as single membrane vesicles. **C**. In chaperone-mediated autophagy (CMA), a targeting motif in the substrate proteins is recognized by a cytosolic chaperone that delivers it to the surface of the lysosome. Once there, the substrate protein binds to a lysosomal receptor that multimerizes to form a translocation complex. A luminal chaperone mediates the translocation of the substrate protein into the lumen where it is rapidly degraded [Adapted from (Wong and Cuervo, 2010)].

Microautophagy is somewhat similar to macroautophagy, but in this case the lysosomal membrane invaginates or generates protrusions and tubulations to sequester the cytosolic content “in bulk.” Microautophagy is a constitutively active pathway that contributes to the continuous, slow turnover of cytosolic proteins (Mortimore et al., 1988).

In contrast to “in bulk” degradation, cytosolic proteins can also be transported one-by-one into lysosomes for degradation by CMA. The intrinsic selectivity associated with this pathway permits the removal of damaged proteins without affecting normal proteins in the vicinity. Through CMA just cystosolic proteins containing the pentapeptide targeting motif KFERQ (Dice, 1990) are selectively recognized by a chaperone complex in the cytosol, including the heat shock cognate (HSC70) and its associated co-

chaperones (Chiang et al., 1989). This complex is targeted to the lysosome-associated membrane protein type 2A (LAMP-2A), the lysosomal receptor for this pathway (Cuervo and Dice, 1996). After unfolding, substrate proteins cross the lysosomal membrane and are assisted by a luminal chaperone (Lys-hsc70) to be degraded within the lysosomal lumen. Although some level of basal CMA activity is detectable in almost all cell types, this pathway is maximally activated under conditions of stress. Stressors known to activate this pathway include prolonged starvation, mild oxidative stress, and exposure to toxic compounds that alter the conformation of particular proteins (Massey et al., 2004).

Among the three main types of autophagy, macroautophagy is the best characterized process and will henceforth be referred to as autophagy.

1.4.1 Molecular orchestration of autophagy

1.4.1.1 Autophagy-related proteins: the basic core machinery

The molecular understanding of autophagy was initiated by the pioneering work in yeast utilizing genetic screenings that led to the discovery of more than 30 autophagy-related (Atg) genes, followed by the identification of homologs in mammals (Noda et al., 2002; Nakatogawa et al., 2009). Although autophagy occurs at basal levels in all cells, basal-level autophagy is very low under normal conditions, therefore an efficient mechanism of induction is crucial for organisms to adapt to stress and extracellular signals (He and Klionsky, 2009).

A central negative regulator of autophagy is the serine/threonine protein kinase mTOR (mammalian target of rapamycin) (Kamada et al., 2004; Neufeld, 2010). mTOR integrates input information from multiple upstream signal transduction pathways and negatively regulates other downstream serine/threonine kinases. Thus, under nutrient-rich conditions, mTOR inhibits autophagy through phosphorylation and inactivation of key targets, the Unc-51-like kinase 1 (ULK1) and -2 (ULK2) (Atg1 in yeast), mammalian Atg13 (mAtg13), and the focal adhesion kinase family-interacting protein of 200 kD (FIP200, Atg17 in yeast), which seem to form a stable complex regardless of nutritional conditions in mammalian cells (Kamada et al., 2000; He and Klionsky, 2009; Hosokawa et al., 2009). In contrast, upon mTOR inhibition by starvation or rapamycin, ULK1 and ULK2 undergo autophosphorylation that is conducive to a conformational change essential for their activation (Chan et al., 2009b), and further phosphorylate mAtg13 and FIP200, forming a complex essential for autophagy activity (Hosokawa et al., 2009; Jung et al., 2009) **(Figure I.8)**.

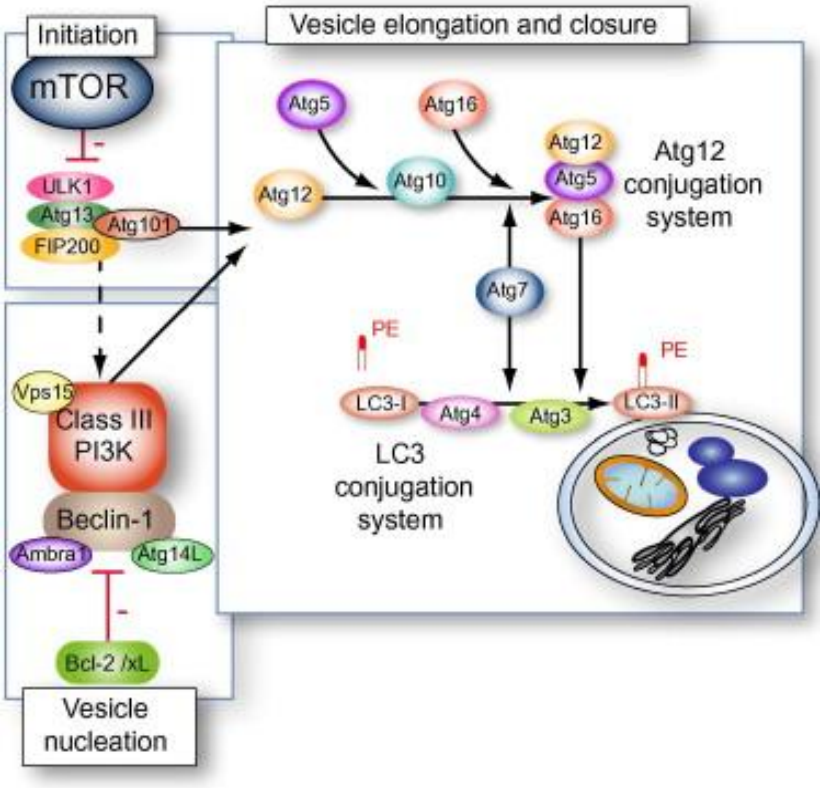

Figure I.8. Basic molecular machinery of autophagy.

There are at least three steps in the formation of autophagosomes: initiation, nucleation, and elongation/closure. Autophagy is initiated by the ULK1 complex. This complex is formed by ULK1 Ser/Thr protein kinase, Atg13, and FIP200. Among the initial steps of vesicle nucleation is the activation of the phosphatidylinositol 3-kinase class III (Vps34) to generate phosphatidylinositol 3-phosphate (PtdIns(3)P). This activation depends on the formation of a multiprotein complex that includes Beclin-1, p150 (Vps15), mAtg14 (Atg14-like protein), and Ambra1. Beclin-1 constitutively interacts with Bcl-2 or its close homolog Bcl-XL and autophagy induction requires the dissociation of Beclin-1 from its inhibitors Bcl-2 or Bcl-XL. The membrane formed elongates and closes on itself to form an autophagosome. Two conjugation systems are successively involved. The first involves the covalent conjugation of Atg12 to Atg5, with the help of Atg7 and Atg10. This conjugate is organized into a complex by associating with Atg16 to form the Atg16–Atg5–Atg12 complex. The second involves the conjugation of phosphatidylethanolamine (PE) to LC3 by the sequential action of the Atg4, Atg7, and Atg3. This lipid conjugation leads to the conversion of the soluble form of LC3 (named LC3-I) to the autophagic vesicle-associated form (LC3-II), allowing for the closure of the autophagic vacuole. *Abbreviations:* Ambra1, activating molecule in Beclin-1-regulated autophagy; Atg, autophagy genes; Bcl, B-cell leukemia/lymphoma; FIP200, 200-kDa focal adhesion kinase family-interacting protein; LC3, microtubule-associated protein light chain 3; mTOR, mammalian target of rapamycin; PI3K, phosphatidylinositol 3-kinase; ULK1, uncoordinated 51-like kinase 1; Vps, vacuolar protein sorting. [Adapted from (Rautou et al., 2010)].

In addition, the activation of autophagy in response to starvation requires the dissociation of Beclin-1 (Atg6 in yeast) from its binding partner Bcl-2 in the cytosol (Wei et al., 2008). Beclin is then free to complex with the phosphatidylinositol 3-kinase class III (Vps34 in yeast), p150 (Vps15 in yeast) and mAtg14 (Atg14 in yeast) to form the active class III phosphatidylinositol 3-kinase (PtdIns3K) complex (Backer, 2008; Itakura et al., 2008). The lipid kinase activity of the class III PtdIns3K produces phosphatidylinositol 3-phosphate (PtdIns(3)P) and is involved in the targeting of a number of Atg proteins essential to generate the nucleation complex or the phagophore (in yeast), which gives rise to the pre-autophagosomal membrane. Various sources, including the ER, mitochondria, the plasma membrane, and the Golgi complex have been proposed to be the origins of the autophagosomal membrane (Arstila and Trump, 1968; Geng et al., 2010; Hailey et al., 2010; Ravikumar et al., 2010; Bodemann et al., 2011). The PtdIns3K complex, in part together with the above Atg proteins, further recruits two interrelated ubiquitin-like (Ubl) conjugation systems, the mAtg12–Atg5-Atg16 and the light chain-3 (LC3, Atg8 in yeast), to the autophagosomal membrane (Suzuki et al., 2007; Geng and Klionsky, 2008; Sou et al., 2008), which play an essential role in regulating the membrane elongation and expansion of the forming autophagosome. Then, both Atg12 and LC3 undergo conjugation and are activated by the ubiquitin E1-like ligase, mAtg7. In addition, the shuttling and self-multimerization of mAtg9, the only identified integral membrane protein required for autophagosome formation, to the site of autophagosome formation facilitates membranes supply for the elongation of the limiting membrane (Mari et al., 2010). When autophagosome formation is completed, LC3 attached to the outer membrane is cleaved from phosphatidylethanolamine (PE) by Atg4 and released back to the cytosol (Kirisako et al., 2000). The mechanism of autophagosome formation is such that the sequestering membrane can accommodate basically any sized cargo. After fusion, degradation of the inner vesicle components and cargo is dependent on a series of lysosomal acid hydrolases, including cathepsins B, D, and L (Tanida et al., 2005). The resulting small molecules from the degradation, particularly amino acids, are transported back by permeases to the cytosol for *de novo* protein synthesis and maintenance of cellular functions under starvation conditions.

1.4.1.2 Microtubule network: a crucial component required for autophagy

Besides the aforementioned Atg proteins, certain subcellular systems, including the MT network, may also carry out essential functions during autophagy, such as facilitating autophagosome transport and enabling clearance of autophagic substrates.

Within neurons, autophagosomes are actively formed in synapses and along neurites but the proper clearance of these compartments involve their retrograde transport towards the neuronal cell body, where lysosomes are concentrated. Several lines of evidence suggest that, in mammals, autophagosomes associate with MT tracks, move towards the microtubule-organizing centre (MTOC), and fuse with endosomes or lysosomes, and the dynamic process is driven by the dynein motors. Indeed, pioneering studies demonstrated that autophagic flow is MT-dependent since disruption of MT network using agents such as nocodazole and vinblastine, which interfere with MT polymerization, blocks fusion of autophagosomes with endosomes and lysosomes (Aplin et al., 1992; Seglen et al., 1996; Webb et al., 2004). Also, disruption of the MT network results in a decreased clearance of autophagy substrates (Ravikumar et al., 2005). However, a number of more recent studies revealed that, in mammalian cells, compromised functional integrity of MTs provoke a delay in autophagy rather than a complete block in this process (Fass et al., 2006; Kochl et al., 2006). In addition, it was shown that knockdown of dynein leads to similar effects (Jahreiss et al., 2008) corroborating that dyneins are the key motor proteins that mediate the transport of autophagosomes along MTs towards lysosomes (Kimura et al., 2008).

In addition, proteins associated to familial forms of PD, such as α-synuclein, LRRK2, PINK1 or Parkin have been reported to interact with, and potentially impair MT-mediated trafficking (Schon and Przedborski, 2011). In fact, misfolded and aggregated proteins are also transported to, and deposited in the pericentriolar region via the MT system (Johnston et al., 1998; Kopito, 2000). These MT dependent deposits of aggregates are called aggresomes and may explain the biogenesis of the LBs found in PD. Therefore, impairment of MT system is being increasingly associated with abnormal accumulation of α-synuclein (Lee et al., 2006). Although the mechanism whereby α-synuclein accumulates in LBs is not fully understood, evidence suggests that defective axonal transport of α-synuclein itself may contribute to the process. Mutant forms of α-synuclein but not wild-type were found to exhibit reduced axonal transport in transfected cultured neurons (Saha et al., 2004). Further evidence revealed that overexpression of α-synuclein causes disruption of MT network and impairment of MT-dependent trafficking (Lee et al., 2006). In addition, Kim *et al.* demonstrated that exposing yeast cells to a MT assembly inhibitor or by deleting genes involved in MT biogenesis, α-synuclein

aggregation and toxicity increases, suggesting that tubulin can stimulate α-synuclein fibrillization in yeast (Kim et al., 2008a). Therefore, there are two possible mechanisms underlying the crosstalk between α-synuclein and MT function and, interestingly, they seem to be not exclusive from each other. Consistent with this observation, wild-type α-synuclein has also been considered a functional MT-associated protein able to induce the polymerization of purified tubulin into MTs whereas mutant forms of α-synuclein lose this potential (Alim et al., 2002; Alim et al., 2004).

With long axons and elaborated dendrites, neurons require a more coordinated and widespread regulation of the MT network and membrane trafficking system. Potentially important mechanisms for controlling MT dynamics are the post-translational modifications of tubulin subunits. Acetylation is the major post-translational modification of α-tubulin and occurs on Lys40 (L'Hernault and Rosenbaum, 1985; LeDizet and Piperno, 1987; Edde et al., 1991) which, according to structural data, is localized to the luminal face of the microtubule (Nogales, 1999; Draberova et al., 2000). The acetylation of α-tubulin could regulate the presence of MTs in specific intracellular spaces by selective stabilization, promoting the scafold indispensable for an efficient mobilization of cargos within neurons. Indeed, α-tubulin acetylation results from dynamic processes targeting a MT subset that may restrict to stable MTs (Webster and Borisy, 1989) in most cell types, but that may also extend to the whole MT network (Belmadani et al., 2004). Like other post-translational modifications of α-tubulin, the level of acetylation is regulated by the balance of tubulin acetyltransferase and tubulin deacetylase activities (Laurent and Fleury, 1996). As acetylation of tubulin most often compartmentalizes on the stable MT subset, it was widely accepted that deacetylases would act preferentially on soluble tubulin and that acetylases operate on stable polymers.

Although α-tubulin acetylation was firstly described more than 25 years ago, the enzymes that control α-tubulin deacetylation and acetylation were identified only in the past decade. The first discovery came from the finding that histone deacetylase 6 (HDAC6), a member of the class II histone deacetylases, which is mainly cytoplasmic (Bertos et al., 2004), associates with MTs and deacetylates α-tubulin both in vitro on preassembled MTs and in cells (Hubbert et al., 2002; Matsuyama et al., 2002; Zhang et al., 2003) Interestingly, and in contrast with the “classical” view of α-tubulin post-translational modifications, HDAC6 does not deacetylate soluble tubulin dimers in vitro (Hubbert et al., 2002). HDAC6 was also found to deacetylate Hsp90, a chaperone that was known for a long time to associate with MTs (Redmond et al., 1989; Bali et al., 2005) and with soluble tubulin (Garnier et al., 1998), and was recently described to bind MTs in a tubulin acetylation-dependent manner (Giustiniani et al., 2009). The links between HDAC6 and the cytoskeleton also extend to actin microfilaments as HDAC6

binds to and deacetylates cortactin (Zhang et al., 2007; Lee et al., 2010b; Lee and Yao, 2010). Its deacetylation has an impact on actin dynamics by enhancing the interaction of cortactin and F-actin thus leading to an increased actin polymerization (Zhang et al., 2007). Therefore, HDAC6 is seen as a cytoplasmic regulator of cell motility and protein transport.

A recently emerging aspect is the direct involvement of HDAC6 in autophagy progression and clearance, which is of great interest for revealing disease mechanisms in neurodegeneration. HDAC6 facilitates the MT and dynein motor-based transport of ubiquitinated proteins to aggresomes (Kawaguchi et al., 2003; Pandey et al., 2007). A central role for HDAC6 for misfolded protein clearance is further supported by the recent study of Lee *et al.*, which shed some light on the question how HDAC6 is linked to autophagic clearance mechanistically, and described the fusion of the autophagosome with the lysosome as a HDAC6-dependent step in autophagy, depending on the HDAC6 substrate cortactin and assembly of the actin network (Lee et al., 2010b). In addition, the crucial role of HDAC6 in manageing cytotoxic protein overload was also demonstrated in a *Drosophila* model where ectopic expression of HDAC6 could rescue proteasome impairment as well as a neurodegenerative phenotype in an autophagy-dependent manner (Pandey et al., 2007). The role of HDAC6 in the degradation of protein aggregates suggests its involvement in the formation of LBs in PD. In fact, HDAC6 was found to colocalize with α-synuclein and ubiquitin in brain sections of PD patients, demonstrating that HDAC6 is also a component of LBs (Kawaguchi et al., 2003). In cell culture, the association of HDAC6 with polyubiquitinated mutant DJ-1, a protein involved in an early onset form of PD, promoted the formation of aggresomes containing DJ-1 upon proteasome inhibition (Olzmann et al., 2007). This study further demonstrates that HDAC6 preferentially binds K63-linked polyubiquitinated DJ-1 in vivo. DJ-1 ubiquitination recruits HDAC6, which facilitates the transport of DJ-1 to the MTOC, forming the inclusion body. This observation suggests that K63-linked polyubiquitination of DJ-1 may act as a novel signal for the dynein-mediated transport and sequestration of misfolded proteins in the aggresome. Moreover Parkin, an ubiquitin E3 ligase (often mutated in PD), tightly binds to HDAC6 and is also transported by HDAC6 in a MT motor-dependent manner to the forming aggresome. There may be ongoing Parkin-mediated ubiquitination of misfolded proteins during transport along the MTs (Jiang et al., 2008).

The second tubulin deacetylase that was identified is the sirtuin SIRT2, a class III histone deacetylase which depends on NAD^+ as a cofactor (North et al., 2003). Like HDAC6, it mainly resides in the cytoplasm as a result of an active nuclear exportation mechanism (North and Verdin, 2007). In contrast to HDAC6, it may use both soluble and polymerized tubulin as substrates (North et al., 2003). HDAC6 and SIRT2 do not only

share tubulin as a common substrate but they were found to interact in a complex that also comprises α-tubulin (Nahhas et al., 2007). Like HDAC6 does, SIRT2 may also deacetylate non-tubulin substrates like the transcription factors FOXO1(Jing et al., 2007; Wang and Tong, 2009) and p53 (an activity that also requires SIRT1) (Peck et al., 2010) or it may control the self-acetylation of the histone acetylase p300 that functions as a broad coactivator in regulating gene expression (Black et al., 2008). Conversely, p300 may also acetylate SIRT2 to down-regulate its enzyme activity (Han et al., 2008).

Relevant to PD, inhibition of SIRT2 prevented α-synuclein cytotoxicity and modulated its aggregation in cultured cells; ameliorated mutant α-synuclein neurotoxicity in rat primary dopamine-positive neurons and rescued degeneration of dopaminergic neurons from α-synuclein toxicity in a *Drosophila* animal PD model (Outeiro et al., 2007). However, the mechanisms by which SIRT2 inhibition protects neurons from cell death remain uncertain. In addition, it was demonstrated that SIRT2-mediated tubulin deacetylation abolished degeneration resistance in the Wallerian mouse model subjected to axonal injury induced by MT depolymerizing drugs, suggesting that tubulin deacetylation promotes axonal MT destabilization (Suzuki and Koike, 2007).

1.4.2 Selective autophagy and protein turnover

Although autophagy had been primarily considered a nonselective degradative pathway induced by starvation, constitutive basal autophagic activity has now emerged as a main QC process that selectively dispose aberrant protein aggregates and damaged organelles for degradation (Lee et al., 2010b; Lee et al., 2010a). In fact, several autophagy selective processes have been described in recent years based on the nature of the cargo degraded by each of them: mitophagy (autophagy of mitochondria), pexophagy (autophagy of peroxisomes), lipophagy (autophagy of lipid droplets), and aggregophagy (autophagy of aggregates). A specific subset of proteins, known as cargo-recognition proteins, is involved in each of these subtypes of autophagy, concurring for their selectivity (Klionsky et al., 2003; Yang and Klionsky, 2010). All of these proteins, including among others p62, the neighbor of Brca1 gene (NBR1) and NIX, contain a region that binds to components of the autophagic system (LC3) and a second region that recognizes specific tags in the cargo (Lamark et al., 2009). In addition, ubiquitin can target organelles such as mitochondria, peroxisomes and protein aggregates for autophagic degradation (Bjorkoy et al., 2005; Kim et al., 2008b), making autophagy an alternative mechanism to degrade superfluous material that cannot be processed by the proteasome. Thus, it is not surprising that malfunction of autophagy could contribute to neurodegeneration associated to PD as efficient sequestration and clearance of

unneeded or damaged cellular or nonself components is crucial for cell survival and function.

The most compelling evidence supporting a significant role for autophagy dysfunction in PD came from the demonstration that α-synuclein is degraded either by macroautophagy and CMA (Webb et al., 2003; Cuervo et al., 2004; Vogiatzi et al., 2008; Xilouri et al., 2009). Actually, although α-synuclein can be degraded by the UPS, it also contains the KFERQ targeting motif that mediates its degradation through CMA (Webb et al., 2003; Cuervo et al., 2004). However, A53T and A30P α-synuclein mutants, that cause autosomal dominant PD, are unsuccessfully degraded by CMA because they cannot be internalized into lysosomes, despite their higher binding affinity to the lysosomal receptor LAMP-2A compared with wild type α-synuclein (Cuervo et al., 2004). In addition, due to their tight binding to the lysosomal receptor, α-synuclein mutants often end up clogging the CMA translocation system and inhibit their own degradation and that of other CMA substrates, leading to a “wide-range” CMA blockage (Cuervo et al., 2004). Inhibition of CMA by α-synuclein mutants is accompanied by a compensatory activation of macroautophagy that could help alleviate that conditions (Wong and Cuervo, 2010), although the physiological significance of this event is not completely understood. In addition to the rare α-synuclein mutations, phosphorylated, ubiquitinated, nitrated and oxidized forms of α-synuclein impair, to some extent, further degradation of α-synuclein by CMA, but not degradation of other substrates (Cuervo et al., 2004; Engelender, 2008). However, modification of the protein via a noncovalent interaction with oxidized dopamine gives a phenotype that more closely resembles the point mutations (Maguire-Zeiss et al., 2005; Norris et al., 2005). Dopamine-modified α-synuclein is not only poorly degraded by CMA, but also blocks degradation of other substrates, thereby increasing cellular vulnerability to stressors (Martinez-Vicente et al., 2008). This is especially relevant because oxidized metabolites of dopamine such as dopamine quinone derivatives are thought to play a critical role in the preferential loss of dopaminergic neurons in PD (Martinez-Vicente et al., 2008). The blockage of CMA activity with mutant forms of α-synuclein not only results in the direct buildup of toxicity in the neuron through the formation of aggregates, but it also prevents the protective activity of the protein myocyte enhancer factor 2D (MEF2D), a transcription factor required for neuronal survival, and CMA substrate (Yang et al., 2009). Interestingly, it was demonstrated that both wild-type and A53T mutant α-synuclein interfere with the binding of MEF2D to the chaperone HSC70 in the CMA degradation machinery. Consistent with this observation, the cytoplasmic pool of MEF2D is increased in A53T α-synuclein transgenic mice and in postmortem brain tissue from PD patients (Smith et al., 2006), and a similar increase of inactive MEF2D in the cytoplasm has been found in neurons upon inhibition of CMA

(Yang et al., 2009). These findings rise up two interesting possibilities: (1) α-synuclein promotes neuronal cell death through the formation of aggregates, but also by the inhibition of cell survival proteins; (2) compromised neuronal viability observed in PD results, at least in part, from CMA dysfunction.

As abovementioned, inhibition of CMA by aberrant α-synuclein leads to an increase in autophagy. This appears to be a compensatory response, but rather than leading to cell survival, the induction of autophagy can be detrimental causing autophagic cell death. For example, alterations in macroautophagy have been associated with wild-type α-synuclein accumulation, suggesting that this lysosomal pathway is also involved in normal α-synuclein turnover (Vogiatzi et al., 2008). Nevertheless, blocking autophagy by knocking down the autophagy protein Atg5 in cells expressing the A53T a-synuclein mutant can rescue the cell from toxicity-induced cell death (Xilouri et al., 2009). More recently, it was also demonstrated that α-synuclein overexpression not only impairs CMA but also macroautophagy through RAB1A and omegasome formation as observed in both cell and mouse models (Winslow et al., 2010). α-Synuclein blocks autophagy by inhibiting the activity of RAB1A, a GTPase involved in the early secretory pathway, specifically in the ER-to-Golgi transport. These data show an Atg9 mislocalization and consequent inhibition of autophagosome formation (Winslow et al., 2010).

1.4.3 Mitophagy: the autophagic mitochondria removal

The role of autophagy dysfunction in PD is not restricted to the removal of cytosolic PD-related or other damaged proteins but also involve removal of dysfunctional organelles, such as mitochondria. Accumulating data suggests that mitochondrial dysfunction by itself triggers mitophagy. Changes in the MPT that result in loss of mitochondria membrane potential were initially found to be a selective marker for mitochondria degradation (Lemasters et al., 1998; Kim et al., 2007). More recently, a predicted mitochondrial targeting signal (MTS) was identified in the N-terminus of PINK1 after mitochondria depolarization (Jin et al., 2010), which can determine the selective recruitment and the binding of cytosolic proteins to the surface of the dysfunctional mitochondria (Narendra et al., 2008; Narendra et al., 2010). Additionally, other studies have also revealed the involvement of α-synuclein, Parkin, PINK1 and LRRK2 in the regulation of mitochondrial degradation and homeostasis. Overexpression of α-synuclein, Parkin and PINK1 results in enhanced mitochondrial fragmentation, followed by activation of mitophagy (Kamp et al., 2010; Kawajiri et al., 2010; Vives-Bauza et al., 2010), supporting an essential role of autophagy in the clearance of defective

mitochondria in PD. In cells expressing the A53T α-synuclein mutant, an increased colocalization of autophagosomes with normal and polarized mitochondria occurs. In addition, there is a decrease in the number and length of mitochondria in these cells (Choubey et al., 2011). The increase in mitochondria clearance in these cell lines is dependent on mitochondrial fragmentation and on the protein Parkin. Parkin is selectively recruited to dysfunctional mitochondria with low membrane potential in mammalian cells (Narendra et al., 2008) and relies on the expression of wild-type PINK1, but not PD related PINK1 mutants, due to a decreased physical binding of PINK1 to Parkin (Geisler et al., 2010b). This occurs via phosphorylation-dependent regulation of Parkin (Sha et al., 2010), suggesting a pathogenic role of PINK1 and Parkin loss-of-function mutations in PD. Once in mitochondria, Parkin activates the UPS, that will mediate the ubiquitination of VDAC-1 (Geisler et al., 2010a), mitofusins Mfn1 and Mfn2, among other mitochondrial proteins (Gegg et al., 2010), and serve to recruit the ubiquitin-binding histone deacetylase HDAC6 and p62, which assemble the autophagic machinery (LC3) for efficient degradation of impaired mitochondria (Geisler et al., 2010a; Chan et al., 2011). In addition, Parkin was recently shown to interact with Ambra 1, an autophagy/Beclin-1 regulator, that critically determines the final step of Parkin-mediated mitochondrial clearance (Van Humbeeck et al., 2011)

The role of LRRK2 in regulating autophagy was also addressed. Interestingly, it was demontrated that LRRK2 specifically localizes to specific membrane subdomains and endosomal-autophagic structures, suggesting a functional relationship between LRRK2 and mitophagy (Alegre-Abarrategui et al., 2009). Furthermore, increased autophagic activity upon LRRK2 knockdown was observed, which indicates that LRRK2 may normally act as a negative regulator of autophagy (Alegre-Abarrategui et al., 2009). Alternatively, LRRK2 regulation in neurite blunting and remodeling requires autophagy (Plowey et al., 2008). Thus, by impairing this pathway, mutations in parkin, PINK1, and LRRK2 may alter autophagy-dependent mitochondrial turnover which, in turn, may cause the accumulation of defective mitochondria and, ultimately, neurodegeneration in PD.

1.5 Aims and thesis outline

Understanding the molecular basis of sPD has proven to be a major challenge in the field of neurodegenerative diseases. Although several hypotheses have been proposed to explain the molecular mechanisms underlying the pathogenesis of sPD, growing evidence has highlighted the role of mitochondrial dysfunction and the disruption of mechanisms which rely on mitochondrial bioenergetics in sPD. But the role of mitochondria in sPD extends beyond defective mitochondrial respiratory chain and may involve mitochondrial dynamics, intracellular trafficking, protein quality control, or redox homeostasis.

Data from human genetics and studies in model organisms, as well as from biochemical and biophysical characterization of the proteins involved in PD, have demonstrated that most cases of PD can be considered as arising from protein misfolding, protein aggregation, or defective degradation and clearance, and that proteostasis network pathways are also altered in sPD. However, it remains an open question whether alterations of these pathways lead to different aspects of PD or whether they converge at a point that is the common denominator of sPD pathogenesis. In addition, clear insights of exactly how and when mitochondria and proteostasis network pathways interconnect, overlap or converge to produce nigral neuronal degeneration will be crucial to understanding the pathogenesis of sPD.

In this work, we aim to address the potential implications of an altered structural and functional crosstalk between mitochondria and the ER, two important metabolic organelles for the maintenance of cellular protein homeostasis. In addition, we will assess the role of mitochondrial metabolism in the regulation of the autophagy-lysosomal pathway, a major cellular homeostatic process essential for bulk and/or selective degradation of cytoplasmic contents.

The data obtained will be presented according with the following specific aims:

- Address the molecular mechanism underlying the interplay between mitochondria and ER dysfunctions under particular stressfull conditions of sPD;

- Investigate whether the modulation of ER-mitocondria interaction, as well as the Ca^{2+} shuttling between ER and mitochondria, has repercursions to the intracellular homeostasis and consequently to lowering the cell's threshold to survival;

- Establish a molecular framework between deregulation of the autophagy pathway observed in PD patients brains and mitochondrial dysfunction;

- Explore the hypothesis that dysfunctional mitochondria lead to impaired vesicular trafficking and protein turnover;

- Unravel the mechanistic link between mitochondria-, autophagy-, and microtubule network dysfunctions.

CHAPTER II

Materials & Methods

2.1 Materials

2.1.1 Chemicals and cell media

The most common chemicals and media used were as categorized in the Table II.1.

Table II.1 Chemicals and cell media, with the corresponding company.

CHEMICAL	COMPANY
Antibodies	
Alexa Fluor® 488-conjugated goat anti-rabbit	Molecular Probes (Eugene, OR, USA)
Alexa Fluor® 594-conjugated goat anti-mouse	Molecular Probes (Eugene, OR, USA)
Goat alkaline phosphatase-conjugated anti-mouse	GE Healthcare (Buckinghamshire, UK)
Goat alkaline phosphatase-conjugated anti-rabbit	GE Healthcare (Buckinghamshire, UK)
Mouse mAb* anti-Beclin	BD Biosciences (San Diego, CA, USA)
Mouse mAb anti-BiP/GRP78	BD Biosciences (San Diego, CA, USA)
Mouse mAb anti-class III β -tubulin (clone TU-20)	Cell Signaling (Danvers, MA, USA)
Mouse mAb anti-class III β-tubulin (clone TUJ)	Covance Inc. (Princeton, NJ, USA)
Mouse mAb anti-GAPDH	AbCam (Cambridge, UK)
Mouse mAb anti-Hsp60	Millipore (Billerica, MA, USA)
Mouse mAb anti-LAMP-1 (clone H4A3)	Developmental Studies Hybridoma Bank (University of Iowa, Iowa, USA)
Mouse mAb anti-MAP2	Sigma-Aldrich Co. (St. Louis, MO, USA)
Mouse mAb anti-TATA binding protein TBP	AbCam (Cambridge, UK)
Mouse mAb anti-α-synuclein (clone LB509)	Invitrogen Corporation (Camarillo, CA, USA).
Rabbit mAb anti-LC3B (D11) XP®	Cell Signaling (Danvers, MA, USA)
Rabbit mAb anti-α-tubulin (clone 11H10)	Cell Signaling (Danvers, MA, USA)
Rabbit pAb* anti-Bcl-2	Cell Signaling (Danvers, MA, USA)
Rabbit pAb anti-Beclin	Cell Signaling (Danvers, MA, USA)
Rabbit pAb anti-COX IV	Cell Signaling (Danvers, MA, USA)
Rabbit pAb anti-LC3B	Cell Signaling (Danvers, MA, USA)

Rabbit pAb anti-NDUFA2	Generous gift of Dr. Leo Nijtmans (Radboud University Nijmegen Medical Center, The Netherlands)
Rabbit pAb anti-SIRT2	Cell Signaling (Danvers, MA, USA)
Rabbit pAb anti-SQSTM1/p62	Cell Signaling (Danvers, MA, USA)
Rabbit pAb anti-TOM20	Santa Cruz Biotechnology (Santa Cruz, CA, USA)
Rabbit pAb anti-VDAC/Porin	AbCam (Cambridge, UK)
Rabbit pAb anti-Vimentin	Cell Signaling (Danvers, MA, USA)

Cell culture chemicals and media	
5-fluoro-2'-deoxyuridine (FUdR)	Sigma-Aldrich Co. (St. Louis, MO, USA)
all-trans retinoic acid (ATRA)	Sigma-Aldrich Co. (St. Louis, MO, USA)
B-27 supplement	Gibco™, Invitrogen Corporation (Camarillo, CA, USA).
Bovine serum albumin (BSA) fatty acid free	Sigma-Aldrich Co. (St. Louis, MO, USA)
Cytosine β-D-arabinofuranoside (araC)	Sigma-Aldrich Co. (St. Louis, MO, USA)
Deoxyribonuclease I (DNAse I)	Sigma-Aldrich Co. (St. Louis, MO, USA)
Dialyzed fetal bovine serum (FBS)	Gibco™, Invitrogen Corporation (Camarillo, CA, USA).
Dulbecco's Modified Eagle (DMEM) Medium	Gibco™, Invitrogen Corporation (Camarillo, CA, USA).
L-glutamine	Sigma-Aldrich Co. (St. Louis, MO, USA)
Minimum Essential Medium (S-MEM)	Gibco™, BRL, Life Technologies (Scotland, UK)
Neurobasal medium	Gibco™, Invitrogen Corporation (Camarillo, CA, USA).
Non-dialyzed FBS	Gibco™, Invitrogen Corporation (Camarillo, CA, USA).
Opti-MEM® I Reduced Serum Medium	Gibco™, BRL, Life Technologies (Scotland, UK)
Penicillin	Gibco™, Invitrogen Corporation (Camarillo, CA, USA).
Poli-D-lysine,	Sigma-Aldrich Co. (St. Louis, MO, USA)
Poli-L-lysine	Sigma-Aldrich Co. (St. Louis, MO, USA)
Polyethylene glycol 1000 (PEG 1000)	Merck (Darmstadt, Germany)
Sodium pyruvate solution	Sigma-Aldrich Co. (St. Louis, MO, USA)
Streptomycin	Gibco™, Invitrogen Corporation (Camarillo, CA, USA).

Trypsin/Ethylenediamine tetraacetic acid (EDTA) solution	Sigma-Aldrich Co. (St. Louis, MO, USA)
Uridine (Urd)	Sigma-Aldrich Co. (St. Louis, MO, USA)
Enzyme inhibitors	
3-Methyladenine (3-MA)	Sigma-Aldrich Co. (St. Louis, MO, USA)
AK-1	Sigma-Aldrich Co. (St. Louis, MO, USA)
Chymostatin	Sigma-Aldrich Co. (St. Louis, MO, USA)
Leupeptin	Sigma-Aldrich Co. (St. Louis, MO, USA)
Pepstatin A	Sigma-Aldrich Co. (St. Louis, MO, USA)
Phenylmethylsulfonyl fluoride (PMSF)	Sigma-Aldrich Co. (St. Louis, MO, USA)
Rapamycin	Sigma-Aldrich Co. (St. Louis, MO, USA)
Trypsin inhibitor type-II soybean	Sigma-Aldrich Co. (St. Louis, MO, USA)
Tubastatin A	BioVision Inc. (Milpitas, CA, USA)
Enzyme substrates	
N-Ac-Asp-Glu-Val-Asp-*p*NA (NAc-DEVD-*p*NA)	Calbiochem, Merck KGaA (Darmstadt, Germany)
N-Ac-Leu-Glu-His-Asp-*p*NA (NAc-LEDH-*p*NA)	Calbiochem, Merck KGaA (Darmstadt, Germany)
N-Ac-Leu-Glu-Val-Asp-*p*NA (NAc-LEVD-*p*NA)	MBL International Corporation (Woburn, MA, USA)
N-Ac-Val-Asp-Val-Ala-Asp-pNA (NAc-VDVAD-*p*NA)	Sigma-Aldrich Co. (St. Louis, MO, USA)
Fluorescent dyes	
Acetoxymethyl ester of Fura-2 (Fura-2, AM)	Molecular Probes®, Invitrogen (Eugene, OR, USA)
Acetoxymethyl ester of Rhod-2 (Rhod-2, AM)	Molecular Probes®, Invitrogen (Eugene, OR, USA)
Hoechst 33342	Molecular Probes®, Invitrogen (Eugene, OR, USA)
Mitotracker Green	Molecular Probes®, Invitrogen (Eugene, OR, USA)
Rhodamine 123	Sigma Chemical Co (St. Louis, MO, USA)
Western blotting purpose	
Enhanced chemifluorescence (ECF) reagent	GE Healthcare (Buckinghamshire, UK)
Hybond™-P PVDF membrane	GE Healthcare (Buckinghamshire, UK)
Immobilon™-P PVDF membrane	Millipore (Billerica, MA, USA)

Low range all blue prestained protein standard	Bio-Rad (Hercules, CA, USA)
Others	
1-methyl-4-phenylpyridinium (MPP^+)	Sigma-Aldrich Co. (St. Louis, MO, USA)
Ammonium chloride (NH_4Cl)	Merck KGaA (Darmstadt, Germany)
Brefeldin	Sigma-Aldrich Co. (St. Louis, MO, USA)
BSA (Fraction V, Low heavy metals)	Calbiochem™, Merck (Darmstadt, Germany)
Calimycin (A23187)	Sigma-Aldrich Co. (St. Louis, MO, USA)
Carbonyl cyanide-p trifluoromethoxyphenylhydrazone (FCCP)	Sigma-Aldrich Co. (St. Louis, MO, USA)
Dantrolene	Sigma-Aldrich Co. (St. Louis, MO, USA)
Dithiothreitol (DTT)	Sigma-Aldrich Co. (St. Louis, MO, USA)
Histopaque – 1077	Sigma-Aldrich Co. (St. Louis, MO, USA)
Nocodazole	Sigma-Aldrich Co. (St. Louis, MO, USA)
Oligomycin	Sigma-Aldrich Co. (St. Louis, MO, USA)
Paclitaxel (Taxol)	Sigma-Aldrich Co. (St. Louis, MO, USA)
Pluronic F-127	Molecular Probes®, Invitrogen (Eugene, OR, USA)
Potassium cyanide (KCN)	Sigma-Aldrich Co. (St. Louis, MO, USA)
Thapsygargin	Sigma-Aldrich Co. (St. Louis, MO, USA)
Tunicamycin	Sigma-Aldrich Co. (St. Louis, MO, USA)
Ubiquinone	Sigma-Aldrich Co. (St. Louis, MO, USA)

**mAb: monoclonal antibody; pAb: polyclonal antibody*

All other chemicals were of the best analytical grade and were purchased from Merck (Darmstadt, Germany) or Sigma-Aldrich Co. (St. Louis, MO, USA).

2.1.2 Biological materials

2.1.2.1 Human subjects' characteristics

Sporadic PD (sPD) patients and healthy individuals were all recruited after approval by the University of Kansas School of Medicine Institutional Review Board. Individuals in the PD group were followed regularly in a tertiary referral movement disorders clinic at the Kansas University Medical Center and met criteria commonly used to diagnose PD in clinical and research settings (Litvan et al., 2003). None of the patients were believed to have alternative diagnoses, degeneration of related systems, drug-induced Parkinsonism, or any other serious medical illness. Enrollment was also contingent on the absence of a diagnosis for another neurodegenerative disease.

The control (CT) subjects were participants of a longitudinal “normal ageing” cohort that is characterized serially by the Brain Ageing Project at the University of Kansas School of Medicine. These CT subjects have not been diagnosed with a neurodegenerative or pre-neurodegenerative disease condition. The age of the PD subjects who participated in this study was 64±12.8 years, and for the CT subjects it was 74.3±5.5 years.

After informed consent was given, sPD (n=9) and age-matched CT (n=5) subjects underwent a 10 ml phlebotomy using tubes containing acid-citrate-dextrose, as an anticoagulant, to provide the platelets needed for cell fusions.

2.1.2.2 Animals

Experiments involving animals were approved by and performed in accordance with the University of Coimbra Institutional Animal Care and Use Committee guidelines and European Community Council Directive for the Care and Use of Laboratory Animals (86/609/ECC).

2.2 Cell Culture

2.2.1 Human Cell Lines Culture

2.2.1.1 Parental Teratocarcinoma (NT2 Rho+) cell line

The NT2 (Ntera2/ clone D1) cells, from a neuronally committed human teratocarcinoma cell line (Pleasure and Lee, 1993; Sodja et al., 2002), were purchased from Stratagene Cloning Systems (La Jolla, CA, USA) and were cultured as described previously (Cardoso et al., 2001). Briefly, cells were grown in 75 cm^2 tissue culture flasks in Opti-MEM® medium (a modification of Eagle's Minimum Essential Medium) supplemented with 10% heat-inactivated fetal bovine serum (FBS), 10,000U/mL penicillin and 10 µg/mL streptomycin. Cells were maintained under a humidified atmosphere of 95% air, 5% CO_2, at 37ºC and and were split by incubating them in 0.05% (v/v) trypsin solution whenever flasks were 80-100% confluent. In early passages, cells were split 1:4; at later passages, cells were split 1:5 or 1:6 because cell growth rate increase at later passages.

2.2.1.2 mtDNA depleted (NT2 Rho0) cell line

The mtDNA-free Rho0 cell-line used for these studies was kindly provided by Dr. RH Swerdlow (University of Kansas School of Medicine, Kansas City, Kansas, USA). This cell line was created in the NT2 cells background by long-term exposure (at least 150 days) to 5 µg/mL ethidium bromide (Sigma-Aldrich Co., St. Louis, MO, USA) in growth medium to deplete selectively mitochondrial DNA (mtDNA) (Swerdlow et al., 1996).

Cells were grown in 75 cm^2 tissue culture flasks in Opti-MEM® medium, supplemented with 10% heat-inactivated FBS, 10,000 U/mL penicillin and 10 µg/mL streptomycin, 150 µg/mL uridine and 200 µg/mL pyruvate. Cells were maintained under a humidified atmosphere of 95% air, 5% CO_2, at 37ºC and and were split by incubating them in 0.05% (v/v) trypsin solution whenever flasks were 80-100% confluent. In early passages, cells were split 1:2; at later passages, cells were split 1:4 because cell growth rate increase at later passages.

2.2.1.3 Generation of transmitochondrial hybrid (cybrids) cell lines

Cybrid approach consists of the transfer of sPD or healthy subjects' platelet mitochondria to mtDNA-depleted recipient cells (Rho0 cells), generating hybrid cell lines (cybrids). Platelets (which contain mtDNA but not nDNA) from PD subjects are known to have reduced complex I activity relatively to control subjects' (Parker et al., 1989). We used platelet mitochondria to generate cybrid cell lines from both sPD and disease-free control subjects. Thus, the resulting cybrid cell lines express the nuclear genes of the recipient Rho0 cell line and the mitochondrial genes of the platelet donor **(Figure II.1)**.

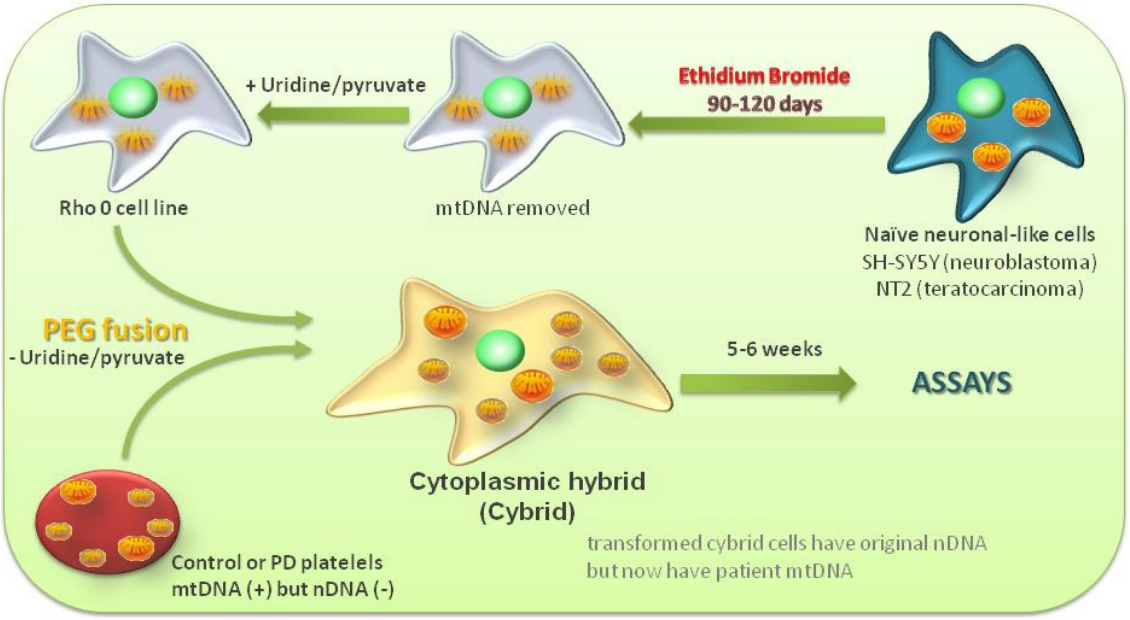

Figure II.1 Generation of cybrid cell lines.

Tumor or immortalized cell lines are grown in the presence of ethidium bromide, which effectively eliminates functional mtDNA to result in a Rho0 cell line. Rho0 cells are then fused with patient platelets, which contain mitochondria but not nuclei. This creates cytoplasmic hybrid (cybrid) cells that can be isolated and expanded. The expanded cybrid cell cultures are biochemically analyzed. Differences in function between cell lines mostly likely arise through differences in their mtDNA.

The preparation and fusion of donor and host cells and selection of repopulated cybrid cell lines was as detailed subsequently:

- ***Isolation of platelets***

Previously, platelets were isolated from the individual blood sample which was drawn aseptically into a tube containing 2.2% citrate, 0.8% citric acid, and 2.45% dextrose. Ten milliliters of blood were separated over three mL of Histopaque-1077-1 in a 12 mL Accuspin^{TM} tube (Sigma-Aldrich Co., St. Louis, MO, USA) by centrifugation at 1000 ×*g* for 10 min, at room temperature. The platelet (top) layer was washed with 15 mL of Minimum Essential Medium (S-MEM). Platelets were counted, then washed again, and resuspended to 1×10^8 cells/mL. Aseptic blood drawing and sample collection were essential to eliminate the propagation of mycoplasma and other organisms.

- ***Fusion***

Fusion of human platelets with NT2 Rho0 cells was facilitated by the presence of dilute polyethylene glycol 1000 (PEG 1000). Autoclaved PEG was melted and mixed 1:1 (w/v) with S-MEM and pH was adjusted to 7.2 with sterile 0.1 N NaOH. Then, one mL of platelets (1×10^8) and one mL Rho0 cells (1.5×10^6) were mixed and allowed to adhere at room temperature for 10 min. The mixture was then centrifuged at 200 ×*g* for 5 min and supernatant was removed. To fuse cells, 150 µL S-MEM-diluted pH 7.2 PEG solution was added to the pellet and allowed to penetrate for 10 s. This mixture was then gently ressuspended 10 times with a wide bore pipet tip until smooth. At 90 s, 12 mL growth medium was added to the pellet and the whole content was transferred to a 75 cm^2 flask. Media were changed at 24 h after cells have adhered to the flask. As a control, "mock fusions", in which NT2 Rho0 cells were not co-incubated with platelets, were performed in parallel with the proper fusions. The resulting cybrids were maintained for one week or until cells were 90% confluent in Rho0 growth medium, that was changed every 2–3 days.

- ***Cybrid selection***

NT2 Rh0 cells lack intact mtDNA, do not possess a functional mitochondrial electron chain, and are auxotrophic for pyruvate and uridine. Maintaining cells in selection medium removes Rh0 cells that have not repopulated their mtDNA with platelet mtDNA.
The cybrid selection process began by substituting Rho0 growth medium (with pyruvate and uridine) for the selection medium (growth medium that lacked pyruvate and uridine and contained dialyzed heat-inactivated serum). After 4 days in selection medium, Rho0 cells that had not fused with platelets began to die. Cybrids were typically split every 5 days. Cells in the mock fusion were always split 1:1 and decreased in numbers over time. Selection was considered complete when the mock fusion flask contained fewer than 20 cells.

After selection was complete, the cybrids were changed to cybrid growth medium. Flasks were maintained in this medium at 37ºC, 5% CO_2 for 24 hours prior to harvesting. Afterward, cybrids were maintained in growth medium under a humidified atmosphere of 95% air, 5% CO_2 at 37ºC and were split by incubating them in 0.05% (v/v) trypsin solution whenever flasks were 80-100% confluent. In early passages, cybrids were split 1:4; at later passages, cells were split 1:6 or 1:8 because cell growth rate increase at later passages.

2.2.1.4 Cybrid cell line neuronal differentiation and culture

Cybrid cell lines with an NT2 background present a commited neuronal precursor stage of differentiation. NT2 precursor cells can be induced by *all-trans* retinoic acid (ATRA) to differentiate *in vitro* into post mitotic central nervous system neurons.

Cybrid cell lines were induced to form process-bearing neuronal cells according to the procedure of Paquet-Durand *et al.* (Paquet-Durand et al., 2003). Cells were allowed to form free floating conglomerates in non-tissue culture plastic, 10 cm diameter dishes in growth medium supplemented with 10 μM ATRA, renewed every 2 days. After 8 days in culture, the conglomerates were seeded in 75 cm^2 cell culture flasks and cultures were kept for 10 days to completely generate a large number of cell aggregates. A single-cell suspension was then derived from the conglomerates by trypsinization and transferred to 175 cm^2 culture flasks. Cells were cultured for 4 days to expand the culture and to further obtain conditioned medium. After that, cells were selectively trypsinized and transferred again to 75 cm^2 culture flasks, where they were kept for 2 weeks to eliminate persistent undifferentiated cells by adding mitotic inhibitors (AraC 1 μM, FudR 10 μM, Urd 10 μM) in the growth medium. Finally, neuron-like cells (1×10^5 per coverslip) were plated onto glass coverslips (16 mm diameter) pre-coated with poly-D-lysine in 50:50 conditioned medium and were allowed to improve neurite outgrowth for 4 days for further immunocytochemical experiments.

The enrichment and purity of neuronal-like cultures was evaluated by comparing the number of cells staining positively with antibodies directed against neuronal marker β-tubulin III (clone TU20), with the number of nuclei stained with Hoechst 33342 dye. The number of β-tubulin III-positive cells and Hoechst 33342-positive nuclei were counted in 10 randomly selected visual fields. This was performed for two independent experiments.

2.2.2 Isolation of human peripheral blood mononuclear cells (PBMCs)

Data obtained using cell lines were corroborated in human PBMCs obtained from control and sPD patients. PBMCs were composed of 90% of lymphocytes and 10% monocytes and in this study were considered as a lymphocytic population.

For this purpose, 20 ml of venous blood from both sPD and disease-free CT subjects were collected by venipuncture in K_2EDTA-containing tubes. PBMCs were isolated by Histopaque-1077 density gradient centrifugation, according to the manufacturer's instruction. Briefly, blood samples were diluted with the same amount of Hanks's balanced salt solution (HBSS), layered on Histopaque-1077-1 and centrifuged

for 30 min at 300 ×*g*, at room temperature. PBMCs were collected from the interface between serum and Histopaque-1077-1 gradients and washed once with HBSS.

2.2.3 Mouse primary cortical neurons isolation and culture

Primary neuronal cultures were prepared as described previously (Agostinho and Oliveira, 2003), with minor modifications. Cerebral cortices were removed from embryonic day 15-16 of Wistar rats and were aseptically dissected and combined in Ca^{2+}- and Mg^{2+}-free Krebs buffer [10 mM HEPES (pH 7.4), 1.2 mM KH_2PO_4, 120 mM NaCl, 4.8 mM KCl, 13 mM glucose] and then incubated in Krebs solution supplemented with 0.3 g/L BSA containing 0.5 g/L trypsin and 0.04 g/L DNase I for 10 min, at 37ºC. Tissue digestion was stopped by the addition of trypsin inhibitor (type II-S; 0.75 g/L) in Krebs buffer containing 0.04 g/L DNase I, followed by a centrifugation at 140 ×*g* for 5 min. After washing the pellet once with Krebs buffer, the cells were dissociated mechanically and resuspended in fresh Neurobasal medium supplemented with 2 mM L-glutamine, 2% (v/v) B-27 supplement, 100,000 U/L penicillin, and 100 mg/L streptomycin. The cells were seeded on poly-L-lysine (0.1 g/L)-coated dishes at a density of 0.75×10^6 cells/mL for Western blotting. For immunofluorescence studies, neurons were mounted on poly-L-lysine-coated glass coverslips at a density of 1.6×10^6 cells/mL. The cultures were maintained in serum-free Neurobasal medium supplemented with B-27 at 37ºC in a humidified atmosphere of 5% CO_2, 95% air for 6 days before treatment, in order to allow neuronal differentiation. After 6 days *in vitro* (6 DIV), cultured neurons were treated with 50 µM MPP^+, 24h before fixation or harvesting. Where indicated, 20 mM ammonium chloride and 20 µM leupeptin, and 10 mM 3-MA or 10 nM rapamycin were added in the culture medium in the last 4 h of MPP^+ treatment. The composition of the cultures was determined by immunolabeling in addition to physiological characterization. The majority of cells (90–95%) were positive for neuronal markers (MAP2, TUJ1), whereas <10% of cells showed immunolabeling for the astrocytic marker glial fibrillary acidic protein (GFAP).

2.3 Evaluation of mitochondrial structure and function

2.3.1 Mitochondrial ultrastructure

Cybrids and Rho0 cells were grown in 75 cm^2 culture flasks till 90% confluence and growth medium was changed 1–3 h before harvesting. Then cellular suspensions from each cell lines were obtained and were fixed with 2.5% gluteraldehyde/2% paraformaldehyde in 100 mM sodium cacodylate (SC), pH 7.43, and post-fixed in 1% osmium tetroxide in SC followed by 1% uranyl acetate. After ethanol dehydration and embedding in LX112 resin (LADD Research Industries), ultrathin sections were stained with uranyl acetate followed by lead citrate. Grids were viewed on a JEOL JEM 1400 transmission electron microscope operated at 80 kV. For the quantification of mitochondria in cells, 10-15 different electronmicrographs for each cell line were analyzed.

2.3.2 Mitochondrial morphology

Cybrid cells growing in 75 cm^2 flasks were replated on treated glass coverslips (16 mm diameter) in 12-well plates at the concentration of 1.0×10^5 cells/mL. After 24 h, cells were washed twice with serum-free growth medium and once with (1:1) serum-free growth medium: 4% (v/v) paraformaldehyde in PBS solution, for 10 min. Then cells were fixed with 4% (v/v) paraformaldehyde in PBS solution for 20 minutes, at room temperature. The fixed cells were washed again with PBS, permeabilized with 0.2 % (v/v) Triton X-100 in PBS and incubated with 3% (w/v) BSA in PBS, for 30 min, to prevent nonspecific binding. Then, cells were incubated with the primary rabbit polyclonal anti-TOM-20 (1:200) antibody overnight followed by washing with PBS and incubation with the secondary antibody Alexa Fluor® 488-conjugated goat anti-rabbit for 1 h. After washing twice with PBS, nuclei were counterstained with 5 μg/mL Hoechst 33342 dye in PBS. After a final wash, the coverslips were immobilized on a glass slide with mounting medium (DakoCytomation, Dako, Glostrup, Denmark). Negative CTs omitting primary antibody were performed in each case, and no staining was seen (data not shown). Images were acquired on a Zeiss LSM 510 meta-confocal microscope (63 × 1.4NA plan-apochromat oil immersion lens) by using the Zeiss LSM510 v3.2 software (Carl Zeiss, Inc., Thornwood, NY, USA) and analyzed using Zeiss LSM Image Examiner.

Fluorescence microscopy images were optimized by adjusting the contrast and afterwards binarized by conversion to 8-bit images. After unspecific noise of the

fluorescence signal was reduced, a spatial filter (convolution filter) as well as a threshold was applied to the images to define mitochondrial structures. Using a custom-written macro containing plug-ins (Dagda et al., 2009) from ImageJ1.46e software (Wayne Rasband; National Institutes of Health, USA), every single mitochondrion of the investigated cells was marked to analyze morphological characteristics such as its area, perimeter, major and minor axes. The area/perimeter ratio was employed as an index of mitochondrial interconnectivity, and inverse circularity was used as a measure of mitochondrial elongation.

2.3.3 Mitochondrial content

Cybrid cell lines growing in 75 cm^2 flasks were replated into 10 cm petri-dishes at the concentration of 3.0×10^5 cells/mL. After 24 h in culture, individual cell lines were washed once with ice-cold PBS, scraped and harvested on ice with a 1% (v/v) Triton X-100 containing hypotonic lysis buffer [25 mM HEPES (pH 7.5), 2 mM $MgCl_2$, 1 mM EDTA and 1 mM EGTA, supplemented with 2 mM DTT, 0.1 mM PMSF and a 1:1000 dilution of a protease inhibitor cocktail]. The cellular suspension was frozen/thawed three times on liquid nitrogen and centrifuged at 20,000 ×*g*, for 10min at 4ºC. The resulting supernatant was collected and assayed for protein concentration using the Bio-Rad Protein Assay (Bio-Rad, Hercules, CA, USA).

For each sample, 50 µg of protein were separated under reducing conditions on 12% sodium dodecyl sulphate-polyacrylamide gel electrophoresis (SDS-PAGE) after denaturation at 100ºC, for 5 min, in a 6 × concentrated sample buffer [100 mM Tris-HCl (pH 6.8), 100 mM DTT, 4% (w/v) SDS, 0.2% (w/v) bromophenol blue and 20% (v/v) glycerol]. Proteins were then transfered to a Immobilon^{TM}-P PVDF (polyvinylidene difluoride) membrane, which was further blocked with 5% (w/v) non fat milk in Tris-buffered saline buffer [50 mM Tris (pH 7.6), 150 mM NaCl], 0.1% (v/v) Tween 20 (TBS-T), for 1h, at room temperature. After blocking, membranes were subjected to an overnight incubation with the anti-Hsp60 (1:1000), anti-VDAC/Porin (1:800), anti-COXIV (1:1000), anti-TOM20 (1:1000), anti-NDUFA2 (1:200) or anti-α-tubulin (1:10,000) primary antibodies, at 4ºC. Membranes were further washed three times with TBS-T and then incubated with the corresponding alkaline phosphatase-conjugated secondary antibody (1:15,000) for 1h, at room temperature. The membranes were washed again three times and bound antibodies detected using the enhanced chemifluorescence reagent (ECF) according to the manufacturer's instructions.

Blots were visualized using a VersaDoc imageing system (Bio-Rad, Hercules, CA, USA) and protein bands densitometry quantified using the Quantity-One software (Bio-Rad, Hercules, CA, USA).

2.3.4 mtDNA screening

Total DNA was extracted from three PD and three CT cybrids by using standard methods and quantified by UV spectrophotometry (λ=260 nm). Automated sequencing analysis was used, according to the manufacturer's instructions (3130 ABI Prism sequencing system), with BigDye® Terminator Ready Reaction Mix v3.1 (Applied Biosystems), for the investigation of the seven mtDNA genes coding for complex I subunits, corresponding to ND1, ND2, ND3, ND4L, ND4, ND5 and ND6, allowing the screening of confirmed pathogenic mutations, reported mutations, polymorphisms and novel sequence variations in these genes, according to MITOMAP (www.mitomap.org). All sequences were analysed using Sequencing Analysis v5.4 and SeqScape v.2.5 software, by comparison with reference sequence obtained from GenBank database.

In silico analysis was performed for unpublished sequence variations found, using PolyPhen-2® and ClustalW2® for evolutionary conservation analysis among species.

2.3.5 Analysis of mitochondrial membrane potential

NT2 Rho^+ cells growing in 75 cm^2 flasks were replated into 24-well plates at the concentration of 2.1×10^5 cells/mL. Where indicated, cell treatment conditions included 1 mM MPP^+; 2 μM brefeldin A and 2 μM tunicamycin added to the growth medium for 2, 4, 6 and 24 h. For all experimental procedures, controls were performed in the absence of the stress agents.

The distribution and subsequent quenching of the fluorescent lipophilic cation rhodamine 123 (Rh123) was used to monitor changes in $\Delta\psi_m$. An increase in Rh 123 fluorescence indicates depolarization of $\Delta\psi_m$, as shown by the observation that mitochondrial uncouplers increase the Rh123 fluorescence signal (Duchen, 1992; Duchen and Biscoe, 1992). This is interpreted in terms of the well-established biophysics of a variety of lipophilic cations in response to partitioning into negatively charged organelles. The concentration of the dye by mitochondria leads to the forced aggregation of dye molecules and to an associated quenching of the fluorescence signal (Emaus et al., 1986; Bunting, 1992). Some dye must remain in the cytosol, prevented from leaving the cell by the plasma membrane potential. Thus, hyperpolarization of $\Delta\psi_m$ will increase the partitioning of dye into the mitochondria, and increase the concentration-dependent

quenching. Depolarization of $\Delta\psi_m$ allows dye to redistribute from the mitochondria into the cytosol, increasing the signal.

Cells were loaded with 0.5 µM Rh123 in Krebs buffer [10 mM HEPES, 10 mM $NaHCO_3$ (pH 7.4), 132 mM NaCl, 4 mM KCl, 1.4 mM $MgCl_2$, 6 mM glucose, 1 mM $CaCl_2$] at 37°C, in the dark. Simultaneously, the fluorescence (λ_{ex} = 505 nm and λ_{em}= 525 nm) was recorded for 45 min before, and 10 min after mitochondrial depolarization, using a Spectramax Plus 384 spectrofluoremeter (Molecular Devices, Sunnyvale, CA, USA). Maximal mitochondrial depolarization ($\Delta\psi_m$ collapse) was performed in every individual experiment by adding 1 µM carbonyl cyanide 4-(trifluoromethoxy)phenylhydrazone (FCCP, protoionophore), which was always preceded by oligomycin (2 µg/mL) to prevent ATP synthase reversal.

Rh123 retention was determined by the difference between total fluorescence (after depolarization) and the initial value of fluorescence. Since positively charged Rh123 is retained by functional mitochondria with a high $\Delta\psi_m$, a decrease of cellular retention of Rh123 has been associated with a decrease in $\Delta\psi_m$.

2.3.6 Evaluation of mitochondrial respiratory chain NADH–ubiquinone oxidoreductase activity

NT2 Rho^+ cells growing in 75 cm^2 flasks were replated into 10 cm petri-dishes at the concentration of 3.0×10^5 cells/mL. Cell treatment conditions were as mentioned in the section 2.3.2.

The activity of mitochondrial NADH-ubiquinone oxidoreductase (complex I: EC 1.6.99.3) was determined by using a modified version of the method of Ragan *et al.* (Ragan, 1987). Briefly, after treatments, cells were harvested on ice with a low stringency lysis buffer [20 mM HEPES (pH 7.4), 250 mM sucrose, 1 mM EDTA, 1 mM EGTA]. Then, protein lysates of homogenated cells were prepared using a Teflon-fitted glass hand homogenizer and assayed for protein concentration using the Bio-Rad Protein Assay (Bio-Rad, Hercules, CA, USA). Complex I activity was measured by following the decrease in NADH absorbance at 340 nm (ε=6.81$mM^{-1}cm^{-1}$) that occurs when ubiquinone is reduced to form ubiquinol. The reaction was initiated by adding 50 µM ubiquinone to the reaction mixture, containing 30 µg of protein lysate suspended in potassium phosphate buffer [25 mM K_2HPO_4, 25mM KH_2PO_4 (pH 7.2)], in the presence of 2.5 mg/mL BSA (which increases rotenone sensitivity), 4 mM $MgCl_2$, and 1 mM KCN at 30°C. After 5 min, 10 µM rotenone was added and the reaction was monitored for a

further 5 min period. Complex I specific activity was expressed in nanomoles per minute per milligram of protein and represents the rotenone sensitive rates.

2.3.7 Quantitative determination of total NAD levels

Total nicotinamide adenine dinucleotide (NAD^+ plus NADH) levels were determined using the NAD^+/NADH colorimetric assay kit (MBL International Corporation, Woburn, MA, USA) according to the manufacturer's instructions. Standard curves generated with known amounts of purified NADH were used to whole cell concentrations.

2.3.8 Evaluation of mitochondrial Ca^{2+} uptake ability

NT2 Rho^+ cells growing in 75 cm^2 flasks were replated into 12-well plates at the concentration of 2.1×10^5 cells/mL. Cells treatment conditions included 1 mM MPP^+, 2 μM brefeldin A and 2 μM tunicamycin added to the growth medium for 2, 4, 6 and 24 h.

To monitor mitochondrial Ca^{2+} levels we used the fluorescent cell permeant probe Rhod-2, AM (λ_{ex}= 552 nm and λ_{em}= 581 nm). In its AM form, Rhod-2 carries a delocalized positive charge that causes preferential accumulation of this probe in mitochondrial matrix driven by $\Delta\psi_m$ according to the Nernst equation. After deesterification, this dye remains trapped in the mitochondria and reports Ca^{2+} levels variations in the mitochondrial lumen.

Treated and CT cells were washed twice with Krebs buffer [10 mM HEPES, 10 mM $NaHCO_3$ (pH 7.4), 132 mM NaCl, 4 mM KCl, 1.4 mM $MgCl_2$, 6 mM glucose, 1 mM $CaCl_2$] and loaded with 10 μM Rhod-2 in Krebs buffer, supplemented with 0.01% (v/v) Pluronic F-127 (Molecular Probes, Eugene, OR, USA) and 1% (w/v) BSA, for 40 min, at 37 °C. To assure a selective loading of Rhod-2, AM into mitochondria, probe loading procedure was performed at low temperature followed with warm incubation at 37ºC. After loading, cells were washed three times in calcium-free Krebs buffer and were kept in Ca^{2+} and dye free-medium at 37°C, for 30 min, thereby permitting the cells to hydrolyze the acetoxymethyl ester completely. From the entire loading process onwards, cells were shielded from ambient light. Then, recordings were carried out. After establishment of a stable fluorescence baseline, mitochondrial maximal Ca^{2+} uptake ability was further assessed by challenging mitochondria with the subsequent addition of 5 μM Ca^{2+} ionophore A23187 as described previously by Deniaud *et al.* (Deniaud et al., 2008). The variations of fluorescence were monitored using a Spectramax Plus 384 spectrofluorometer (Molecular Devices, Sunnyvale, CA, USA).

The ratio between mitochondrial matrix Ca^{2+} before and after challenging with A23187 was taken as an indirect measure of mitochondrial Ca^{2+} content.

2.3.9 Evaluation of mitochondrial distressing on cell-death related events

Induction of apoptic cell death mechanisms was determined by caspase activation assays that were performed by using the method described by Cregan *et al.* (Cregan et al., 1999), with minor modifications.

NT2 Rho^+ cells growing in 75 cm^2 flasks were replated into 6-well plates at the concentration of 2.5×10^5 cells/mL. Where indicated, cells were treated with 1 mM MPP^+ added in the culture medium for 24 h. In another set of experiments, cells were preincubated for 1h with 10 μM dantrolene, an inhibitor of ryanodine receptors of ER. After treatments, cells were washed once in ice-cold PBS and harvested on ice with a hypotonic lysis buffer [25 mM HEPES (pH 7.5), 2 mM $MgCl_2$, 1 mM EDTA and 1 mM EGTA, supplemented with 2 mM DTT, 0.1 mM PMSF and a 1:1000 dilution of a protease inhibitor cocktail]. The cellular suspension was frozen/thawed three times on liquid nitrogen and centrifuged at 20,000 ×*g*, for 10min, at 4ºC. The resulting supernatant was collected and assayed for protein concentration using the Bio-Rad Protein Assay (Bio-Rad, Hercules, CA, USA).

To evaluate caspases activation, in parallel sets of assays, whole cellular extracts containing 50 μg or 100 μg of protein were individually incubated, for 2 h, at 37ºC in a reaction buffer [25mM HEPES (pH 7.5), 0.1% (w/v) 3[(3-cholamidopropyl) dimethylammonio]-propanesulfonic acid (CHAPS), 10% (w/v) sucrose, 2 mM DTT] with 100 μM Ac-VDVAD-*p*NA, 100μM Ac-DEVD-*p*NA, 50 μM Ac-LEVD-*p*NA and 50 μM Ac-LEDH-*p*NA, specific colorimetric substrates for caspase-2, -3, -4 and -9, respectively.

The enzymatic cleavage of the chromophore *p*-nitroaniline (*p*NA) from the substrate was detected at 405 nm using a Spectramax Plus 384 spectrophotometer (Molecular Devices, Sunnyvale, CA, USA).

2.4 Evaluation of ER stress and UPR activation

2.4.1 Analysis of Bip/GRP78 levels

NT2 Rho^+ cells growing in 75 cm^2 flasks were replated into 6-well plates at the concentration of 2.5×10^5 cells/mL. Cells treatment conditions included 1 mM MPP^+, 2 μM brefeldin A and 2 μM tunicamycin added to the growth media for 2, 4, 6 and 24 h.

After treatments, cells were washed once in ice-cold PBS and harvested on ice with a 1% (v/v) Triton X-100 containing hypotonic lysis buffer [25 mM HEPES (pH 7.5), 2 mM $MgCl_2$, 1 mM EDTA and 1 mM EGTA, supplemented with 2 mM DTT, 0.1 mM PMSF

and a 1:1000 dilution of a protease inhibitor cocktail]. The cellular suspension was frozen/thawed three times on liquid nitrogen and centrifuged at 20,000 ×*g*, for 10min at 4ºC. The resulting supernatant was collected and assayed for protein concentration using the Bio-Rad Protein Assay (Bio-Rad, Hercules, CA, USA).

For each sample, 40 µg of protein were separated under reducing conditions on 12% SDS-PAGE gel after denaturation at 100ºC, for 5 min, in a 6 × concentrated sample buffer [100 mM Tris-HCl (pH 6.8), 100 mM DTT, 4% (w/v) SDS, 0.2% (w/v) bromophenol blue and 20% (v/v) glycerol]. Proteins were then transfered to a Hybond-P PVDF membrane, which was further blocked with 5% (w/v) non fat milk in TBS-T, for 1 h, at room temperature. After blocking, membranes were subjected to an overnight incubation with the anti-BiP/GRP78 (1:500) or anti-α-tubulin (1:10,000) primary antibodies, at 4ºC. Membranes were further washed three times with TBS-T and then incubated with the corresponding alkaline phosphatase-conjugated secondary antibody (1:20,000) for 2 h, at room temperature. The membranes were washed again three times and bound antibodies detected using the enhanced chemifluorescence reagent (ECF) according to the manufacturer's instructions.

Blots were visualized using a VersaDoc imageing system (Bio-Rad, Hercules, CA, USA) and protein bands densitometry quantified using the Quantity-One software (Bio-Rad, Hercules, CA, USA).

2.4.2 Evaluation of ER Ca^{2+} content

Measurement of ER Ca^{2+} content was assessed according to the method described by Nutt *et al.* (Nutt et al., 2002), with some modifications. Briefly, 2.1×10^5 cells/mL were seeded in 12-well plates and treated with 1 mM MPP^+, 2 μM brefeldin A and 2 μM tunicamycin added in the growth medium for 2, 4, 6 and 24 h.

Afterward, treated and control cells were washed twice in Krebs buffer [10 mM HEPES, 10 mM $NaHCO_3$ (pH 7.4), 132 mM NaCl, 4 mM KCl, 1.4 mM $MgCl_2$, 6 mM glucose, 1 mM $CaCl_2$] and loaded with 5 µM Fura-2, AM in Krebs buffer, supplemented with 0.01% (v/v) Pluronic F-127 and 1% (w/v) BSA, for 40 min, at 37 °C. After loading, cells were washed three times in Ca^{2+}-free Krebs buffer and they were kept in Ca^{2+} and dye free-medium at 37°C, for 30 min, thereby permitting the cells to hydrolyze the acetoxymethyl ester completely. From the entire loading process onwards, the cells were shielded from ambient light. Then, recordings were carried out. After fluorescence baseline stabilization, cells were stimulated with 5 µM thapsigargin, in the absence of

extracellular Ca^{2+}, to empty Ca^{2+} from ER. Fura-2, AM fluorescence was recorded at 340/380 nm excitation and 512 nm emission.

The variations of fluorescence were monitored using a Spectramax Plus 384 spectrofluoremeter (Molecular Devices, Sunnyvale, CA, USA). The peak amplitude of Fura-2, AM fluorescence (ratio at 340/380 nm) was used to evaluate ER Ca^{2+} levels.

2.4.3 Evaluation of ER stress on apoptosis induction

NT2 Rho^+ cells growing in 75 cm^2 flasks were replated into 6-well plates at the concentration of 2.5×10^5 cells/mL. Cells treatment conditions included 2 μM brefeldin A and 2 μM tunicamycin added in the growth media for 24 h.

Induction of apoptic mechanisms was determined by caspase -2, -4 and -9 activation assays performed as described in the section 2.3.9.

2.5 Assessment of the autophagy-lysosomal pathway

2.5.1 Autophagic vacuole ultrastructural analysis

Cybrids and Rho0 cells were grown in 75 cm^2 culture flasks till 90% confluence and growth medium was changed 1–3 h before harvesting. Then cellular suspensions from each cell line were obtained and were fixed with 2.5% gluteraldehyde/2% paraformaldehyde in 100 mM sodium cacodylate (SC), pH 7.43, and post-fixed in 1% osmium tetroxide in SC followed by 1% uranyl acetate. After ethanol dehydration and embedding in LX112 resin (LADD Research Industries), ultrathin sections were stained with uranyl acetate followed by lead citrate. Grids were viewed on a JEOL JEM 1400 transmission electron microscope operated at 80 kV. For the quantification of autophagic vacuoles in cells, 10-15 different electronmicrographs for each cell line were analyzed. Autophagic vacuoles were identified using previously established criteria (Nixon et al., 2005).

2.5.2 Evaluation of autophagic flux and turnover

2.5.2.1 Western blotting

NT2 Rho^+, Rho0 and cybrid cells growing in 75 cm^2 flasks were replated into 10 cm petri-dishes at the concentration of 3.0×10^5 cells/mL. Cell lines treatment conditions included normal-nutrient (serum +) and serum-starvation (hereafter simply starvation) by culturing

cells in serum-free medium (serum -) for 6 h before harvesting. Compounds included 1 mM MPP^+, 5 μM AK-1 or 10 μM Tubastatin A added in the growth medium for 24 h before harvesting. Where indicated, 20 mM ammonium chloride and 100 μM leupeptin were added in the culture medium in the last 4 h of fed/starved cells.

Regarding primary neuronal cultures, after 6 DIV, cultured cortical neurons were treated with 50 μM MPP^+, 24 h before harvesting. Where indicated, 20 mM ammonium chloride and 20 μM leupeptin, 10 mM 3-MA or 10 nM rapamycin were added in the culture medium in the last 4 h of MPP^+ treatment.

After cell treatments, individual cell lines or cultured cortical neurons were washed once with ice-cold PBS, scraped and lysed on ice in RIPA buffer [50 mM Tris-HCl (pH 7.4), 150 mM NaCl, 1% (v/v) NP40, 0.1% (v/v) SDS, 0.5% (v/v) sodium deoxicholate (DOC), supplemented with 0.1 mM PMSF, 2 mM DTT and a 1:1000 dilution of a protease inhibitor cocktail]. Cell suspensions were incubated on ice for 15 min and centrifuged at 20,000 ×*g* for 15 min. Cleared lysates were assayed for protein concentration using the Pierce® BCA Protein Assay Kit (Thermo Fisher Scientific Inc., Rockford, IL, USA).

Regarding PBMCs, protein extracts were obtained by using 1% Triton X-100 containing hypotonic lysis buffer [25 mM HEPES (pH 7.5), 2 mM $MgCl_2$, 1mM EDTA and 1mM EGTA, supplemented with 2 mM DTT, 0.1 mM PMSF and a 1:1000 dilution of a protease inhibitor cocktail]. The cellular suspension was frozen/thawed three times on liquid nitrogen and centrifuged at 20,000 ×*g*, for 10 min at 4ºC. The resulting supernatant was collected and assayed for protein concentration using the Bio-Rad Protein Assay (Bio-Rad, Hercules, CA, USA).

For each sample, equal amounts of protein (50 μg) were separated under reducing conditions on 15% SDS-PAGE gels. Following electrophoretic transfer onto a Immobilon™-P PVDF membrane and blocking with 5% (w/v) BSA in TBS-T solution, membrane was incubated overnight with the rabbit polyclonal anti-LC3B (1:1000) antibody, at 4ºC with gentle agitation. Membranes were further washed three times with TBS-T and then incubated with the corresponding alkaline phosphatase-conjugated secondary antibody (1:15,000), for 2h at room temperature. The membranes were washed again three times and bound antibodies detected using ECF according to the manufacturer's instructions.

Blots were visualized using a VersaDoc imageing system (Bio-Rad, Hercules, CA, USA) and protein bands densitometry performed using the Quantity-One software (Bio-Rad, Hercules, CA, USA).

2.5.2.2 Immunocytochemistry

Rho0 and cybrid cells growing in 75 cm^2 flasks were replated on treated glass coverslips (16 mm diameter) in 12-well plates at the concentration of 1.0×10^5 cells/mL. Cybrid neuron-like cells (1×10^5 per coverslip) were plated onto glass coverslips (16 mm diameter) pre-coated with poly-D-lysine in 50:50 conditioned medium and were allowed to improve neurite outgrowth for 4 days, for further immunocytochemical experiments. Cortical neurons were mounted on poly-L-lysine-coated glass coverslips (16 mm diameter) at a density of 0.75×10^6 cells/mL. Cell treatment conditions were as mentioned in the section 2.5.2.1.

Following treatments, cells were analyzed by indirect immunofluorescence as described in the section 2.3.2, using the primary rabbit polyclonal anti-LC3B (1:200) antibody overnight and the secondary antibody Alexa Fluor® 488-conjugated goat anti-rabbit for 1 h. LC3 puncta number and size were quantified using the 'analyze particles' function of the ImageJ v1.46e software (Wayne Rasband; National Institutes of Health, USA) after thresholding of images with size settings from 0.2–10 $pixel^2$ and a circularity of 0–1. At least 20 cells were examined for each condition.

2.5.3 Autophagy induction and nucleation complex

2.5.3.1 Beclin and Bcl-2 levels

Cybrid cells growing in 75 cm^2 flasks were replated into 10 cm petri-dishes at the concentration of 3.0×10^5 cells/mL. Cell line treatment conditions included normal nutrient (serum +) and starvation for 6 h before harvesting. Where indicated, 20 mM ammonium chloride and 100 μM leupeptine were added in the culture medium in the last 4 h of fed/starved cells.

Following treatments, individual cell lines were washed once with ice-cold PBS, scraped and lysed on ice in RIPA buffer [50 mM Tris-HCl (pH 7.4), 150 mM NaCl, 1% (v/v) NP-40, 0.1% (v/v) SDS, 0.5% (v/v) sodium deoxicholate (NaDOC), supplemented with 0.1mM PMSF, 2 mM DTT and a 1:1000 dilution of a protease inhibitor cocktail]. Cell suspensions were incubated on ice for 15 min and centrifuged at 20,000 ×*g* for 15 min. Cleared lysates were assayed for protein concentration using the Pierce® BCA Protein Assay Kit (Thermo Fisher Scientific Inc., Rockford, IL, USA). For each sample, equal amounts of protein (50 μg) were separated under reducing conditions on 12% SDS-PAGE gels.

Following electrophoretic transfer onto a Immobilon™-P PVDF membrane and blocking with 5% (v/v) non fat milk TBS-T solution, membrane was incubated overnight

with the rabbit polyclonal anti-Bcl-2 (1:1000) or the mouse monoclonal anti-Beclin (1:1000) primary antibodies, at 4ºC, with gentle agitation. Membranes were further washed three times with TBS-T and then incubated with the corresponding alkaline phosphatase-conjugated secondary antibody (1:15,000) for 2 h at room temperature. The membranes were washed again three times and bound antibodies detected using ECF, according to the manufacturer's instructions.

Blots were visualized using a VersaDoc imageing system (Bio-Rad, Hercules, CA, USA) and protein bands densitometry performed using the Quantity-One software (Bio-Rad, Hercules, CA, USA).

2.5.3.2 Beclin and Bcl-2 subcompartmentalization

Cybrid cells were grown in 75 cm^2 flasks and were treated under the conditions mentioned in the section 2.5.3.1. Following treatments, mitochondria- and cytosol-enriched fractions were obtained by using the ProteoExtract Subcellular Proteome Extraction Kit (Calbiochem™, Merck KGaA, Darmstadt, Germany). Cells were harvested and subcellular fractions were prepared according to the manufacturer's specifications. To prepare samples for Western blotting, protein concentrations were determined using the Pierce® BCA Protein Assay Kit (Thermo Fisher Scientific Inc., Rockford, IL, USA) according to the manufacturer's instructions for plate reader.

For each sample, equal amounts of protein (20 μg) were separated under reducing conditions on 12% SDS-PAGE gels and analyzed by Western blotting using the rabbit polyclonal anti-Bcl-2 (1:1000) and the rabbit polyclonal anti-Beclin (1:1000) primary antibodies, as described in the section 2.5.3.1. The rabbit monoclonal anti-α-tubulin (clone 11H10) (1:1000) and the rabbit polyclonal anti-TOM20 (1:1000) primary antibodies were used as loading controls for cytosol- and mitochondria-enriched fractions, respectively.

2.5.3.3 Beclin/Bcl-2 physical interaction

Cybrid cells were grown in 75 cm^2 flasks and were treated under the conditions mentioned in the section 2.5.3.1. After starvation conditions, cells were scraped and lysed on ice in a non-denaturing lysis buffer [20 mM Tris-HCl (pH 7.0), 100 mM NaCl, 2 mM EDTA, 2 mM EGTA, supplemented with 0.1% (v/v) SDS, 1% (v/v) Triton X-100, 2 mM DTT, 0.1 mM PMSF and a 1:1000 dilution of a protease inhibitor cocktail]. Cellular suspensions were centrifuged at 20,000 ×*g*, for 10 min at 4ºC and whole lysates were assayed for protein concentration as mentioned in the section 2.5.3.1.

Afterward, 500 µg of each sample were precleared with Protein A Sepharose beads (GE Healthcare Bio-Sciences, Uppsala, Sweden) for 1 h, at 4ºC, and then incubated with the primary rabbit polyclonal anti-Beclin (1:100) antibody, overnight at 4ºC and with nutation. Protein A-Sepharose beads were then added to samples followed by 2 h incubation. The beads were spun down and washed seven times with the previously referred washing buffer (each time centrifuging at 4°C and discarding the supernatant). For the first two washes the buffer was supplemented with 1% (v/v) Triton X-100. For the next three washes the buffer was supplemented with 1% (v/v) Triton X-100 and 500 mM NaCl. The final two washes were performed using unsupplemented buffer. The last supernatant was collected and 25 µl of 2 × concentrated sample buffer was added. The samples were boiled at 95-100°C for 5 min to denature the protein and to separate it from the protein-A beads. The boiled proteins were centrifuged at 20,000 ×*g* for 5 min at room temperature and the supernatants collected. Samples including the input, flow trough and immunoprecipitated complex, were separated by SDS–PAGE and analyzed by Western blotting using the rabbit polyclonal anti-Bcl-2 (1:1000) and the rabbit polyclonal anti-Beclin (1:1000) primary antibodies, as mentioned in the section 2.5.3.1. A shift < 5 kDa is observed in the molecular weight of Bcl-2 in the IP, which might be due to different salt concentrations between the lysis buffer and the IP buffer.

2.5.4 Clearance of autophagic substrates

2.5.4.1 p62 levels

Cybrid cells growing in 75 cm^2 flasks were replated into 10 cm petri-dishes at the concentration of 3.0×10^5 cells/mL. Cell lines treatment conditions included normal nutrient (serum +) and starvation for 6 h before harvesting. Where indicated, 20 mM ammonium chloride and 100 µM leupeptin were added in the culture medium in the last 4 h of fed/starved cells.

Following cell treatments, cells were harvested and samples were processed and subjected to SDS-PAGE and immunoblotting analysis using the rabbit polyclonal anti-SQSTM1/p62 (1:1000) antibody, as described in the section 2.5.2.1.

2.5.4.2 α-Synuclein oligomerization patterns

Cybrid cells were grown in 75 cm^2 flasks and were treated under the conditions mentioned in the section 2.5.2.1.

For the analysis of α-synuclein oligomerization patterns, a detergent solubility fractionation was performed by using 1% (v/v) Triton X-100 containing hypotonic lysis buffer [25 mM HEPES (pH 7.5), 2 mM $MgCl_2$, 1 mM EDTA and 1 mM EGTA, supplemented with 2 mM DTT, 0.1 mM PMSF and a 1:1000 dilution of a protease inhibitor cocktail] and incubating cells suspensions for 15 min on ice followed by ultracentrifugation (163,400 ×*g*, 15 min, 4°C). The supernatant was designated Triton X-100-soluble fraction, and the pellet was redissolved in 1% (v/v) SDS-containing lysis buffer and sonicated for 10 s (Triton X-100-insoluble fraction). Seventy-five micrograms of each cell lysate was loaded onto 10% SDS-PAGE gels under non-reducing and non-denaturating conditions and subjected to SDS-PAGE and immunoblotting analysis using the mouse monoclonal anti-α-synuclein [clone LB509, (1:100)] antibody, as described in the section 2.5.2.1.

2.5.4.3 Autophagosome-lysosome fusion

Autophagosome-lysosome fusion can be visualized via immunofluorescence imageing as the co-localization of LC3 positive vesicles with a lysosome marker (e.g., LAMP-1) (Bains and Heidenreich, 2009).

Cybrid cells growing in 75 cm^2 flasks were replated on treated glass coverslips (16 mm diameter) in 12-well plates at the concentration of 1.0×10^5 cells/mL. To modulate microtubule dynamic instability 5 nM taxol and 1 μM nocodozole were added in the culture medium for 24 h, and 20 mM ammonium chloride and 100 μM leupeptin in the last 4 h.

Following treatment, cells were analyzed by indirect immunofluorescence as mentioned in the section 2.3.2, using the rabbit monoclonal anti-LC3 XP® (1:400) and the mouse monoclonal anti-LAMP-1 [clone H4A3, (1:100)] primary antibodies. Colocalization of the two antibodies (LC3/LAMP-1) was quantified in thresholded images with the JACoP plug-in of the ImageJ software, according to Bolte and Cordelières (Bolte and Cordelieres, 2006).

2.5.5 Evaluation of autophagy modulation on cell death-related events

NT2 Rho^+, Rho0 and cybrid cells growing in 75 cm^2 flasks were replated into 6-well plates at the concentration of 2.5×10^5 cells/mL. Cells treatment conditions included 20 mM ammonium chloride and 100 µM leupeptin, 10 mM 3-MA or 0.5 µM rapamycin added in the culture medium in the last 4 or 6 h before harvesting, respectively.

Induction of apoptic cell death related mechanisms was determined by the caspase-3 activation assay as described in the section 2.3.9.

2.6 Microtubule network status and intracellular trafficking

2.6.1 Microtubule network morphology

Cybrid cells growing in 75 cm^2 flasks were replated on treated glass coverslips (16 mm diameter) in 12 well plates at the concentration of 1.0×10^5 cells/mL. Where indicated, cells were treated with 5 µM AK-1 and 10 µM Tubastatin A added in the culture medium for 24 h. Following treatment, cells were analyzed by indirect immunofluorescence as described in the section 2.3.2, using the mouse polyclonal anti-α-tubulin (1:1000) primary antibody.

2.6.2 Microtubule network postranslational modifications: acetylation

Cybrid cells growing in 75 cm^2 flasks were replated into 10 cm petri-dishes at the concentration of 3.0×10^5 cells/mL. Cell line treatment conditions were as described in the section 2.6.1. Following cell treatments, cells were harvested and samples were processed and subjected to SDS-PAGE and immunoblotting analysis using the mouse polyclonal anti-acetyl-α-tubulin (1:2000) primary antibody, as described in the section 2.5.2.1.

2.6.3 Microtubule network structural integrity

Cybrid cells growing in 75 cm^2 flasks were replated into 10 cm petri-dishes at the concentration of 3.0×10^5 cells/mL. Cell lines treatment conditions were as described in the section 2.6.1.

Following cell treatments, soluble and polymeric fractions of cell tubulin were prepared according to the method described by Joshi and Cleveland (Joshi and Cleveland, 1989), with slight modifications. Cells were washed twice, very gently, with a

microtubule stabilizing buffer (0.1 M N-morpholinoethanesulfonic acid, pH 6.75, 1 mM MgSO4, 2 mM EGTA, 0.1 mM EDTA, 4 M glycerol). Soluble proteins were extracted at 37°C for 4-6 min in 100 µl of microtubule stabilizing buffer containing 0.1% Triton X-100. The soluble extract was removed and centrifuged for 2 min in order to pellet any cytoskeletal material dislodged from the culture dish during extraction. The remaining cytoskeletal fraction in the culture dish was scraped in 100 µl of 25 mM Tris (pH 6.8) and 0.5% SDS. This suspension was frozen three times in liquid nitrogen. Then, samples were processed and subjected to SDS-PAGE and immunoblotting analysis using the mouse polyclonal anti-α-tubulin (1:10,000) primary antibody, as described in the section 2.5.2.1.

2.6.4 SIRT2 tubulin deacetylase subcompartmentalization

Cybrid cells were grown in 75 cm^2 flasks and were treated under the conditions mentioned in the section 2.6.1. Following treatments, mitochondria-, cytosol-, nuclei-, and cystoskeleton-enriched fractions were obtained as described in 2.5.3.2.

For each sample, equal amounts of protein (50 µg) were separated under reducing conditions on 12% SDS-PAGE gels and analyzed by Western blotting using the rabbit polyclonal anti-SIRT2 (1:1000) antibody, as described in the section 2.5.2.1. The rabbit monoclonal anti-α-tubulin (clone 11H10, 1:1000), the rabbit polyclonal anti-TOM20 (1:1000), the mouse monoclonal anti-TATA binding protein (1:1000), and the rabbit polyclonal anti-Vimentin (1:1000) primary antibodies were used as loading controls for cytosol-, mitochondria-, nuclei-, and cystoskeleton-enriched fractions, respectively.

2.6.5 Intracellular transport of mitochondria and autophagosomes

2.6.5.1 Modulation of microtubule-dependent trafficking of autophagosomes

Cybrid cells growing in 75 cm^2 flasks were replated into 10 cm petri-dishes at the concentration of 3.0×10^6 cells/mL. To modulate microtubules dynamic instability 5 nM taxol and 1 µM nocodozole were added in the growth medium in normal nutrient conditions for 24h. Following cell treatments, cells were harvested and samples were processed and subjected to a SDS-PAGE and immunoblotting analysis using the rabbit polyclonal anti-LC3B (1:1000) antibody, as described in the section 2.5.2.1.

2.6.5.2 Live-cell imaging of mitochondria movement

Cybrid cells growing in 75 cm^2 flasks were replated into ibidiTreat µ-Slide eight-well plates at the concentration of 2.0×10^4 cells/mL. Cells treatment conditions included normal nutrient (serum +) and starvation for 6h. To modulate microtubule dynamic instability 5 nM taxol and 1 µM nocodozole were used in normal nutrient conditions for 24 h. Where indicated, 20 mM ammonium chloride and 100 µM leupeptin, were added in the culture medium in the last 4h of fed/starved cells.

Following treatments, cells were washed twice with HBSS, and to label mitochondria, cells were then incubated with 100 nM MitoTracker Green in HBSS for 30 min, at 37°C, in the dark, according to Du *et al.* (Du et al., 2010). After a gentle wash cells were kept in HBSS, and were imaged for mitochondrial movements. Time-lapse images were captured under a Zeiss LSM 510 meta confocal microscope with a stage-based chamber (5% CO_2, 37°C). The inverted microscope was driven by the LSM software and images were taken every 2 s for a total of 4 min under 63 × magnification (Zeiss Plan-ApoChromat 63 ×, 1.4NA).

For transport analysis, mitochondria were considered not mobile if they remained stationary for the entire recording period. Movement was counted only if the displacement was more than the length of the mitochondrion (~2 µm).

For each time-lapse movie, mitochondria were manually tracked and transport parameters of mitochondria movements were generated using the ImageJ software plug-in Multiple Kymograph, submitted by J. Rietdorf and A. Seitz (European Molecular Biology Laboratory, Heidelberg, Germany). Mitochondrial movement velocity data were determined from the kymographic images and were calculated based on the slope ($v=dx/dt$) obtained for each mitochondrion movement profile along the recording time. Each series of images was recorded for at least three randomly selected MitoTracker Green-labeled cells per culture and three independent cultures per condition.

2.6.5.3 Live-cell imaging of autophagosome movement

Cybrid cells growing in 75 cm^2 flasks were replated into ibidiTreat µ-Slide eight-well plates at the concentration of 2.0×10^4 cells/mL. To modulate microtubule dynamic instability 5 nM taxol and 1 µM nocodozole were used in normal nutrient conditions for 24 h. Where indicated, 20 mM ammonium chloride and 100 µM leupeptin, were added in the culture medium in the last 4h.

Following treatments, cells were washed twice with HBSS and late autophagosomes and earlier vacuoles in the autophagy pathway were labeled using the Cyto-ID™ Green detection reagent provided in the Cyto-ID™ Autophagy detection kit

(Enzo, Lausen, Switzerland) according to the manufacturer's instructions. After a gentle wash, cells were kept in HBSS and were imaged for autophagosome movements. Time-lapse images acquisition and transport analysis were performed as described in the section 2.6.5.2. Movement was counted only if the displacement was more than the length of the autophagosome (~500 nm). Each series of images was recorded for at least three randomly selected Cyto-ID™ Green-labeled cells per culture and three independent cultures per condition.

2.7 Data Analysis

All data were expressed as mean ± SEM of at least three independent experiments. Statistical analyses were performed using GraphPad Prism 5 (GraphPad Software, San Diego, CA, USA). Differences between two data sets were evaluated by two tailed unpaired Student's *t*-test. Statistical tests between multiple data sets and conditions were carried out using a one way or two-way analysis of variance (ANOVA) followed by Bonferroni *post hoc* test or the Newman-Keuls multiple comparison test to determine statistical significance, as appropriate. A P-value<0.05 was considered statistically significant.

CHAPTER III

Endoplasmic reticulum and mitochondria interplay mediates apoptotic cell death: relevance to Parkinson's disease

3.1 Summary

Sporadic Parkinson's disease (sPD) is a progressive neurodegenerative disease characterized by a loss of dopaminergic neurons in the substantia nigra pars compacta. Many cellular mechanisms are thought to be involved in the death of these specific neurons in sPD, including oxidative stress, changes in intracellular calcium (Ca^{2+}) homeostasis, and mitochondrial dysfunction. In addition, recent studies have revealed that also the endoplasmic reticulum (ER) stress in conjunction with abnormal protein degradation can contribute to the sPD pathophysiology.

Here, we investigated the molecular mechanisms underlying the interplay between the ER and mitochondria and its relevance for the control of neuronal cell death in sPD. We observed that 1-methyl-4-phenylpyridinium (MPP^+) induces changes in the mitochondrial function, affecting the mitochondrial membrane potential and the electron transport chain function. Likewise, it was also evident the activation of the unfolded protein response by the overexpression of the chaperone BiP/GRP78.

Moreover, MPP^+ stress stimuli caused the release of Ca^{2+} from the ER, which consistently induced mitochondrial Ca^{2+} uptake, with a rise in the mitochondrial matrix free Ca^{2+}. Besides, inhibition of Ca^{2+} release from the ER prevented the activation of mitochondria-dependent caspases induced by MPP^+.

Our findings show that the ER and mitochondria are in a close communication, establishing a dynamic ER-Ca^{2+}-mitochondria interconnection that can play a prominent role in the neuronal cell death induction under particular stressful circumstances of sPD pathology.

3.2 Introduction

Sporadic Parkinson's disease (sPD) is a severe and progressive neurodegenerative disease of unknown cause, characterized by a selective and profound loss of dopaminergic neurons in the substantia nigra pars compacta (SNpc) and norepinephrinergic neurons of the locus coeruleus. The most prominent histopathological hallmark of sPD is the intracellular accumulation of insoluble fibrous material, named Lewy bodies (LBs), found in the cytoplasm of neurons (Cardoso et al., 2005). LBs are formed by aggregates of several proteins, including α-synuclein, ubiquitin, synphilin and tubulin (Shimura et al., 2000).

Several reports support a link between the endoplasmic reticulum (ER) stress and sPD. Thus, it has been demonstrated the up-regulation of ER chaperones, such as protein disssulfide isomerase (PDI), in postmortem brain tissues and cell culture models of sPD, and the accumulation of PDI in LBs (Conn et al., 2004). Other evidences come from studies of certain neurotoxins that are used as model compounds to mimic the disease process both in neuronal cells and *in vivo* (Ryu et al., 2002; Holtz and O'Malley, 2003). Compounds, such as 6-hydroxydopamine (6-OHDA) and *N*-methyl-4-phenyl-1,2,3,6 tetrahydropyridine (MPTP), or its active metabolite, 1-methyl-4-phenylpyridinium (MPP^+), induce oxidative stress and impair mitochondrial respiration and energy metabolism. Recent studies in cultured cells, including dopaminergic neurons, have demonstrated that these compounds trigger ER stress and are also involved in the up-regulation of diverse components of the unfolded protein response (UPR) (Ryu et al., 2002; Holtz and O'Malley, 2003). It has also been well-established that mitochondrial function is altered in the course of sPD, particularly at the mitochondrial NADH-ubiquinone oxidoreductase (complex I) level (Cardoso et al., 2005). The complex I deficiency in the SNpc and platelets of patients with sPD has been consistently noticed (Parker et al., 1989; Schapira et al., 1989; Mann et al., 1994; Haas et al., 1995). Accordingly, it seems that sPD has a mitochondrial component and that probable factors which directly or indirectly modulate normal mitochondrial functions could compromise neuronal survival.

The fundamental contribution of mitochondria and ER to the cellular fate has been increasingly recognized. Moreover, mitochondria are often closely associated with the ER providing the conditions for a local and privileged communication between the two organelles (Csordas et al., 2006).

Therefore, it seems worthwhile to unveil the molecular mechanisms that coordinate the interplay between mitochondrial dysfunction and the ER stress and its relevance for the control of neuronal cell death in a sPD context.

In the present work, we report that an altered mitochondrial function renders cells more susceptible to develop an ER stress response. We propose that calcium (Ca^{2+}) is the main intervenient in the ER and mitochondria crosstalk, functioning as a key modulator of cell death signals triggered by the ER and mitochondria.

3.3 Results

3.3.1 Characterization of mitochondrial function

Concentrations of high micromolar or millimolar range of MPP^+ are usually used to study its neurotoxic effects and apoptosis induction (Bando et al., 2005; Domingues et al., 2008a; Esteves et al., 2008). We have previously reported that MPP^+ triggers apoptotic cell death, upon 24 h, in different PD cellular models (Arduino et al., 2008; Domingues et al., 2008a; Esteves et al., 2008).

In this study, to characterize the mitochondrial function in the NT2 cell line after short- (2, 4, 6 h) and long-term (24 h) periods of MPP^+ exposure, we have evaluated the mitochondrial respiratory chain complex I activity and changes in the mitochondrial membrane potential ($\Delta\psi_m$). As expected, results detailed in **Table III.1** demonstrate that MPP^+ induced a statistically significant decrease of this mitochondrial respiratory chain complex activity.

Table III.1. Mitochondrial respiratory chain NADH-ubiquinone oxidoreductase (complex I) activity (nmol.min^{-1}.mg^{-1}). Data represent mean ±SEM.

Condition	Complex I activity (nmol.min^{-1}.mg^{-1})			
	2h	4h	6h	24h
Control	5.60±0.232	5.32±0.521	5.23±0.547	4.72±0.540
MPP^+	1.44±0.155***	1.45±0.084***	1.35±0.119***	1.21±0.014***

*** p<0.001 relative to the corresponding control.

Nevertheless, as shown in the **Figure III.1**, we were unable to observe a significant alteration in rhodamine 123 (Rh123) retention induced by MPP^+ for the first 6 h.

These results suggest that, although NT2 cells harbour deficits in mitochondrial respiratory chain complex I and show an increase in reactive oxygen species (ROS) production during the first 6 h period (Domingues et al., 2008b), they are able to maintain $\Delta\psi_m$ until 24 h.

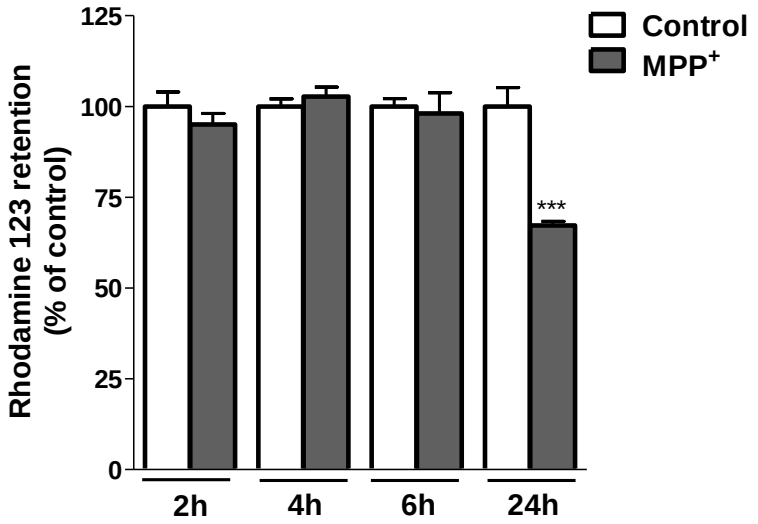

Figure III.1. Mitochondrial function is affected in NT2 neuron-like cells after long-term exposure to MPP^+.

Changes in mitochondrial membrane potential ($\Delta\psi_m$) induced by MPP^+ were estimated using the fluorescent cationic dye Rh123 as depicted in Chapter II. Rh123 retention was determined by the difference between total fluorescence (after mitochondrial membrane depolarization) and the initial value of fluorescence. Data are expressed as a percentage of the untreated cells values (control) and are mean±SEM (n=3; *** $p<0.001$, relative to control).

3.3.2 MPP^+ activates UPR in an early phase

Our next step was to clarify the effect of a decreased activity of the mitochondrial respiratory chain complex I on the ER stress induction. The initial cellular response following ER stress, also called UPR, protects the cell through adaptive mechanisms that re-establish normal ER function (Xu et al., 2005; Boyce and Yuan, 2006). For this purpose, we have analyzed the expression levels of a specific UPR marker, BiP/GRP78, a chaperone known to be localized in the ER lumen and that function in Ca^{2+} sequestration or that assist to the correct folding and assembly of nascent proteins (Nigam et al., 1994; Lievremont et al., 1997).

Overall**, Figure III.2** shows a representative BiP/GRP78 immunoblot (**Figure III.2A**) and the corresponding protein levels (**Figure III.2B**) in cells treated with MPP^+ for the different time points (2, 4, 6 and 24 h) .

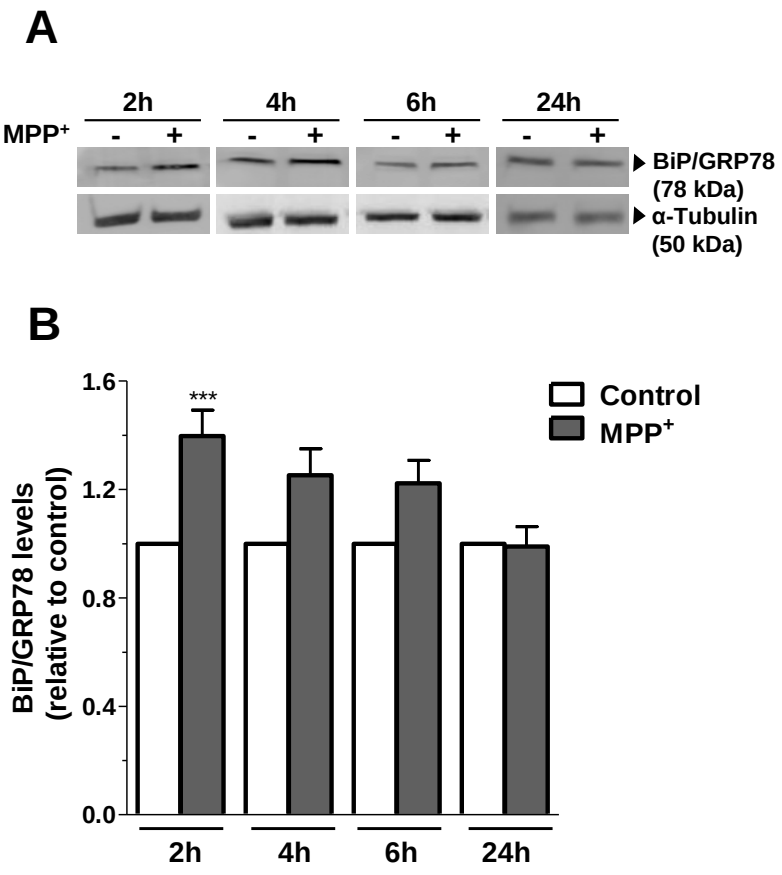

Figure III.2. The unfolded protein response is activated in an early phase by MPP+ in NT2 neuron-like cells.

A. Whole-cell lysates from untreated and MPP^+-treated cells were prepared as described in Chapter II and the levels of BiP/GRP78 were determined by immunobloting analysis for 2, 4, 6 and 24 h. The blots were reprobed for α-tubulin to confirm equal protein loading. The data are from representative blots. **B.** Quantification of BiP/GRP78 levels by densitometric analysis of each time point corresponding blots. Data are reported as the fold increase over the untreated cell values (control) (n=3-10; ***p<0.001, relative to control).

Surprisingly, the levels of this ER chaperone was extensively up-regulated by MPP^+ treatment upon 2 h, being observed a suppression of its expression pattern along the time course studied.

We suggest that, eventually, an increase in ROS production elicited by mitochondrial deficits at respiratory chain level potentiated this ER stress response.

3.3.3 Ca^{2+} is the mediator in the ER and mitochondria communication

Mitochondria and the ER form two intertwined endomembrane networks and their dynamic physical interactions control metabolic flow, protein transport and intracellular Ca^{2+} homeostasis (Ferri and Kroemer, 2001; Berridge et al., 2003; Levine and Rabouille, 2005). Therefore, we appointed Ca^{2+} as a potential mediator in the communication between these two organelles in the context of sPD pathology.

To investigate this point, we determined the ER Ca^{2+}-content after cell treatment with MPP^+ for the different time points studied. The ER Ca^{2+}-content was evaluated by changes in cytosolic Ca^{2+}, monitored using the Fura-2AM probe. Cytosolic Ca^{2+} was measured before and after the addition of thapsigargin (TPG), which evokes Ca^{2+} release from the ER (**Figures III.3A-D**). Overall, **Figure III.3E** shows that MPP^+ promoted a gradual and sustained decrease of Ca^{2+} content in the ER.

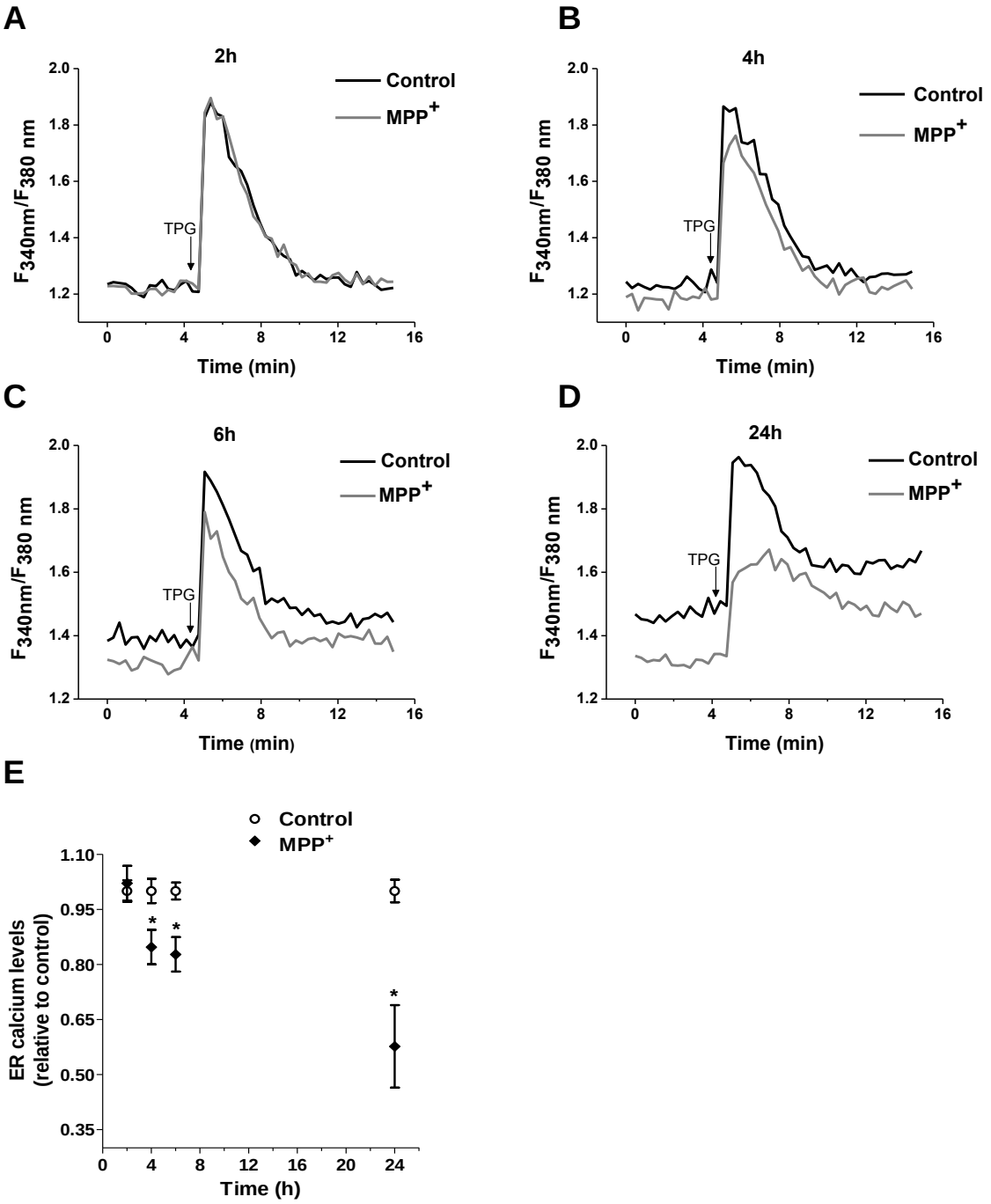

Figure III.3. MPP^+ triggers Ca^{2+} release from ER stores.

Untreated (control) and MPP^+-treated cells were loaded with 5 µM of Fura-2,AM for the fluorescence measurement of the ER Ca^{2+}-content. **A-D** Representative traces of the fluorometric measurement of cytosolic Ca^{2+} levels for the indicated time points. Cytosolic Ca^{2+} was measured before and after the addition of 5 µM thapsigargin (TPG) to evoke ER Ca^{2+} release (denoted as an arrow on the graphs). **E.** Measurement of ER Ca^{2+} released after TPG stimulation. The measurement of Ca^{2+} released was obtained by subtracting the fluorescence after to the fluorescence before TPG addition (n=4; *p<0.05, relative to control).

We further investigated whether the observed ER Ca^{2+} changes are accompanied by changes in mitochondrial Ca^{2+}-content. Mitochondria, by virtue of their membrane potential (**Figure III.1**) provide a sink for the buffering of cytoplasmic Ca^{2+} after the ionophore calimycin (A23187) stimuli. Therefore, we have also evaluated Ca^{2+} clearance by mitochondrial uptake and subsequent Ca^{2+} accumulation in the mitochondrial compartment following MPP^+ treatment. After establishment of a stable baseline, cells were challenged with A23187, which rapidly increased the Rhod-2AM fluorescence, demonstrating Ca^{2+} accumulation in the mitochondrial matrix (**Figures III.4 A-D**).

We have also observed that MPP^+ led to an accumulation of Ca^{2+} in the mitochondrial matrix after 4 h treatment, which is in accordance with the decrease in the ER compartment for the same time point (**Figures III.3E and III.4E**).

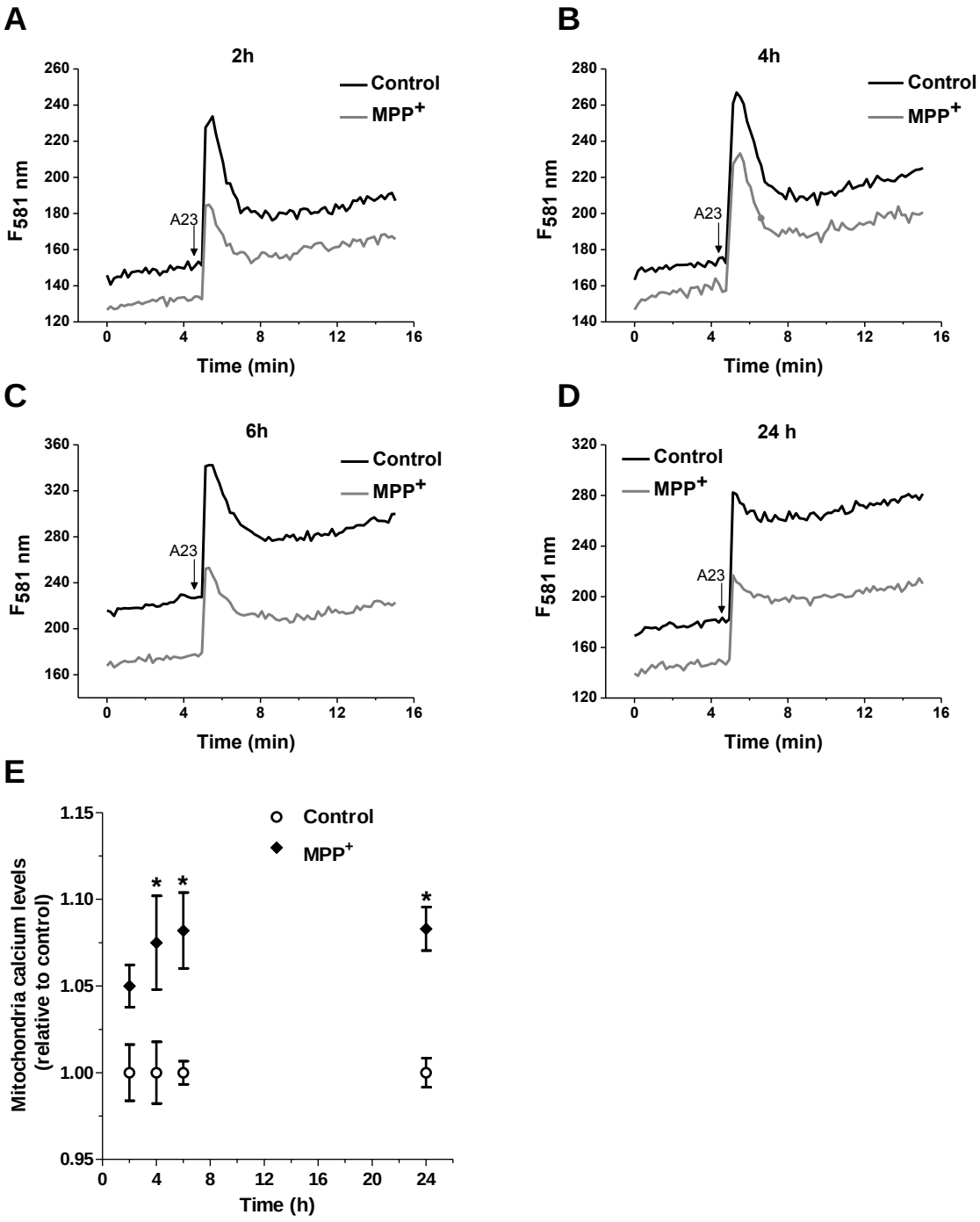

Figure III.4. MPP$^+$ triggers Ca^{2+} uptake by mitochondria from cytosolic pools.

Untreated (control) and MPP$^+$-treated cells were loaded with 10 µM of Rhod-2, AM for the fluorescence measurement of mitochondrial Ca^{2+}-content. **A-D** Representative traces of the fluorometric measurement of mitochondrial matrix Ca^{2+} levels for the indicated time points. Mitochondrial matrix Ca^{2+} was measured before and after the addition of 5 µM of calimycin (A23187, A23) to take the mitochondrial maximal uptake ability (denoted as an arrow on the graphs). **E.** Measurement of Ca^{2+} uptake by mitochondria. The measurement of mitochondrial Ca^{2+} uptake was obtained by the ratio of fluorescence before over total fluorescence after A23187 addition (n=4; *p<0.05, relative to control).

Taken collectively, these results demonstrate that Ca^{2+} release from the ER incited by MPP^+ invariably induces mitochondrial Ca^{2+} uptake with a rise in mitochondrial matrix free Ca^{2+} after MPP^+ treatment for 4 h. This suggests a qualitative inverse relationship between Ca^{2+} changes in the ER and mitochondria compartments.

Besides, these findings are consistent with the $\Delta\psi_m$ data (**Figure III.1**), which pointed that $\Delta\psi_m$ is not affected by the presence of MPP^+ until 24 h and that there is a correlation between the maintenance of $\Delta\psi_m$ and the ability of mitochondria to take up Ca^{2+}.

3.3.4 Mitochondria stress initiates ER and mitochondria caspase-dependent cell death

We next decided to examine the mechanisms that the ER and mitochondria use to initiate and propagate cell death signals and its involvement in the control of neuronal death in a sPD context.

Firstly, following the cascade of death signalling downstream of the ER, we have analyzed the involvement of caspase-4 induced by MPP^+. As shown in **Figure III.5A**, an increase in Ac-LEVD-*p*NA cleavage (caspase-4 activation) was only observed upon treatment with MPP^+ for 24 h.

We have also analyzed caspase-2 and caspase-9 activities, which are thought to be involved in the cell death signals propagation triggered by mitochondria (Slee et al., 1999; Susin et al., 1999; Guo et al., 2002). As shown in **Figures III.5B** and **C**, the activation pattern of caspase-2 (Ac-VDVAD-*p*NA cleavage) was similar to caspase-9 (Ac-LEDH-*p*NA cleavage) and it was more marked in later stages following the treatments with MPP^+.

Additionally, since caspase-3 is an effector caspase in the apoptotic process, and to better characterize the cell death mechanisms mediated by MPP^+, it was also our interest to analyze its effects on caspase-3 activation. We observed an increase in Ac-DEVD-*p*NA cleavage (caspase-3 activation) within 6 h, which was detectable till to 24 h treatment with MPP^+ (**Figure III.5D**). To confirm the involvement of the ER Ca^{2+} in the activation of this caspase-cascade, we analyzed caspase-3 activation by MPP^+ in cells exposed previously to dantrolene. We have observed that dantrolene, which blocks the ER Ca^{2+} release, was able to prevent MPP^+-mediated caspase-3 activation (**Figure III.5E**).

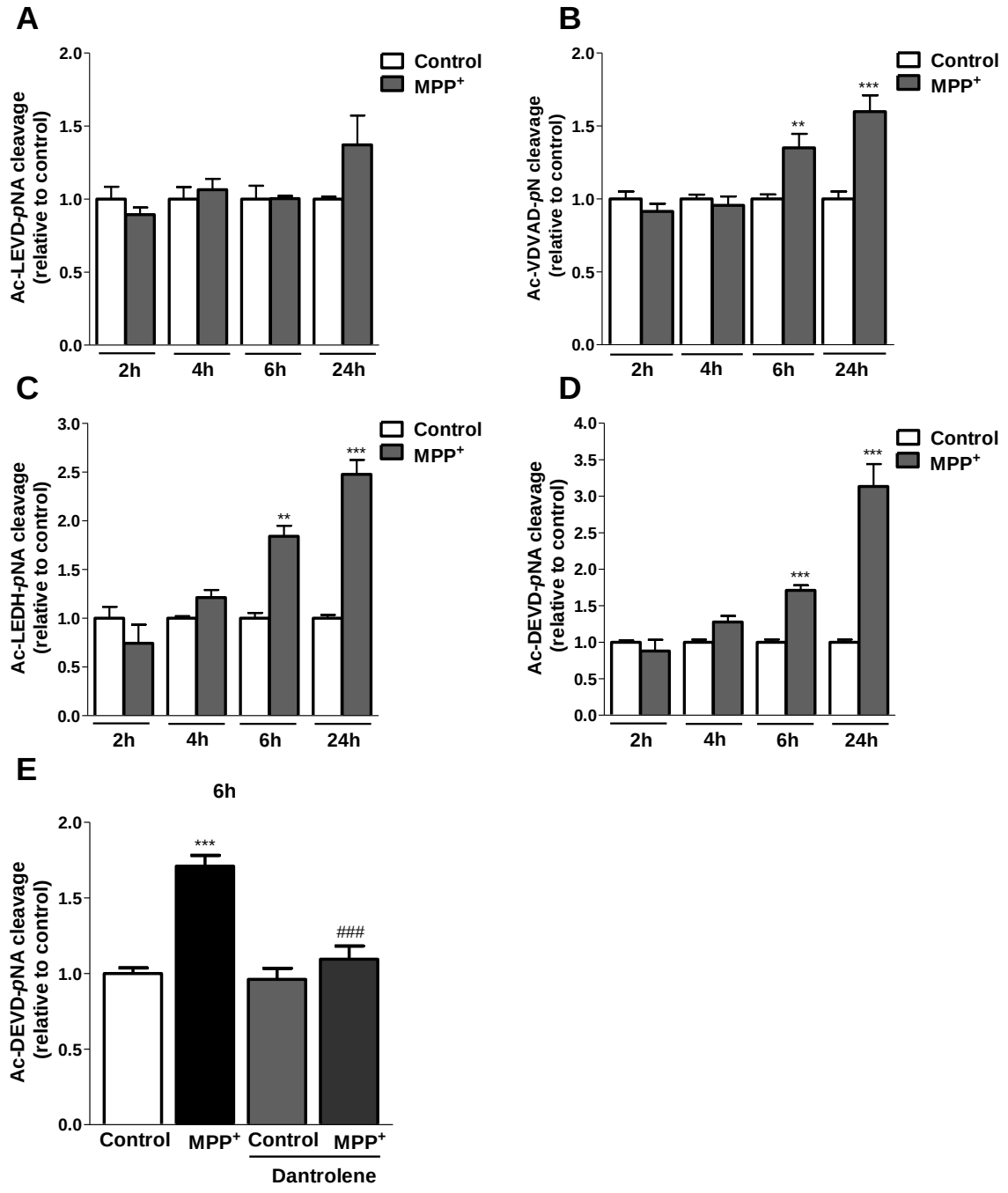

Figure III.5. MPP$^+$-induced ER and mitochondria stress activates ER and mitochondria-dependent apoptotic pathways. A-D Effect of MPP$^+$ on caspase 4-like activity (Ac-LEVD-*p*NA cleavage) (**A**), caspase 2-like activity (Ac-VDVAD-*p*NA cleavage) (**B**), caspase 9-like activity (Ac-LEDH-*p*NA) (**C**), and caspase 3-like activity (Ac-DEVD-*p*NA cleavage) (**D**), respectively. Caspase activation was evaluated spectrophotometrically at 405 nm as described in Chapter II. Data are expressed relative to the basal activity observed in the untreated NT2 cells (n=4-8; **p<0.01, ***p<0.001 relative to control). **E.** Protective effect of dantrolene on MPP$^+$-induced caspase-3 activation. Data are expressed relative to the basal activity observed in the untreated NT2 cells (n=3; **p<0.01; ***p<0.001, relative to control; $^{###}$p<0.001, relative to MPP$^+$-treated cells).

3.4 Discussion

In this study, we have investigated the molecular mechanisms underlying the crosstalk between the ER and mitochondria and their relevance to the sPD pathology. We provide some lines of direct evidence indicating that mitochondria and the ER can establish a dynamic signaling pathway, which is crucial for the activation of a cascade of cellular signals that culminates in apoptotic cell death.

First, we have characterized mitochondrial function upon MPP^+ treatments. Our results demonstrate that MPP^+, as expected, led to a steady decrease in the complex I oxidoreductase activity as soon as 2 h, but only induced considerable changes in $\Delta\psi_m$ at 24 h. Second, our results also indicate that an altered mitochondrial respiratory chain complex I activity seems to play an essential role in the ER-induced stress response. UPR as a consequence of ER stress was elicited by MPP^+ at 2 h, indicating that mitochondria complex I activity may regulate an ER response. These results are in agreement with previous ones that reported the activation of UPR induced by 6-OHDA and MPP^+ in cellular models of PD and in dopaminergic neurons of the SNpc of PD patients (Ryu et al., 2002; Holtz and O'Malley, 2003; Cooper et al., 2006; Hoozemans et al., 2007). MPP^+ is thought to induce oxidative stress by mitochondrial function inhibition. The consequent accumulation of oxidized proteins that hinder the cellular protein degradation mechanisms leads to an accumulation of misfolded proteins into the ER (Friedlander et al., 2000). Interestingly, we have previously demonstrated, in the same cellular model, that MPP^+-treatment for 2 h induces an increased generation of ROS (Domingues et al., 2008).

Moreover, changes in the redox state and the presence of ROS also affect the Ca^{2+} homeostasis by modulating the functionality of ER-based channels and buffering chaperones [for review see (Gorlach et al., 2006)]. In such instance, we suggest that a close relationship exists between ROS generation mediated by MPP^+ and the ER stress, further contributing to the disruption of the mitochondrial function.

Our hypothesis is that the ER and mitochondria communicate via Ca^{2+} exchanges facilitated by the close proximity of their membranes that easily exchange lipids, Ca^{2+} and glycoproteins (Chandra et al., 1998; Rizzuto et al., 1998).

Ca^{2+} is one of the most important elements in cellular signaling. The ER, besides playing a major role in regulating synthesis, folding and transport of proteins, functions also as a dynamic Ca^{2+} store. The dynamic changes in free-cytosolic and in the ER Ca^{2+} are regulated by a number of factors including intracellular Ca^{2+} buffers (Ca^{2+} binding proteins, nucleotides and phosphate) and Ca^{2+}-transporting systems (Ca^{2+} channels and Ca^{2+}-ATPases). Moreover, mitochondria have been postulated to play an important role

as Ca^{2+} buffers participating in the intracellular Ca^{2+} handling machinery in stimulated cells (Hoth et al., 1997; Hajnoczky et al., 1999; Hoth et al., 2000). More recently, mitochondria have been considered not only as high-capacity Ca^{2+} buffers but also as active elements of the intracellular signaling system (Parekh, 2003; Butow and Avadhani, 2004).

In this work, we have found that MPP^+ evokes a gradual decrease in the ER Ca^{2+} content, concomitantly to an Ca^{2+} increase into the mitochondrial matrix. These results demonstrate that a net flux of Ca^{2+} from the ER to mitochondria occurs under ER and mitochondria stress conditions.

In fact, Ca^{2+} release from the ER has been implicated as a key signaling event in many apoptotic models and it may sensitize mitochondria to trigger apoptotic cell death. Furthermore, a growing number of ER proteins have been described to influence apoptosis by either interacting with Bcl-2 family members or altering ER Ca^{2+}-responses, whereas several ER proteins are caspase substrates that may regulate the execution phase of apoptosis [for review see (Breckenridge et al., 2003b)].

Our results revealed that stress in the ER and the subsequent ER Ca^{2+}-release triggers a caspase-4 dependent pathway and also a mitochondrial-dependent apoptotic pathway, which leads to the activation of caspase-2 and -9. We propose that these two components of the ER and mitochondria stress can apparently work together to activate caspase-3, an executer caspase of the apoptotic process. Moreover, we proved, by inhibiting ryanodine receptors-mediated Ca^{2+} release with dantrolene, that ER Ca^{2+} fluxes evoked by MPP^+ were able to induce caspase-3 activation.

Our results highlight the inevitable role of ER to mitochondria Ca^{2+} fluxes and their requirement to mitochondria-dependent cell death induction, enclosing a feedback loop whereas mitochondria signal ER, ER induces further mitochondrial alterations, like $\Delta\psi_m$ loss, leading to the activation of a cascade of signals that culminates in apoptotic cell death.

CHAPTER IV

ER-mediated stress induces mitochondrial-dependent caspases activation in NT2 neuron-like cells

4.1 Summary

Recent studies have revealed that endoplasmic reticulum (ER) disturbance is involved in the pathophysiology of neurodegenerative disorders contributing to the activation of the ER stress-mediated apoptotic cell death pathway.

Here, we investigated the molecular mechanisms underlying the interplay between the ER and mitochondria, focusing on calcium as a potential mediator and its relevance for the control of cell death signals.

Using NT2 cells treated with brefeldin A or tunicamycin, two ER stressors, we observed that ER stress induced changes in the mitochondrial function, affecting the mitochondrial membrane potential and the electron transport chain function. Moreover, stress stimuli at ER level evoked calcium fluxes between the ER and mitochondria. Under these conditions, ER stress activated the unfolded protein response by the overexpression of BiP/GRP78, although this chaperone was unable to prevent mitochondria-dependent caspases activation.

Our findings show that ER and mitochondria interconnection play a prominent role in the neuronal cell death induction under particular ER stress circumstances.

4.2 Introduction

The endoplasmic reticulum (ER) has several important functions including the regulation of intracellular calcium (Ca^{2+}) homeostasis, protein glycosylation, and formation of disulfide bounds and folding and assembly of newly synthesized secretory proteins.

Under various conditions, ER function is disturbed leading to the accumulation of unfolded proteins and activation of a sporadic ER stress response, also known as unfolded protein response (UPR). In an attempt to survive, cells develop self-protective mechanisms, whereby conditions within the ER are communicated to the protein translation machinery and to the nucleus in order to restore cellular homeostasis. When cells are subjected to severe or prolonged ER stress, the transcriptional factor CHOP/Gadd153 is activated and apoptotic cell death may occur (Kaufman, 1999a, b; Paschen et al., 2001). ER stress has been implicated in many important diseases, including neurodegenerative disorders. We have recently demonstrated that the Alzheimer's disease-associated amyloid-β peptide induces ER stress contributing to Ca^{2+} release through ryanodine (RyR) and inositol 1,4,5-triphosphate (IP_3R) receptors, with subsequent increase in intracellular Ca^{2+} levels and induction of apoptosis (Ferreiro et al., 2006). Moreover, it has been demonstrated the up-regulation of ER chaperones, such as protein disulfide isomerase (PDI) in postmortem brain tissues and cell culture models of Parkinson's disease (PD), accumulating preferentially in Lewy bodies (Conn et al., 2004). Recent studies in cultured cells, including dopaminergic neurons, have demonstrated that PD-related neurotoxins, such as 6-hydroxydopamine (6-OHDA) and *N*-methyl-4-phenyl-1,2,3,6 tetrahydropyridine (MPTP) or even its active metabolite 1-methyl-4-phenylpyridinium (MPP^+), trigger ER stress and are also involved in the up-regulation of diverse components of the UPR (Ryu et al., 2002; Holtz and O'Malley, 2003; Arduino et al., 2009a). Moreover, mitochondria are often closely associated with the ER providing the conditions for a local and privileged communication between the two organelles (Csordas et al., 2006).

Therefore, it seems worthwhile to unveil the molecular mechanisms that coordinate the interplay between the ER stress and mitochondrial function and their relevance for the control of cell death.

In the present work, we report that mitochondrial function is sensitive to ER stress stimuli and identify Ca^{2+} fluxes in the ER and mitochondria axis as key factors for cell death signals triggered by the ER and mitochondria stress.

4.3 Results and Discussion

4.3.1 Brefeldin A and tunicamycin activate the unfolded protein response

To induce ER stress, we used two pharmacological agents, employed as ER stress inducers, that block ER to Golgi protein trafficking (brefeldin A, BFA) or that inhibit *N*-linked glycosylation reactions (tunicamycin, TUN).

Upon stress induction, ER activates the UPR by the induction of ER resident stress proteins, referred to as the glucose-regulated proteins (GRPs) (Lee, 1992). GRPs are Ca^{2+}-binding chaperone proteins with protective properties. The best characterized GRP is GRP78, a 78-kDa protein also referred to as BiP. BiP/GRP78 is an essential regulator of the ER function due to its role in protein folding and assembly, ER Ca^{2+} binding and controlling the activation of transmembrane ER stress inducers (Little et al., 1994; Lee, 2001). The cytoprotective function of BiP/GRP78 has been well recognized in several experimental systems (Rao et al., 2002; Reddy et al., 2003; Lee, 2005).

Figure IV.1 shows a representative BiP/GRP78 immunoblot (**Figure IV.1A**) and the corresponding protein levels (**Figure IV.1B**) in cells treated with BFA or TUN. Results show that the levels of this protein were up-regulated by BFA and TUN, indicating that BFA and TUN elicit ER stress.

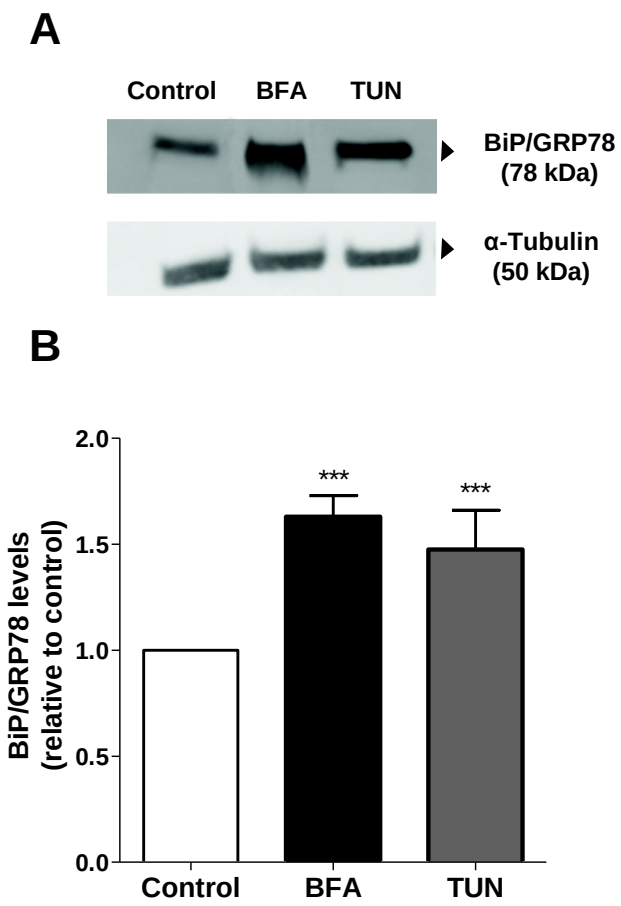

Figure IV.1. Induction of UPR after exposure of NT2 cells to ER stress.

A. Expression of BiP/GRP78 was determined by immunoblot analysis from untreated (control) and ER stressors (BFA, TUN)-treated cells. The blots were reprobed for α-tubulin to confirm equal protein loading. The data are representative blots. **B.** Quantification of BiP/GRP78 levels by densitometric analysis of the corresponding blots. Data are reported as the fold increase over the untreated cell values (n=8; ***p<0.001, relative to control).

4.3.2 Ca^{2+} is the link in the ER to mitochondria communication axis

ER, besides playing a major role in regulating synthesis, folding, and transport of proteins, functions also as a dynamic Ca^{2+} store. The dynamic changes in free/cytosolic and in ER Ca^{2+} are regulated by a number of factors, including intracellular Ca^{2+} buffers and Ca^{2+} transporting systems (channels and ATPases). Moreover, mitochondria have been suggested to play an important role as Ca^{2+} buffers, participating in the intracellular Ca^{2+} handling machinery in stimulated cells (Hajnoczky et al., 1999; Hoth et al., 2000; Butow and Avadhani, 2004). More recently, mitochondria have been considered not only

as high-capacity Ca^{2+} buffers but also as active elements of the intracellular signaling system (Parekh, 2003; Sadek et al., 2004).

Therefore, we appointed Ca^{2+} as a potential mediator in the communication between these two organelles. To investigate this point, we determined ER Ca^{2+} content after cell treatment with ER stressors. ER Ca^{2+} content was assessed by changes in cytosolic Ca^{2+}, monitored using Fura-2, AM. Cytosolic Ca^{2+} was measured before and after the addition of thapsigargin to evoke ER Ca^{2+} release. The difference in cytosolic Ca^{2+}calcium before and after thapsigargin addition was taken as a measure of ER Ca^{2+} store. As shown in **Figure IV.2**, both ER stressors were able to induce Ca^{2+} release from the ER lumen (**Figure IV.2A**), demonstrated by the very low levels of ER Ca^{2+} content (**Figure IV.2B)**.

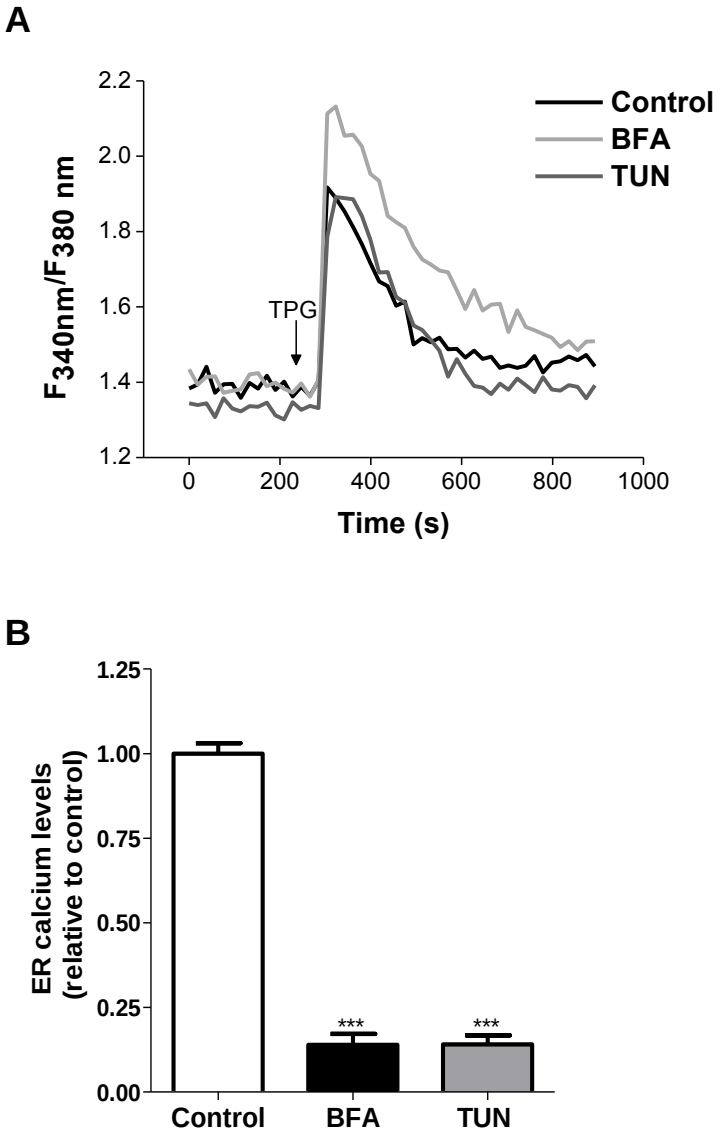

Figure IV.2. Cellular Ca^{2+} fluxes upon ER stress in NT2 cells.

Untreated (control), BFA or TUN treated cells were loaded with 5 µM Fura-2, AM for the fluorescence measurement of ER Ca^{2+} content. **A.** Representative trace of the fluorometric measurement of cytosolic Ca^{2+} levels for the indicated time points. Cytosolic Ca^{2+} was measured before and after the addition of 5 µM TPG to evoke ER Ca^{2+} release (denoted as an arrow on the graph). **B.** Measurement of ER Ca^{2+} released after TPG stimulation. The measurement of Ca^{2+} released was obtained by subtracting the fluorescence after to the fluorescence before TPG addition Data are reported in relation to untreated cells values (control) (n = 4, ***P ＜0.001, compared to control).

We further investigated whether the observed ER Ca^{2+} changes are accompanied by changes in mitochondrial Ca^{2+} content. The mitochondria, by virtue of their sustained membrane potential, provide a sink for the buffering of cytoplasmic Ca^{2+} after the calcium ionophore calimycin (A23187) stimuli. Thus, we evaluated Ca^{2+} clearance by mitochondrial uptake and subsequent Ca^{2+} accumulation in the mitochondrial compartment following the treatments indicated before. After establishment of a stable baseline, as a measure of basal mitochondrial Ca^{2+} stores, cells were challenged with the A23187, which rapidly increased the Rhod-2, AM fluorescence, demonstrating a mitochondrial matrix calcium accumulation (**Figure IV.3A**). The ratio between mitochondrial matrix calcium before and after challenging with A23187 was taken as an indirect measure of mitochondrial calcium content.

In accordance with calcium fluxes release from ER (**Figure IV.2)**, we detected a significant increase in mitochondrial calcium content induced by both ER stressors (**Figure IV.3B**).

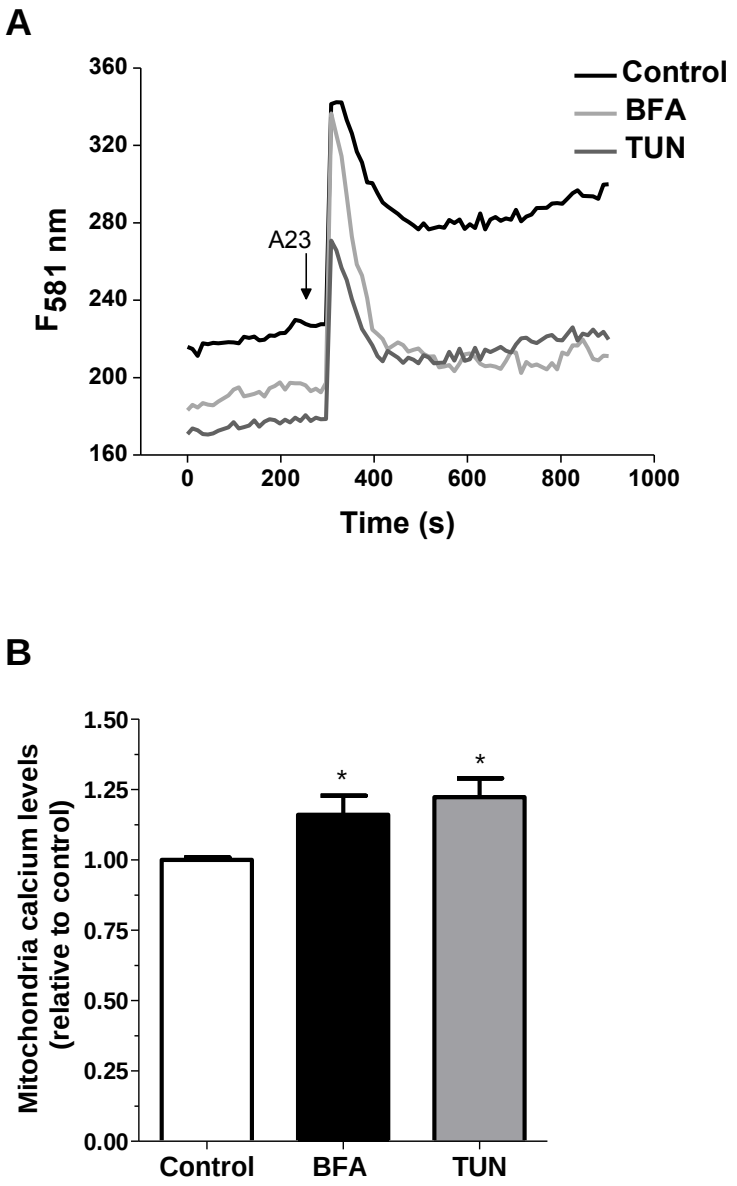

Figure IV.3. Mitochondrial Ca^{2+} uptake fluxes upon ER stress induction in NT2 cells.

Untreated (control) and BFA or TUN treated cells were loaded with 10 µM Rhod-2, AM for the fluorescence measurement of mitochondrial calcium content. **A.** Representative trace of the fluorometric measurement of mitochondrial matrix Ca^{2+} levels. Mitochondrial matrix Ca^{2+} was measured before and after the addition of 5 µM A23187 (A23) to take the mitochondrial maximal uptake ability (denoted as an arrow on the graph). **B.** Measurement of Ca^{2+} uptake by mitochondria. The measure of mitochondrial Ca^{2+} uptake was obtained by the ratio of fluorescence before over the total fluorescence after A23187 addition (n=4; *p<0.05, compared to the control).

These results lead us to presume that ER and mitochondria are in a close communication, establishing a dynamic signalling pathway.

4.3.3 Brefeldin A and tunicamycin-evoked Ca^{2+} fluxes affect mitochondrial function

Although we have demonstrated that ER induced stress potentiates mitochondrial Ca^{2+} uptake, we hypothesized that ER and mitochondria communication via Ca^{2+}exchanges could stimulate alterations in mitochondrial function.

Therefore, we have investigated the functional significance of ER stress induction on mitochondrial function and its contribution to the initiation of cell death. We evaluated changes on $\Delta\psi_m$. As shown in **Figure IV.4A**, a slight decrease in rhodamine 123 (Rh123) retention induced by ER stress inducers was observed, suggesting that these compounds did not incite a substantial mitochondrial depolarization.

In addition, we have also evaluated the mitochondria respiratory chain NADH-ubiquinone oxidoreductase (complex I) activity. Results shown in **Figure IV.4B** demonstrate that both BFA and TUN provoked a statistically significant decrease in mitochondrial respiratory chain complex I activity.

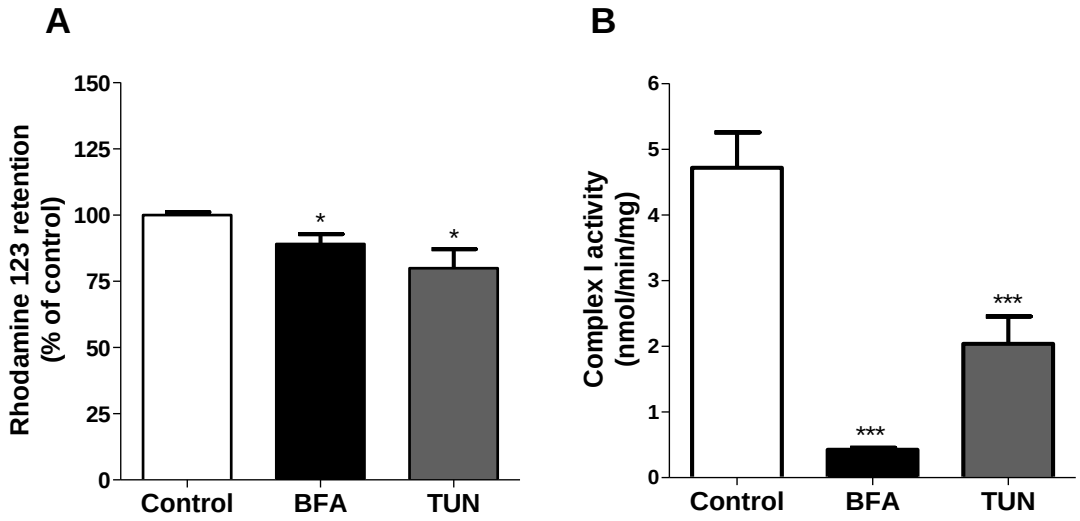

Figure IV.4. Effects of BFA and TUN on mitochondrial function.

A. Changes in mitochondrial membrane potential induced by BFA and TUN stressors were estimated using the fluorescent cationic dye Rh123. Data are expressed as a percentage of the untreated cells values (control) (n=3; *p<0.05, relative to control). **B.** Mitochondrial respiratory chain complex I activity was determined as described in Chapter II. Data are reported in nmol/min/mg as the mean±SEM (n=4; ***p<0.001, relativel to control).

Overall, these results indicate that mitochondrial respiratory chain activity is sensitive to the effects induced by brefeldin A and tunicamycin at ER level.

4.3.4 Brefeldin A- and Tunicamycin-induced stress activates ER- and mitochondria-dependent caspase cascades

Ca^{2+} release from the ER has been implicated as a key signaling event in many apoptotic models and it may influence the sensitivity of mitochondria to apoptotic alterations. Moreover, a recent discovery that a subpopulation of BiP/GRP78 can exist as an ER transmembrane protein implies that it can potentially interact directly with the cytosolic components of the apoptotic pathway and regulate their activity (Rao et al., 2002; Reddy et al., 2003). For instance, GRP78 has been reported to form complexes with procaspases, such as mouse caspase-12, which associates with the outer ER membrane (Reddy et al., 2003). The protective function of BiP/GRP78 against a wide variety of stresses suggests that BiP/GRP78 may also interfere with the activity of key upstream regulators of apoptosis.

Thus, we decided to examine the mechanisms through which ER-induced stress initiate and propagate cell death signals and its involvement in the control of cell death. Firstly, following the cascade of death signalling downstream of ER, we analyzed the involvement of caspase-4. As shown in **Figure IV.5A**, a significant increase in Ac-LEVD-*p*NA cleavage by activated caspase-4 was observed upon BFA treatment only.

Previously, it has been demonstrated that BFA and TUN promote the translocation of cytochrome c from the mitochondrial matrix to the cytosol (Elyaman et al., 2002; Izuta et al., 2008). In line with this, we further analyzed the caspase-2 activity, which appears to act upstream of cytochrome c release and to be involved in the ER stress-mediated death (Guo et al., 2002; Lassus et al., 2002; Seo et al., 2006b), and caspase-9 activity, which is thought to be involved in the cell death signals propagation triggered by mitochondria (Slee et al., 1999). As shown in **Figure IV.5B**, only TUN activated caspase-2 (Ac-VDVAD-*p*NA cleavage). Both ER stressors activated caspase-9 (Ac-LEDH-*p*NA) (**Figure IV.5C**).

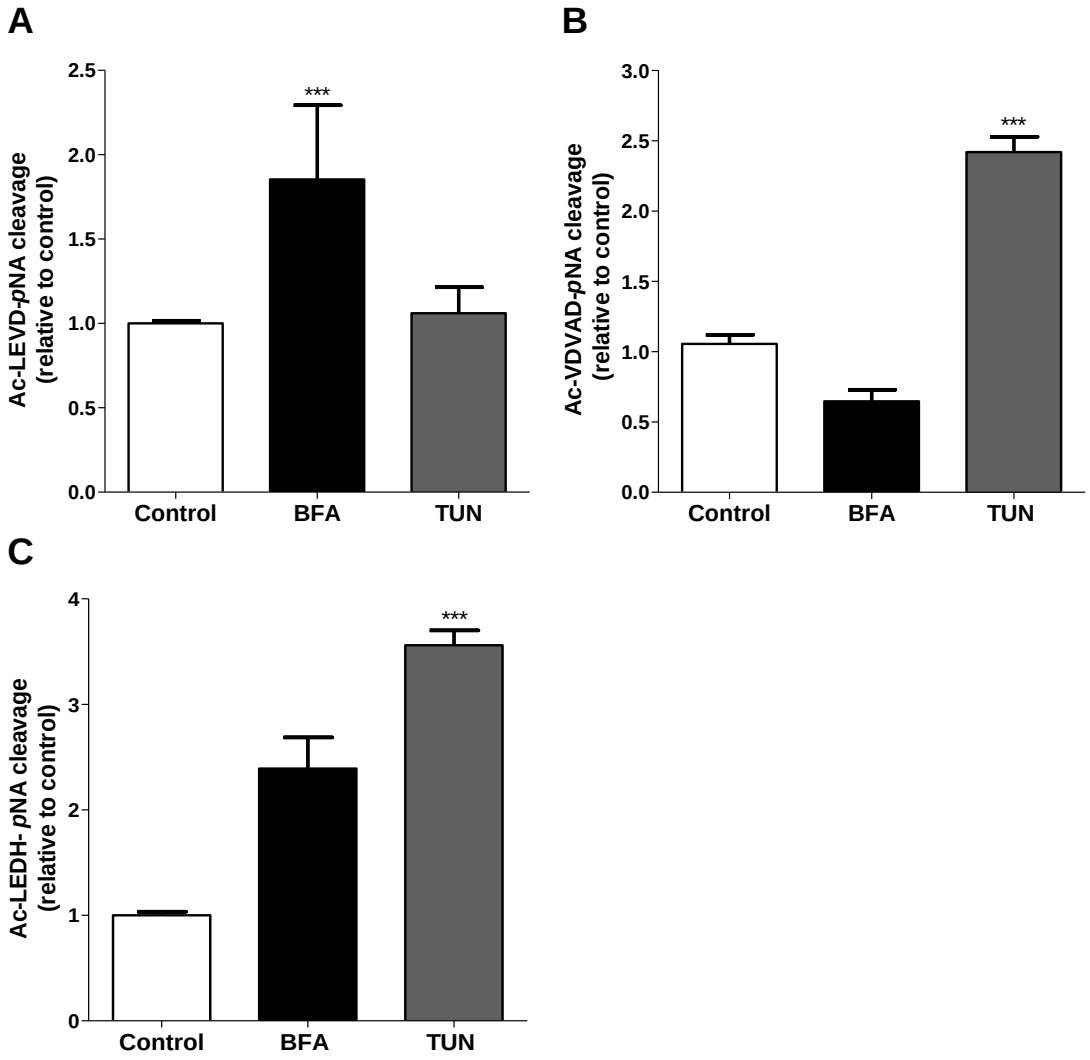

Figure IV.5. Effects of ER stress on caspase activation in NT2 cells.

Effect of brefeldin A (BFA) and tunicamycin (TUN) on caspase 4-like activity (Ac-LEVD-*p*NA cleavage) **(A)**, caspase 2-like activity (Ac-VDVAD-*p*NA cleavage) **(B),** and caspase 9-like activity (Ac-LEDH-*p*NA cleavage) **(C)**. Data are expressed relative to the basal activity observed in the untreated NT2 cells (control) (n=3-6; **p<0.001, ***p<0.001, relative to control).

Interestingly, BFA and TUN differentially regulated the activation of caspase-4 and -2. BFA, by preventing anterograde transport and leading to the backflow of Ca^{2+} into the ER lumen, can activate caspase-4, but TUN, as an inhibitor of the *N*-glycosylation reactions of proteins in ER membrane, cannot. In support of this hypothesis, caspase-4 was shown to be activated by ER stress in a specific-manner and not by membrane- or mitochondria-targeted signals (Hitomi et al., 2004).

Our results revealed that stress in the ER and the subsequent ER Ca^{2+} release triggers a caspase-4 dependent pathway and also a mitochondrial-dependent apoptotic

pathway, which leads to the activation of caspase-2 and -9. We suppose that these two components of the ER and mitochondria stress can apparently work independently. These results are consistent with a previous study which showed that BFA induces typical apoptosis features, such as mitochondrial breach and cell shrinkage, in follicular lymphoma cells (Guo et al., 2002).

First, our results demonstrated that ER stressors induced ER Ca^{2+} release to the cytosol. Second, perturbations at ER level by BFA and TUN potentiated Ca^{2+} uptake by mitochondria. Third, ER stress led to a low decrease of mitochondria membrane potential, with a substantial decline in the rotenone sensitive NADH oxidation.

Taken together, these results led us to infer the inevitable role of Ca^{2+} fluxes between the ER and mitochondria and subsequent caspase activation, representing a link between ER deregulation and mitochondria-dependent apoptotic pathways.

CHAPTER V

Mitochondrial metabolism in Parkinson's disease impairs quality control autophagy by hampering microtubule-dependent traffic

5.1. Summary

Abnormal presence of autophagic vacuoles is evident in brains of patients with Parkinson's disease (PD), in contrast to the rare detection of autophagosomes in a normal brain. However, the actual cause and pathological significance of these observations remain unknown.

Here, we demonstrate a role for mitochondrial metabolism in the regulation of the autophagy-lysosomal pathway in *ex vivo* and *in vitro* models of PD. We show that transferring mitochondria from PD patients into cells previously depleted of mitochondrial DNA is sufficient to reproduce the alterations in the autophagic system observed in PD patient brains. Although the initial steps of this pathway are not compromised, there is an increased accumulation of autophagosomes associated with a defective autophagic activity. We prove that this functional decline was originated from a deficient mobilization of autophagosomes from their site of formation toward lysosomes due to disruption in microtubule-dependent trafficking. This contributed directly to a decreased proteolytic flux of α-synuclein and other autophagic substrates.

Our results lend strong support for a direct impact of mitochondria in autophagy as defective autophagic clearance ability secondary to impaired microtubule trafficking is driven by dysfunctional mitochondria. We uncover mitochondria and mitochondria-dependent intracellular traffic as main players in the regulation of autophagy in PD.

5.2. Introduction

Parkinson's disease (PD) is a common neurodegenerative movement disorder, characterized by a dramatic loss of midbrain dopaminergic neurons in the substantia nigra pars compacta (SNpc), and the presence of ubiquitylated α-synuclein-containing intracytoplasmic inclusions called Lewy bodies (LBs) in surviving SNpc neurons (Forno, 1996).

Ageing is considered the greatest risk factor for sporadic PD (sPD). Accumulation of mitochondrial DNA (mtDNA) mutations and mitochondria-driven oxidative stress is thought to represent a bridge between sPD and the natural ageing process. Mitochondrial association with sPD was established when a mitochondrial NADH dehydrogenase (complex I) activity deficit was identified in the SNpc of post-mortem PD patient brains (Schapira et al., 1989) and in PD patient platelets (Parker et al., 1989). In addition, mtDNA involvement in complex I defects observed in PD platelets was further recognized after transference of platelet mitochondria into mtDNA-deficient cell lines and validated in the resultant cell lines known as ''cybrids'' (Swerdlow et al., 1996). Data obtained using this *ex vivo* cellular model have shown that several pathogenic features observed in PD subject brains are actually recapitulated by PD cybrids (Cardoso, 2011; Swerdlow, 2011). Moreover, the generation of fibrillar and vesicular protein inclusions in sPD cybrids replicating most antigenic and structural features of LBs was reported (Trimmer et al., 2004b; Esteves et al., 2009).

The presence of LBs-like structures in sPD cybrids suggests that mitochondrial dysfunction associated with defective protein handling may account for PD pathogenesis. Relevant to PD pathology, autophagy represents a major mechanism by which intracellular long-lived proteins, protein aggregates (such as α-synuclein oligomers) and entire cytoplasmic organelles (such as mitochondria) are directly degraded within lysosomes. It is now considered that constitutive basal autophagic activity is a main quality control (QC) process that selectively disposes aberrant protein aggregates and damaged organelles for degradation (Lee et al., 2010b; Lee et al., 2010a). Thus, the regulation of QC autophagy may be critical to restrain the neurodegenerative process (Wong and Cuervo, 2010; Arduino et al., 2011b).

In line with this, growing evidence has suggested a role for autophagy deregulation in PD. Increased number of autophagosomes has been observed in cultured cells treated with mitochondrial complex I inhibitors such as 1-methyl-4-phenylpyridinium (MPP^+), rotenone and 6-OHDA (Chen et al., 2007; Dagda et al., 2008), and in postmortem PD patient brains (Anglade et al., 1997). Although these changes have been

commonly interpreted as an abnormal induction of autophagy, the actual origin and significance of these observations for the disease pathogenesis remain elusive.

Here, we investigated cause-and-effect relationships between mitochondrial dysfunction, microtubule network disruption and accumulation of autophagosomes and autophagy substrates. Using sPD cybrid cells, mtDNA-depleted cells and MPP^+-treated primary cortical neurons, we characterized basal and induced autophagic responses and the clearance of autophagy cargos. We found that changes in mitochondrial function *per se* have a severe impact on autophagy since autophagosomes are actually actively formed but inefficiently cleared in sPD cells. Molecular dissection of each of the steps revealed that microtubule disruption rather than abnormal induction of autophagy gives rise to the characteristic patterns of autophagic pathology observed in PD.

5.3. Results

5.3.1. Hybrid cells harboring sPD patient mitochondria and mtDNA-depleted cells accumulate morphologically abnormal mitochondria and nonfused autophagic vacuoles

To directly explore the functional consequences of an altered mitochondrial function over the autophagic-lysosomal system in the context of sPD, we modeled PD by creating transmitochondrial cytoplasmic hybrid cell lines (cybrids) in which endogenous mitochondrial DNA (mtDNA) from sPD or control (CT) subject platelets was transferred to human teratocarcinoma (NT2) cells after complete depletion of endogenous mtDNA (Rho0 cells). By this approach, it is possible to follow the effects of mtDNA heteroplasmy within a nuclear and environmentally controlled context, thus providing a rational basis for the propagation of PD-related mitochondrial dysfunction, including a decline in mitochondrial ATP synthesis capacity and other mitochondria-dependent processes.

In this study, we used the same cohort of cybrids that was previously characterized in terms of mitochondrial bioenergetics (Esteves et al., 2010c). In this cohort, sPD cybrids were found to have a reduced complex I function, though citrate synthase activity, a commonly used quantitative mitochondrial enzyme marker, was not altered. In addition, basal oxygen consumption between sPD and CT cybrids was comparable. However, when mitochondria were challenged via chemical-induced uncoupling into a state of maximum oxygen consumption, sPD cybrids revealed an increase in proton leak in conjunction with a reduced respiratory reserve capacity and ATP production, compared with CT cells. In addition, pathways influenced by aerobic metabolism were also altered in these sPD cybrids. sPD cybrids showed reduced sirtuin-1 (SIRT1) phosphorylation, reduced peroxisome proliferator-activated receptor-gamma coactivator-1alpha (PGC-1α) levels and increased NF-*k*B activation (Esteves et al., 2010c).

In this study, to investigate potential sequence variations that may be functionally relevant and cause mitochondrial dysfunction in sPD, we sequenced cybrid mtDNA derived from three sPD patients and three CT subjects and performed an mtDNA screening analysis of seven mtDNA genes coding for complex I subunits. As shown in **Table V.1**, we identified different patterns of mtDNA variations, in both CT and sPD patients.

Table V.1. Summary of mtDNA investigation results.

Sample	mtDNA sequence variations	Status (according to MITOMAP)	Gene
CT2	3915G>A	CRP	*MTND1*
	4727A>G	CRP	*MTND2*
	11253T>C	CRP; PM reported in LHON and PD	*MTND4*
CT3	3915G>A	CRP	*MTND1*
	4727A>G	CRP	*MTND2*
	11253T>C	CRP; PM reported in LHON and PD	*MTND4*
CT8	10685G>A	CRP	*MTND4L*
	11467A>G	CRP; PM reported in altered brain pH	*MTND4*
	11719G>A	CRP	*MTND4*
	12070G>A	CRP	*MTND4*
	12372G>A	CRP; SM in prostate tumor; PM reported in altered brain pH	*MTND5*
	13617T>C	CRP	*MTND5*
PD4	14470T>A	CRP	*MTND6*
PD5	3992C>T	CRP; SM in thyroid tumor	*MTND1*
	4025A>G	CRP	*MTND1*
	5004T>C	CRP	*MTND2*
	14365C>T	CRP	*MTND6*
	14582A>G	CRP	*MTND6*
PD6	3652A>G*	UnP in Congenital Non-syndromic Deafness	*MTND1*
	4216T>C	CRP; SM in acute leukemia platelets, leukocytes and bone marrow; PM-haplogrup marker JT in LHON/Insulin Resistance	*MTND1*
	4917A>G	CRP; PM reported and haplogroup T marker in LHON/Insulin Resistance/AMD/NRTI-PN	*MTND2*
	11251A>G	CRP	*MTND4*
	11719G>A	CRP	*MTND4*
	11812A>G	CRP	*MTND4*
	13368C>A	CRP	*MTND5*
	13965T>C	CRP	*MTND5*
	14233A>G	CRP	*MTND6*

Notes: the nomenclature of genes is presented according to MITOMAP; CRP: coding region polymorphism; *heteroplasmy; SM: somatic mutation; PM: point mutation; UnP: unpublished polymorphism; LHON: Leber Hereditary Optic Neuropathy; AMD: Age-Related Macular Degeneration; NRTI-PN: Antiretroviral Therapy-Associated Peripheral Neuropathy.

However, no consistent differences were found in terms of mutation patterns or localizations and no PD-related mtDNA variations were detected in sPD cybrids. Our results do not rule out the possible involvement of mtDNA on mitochondrial dysfunction observed in sPD cybrids since other genes outside the regions investigated may be involved in the disease or that mtDNA involvement is related to either deletion events or copy number alterations. We then decided to evaluate whether the phenotypic biochemical changes found earlier in these cybrids are correlated with the mitochondrial content. We performed a comparative analysis for different mitochondrial markers in

order to assess the total mitochondrial pool of CT versus sPD cybrids. As shown in **Figures V.1A** and **B**, we have found variability among the levels of the proteins studied, but no statistically significant differences in sPD cybrids in comparison with CT cells were detected in the most significant structural proteins of mitochondria.

We have also evaluated complex I activity, and, as previously characterized by our group (Esteves et al., 2008; Esteves et al., 2010c), sPD cybrid cell lines show a stable decrease in this mitochondrial activity **(Figure V.1C).**

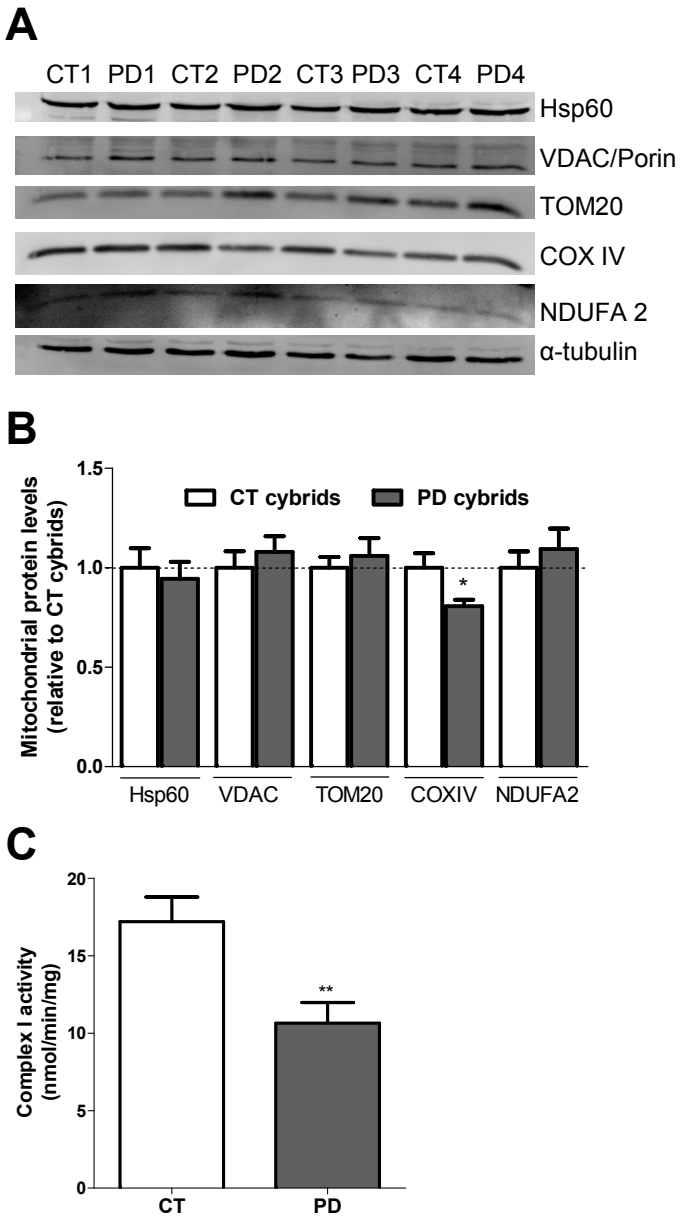

Figure V.1. Mitochondrial deficits are related with an altered ETC complex I activity.

A. Immunoblot for mitochondrial markers (Hsp60, VDAC/Porin, TOM20, COXIV, NDUFA2) from CT and PD cybrids. **B.** Densitometric analysis of mitochondrial marker levels (n=8, *p<0.05, versus CT cybrids). **C.** Mitochondrial respiratory chain complex I activity. Data are reported in nmol/min/mg as the mean ± SEM (n=12; **p<0.01, versus CT cybrids).

To evaluate mitochondrial distribution and morphology, we used TOM20 staining and determined indices of mitochondrial interconnectivity and mitochondrial elongation. Mitochondrial interconnectivity is calculated as the mean area/perimeter ratio and is consistent with the degree of mitochondrial branching, namely the connectivity/dynamics between mitochondria (Koopman et al., 2005b; Koopman et al., 2005a). A higher mitochondrial interconnectivity means a higher access and communication between mitochondria. We have found that, in PD cybrids, mitochondrial distribution was more perinuclear than in CT cybrids (**Figure V.2**). Moreover, PD cybrids showed a decrease in mitochondria elongation and interconnectivity, both features correlating with increased mitochondrial fragmentation. In fact, in PD cybrids, mitochondria appear as small dots instead of a mitochondrial interconnected net.

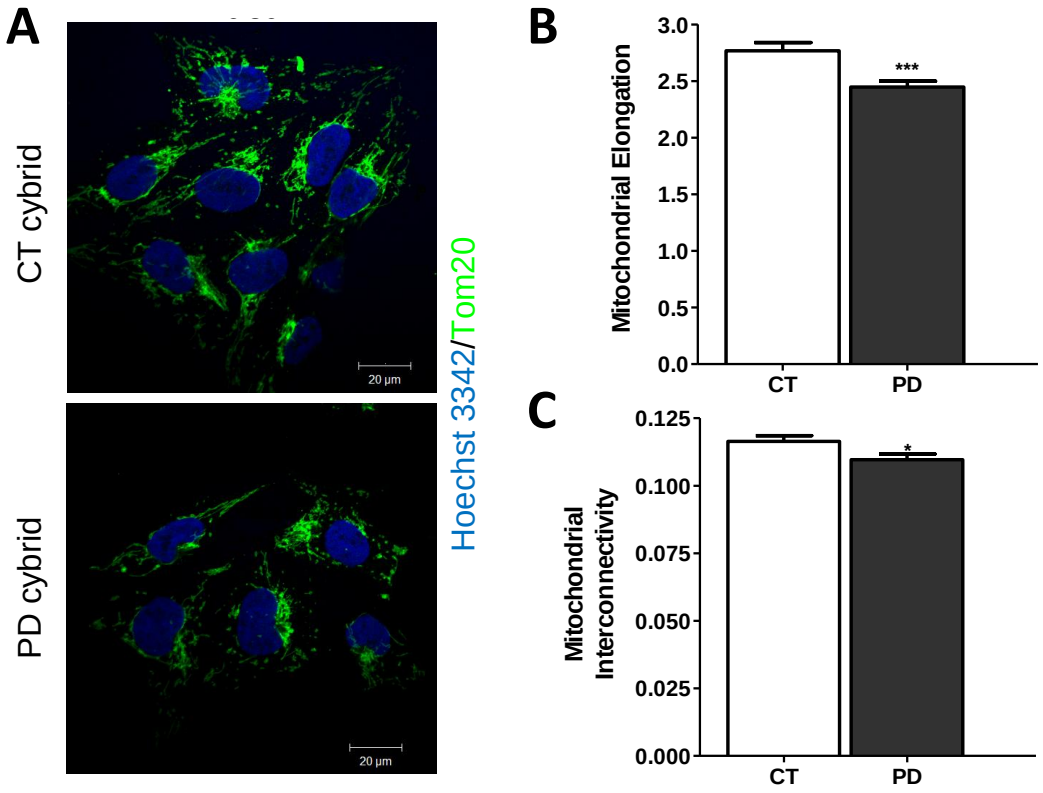

Figure V.2. Mitochondrial distribution, elongation and interconnectivity are altered in sPD cybrids.

A. TOM20 immunostaining (green) of CT and PD cybrids showing alterations in mitochondria distribution, elongation and interconnectivity in PD cybrids. Hoechst 33342-stained nuclei are in blue. Scale bar: 20 µm. **B.** Mitochondrial elongation (n=3, ***p<0.001, PD versus CT cybrids). **C.** Mitochondrial interconnectivity (n=3, *p<0.05, mitochondrial interconnectivity PD versus CT cybrids).

The aforementioned alteration in sPD cybrid morphological and biochemical features is in agreement with an altered mitochondrial ultrastructure and may account for the clinical phenotype of the patients included in this study. Accordingly, in this study, we have examined 15 cell profiles of each cell line and categorized them as to whether they contained predominantly normal or abnormally shaped mitochondria and autophagy-related structures. Regarding mitochondrial structure, we have found that sPD cybrids had many morphologically abnormal mitochondria comparative to CT cybrids. In general, **Figure V.3A** shows that mitochondria in CT cybrids were small and round or rod-like and elongated (**as shown in Figure V.3Aa-d)**. The matrices were dark and uniform and the cristae were homogeneously distributed (**as shown in Figure V.3Ab-d)**. sPD cybrid mitochondria were mostly found enlarged with oval rather than rod-like profiles (**as shown in Figure V.3Ah)**. These abnormal mitochondria contained pale and patchy matrices and disrupted cristae (**as shown in Figure V.3Ai-k**). Some of sPD cybrid mitochondria contained inclusions of electron-dense amorphous substances within matrix that are thought to represent deposits of calcium and inorganic phosphates (**denoted as filled triangles in Figure V.3Aj and k**) (Lloreta-Trull and Serrano, 1998; Ghadially, 2001; Trimmer et al., 2004b).

In order to verify whether these changes in sPD cybrid mitochondrial ultrastructure are exclusively due to the transferred sPD patient mitochondria, we have extended our analysis to the cybrid parental cell line (Rho0 cells). These cells, which lack functional mitochondria due to mtDNA depletion, were found to have high accumulation of swollen pale mitochondria with discontinuous cristae (**denoted as arrows in Figure V.3Ba**). In addition, mitochondrial shape showed a rather circular or oval contour and mitochondria were found apart from each other (**Figure V.3B**)**.** Cristae-like structures were perfectly discernible in Rho+ cell line mitochondria (**Figure V.3A**), whereas in Rho0 cells (**Figure V.3B**) we observed few cristae-like structures with an atypical structure going from one point to another of the mitochondrial peripheral contour (**denoted as filled triangles in Figure V.3Bb and c**). Indeed, these observations suggest that abnormal mitochondria features found in sPD cybrids are clearly due to the transferred mitochondria.

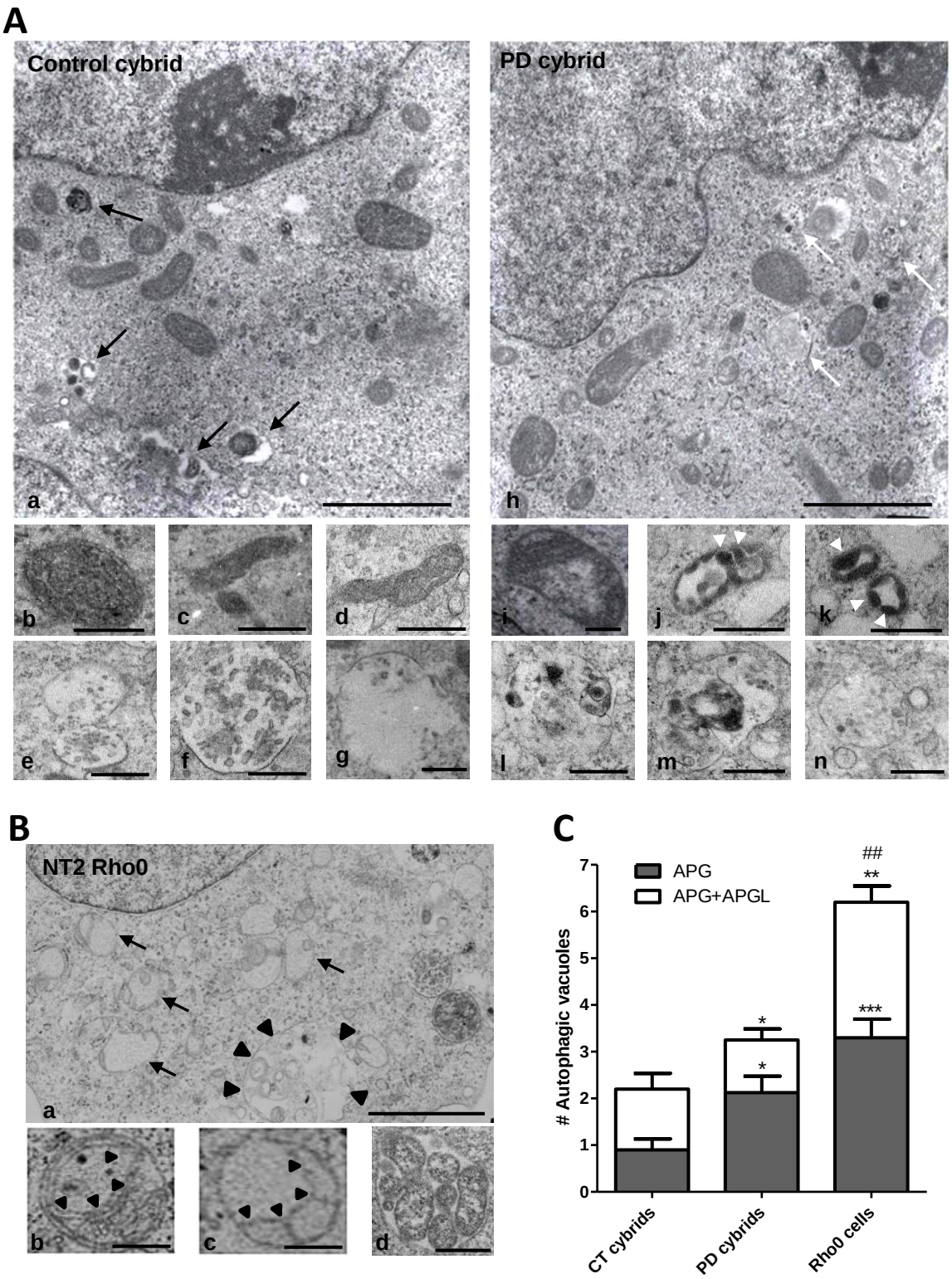

Figure V.3. Mitochondrial deficits induced the accumulation of morphologically abnormal mitochondria and nonfused autophagic vacuoles.

A. Electron micrographs of CT and sPD cybrids. Lower inserts show higher magnification images to illustrate morphological features of mitochondria and individual examples of autophagic vacuoles in both CT and sPD cybrids. Black arrows, autolysosomes; white arrows, autophagosomes; arrows heads, electron-dense amorphous inclusions within mitochondria. Scale bars: 2 μm (top) and 0.5 μm (middle and bottom). **B.** Electron micrographs of NT2 Rho0 cells.

Higher magnification fields show morphological features of mitochondria and autophagic vacuoles in Rho0 cells. (a) Dark arrows: swollen pale mitochondria with discontinuous cristae; Dark arrow heads: enlarged autophagosome enclosing mitochondria and other materials; (b and c) dark arrow heads: abnormal membranous structures. Scale bars: 2 µm (top) and 0.5 µm (bottom). **C.** Quantification of autophagosomes (APG) and autolysosomes (APGL) in cybrid cell lines and mtDNA depleted (Rho0) cells. The total number of vesicles was quantified from 15 cell profiles for each cell line (n=3, *p<0.05, ***p< 0.001, versus APG CT cybrids; *p<0.05, **p< 0.01, versus APG+APGL CT cybrids; $^{\#\#}$p<0.01, versus APG+APGL sPD cybrids).

In addition, ultrastructural analysis revealed that sPD cybrid cells also contain cytosolic vesicles (**denoted as arrows in Figure V.3Ah**) that appear to be autophagic vacuoles enclosing dark bodies and other cytoplasmic inclusions identical to the cytoplasm surrounding the vacuoles, which are compatible with autophagosomes (**Figure V.3Al-n**). In contrast, vesicles containing amorphous materials looking total or partially degraded similar to autolysosomes and/or lysosomes were more prominent and easily detectable in CT cybrids comparative to sPD cybrids (**denoted as arrows in Figure V.3Aa versus h**). Quantitative analysis of the electron micrographs showed an increase in the number of autophagosomes (APG) in those cells compared with CT cybrids (**Figure V.3C)**.

Similarly, Rho0 cells accumulated a large number of autophagic vacuoles (**Figure V.3C**), but apparently no lysosomes or cytoplasmic inclusions (**Figure V.3Ba**). Interestingly, for these cells, we have also detected a great number of mitochondria inside “giant” autophagosomes, indicating a relatively high index of autophagic sequestration (**denoted filled triangles in Figure V.3Ba and d**).

Since newly formed autophagosomes mature and eventually fuse with lysosomes, thereby delivering their contents to lysosomes for degradation, the exacerbated accumulation of autophagosomes observed in sPD cybrids and more evident in Rho0 cells prompted us to assess the effects of sPD-mitochondrial dysfunction on the autophagic activity.

5.3.2 Mitochondrial deficits in cells harboring PD patient mitochondria or in mtDNA-depleted cells compromise quality control autophagic response

We next evaluated autophagosome formation by directly measuring the cellular distribution of endogenous LC3B and by monitoring the autophagic flux, as determined by comparing the accumulation of autophagosomes after the inhibition of lysosomal proteolysis with NH_4Cl/leupeptin (NL) relative to the steady-state levels of autophagosomes (Rubinsztein et al., 2009)

Under basal conditions, sPD cybrids show an increase in both the number and size of endogenous LC3B puncta relative to CT cybrids. (**Figure V.4Aa versus c, and B**), but when lysosomal degradation was inhibited this number increased more markedly in CT cybrids (**Figure V.4Ab versus d, and B**), indicating a higher basal autophagic activity for CT cybrids. Removal of serum further activated autophagy in a higher extent in CT cybrids than in sPD cybrids, as depicted by the higher increase in the number of bright puncta without treatment (**Figure V.4Aa versus e, compared with c versus g, and B**). Similar results were obtained when lysosomal degradation ability was inhibited (**Figure V.4Ab versus f, compared with d versus h, and B**).

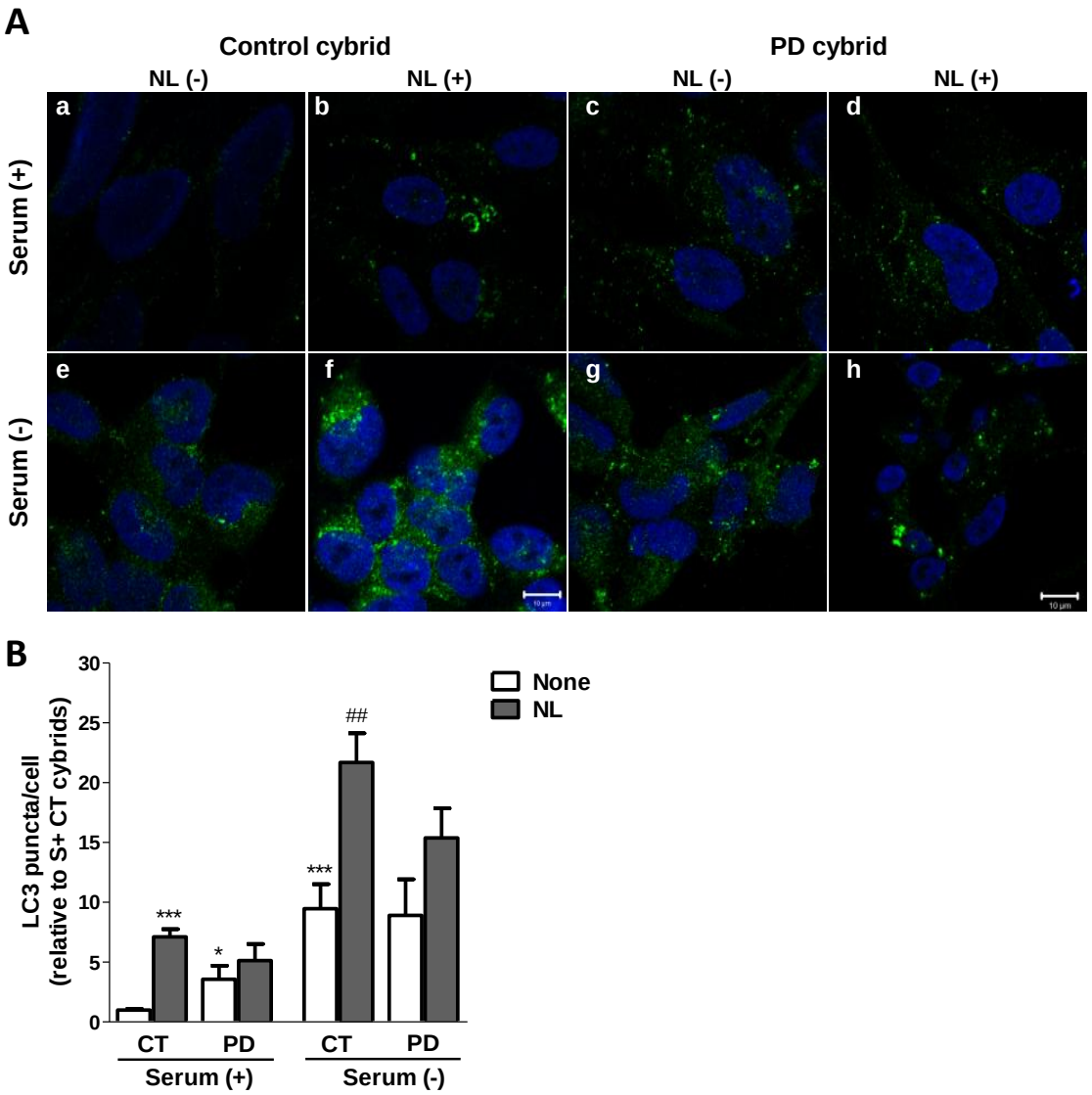

Figure V.4. QC autophagic response is impaired in cells harboring PD patient mitochondria.

A. LC3B immunostaining (green) of CT and PD cybrids maintained in the presence [Serum (+)] or absence [Serum (−)] of serum and inhibitors of lysosomal proteolysis [NL(+); NL(-)]. Hoechst 33342-stained nuclei are in blue. Scale bar: 10 µm. **B.** Mean number of LC3B-positive vesicles per cell profile (n=3, *p<0.05, ***p<0.001 versus S+ CT cybrids; ## p<0.01, versus S- CT cybrids).

These immunofluorescence results were confirmed by determining the autophagic flux by immunoblot. By this approach, we have also detected an increase in the basal levels of LC3B-II, a phosphatidylethanolamine-conjugated form that is localized to autophagosomes, in sPD cybrids when compared with CT cybrids (**Figure V.5A and B**). As in the LC3B puncta staining data, the increase in LC3B-II upon inhibition of lysosomal

degradation was higher for CT cybrids under normal nutrient conditions as well as upon induction of autophagy by starvation [serum (-) conditions]. Accordingly, we observed that, although the basal levels of autophagic vacuoles are increased in sPD cybrids, their rate of autophagic degradation is significantly lower when compared with CT cybrids (**Figure V.5C and D, respectively**). Also, when compared with CT cybrids, sPD cybrids showed increased basal levels of the autophagic substrate p62 which were not potentiated after lysosomal inhibition, demonstrating an impaired lysosomal turnover of protein cargo via autophagy in these cells (**Figure V.23A and B**).

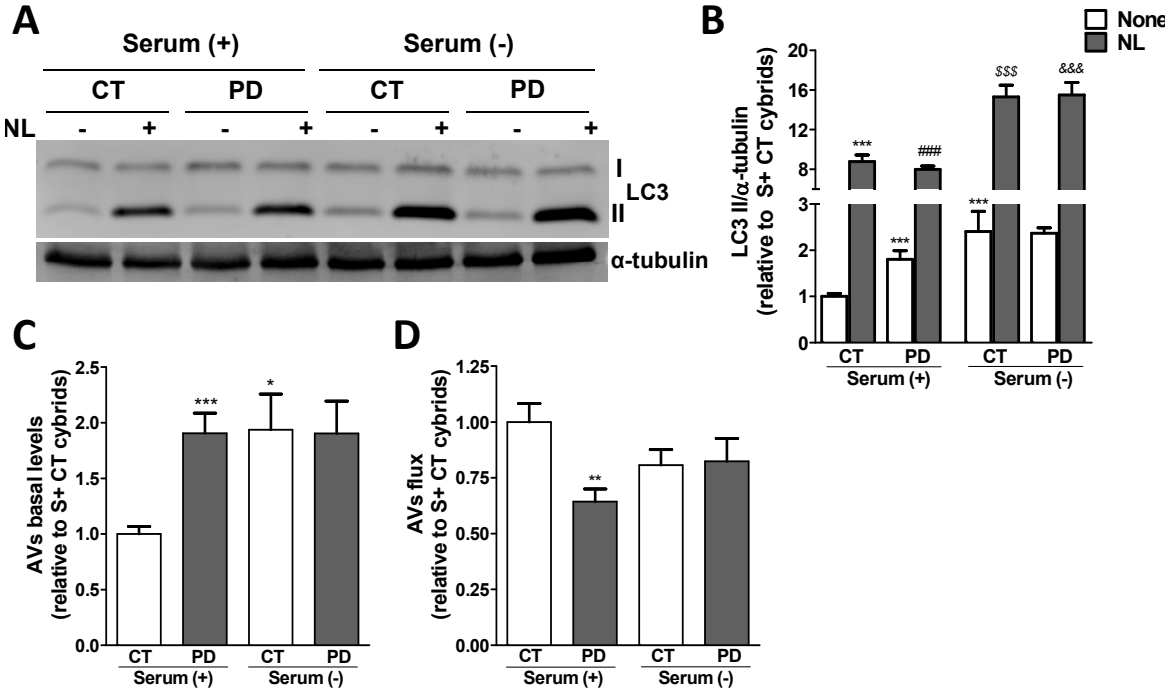

Figure V.5. QC autophagic activity is impaired in cells harboring PD patient mitochondria.
A. Immunoblot for endogenous LC3B from CT and PD cybrids after culture in serum (+) or serum (-) conditions and treatment with NL. **B.** Densitometric analysis of endogenous levels of LC3B (n=18, ***p<0.001 versus S+ CT cybrids; $^{###}$ p<0.001, versus S+ PD cybrids; $^{\$\$\$}$p<0.001, versus S- CT cybrids; $^{\&\&\&}$ p<0.001, versus S- PD cybrids). **C.** Determination of autophagic vacuole (AVs) levels. Values of LC3-II in the absence of NL represent the steady-state AV content (n=18, *p<0.05, ***p<0.001, versus S+ CT cybrids). **D.** Assessment of autophagic flux, calculated as the ratio of LC3-II densitometric value of NL-treated samples over the corresponding untreated samples (n=18, **p<0.01, versus S+ CT cybrids).

We obtained similar results with the parental cell line NT2 when treated with MPP^+ (1 mM, 24 h), a classic inhibitor of complex I (**Figure V.6A-D**).

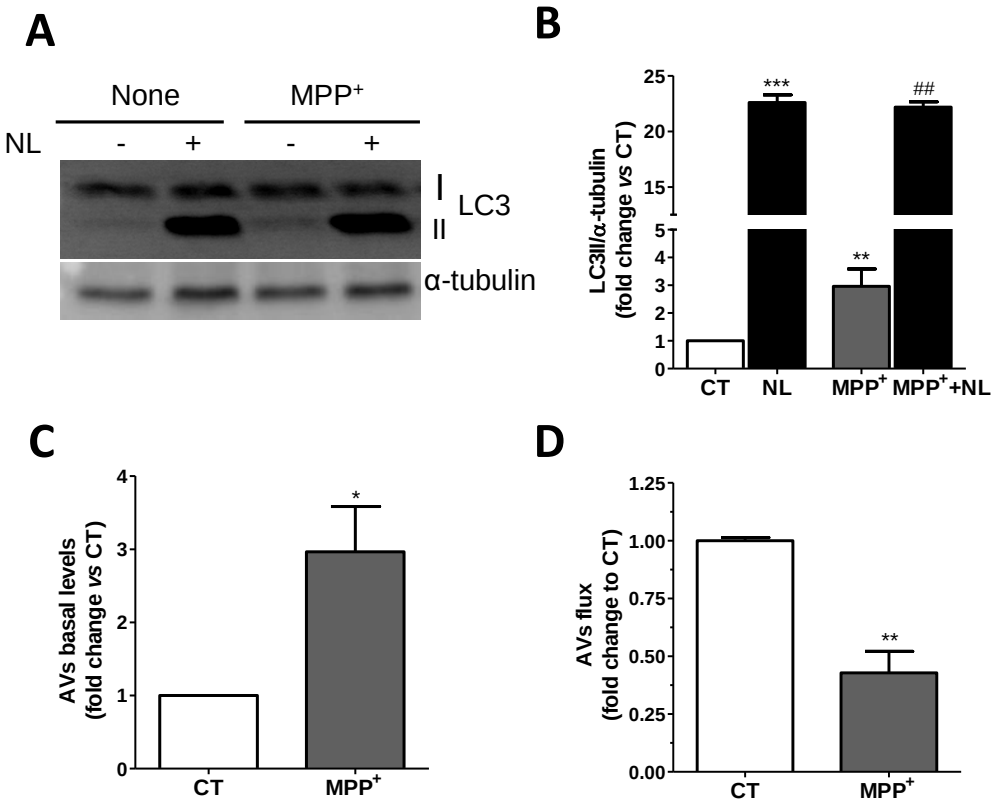

Figure V.6. Mitochondrial dysfunction mediates autophagic stress in MPP^+-treated cells. **A.** Immunoblot for LC3B from NT2-Rho+ cells treated with or without lysosomal inhibitors (NL). **B.** Densitometric analysis of LC3B levels (*n*=3, **p<0.01, ***p<0.001, versus untreated cells; $^{\#\#}$p<0.01, versus MPP^+-treated cells). **C.** Determination of autophagic vacuole (AVs) basal levels. Values of LC3-II in the absence of NL represent the steady-state AV content (*n*=3, *p<0.05, versus untreated cells) **D.** Assessment of autophagic flux, calculated as the ratio of LC3-II densitometric value of NL treated samples over the corresponding untreated samples (*n*=3, **p<0.01, versus untreated cells).

These results were also corroborated in differentiated PD cybrid cell lines that exhibit processes similar to neuronal cells (**Figure V.7A and B**). Consistent with our results in cybrid cells and MPP^+-treated NT2 cells, LC3B content increased significantly more in neuronal-like CT (*n*CT) cybrid cells when exposed to lysosomal inhibition for 4 h, indicating that these cells were more prone to develop an autophagic response rather than *n*PD cybrids (**Figure V.7A and B**).

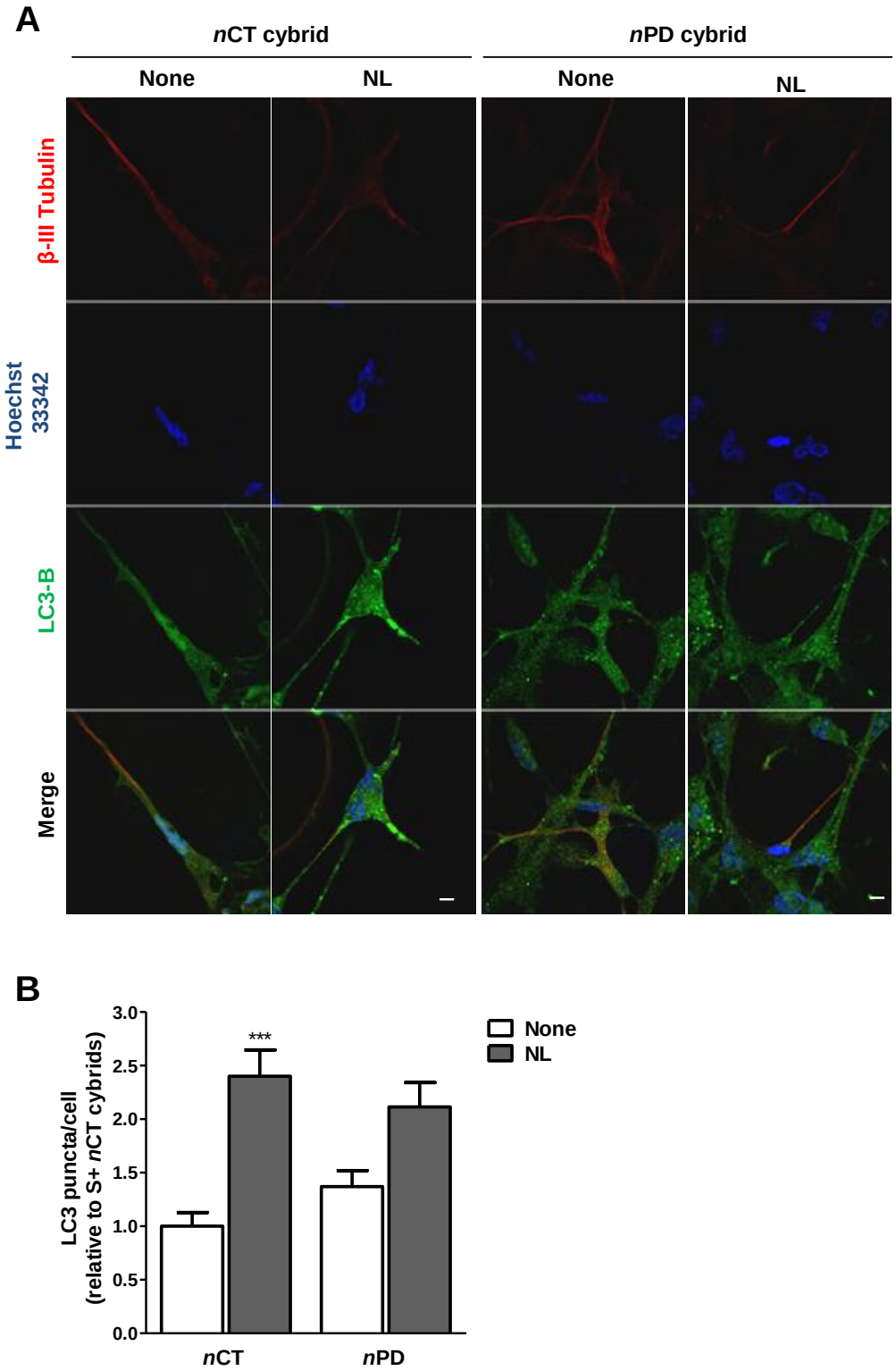

Figure V.7. Autophagic abnormalities are evident in neuronal-like cybrid cell lines.

A. Immunofluorescence for LC3B (green) in neuronal-like CT and PD cybrids treated with or without lysosomal inhibitors (NL). Beta-tubulin III (red) and Hoechst 33342 (blue) co-stainings were used as neuronal and nuclei markers, respectively. Scale bars: 10 µm. **B.** Mean number of LC3B-positive vesicles per cell profile (n=2, ***p<0.001 versus *n*CT cybrids).

The increased accumulation of LC3-II obtained for all those cellular models was also evident in sPD patient peripheral blood lymphocytes **(Figure V.8A and B)**. Moreover, under serum starvation conditions, CT cybrids activated nonselective "bulk" autophagy in a greater extent than PD cybrids, although no alterations were observed in the autophagic flux.

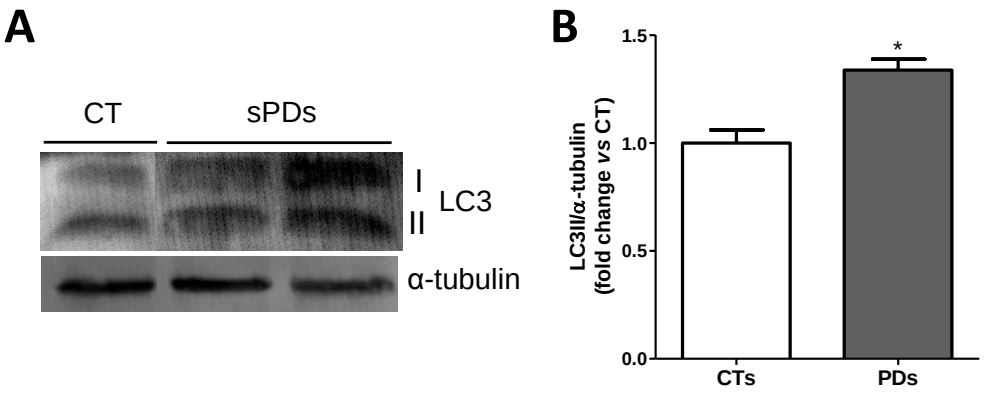

Figure V.8. PBMCs from sporadic PD patients exhibit increased levels of LC3B-II.
A. Immunoblot image for LC3B in PBMCs from control subjects (CT) and sporadic PD patients (sPDs). **B.** Densitometric analysis of LC3B levels (*p<0.05, versus CT subjects).

Similar results were obtained for cells lacking the mitochondrial genome (Rho0 cells) and thereby a dysfunctional mitochondrial respiratory system. In the absence of such system, these cells require alternative mechanisms for the maintenance of an appropriate redox state and energy supply. If sufficient pyruvate and uridine are provided, these cells can grow without a functional mitochondrial electron transport chain and oxidative phosphorylation. Theoretically, this would increase the glycolytic pathway flux for continual regeneration of NAD^+, including that regenerated by the plasma membrane oxidoredutase (Larm et al., 1994), ensuring that glycolytic pathway will provide sufficient ATP to sustain essential cellular metabolic activities and cell viability (Morre et al., 2000).

In agreement with the EM data in **Figure V.3B** , Rho0 cells showed a higher number of autophagic vacuoles in comparison with their parental counterpart cell line containing a full complement of mtDNA (Rho+ cells), distinguished as LC3B-positive puncta by immunofluorescence (data not shown) and by autophagic vacuole basal levels (**Figure V.9A and B**). However, this was not accompanied by an increase in the number of these organelles in response to lysosomal inhibition (**Figure V.9A and B**), supporting a lower autophagic flux in Rho0 cells (**Figure V.9C**).

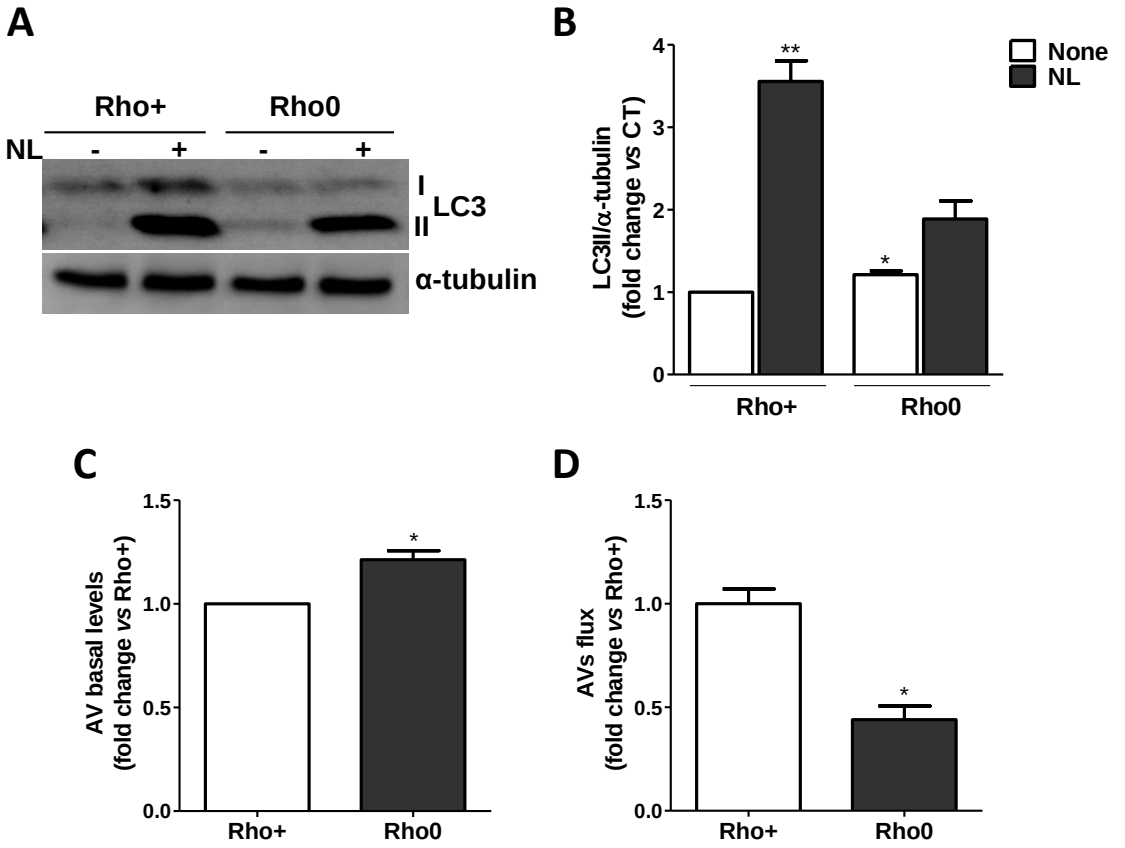

Figure V.9. Autophagic stress is increased in mtDNA-depleted cells relative to full complement mtDNA-containing cells.

A. Immunoblot for LC3B from mtDNA-depleted cells (Rho0) and their parental cells containing a full complement of mtDNA (Rho+) treated with or without lysosomal inhibitors (NL). **B.** Densitometric analysis of LC3B levels (*n*=3, *p<0.05, versus Rho+-untreated cells). **C.** Determination of autophagic vacuole (AVs) basal levels. Values of LC3-II in the absence of NL represent the steady-state AV content (*n*=3, *p<0.05, versus Rho+-untreated cells). **D.** Assessment of autophagic flux, calculated as the ratio of LC3-II densitometric value of NL-treated samples over the corresponding untreated samples (*n*=3, *p<0.05, versus Rho+-untreated cells).

To evaluate whether mitochondrial dysfunction could lead to the impairment in the autophagic response due to a bioenergetic failure, we have also compared the autophagic response of Rho0 cells grown in the presence [pyr/urd (+/+)] or absence [pyr/urd(-/-)] of pyruvate and uridine. Subsequently, autophagy was induced exposing cells to serum starvation conditions. Under these conditions, cells were also maintained in non-supplemented media to determine the extent to which the autophagic response depends on ATP production derived from glycolysis. No statistically significant differences were observed between cells grown in pyr/urd (+/+) or in pyr/urd (-/-) media for 24 h (**Figure V.10Aa versus c and e versus g, and B**). Moreover, the shift to a

punctuate pattern of LC3B upon inhibition of lysosomal-degradative ability was not statistically different between cells subject to both types of pyr/urd treatment, under both normal growing (**Figure V.10Ab versus d, and B**) and serum removal conditions (**Figure V.10Af versus h, and B**).

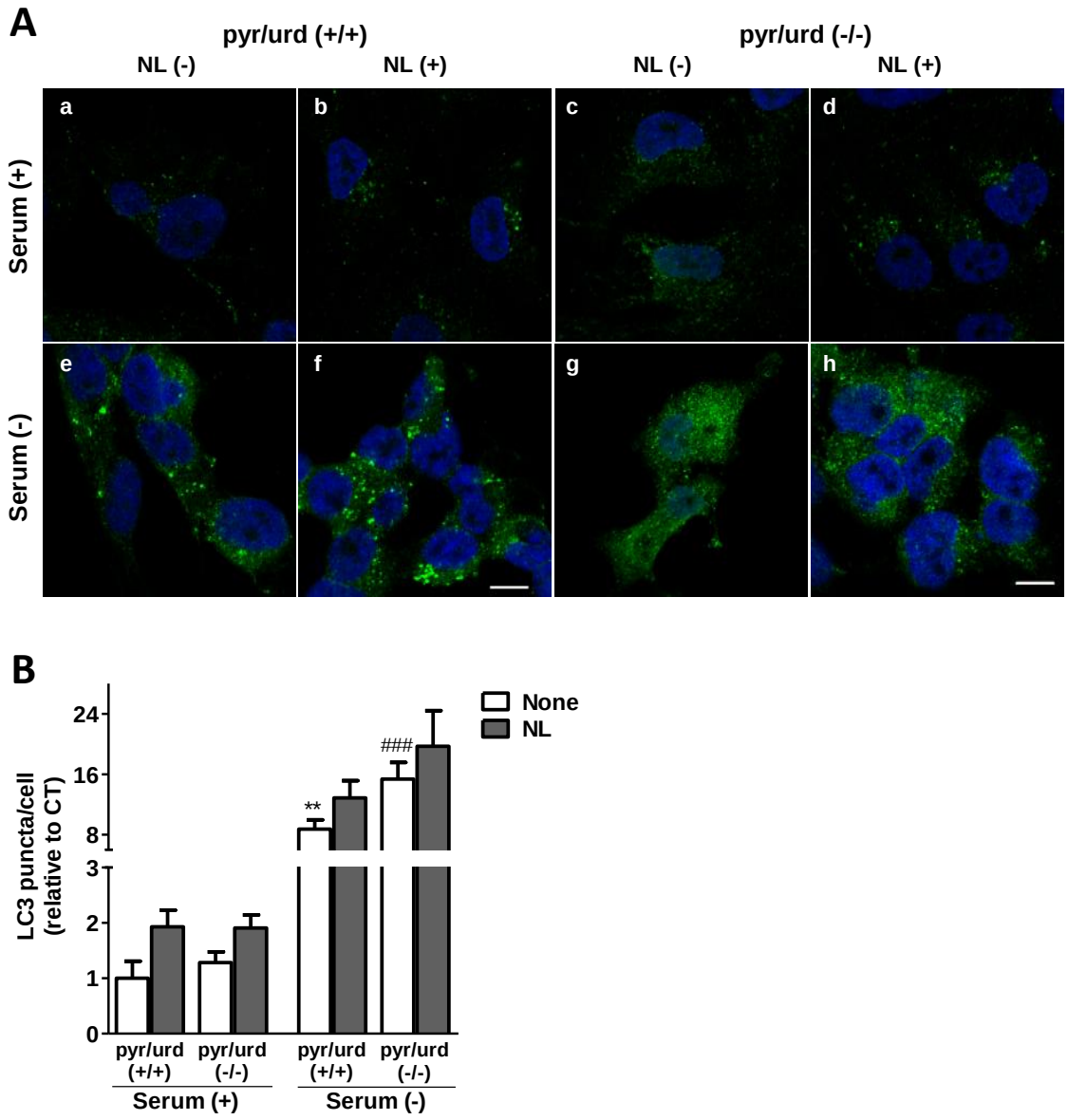

Figure V.10. QC autophagic response is impaired in mtDNA-depleted cells.

A. LC3B immunostaining (green) of Rho0 cells maintained in serum (+) or serum (−) conditions and NL treatment, following growth in the presence [pyr/urd (+/+)] or absence [pyr/urd (-/-)] of pyruvate and uridine. Hoechst 33342-stained nuclei are in blue. Scale bar: 10 μm. **B.** Mean number of LC3B-positive vesicles per cell profile [n=3, **p<0.01, versus S+ pyr/urd (+/+); ### p<0.001 versus S- pyr/urd (+/+)].

We also checked the effect of growing cells in pyr/urd (-/-) medium for 48 h on the autophagic response, but no significant changes were observed (data not shown). These results were supported by our biochemical data showing significantly higher LC3B-II levels only upon serum withdrawal (**Figure V.11A-C**), which was correlated with an impaired autophagic response/activity (**Figure V.11D**).

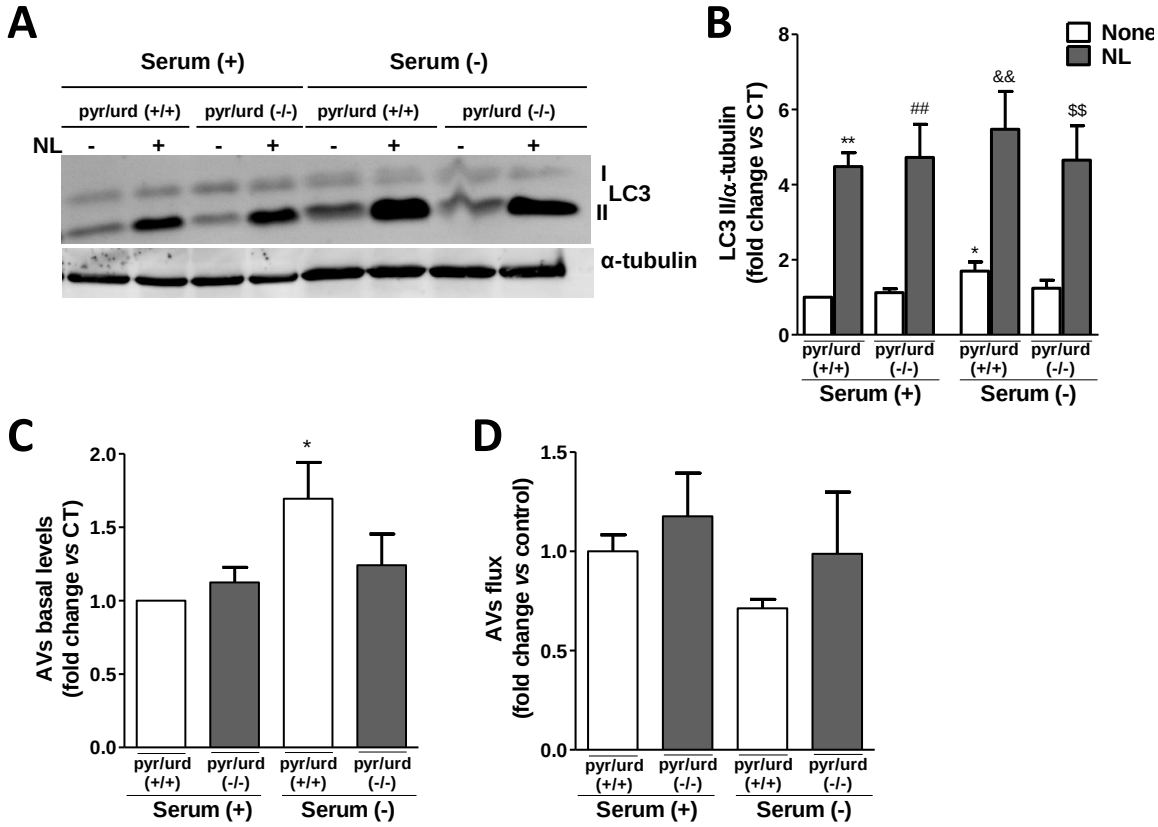

Figure V.11. QC autophagic activity is impaired in mtDNA-depleted cells.

A. Immunoblot for endogenous LC3B from Rho0 cells maintained in serum (+) or serum (−) and NL treatment following growth in pyr/urd (+/+) or pyr/urd (-/-) conditions. **B.** Densitometric analysis of LC3B endogenous levels [n=5, *p<0.05, **p<0.01, versus S+ pyr/urd (+/+); $^{\#\#}$ p<0.01, versus S+ pyr/urd (-/-); $^{\&\&}$ p<0.01, versus S- pyr/urd (+/+); $^{\$\$}$p<0.01, versus S- pyr/urd (-/-)] **C.** Determination of autophagic vacuole (AVs) levels. [n=5, *p<0.05, versus S+ pyr/urd (+/+)]. **D**. Assessment of autophagic flux (n=5).

Overall, these data supports that the defect on both QC and “bulk” autophagy observed in PD cells was not due to changes on ATP availability through glycolysis.

5.3.3. Autophagic degradation is impaired in MPP^+- treated primary cortical neurons

To extend these findings and further confirm our previous observation that mitochondrial deficits can compromise the degradative ability of the autophagic system, we used MPP^+-treated primary cortical neurons, a well-established *in vitro* model of PD-associated neuronal dysfunction directly caused by mitochondrial impairment (Beal, 2001; Nicotra and Parvez, 2002; Martinez and Greenamyre, 2011). In this model, we have also found a rapid accumulation of LC3B-positive vesicles within 4 h after blocking of lysosomal proteolysis, indicating a constitutive autophagic flux in primary cortical neurons (**Figure V.12Aa versus b, and e versus f**). However, we could not observe an increase in the number of LC3B-positive vesicles in MPP^+-treated cells (50 µM, 24 h) when compared with CT cells (**Figure V.12Aa versus c, and B**), both in CT conditions or in the presence of rapamycin, an mTOR inhibitor that induces autophagy (**Figure V.12Ae versus g, and B**).

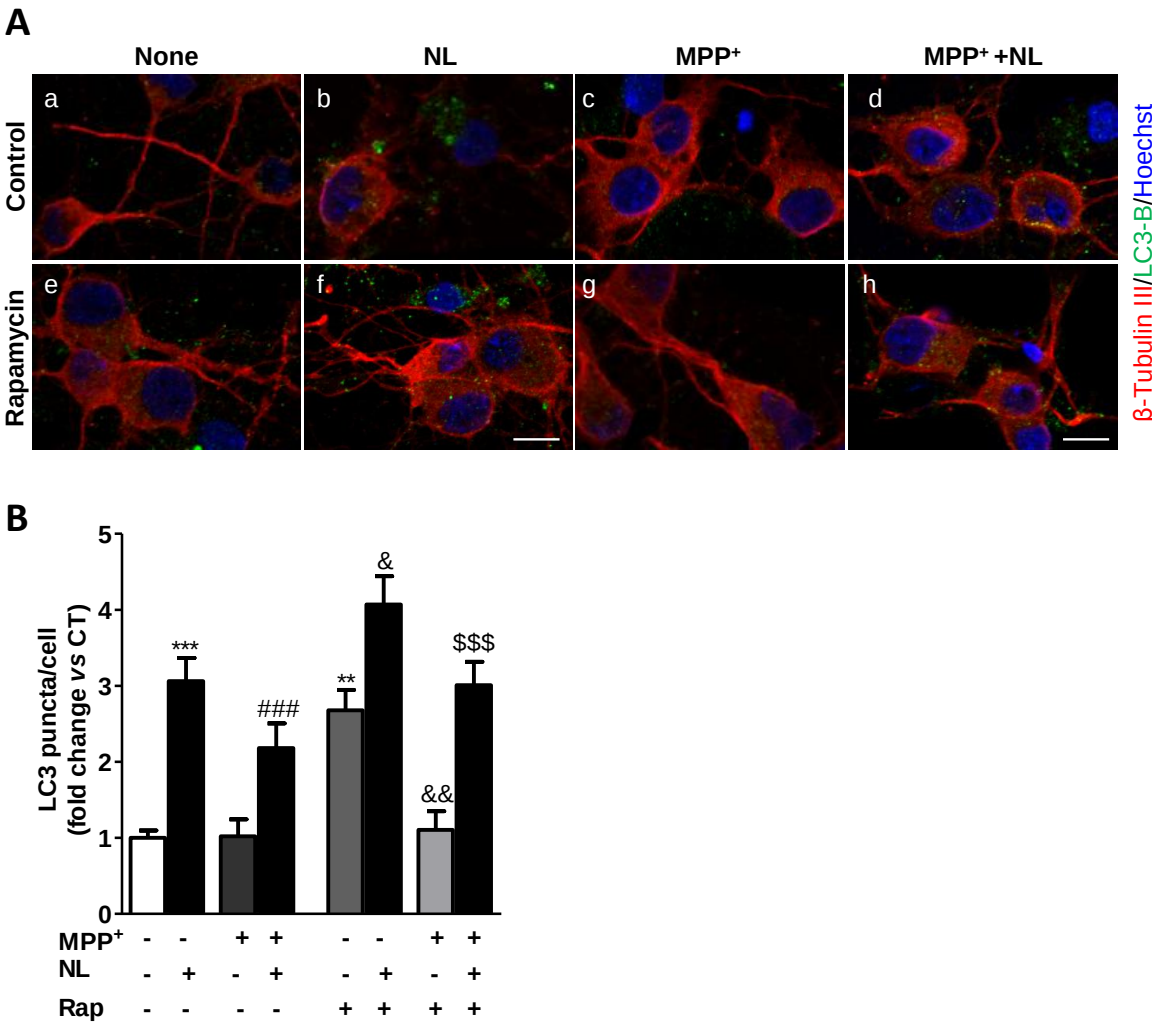

Figure V.12. MPP$^+$-induced mitochondrial dysfunction mediates autophagy-lysosome pathway impairments in primary cortical neurons.

A. LC3B immunostaining (green) of primary cortical neurons treated with MPP$^+$ for 24 h. In the last 4 h, cells were co-treated with or without rapamycin and lysosomal inhibitors (NL). Beta-tubulin III (red) and Hoechst 33342 (blue) co-staining was used as a neuronal and nuclei marker, respectively. Scale bar: 10 µm. **B.** Mean number of LC3B-positive vesicles per cell profile (*n*=3, **p<0.01, ***p<0.001, versus CT; $^{###}$ p<0.001, versus MPP$^+$-treated cells; $^{&}$p<0.05; $^{&&}$p<0.01, versus rapamycin (Rap)-treated cells; $^{\$\$\$}$p<0.001, versus Rap+MPP$^+$-treated cells).

These data were also verified by immunoblotting, showing no significant effect on the levels of LC3B-II when cells were exposed to MPP$^+$ (**Figure V.13A-C**). This was accompanied by a significant reduction on the autophagic flux (**Figure V.13F**), similar to the results obtained using cellular models of mitochondrial dysfunction. Rapamycin was able to develop an autophagic response, which indicates that the decreased flow observed by MPP$^+$ treatment is specific. Even in the presence of rapamycin, MPP$^+$-

treated cortical neurons were unable to develop an efficient autophagic response, since autophagic flux is decreased when compared with rapamycin treatment and did not reach CT values.

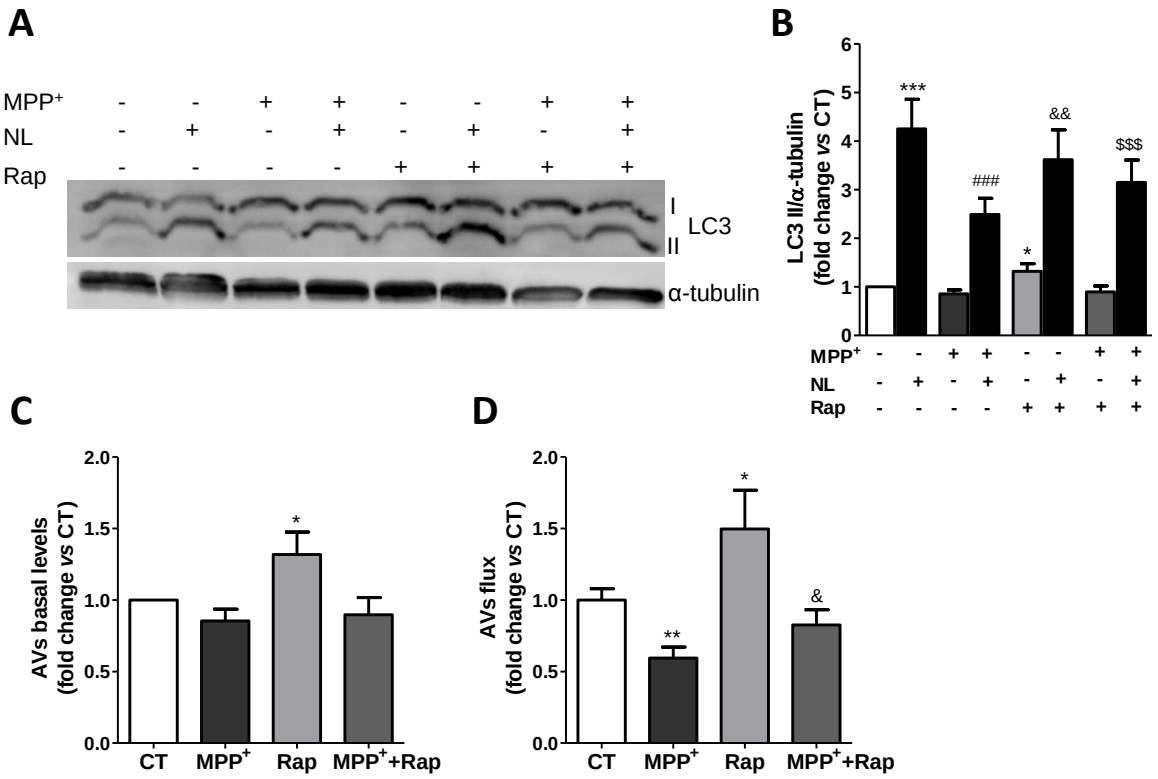

Figure V.13. MPP$^+$-induced mitochondrial dysfunction mediates autophagy-lysosome pathway impairments in primary cortical neurons.

A. LC3B immunoblot of primary cortical neurons treated with MPP$^+$ for 24 h. In the last 4 h, cells were co-treated with or without rapamycin (Rap) and lysosomal inhibitors (NL). **B.** Densitometric analysis of LC3B endogenous levels (*n*=13, *p<0.05, ***p<0.001, versus untreated cells; $^{###}$p<0.001, versus MPP$^+$-treated cells; $^{\&\&}$p<0.01, versus Rap-treated cells; $^{\$\$\$}$p<0.001, versus Rap+MPP$^+$-treated cells). **C.** Determination of autophagic vacuole (AVs) levels. Values of LC3-II in the absence of NL represent the steady-state AV content (*n*=13, *p<0.05, versus CT). **D.** Assessment of autophagic flux, calculated as the ratio of LC3-II densitometric value of NL-treated samples over the corresponding untreated samples (*n*=13, *p<0.05, **p<0.01, versus CT; $^{\&}$p<0.05, versus Rap-treated cells).

Although with minor differences between chronic and acute models, together these data suggest that mitochondrial impairment leads to alterations in the autophagy system, as mainly translated by a reduction in the autophagic flux.

5.3.4 Induction of autophagy is not primarily affected in sPD transmitochondrial cybrids

We further tried to understand the nature of the changes in the autophagy-lysosome pathway found in the context of our sPD transmitochondrial cybrid model. Since this pathway encompasses multiple steps, changes not only in the clearance but also in the initiation could concur for the accumulation of autophagic vesicles observed. In order to clarify if an abnormal induction of autophagy could also be involved and contribute to the observed autophagic vesicles accumulation, we started by analyzing the rates of LC3B-II synthesis. We evaluated possible changes in synthesis in the presence of lysosomal proteolytic activity inhibitors at three different time points (**Figure V.14A**). The changes in LC3B-II levels when degradation is clamped would reflect the synthesis of autophagosomes in the experimental time frame if the autophagy system is under steady-state (Rubinsztein et al., 2009). According to our previous data on LC3B-II flux (**Figure V.5A-D**), the basal levels of LC3B-II were significantly higher in sPD cybrids in comparison with CTs (after 4 h). However, no significant differences between sPD and CT cybrids were observed for the levels of LC3B-II along this time course when lysosomal activity was inhibited (**Figure V.14B**)**.** Since LC3B-II levels were maximal at the earliest time point considered (2 h), we also determined changes in LC3B-II formation between CT and sPD cybrids at earlier time points (30 min and 1 h). As expected, no changes were found between these two cell lines (data not shown). In addition, **Figure V.14C** shows that the rates of autophagosomes synthesis were similar in CT and sPD cybrids when comparisons were defined for 4 versus 2 h as well as 6 versus 4 h, further supporting the notion that the system was under steady-state. These results indicate that the initiation step is not affected in sPD cybrids.

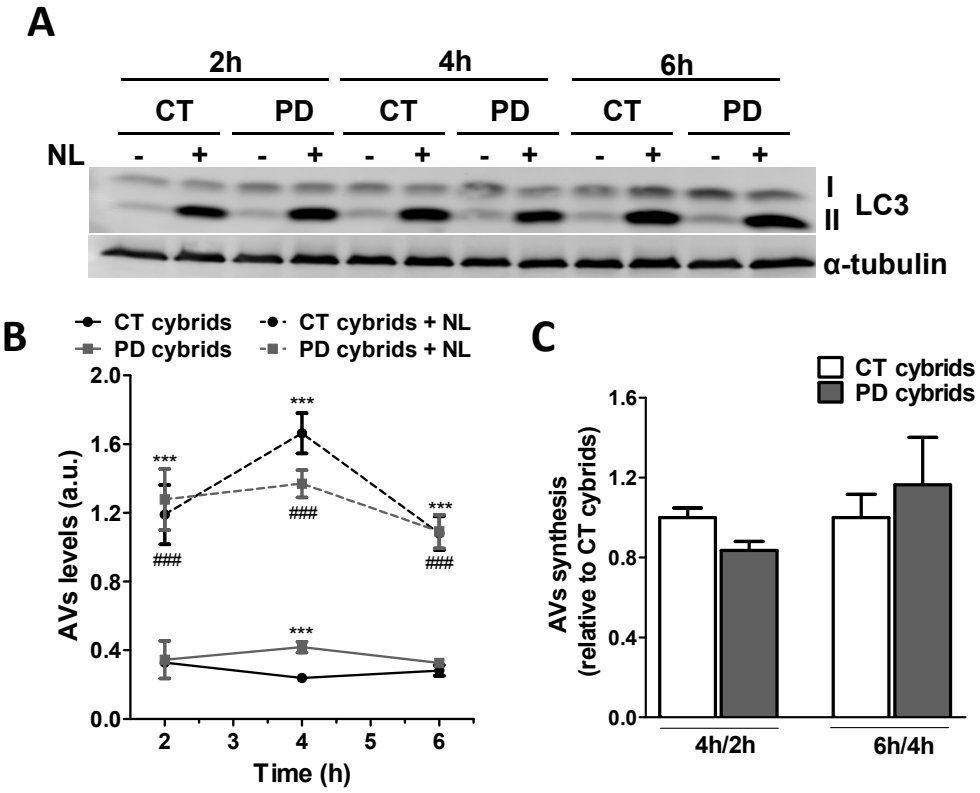

Figure V.14. AV synthesis is not primarily affected in PD cybrid cells.

A. LC3B immunoblot for autophagosome synthesis assessment in CT and PD cybrids treated with or without lysosomal inhibitors (NL) at three different time points (2, 4 and 6 h) (n=4). **B.** Time course for autophagic vacuole (AVs) levels. AV levels correspond to the densitometry values of LC3-II for each condition at each time point (*n*=4, ***p<0.001, versus CT cybrids; ###p<0.001, versus PD cybrids, for each time point). **C.** Assessment of autophagic synthesis. Rates of AV synthesis were determined by comparing LC3-II levels at two different time points after the addition of NL (4 versus 2 and 6 versus 4h) (*n*=4).

We next decided to explore some of the key proteins belonging to the PI3-kinase complex machinery that controls the nucleation of autophagic vesicles. One of these proteins is Beclin-1. Beclin-1 is a key autophagy protein that acts as an essential activator of autophagy and for this reason its cellular abundance has been correlated with autophagic activity (Shibata et al., 2006). Surprisingly, we did not find significant differences in the total cellular levels of this protein in sPD cybrids in comparison with CT cybrids (**Figure V.15A and V.15B**) in the presence of serum. However, when cells were challenged to induce autophagy by serum withdrawal, a large increase in the levels of Beclin-1 was observed for CT cybrids, which was not found for sPD cybrids, demonstrating the inefficient capability of these cells to efficiently prompt a “bulk” autophagic response, as previously observed in **Figure V.5A** and **D**.

Another hypothesis is that the cellular availability of Beclin-1, rather than just total cellular abundance, might be the key point to abnormal induction of autophagy (Wong and Cuervo, 2010). Beclin-1 interacts with the class III phosphatidylinositol 3-kinase (Vps34) to localize other autophagy proteins to the pre-autophagosomal membrane (Funderburk et al., 2010). In conditions in which autophagy is inhibited, Beclin-1 is inactivated by its interaction with Bcl-2, which functions as a brake to autophagy and autophagic cell death by affecting the interaction between Beclin-1 and Vps34. Thus, we sought to determine whether Bcl-2 has a role in modulating the autophagic response observed in our sPD models. Consistent with data from other study involving PD cybrids (Veech et al., 2000), we have found that our sPD cybrids exhibited significantly increased basal levels of Bcl-2 relatively to CT cybrids (**Figure V.15C and D**). Additionally, alterations in the total levels of Bcl-2 were also associated with lysosomal inhibition and serum removal, more remarkably in CT cybrids, which showed dramatic increases in the levels of this protein in such conditions (**Figure V.15C and D**).

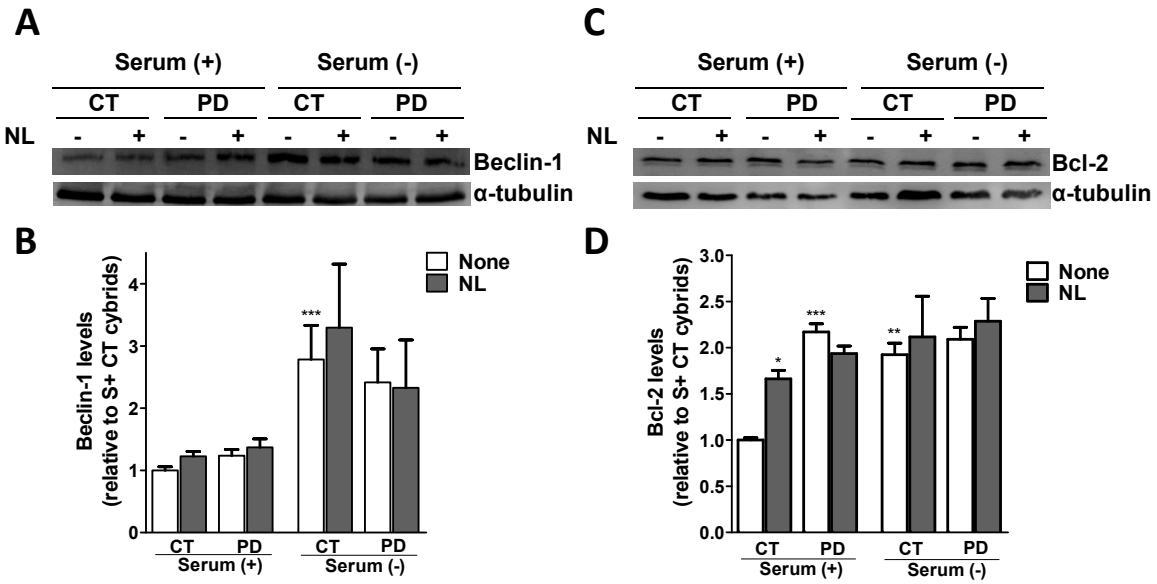

Figure V.15. Autophagic induction is not compromised in PD cybrid cells.

A. Immunoblot for Beclin-1 from CT and PD cybrids after culture in serum (+) or serum (-) conditions and treatment with or without NL. **B.** Densitometric analysis of endogenous levels of Beclin-1. (*n*=8, ***p<0.001, versus S+ CT cybrids). **C.** Immunoblot for Bcl-2 from CT and PD cybrids after culture in serum (+) or serum (-) conditions and treatment with NL. **D.** Densitometric analysis of endogenous levels of Bcl-2. (*n*=6, *p<0.05, **p<0.01, ***p<0.001, versus S+ CT cybrids).

We next assessed the cellular subcompartmentalization of Bcl-2 and Beclin-1 in cytosol and mitochondria-enriched fractions. We have observed that the content of Bcl-2 was increased in the mitochondria-enriched fractions of sPD cybrids relative to CT cybrids (**Figure V.16A and B**), which is in accordance with the results obtained for the whole-cell lysates (**Figure V.15C and D**). Conversely, no major differences were detectable in the levels of Beclin-1 between subcellular fractions of CT and sPD cybrids (**Figure V.16A and C**). However, the changes in the total cellular abundance obtained for both proteins approximately match the sum of their cytosolic and mitochondrial enrichment.

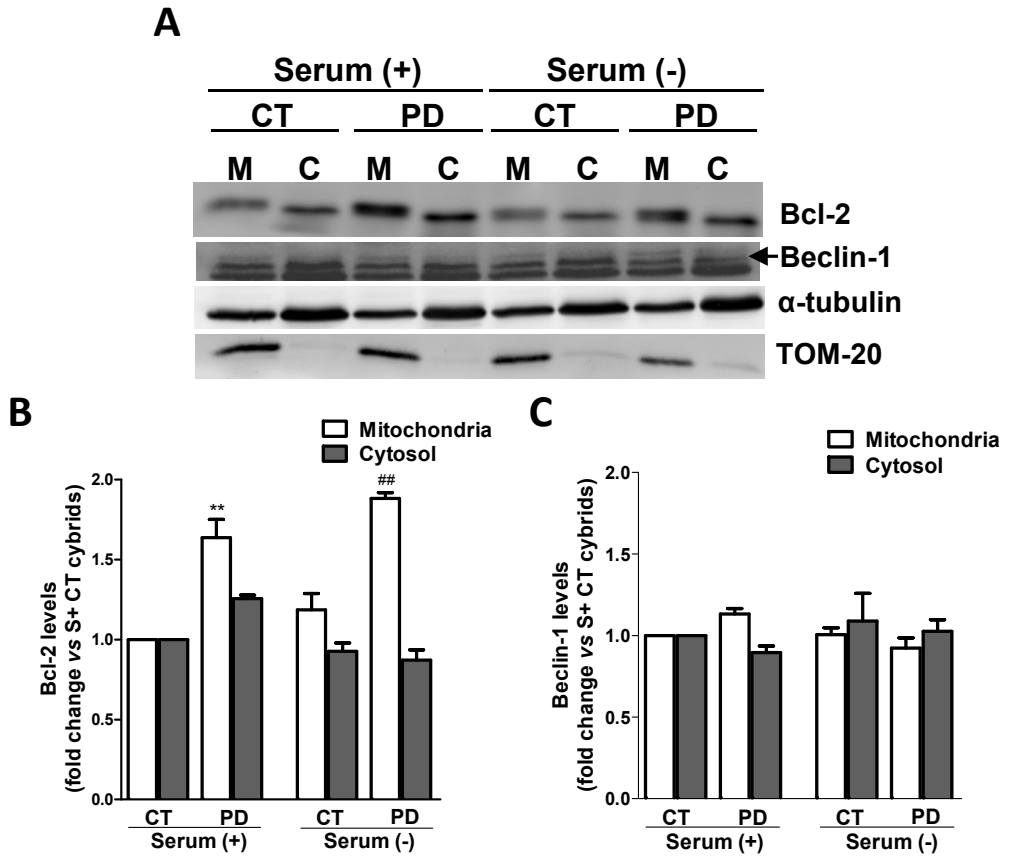

Figure V.16. Beclin-1 cellular availability is not compromised in sPD cybrid cells.

A. Representative immunoblots for Bcl-2 and Beclin-1 cellular subcompartmentalization in mitochondria (M)- and cytosol (C)-enriched fractions. **B.** and **C.** Densitometric analysis of the levels of Bcl-2 (**B**) (*n*=3, **p<0.01, versus S+ CT cybrids; $^{\#\#}$p<0.01, versus S- CT cybrids) and Beclin-1 (**C**) (*n*=3).

As well, the targeting of Beclin-1 by Bcl-2 represents the crucial point to understand the mechanism of autophagy regulation. Therefore, we have also investigated the physical interaction Beclin-1/Bcl-2. When normalized to Beclin-1, the amount of Bcl-2 associated with Beclin-1 did not differ in sPD and CT cybrids (**Figure V.17A and B**). In addition, the anti-apoptotic protein Bcl-2 inhibits starvation-induced autophagy via targeting the BH3-like domain in Beclin-1 (Pattingre et al., 2005; Maiuri et al., 2007). However, the association Beclin-1/Bcl-2 was unchanged in sPD cybrids in comparison with CT cybrids in serum deprivation conditions, which indicates that "bulk" autophagy induction is not compromised in sPD cybrid cells.

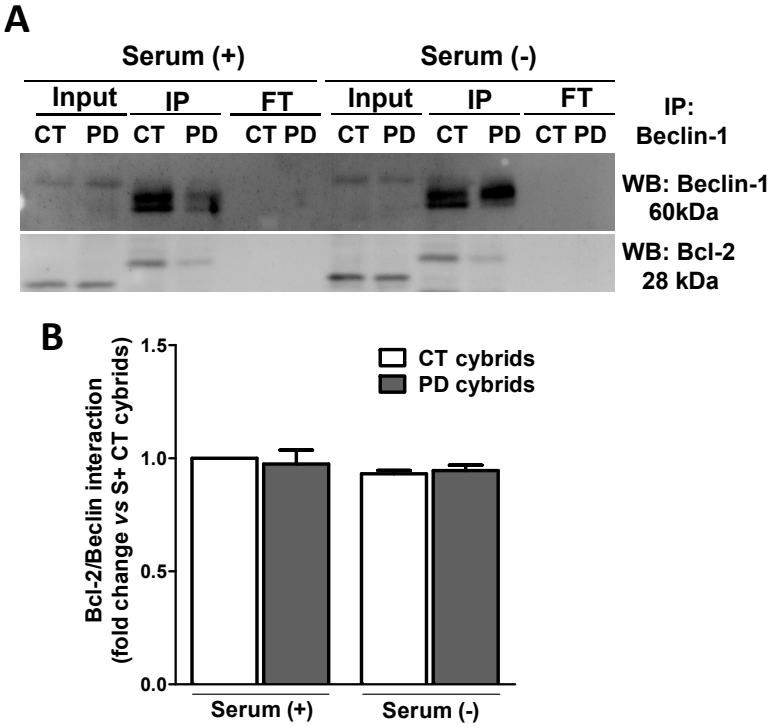

Figure V.17. Bcl-2/Beclin-1 physical interaction is not altered in sPD cybrid cells.
A. Co-immunoprecipitation of Beclin-1 and Bcl-2 in CT and PD cybrids maintained in serum (+) or serum (-) conditions. Levels of Beclin-1 (top) and Bcl-2 (bottom) in the input, immunoprecipitate (IP) and flow through (FT) are shown. **B.** Determination of Bcl-2/Beclin physical interaction (*n*=3).

Taken together, these data strongly suggest that the defects in autophagic flux and more remarkably in the autophagic response under serum starvation conditions are not due to defects in the nucleation complex machinery, and the initiation step of autophagy is not primarily affected in our models of sPD.

5.3.5 Deficient intracellular traffic results in incomplete autophagosome degradation and reduced autophagosome and mitochondria movements in sPD transmitochondrial cybrids

Autophagic failure found in our sPD cybrids model can begin from a delayed or interrupted traffic of autophagosomes along the microtubule system, which provides the tracks necessary for an efficient mobilization of cargos through the autophagy pathway. In support of this hypothesis, we have shown earlier that mitochondrial deficits induce alterations in microtubule network, mainly characterized by an increase in free/polymerized tubulin ratio that was responsible for high levels of α-synuclein oligomeric forms (Esteves et al., 2010a).

In order to correlate our previous findings with defective autophagic clearance, we have modulated microtubule-dependent trafficking of autophagosomes by using taxol (a microtubule polymerizing agent) and nocodazole (a microtubule depolymerizing agent) in concentrations that did not interfere with cell viability (data not shown), in the presence or absence of lysosomal inhibitors. Taxol was effective in promoting autophagy turnover in sPD cybrids, as reflected by decreased autophagosome content (**Figure V.18A and B**) and improved autophagic flux (**Figure V.18A and C**). In contrast, nocodazole considerably enhanced autophagosome accumulation in CT cybrids (**Figure V.18A and B**) associated with a decreased autophagic flux similar to what was observed in sPD cybrids (**Figure V.18A and C**).

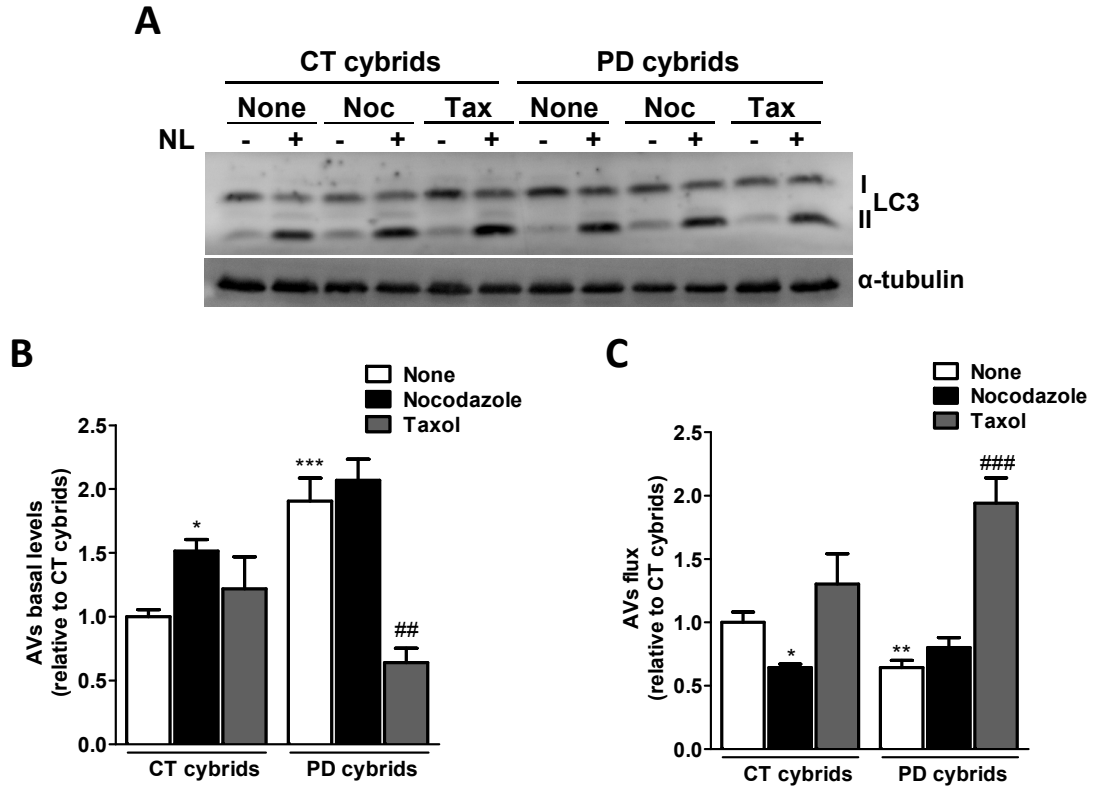

Figure V.18. Disruption of microtubule network results in a deficient autophagic turnover in PD cybrid cells.

A. Immunoblot for endogenous LC3B from CT and PD cybrids after treatment with Taxol (Tax) or Nocodazole (Noc) for 24 h. In the last 4 h, cells were co-treated with or without lysosomal inhibitors (NL). **B.** Determination of autophagic vacuole (AVs) levels. Values of LC3-II in the absence of NL represent the steady-state AV content (*n*=4, *p<0.05, ***p<0.001, versus CT cybrids; ##p<0.01, versus PD cybrids). **C.** Assessment of autophagic flux, determined as the ratio of LC3-II densitometric value of NL-treated samples over the corresponding untreated samples. (*n*=4, *p<0.05, **p<0.01, versus CT cybrids; ###p<0.001 versus PD cybrids).

These findings suggest that autophagosomes clearance may be dependent on the functional status of the microtubule-dependent intracellular traffic. If so, the dynamic interaction of autophagic vacuoles with the microtubule system tracks may be altered in our sPD models hampering autophagosome transport and so the fusion with lysosome. Accordingly, we observed a decreased degree of co-localization between LC3-positive vacuoles and Lamp-1-positive vacuoles in sPD cybrids, an effect that was reversed by taxol treatment **(Figure V.19A and B)**. This result may indicate an impairment of autophagosome-lysosome fusion, but could also point to a disruption in the

autophagosomal intracellular trafficking. In contrast, nocodazole treatment decreased LC3B/Lamp-1 co-localization in both CT and sPD cybrids **(Figure V.19A and B)**.

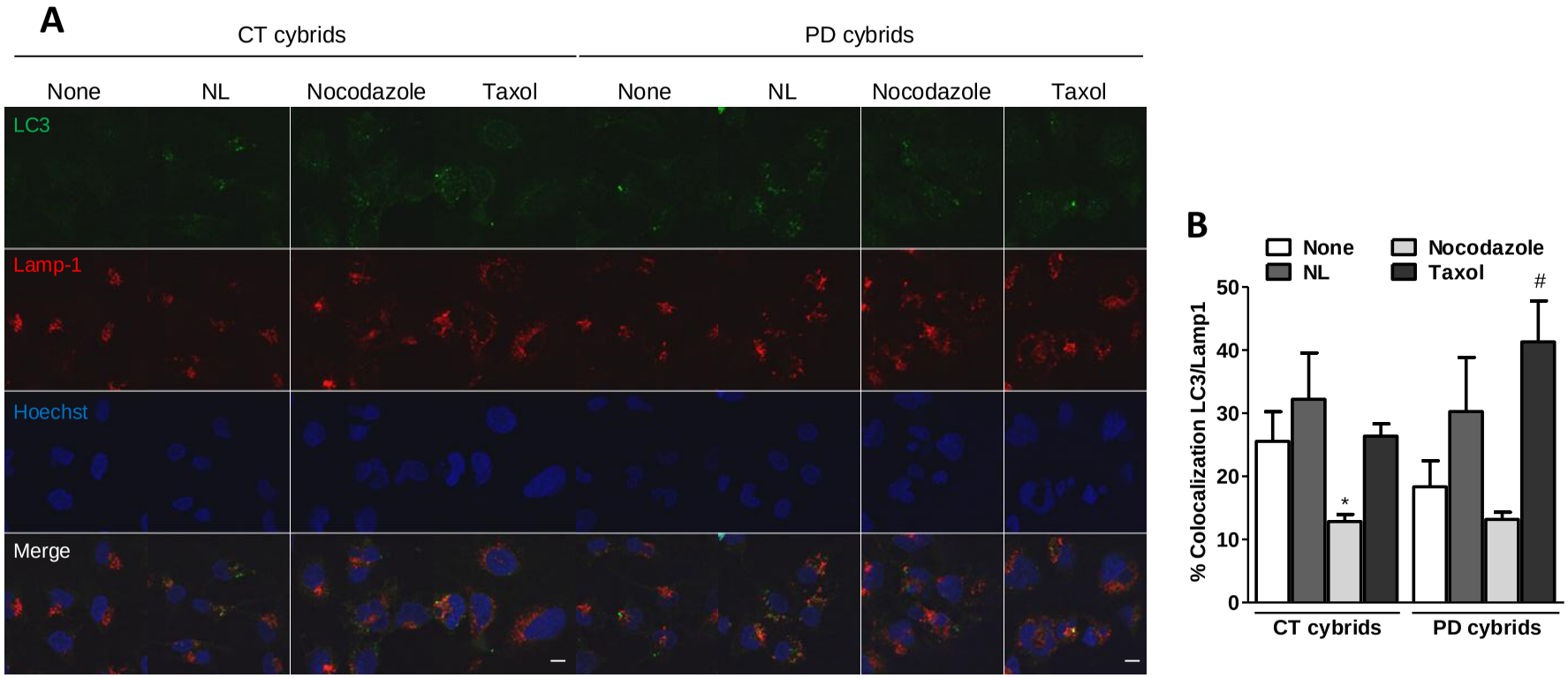

Figure V.19. Autophagosome-lysosome fusion is altered in PD cybrids.

A. LC3B (green) and Lamp-1 (red) immunostaining of CT and PD cybrids treated with Taxol (Tax) or Nocodazole (Noc) for 24 h. In the last 4 h, cells were co-treated with or without lysosomal inhibitors (NL). Scale bars: 10 µm. **B.** Assessment of LC3B and Lamp-1 colocalization (n=2, *p<0.05, versus untreated CT cybrids; $^{\#}$p<0.05, versus untreated PD cybrids).

Moreover, changes in autophagy progression between CT and sPD cybrids were also addressed by measuring the vesicle size distribution profile in the absence and presence of lysosomal inhibition (NL) (Bains and Heidenreich, 2009). Comparing the vesicle size distribution in these conditions reveals a further increase in larger vesicles > 1.5 μm, which under normal autophagy conditions are supposed to be quickly degraded (Bains and Heidenreich, 2009). In addition, we observed that in sPD cells there is a significant increase of the largest size autophagic vacuoles (>2.25 μm) indicating an accumulation of these structures which positively correlates with a decreased vesicular trafficking (**Figure V.20**).

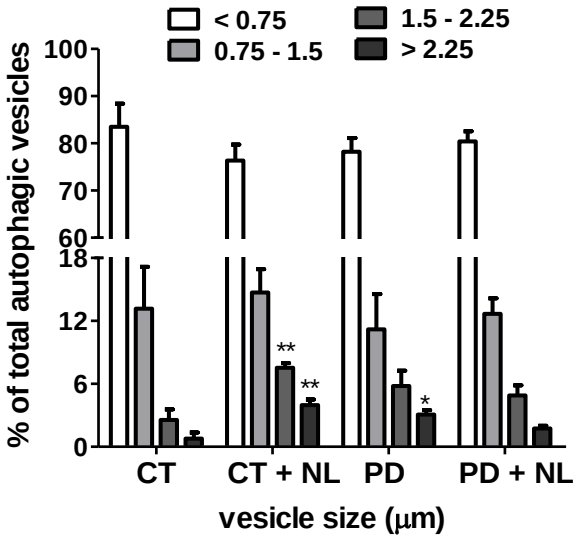

Figure V.20. Accumulation of autophagic vacuoles in CT and sPD cybrid cells.

LC3B immunostaining was used to determine AV size distribution from CT and PD cybrids after treatment with or without lysosomal inhibitors (NL). AV size distribution was graphed as percent of total vacuoles within the indicated size ranges. (*n*=4, *p<0.05, **p<0.001, versus CT cybrids).

In this context, we have also monitored autophagic vacuoles movements. For each observed autophagic vacuole, we recorded whether it moved or remained static (**Figure V.21A**), and subsequently the relative percentages of stationary or movable events were calculated (**Figure V.21B**). As shown in **Figure V.21B,** sPD cybrids exhibited a significant decreased number of movable autophagic vacuoles. In addition, microtubule disruption by nocodazole promoted a decrease in the number of movable autophagic vacuoles to similar values in both CT and sPD cybrids.

We have also determined autophagic vacuole transport velocity as described previously (Lee et al., 2011). Cumulative percentage data displayed a left shift in autophagic vacuole transport velocity in sPD cybrids compared with basal CT cybrids (**Figure V.21C1 and 2**). The shift in curve profiles was minimized when cells were treated with nocodazole or taxol (**Figure V.21C1 and 2**). Intriguingly, the effect of taxol was more pronounced for sPD cybrids, resulting in a deflection of the cumulative curve to a similar profile observed for CT cybrids (**Figure V.21C2**). Concerning average velocities, sPD cybrids demonstrated a significant reduction in autophagic vacuole movement velocity similar to what was observed for CT cybrids treated with nocodazole. On the other hand, taxol was able to restore autophagic vacuole velocity in sPD cybrids (**Figure V.21D**).

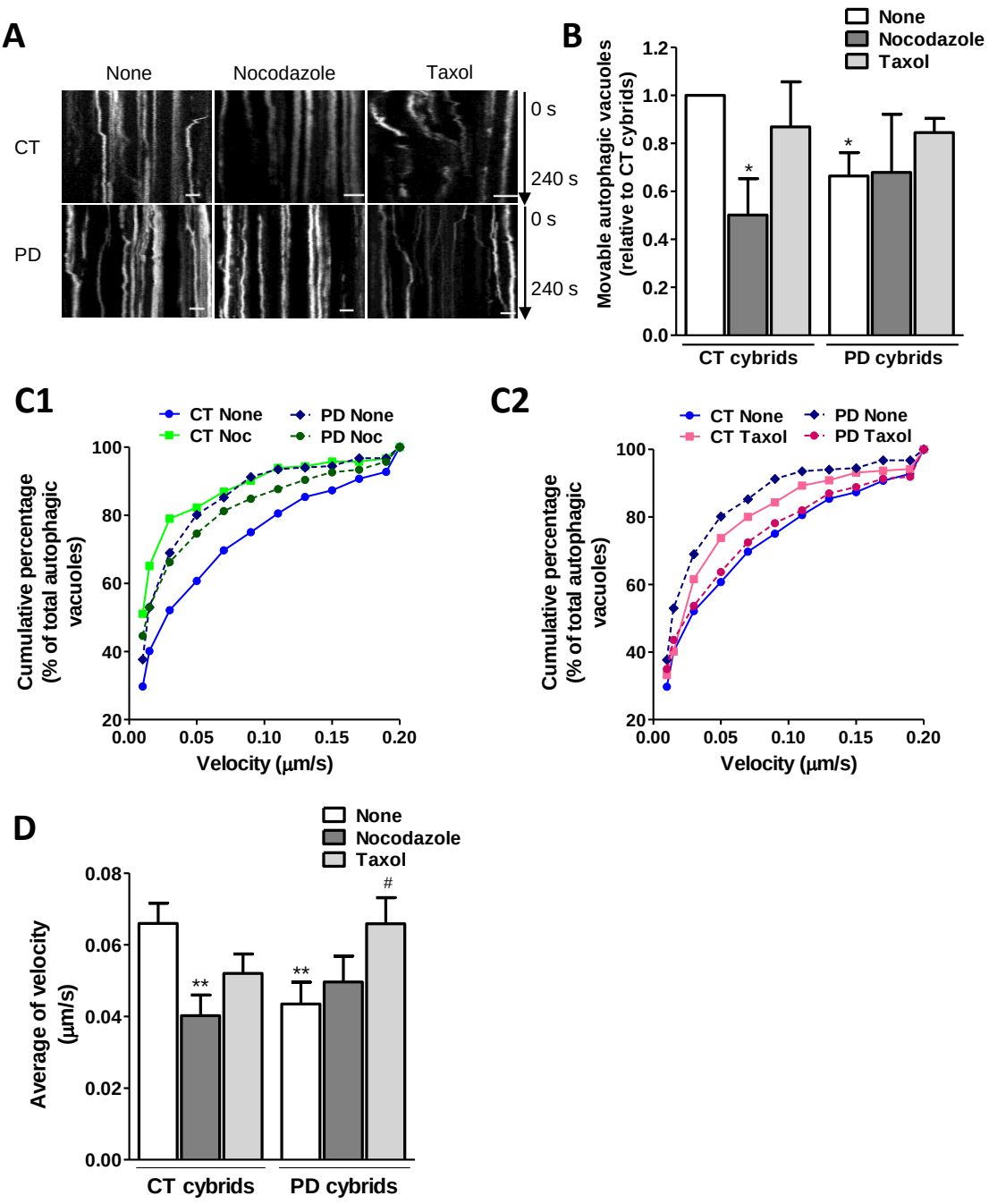

Figure V.21. Disruption of microtubule network results in reduced autophagic vacuole movements in PD cybrid cells.

A. Representative kymograph images (out of three experiments) of AV movement in CT and PD cybrid cells treated with nocodazole (24 h), taxol (24 h). Scale bars: 5 µm. **B.** Number of movable AVs when compared with those of total AVs (*n*=3, *p<0.05, versus CT cybrids). **C1.** and **C2.** Cumulative data for AV transport velocity in CT and PD cybrid cells treated with Noc (**C1**) or treated with taxol (**C2**) (*n*=3). **D.** Average transport velocity of AVs (µm/s) (*n*=3, **p<0.01, versus CT cybrids; $^{\#}$p<0.05, versus PD cybrids).

We believe that this process relies on a dynamic state of mitochondria at several levels of organization and interaction, such as the distribution of mitochondria within a cell, and the dynamic interaction with the vesicular trafficking and turnover mechanisms, as both autophagic vacuoles and mitochondria are driven by dynein and kinesin motors and depends on microtubule system tracks for transport within the cell (Arduino et al., 2010; Arduino et al., 2011a).

This premise led us to analyze alterations in mitochondrial movements in sPD cybrids. Similar to what was performed for autophagic vacuoles, we recorded whether mitochondria moved or remained static (**Figure V.22A**), and subsequently the relative number of stationary or movable events was calculated (**Figure V.22B**). As shown in **Figure V.22B,** sPD cybrids exhibited a significant decreased number of movable mitochondria in the fields studied. In addition, microtubule disruption by nocodazole, disruption of vesicular traffic by neutralizing acidic vesicles with NH_4Cl/leupetin (Strous et al., 1985), and serum removal further promoted a decrease in the number of movable mitochondria to similar values in both CT and sPD cybrids. In contrast, taxol was able to re-establish the number of movable mitochondria in sPD cybrid cells.

We have also measured mitochondrial transport velocity as described previously (Macaskill et al., 2009). Regarding average velocities, sPD cybrids demonstrated a significant decline in mitochondrial movement velocity. As expected, taxol promoted an increase in moving mitochondria velocity in both CT and sPD cybrids (**Figure V.22C**). A dramatic negative effect was found with nocodazole and even more remarkably following autophagic modulation (serum removal and lysosomal degradation inhibition) (**Figure V.22C**). As observed previously for autophagic vacuoles, cumulative percentage data displayed a left shift in mitochondrial transport velocity in sPD cybrids when compared with basal CT cybrids (**Figure V.22D1-4)**. In addition, this difference in curve profiles was abolished when cells were treated with nocodazole (**Figure V.22D1**) and under starvation (**Figure V.22D3**). Interestingly, the effect of lysosomal degradation inhibition was more pronounced for CT cybrids, resulting in a cumulative curve that was left-shifted relative to the sPD cybrid subjected to the same treatment (**Figure V.22D2**). Such effects were completely counteracted by taxol, reflected by a pull-down change in the cumulative curve profile (**Figure V.22D4**)**.** Surprisingly, this change was more obvious for sPD cybrids rather than for CT cybrids.

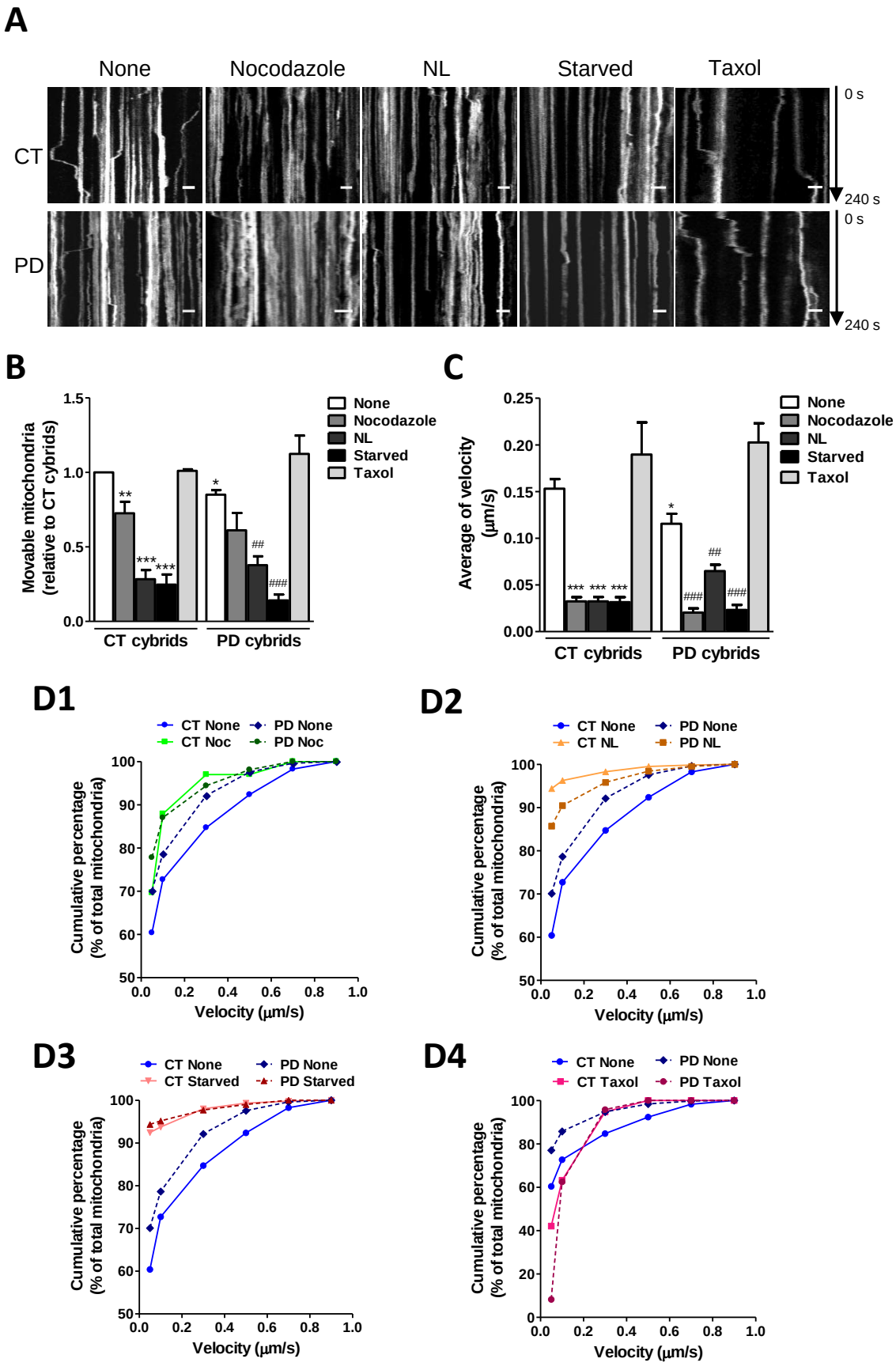
A
None
Nocodazole
NL
Starved
Taxol
CT
PD
0 s
240 s
0 s
240 s
B
Movable mitochondria (relative to CT cybrids)
None
Nocodazole
NL
Starved
Taxol
CT cybrids
PD cybrids
C
Average of velocity (µm/s)
None
Nocodazole
NL
Starved
Taxol
CT cybrids
PD cybrids
D1
CT None
PD None
CT Noc
PD Noc
Cumulative percentage (% of total mitochondria)
Velocity (µm/s)
D2
CT None
PD None
CT NL
PD NL
Cumulative percentage (% of total mitochondria)
Velocity (µm/s)
D3
CT None
PD None
CT Starved
PD Starved
Cumulative percentage (% of total mitochondria)
Velocity (µm/s)
D4
CT None
PD None
CT Taxol
PD Taxol
Cumulative percentage (% of total mitochondria)
Velocity (µm/s)

Figure V.22. Disruption of microtubule network results in reduced mitochondrial movements in PD cybrid cells.

A. Representative kymograph images (out of three experiments) of mitochondrial movement in CT and PD cybrid cells treated with nocodazole (24 h), taxol (24 h) and lysosomal inhibitors (NL, 4 h) or subjected to starvation (starved, 6h). Scale bars: 5 µm. **B.** Number of movable mitochondria when compared with those of total mitochondria (*n*=3, *p<0.05, **p<0.01, ***p<0.001, versus CT cybrids; $^{\#\#}$p<0.01, $^{\#\#\#}$p<0.001, versus PD cybrids). **C.** Average transport velocity of mitochondria (µm/s) (*n*=3, *p<0.05, ***p<0.001, versus CT cybrids; $^{\#}$p<0.05, $^{\#\#}$p<0.01, $^{\#\#\#}$p<0.001, versus PD cybrids). **D1-4**, Cumulative data for mitochondrial transport velocity in CT and PD cybrid cells treated with Noc (**D1**), NL (**D2**), subjected to starvation (**D3**) or treated with taxol (**D4**) (*n*=3).

Altogether, our data suggest that a correlation exists between mitochondrial motility and autophagic turnover, both processes being dependent on the dynamic stability and functional integrity of microtubule network.

5.3.6 Alterations in autophagic activity and defective microtubule-dependent transport result in a poor α-synuclein aggregate clearance

Autophagy deregulation has long been implicated in cellular ageing and α-synuclein toxicity during PD. Indeed, in PD, α-synuclein accumulation has been linked to alterations in chaperone-mediated autophagy and lysosomal system functioning (Cuervo et al., 2004; Martinez-Vicente et al., 2008; Vogiatzi et al., 2008; Xilouri et al., 2009). Therefore, we next investigated the impact of alterations in the autophagic activity due to mitochondrial deficits and altered microtubule transport in autophagy substrates and PD-related α-synuclein clearance.

We started by evaluating the levels of p62/SQSTM1, a selective substrate for autophagy as this protein is normally localized to the autophagosome via LC3 interaction and is continuously degraded by the autophagy–lysosome system (Bjorkoy et al., 2005). According to our previous data on LC3B-II flux (**Figures V.5A-D**), we have verified that p62 levels were significantly increased in sPD cybrids relative to CT cybrids (**Figure V.23A and B**).

We then analyzed the α-synuclein solubility and its propensity for oligomerization in the presence or absence of lysosomal proteolytic activity inhibitors by performing a Triton X-100 detergent fractionation. Overall, **Figure V.23C** and **E** shows that Triton-soluble and -insoluble a-synuclein band patterns, resulting from a-synuclein oligomerization, were comparable. However, it was clear that α-synuclein was

preferentially accumulated in oligomeric forms, in the detergent-soluble fraction (**Figure V.23C and D**). Interestingly, among them, we detected a band corresponding to the tetrameric form (denoted by an arrow in **Figure V.23C**) that has been recently shown as a helically folded structure in cells under physiological conditions (Bartels et al., 2011). We have observed that the generation of SDS-resistant and high molecular weight-soluble species of α-synuclein was enhanced in sPD cybrids relative to CT cybrids (**Figures V.23D and V.23F**). Moreover, we have also detected in sPD cybrids that lysosomal inhibition did not potentiate α-synuclein oligomers accumulation within cells (**Figures V.23C-V.23F**). Likewise, activation of nonselective autophagy upon serum removal was not able to efficiently shift back to a completely soluble non-oligomerized phenotype, further supporting the argument that the final steps of the autophagy-lysosome pathway are compromised in these cells.

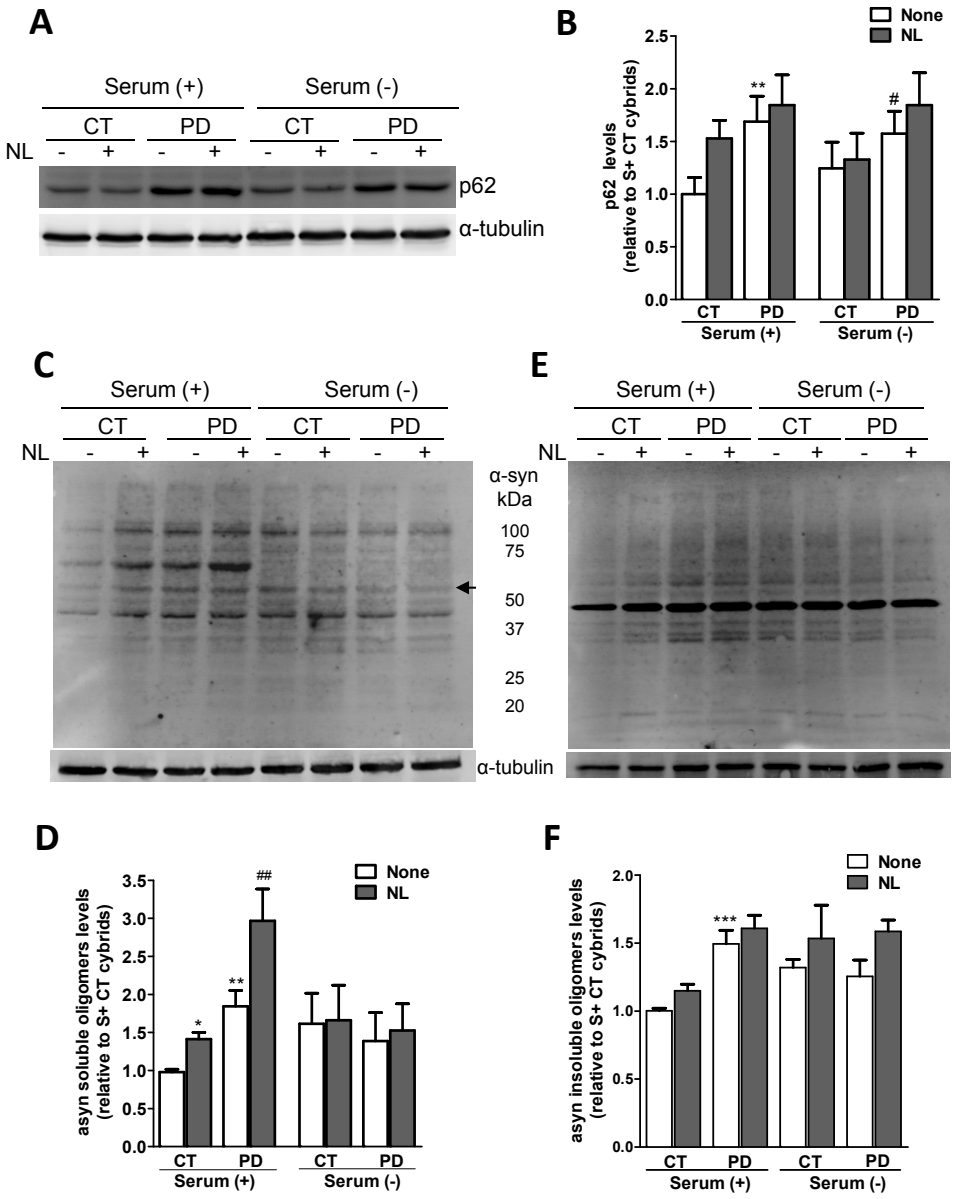

Figure V.23. α-Synuclein and p62 degradation by autophagy is impaired in cells harboring mitochondrial dysfunction.

A. Immunoblot for p62 from CT and PD cybrid cells cultured in S+ or S- conditions and treated with or without lysosomal inhibitors (NL). **B.** Densitometric analysis of p62 levels (*n*=6, **p<0.01, versus S+ CT cybrids; #p<0.05, versus S- CT cybrids). **C.** and **E.** Immunoblots for α-synuclein oligomeric forms from CT and PD cybrid cells cultured in S+ or S- conditions and treated with or without lysosomal inhibitors (NL). Representative blots of Triton X-100-soluble oligomeric species (**C**) and Triton X-100-insoluble, SDS-resistant oligomeric species (**E**). The arrow indicates a band of a tetrameric form of α-synuclein. **D.** and **F.** Densitometric analysis of α-synuclein-soluble oligomers content (**D**) (*n*=12, *p<0.05, **p<0.01, versus S+ CT cybrids; ##p<0.01, versus S+ PD cybrids) and α-synuclein-insoluble oligomers content (**F**) (*n*=12, ***p<0.001, versus S+ CT cybrids).

5.3.7 Impairment of autophagic turnover prompts apoptosis in cells harboring mitochondrial dysfunction

Autophagy is well recognized as a survival mechanism especially during conditions of nutrient limitation. Based on the “bulk” degradation of cytoplasmic material, autophagy is utilized to generate both nutrients and energy in starving cells. Under these conditions, autophagy is critical for maintaining cell survival. We have previously reported that, in our sPD cybrid model and MPP^+-treated cells, both mitochondria and endoplasmic reticulum-dependent apoptotic pathways are initiated during particular stressful circumstances of PD pathology (Esteves et al., 2008; Arduino et al., 2009a; Arduino et al., 2009b).

Here, we examined whether autophagic degradation impairment observed in our cellular models is also related to the apoptotic events described formerly. In order to check whether autophagy could be activated in cells with mitochondrial deficits as an attempt to prevent cell suicide by apoptosis, we used pharmacological modulators of autophagy and determined their roles on caspase-3-mediated apoptosis.

We observed that treatment of our cells with 3-methyladenine (3-MA), a pharmacological compound that inhibits the early sequestration events in autophagy, further stimulated caspase-3 activation in all models studied (**Figures V.24A-C**). Interestingly, co-incubation with MPP^+ significantly enhanced this activation in NT2 cells (**Figure V.24C**).

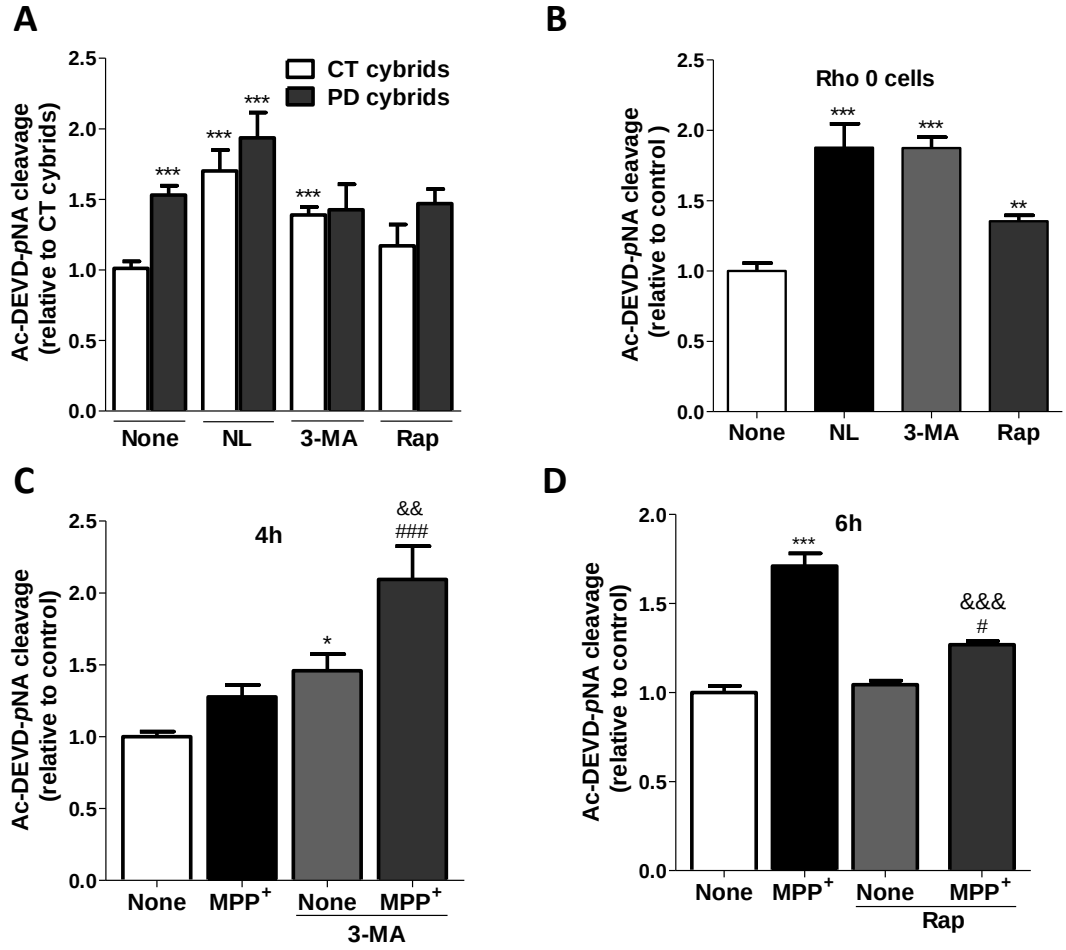

Figure V.24. Impaired autophagic turnover triggers caspase-3 over-activation in cells harboring mitochondrial deficits.

Caspase-3 activation was addressed by Ac-DEVD-*p*NA cleavage in CT and PD cybrids (**A**) (*n*= 12; ***p<0.001, versus S+ CT cybrids); NT2 Rho0 cells (**B**) (*n*= 5; **p<0.01, ***p<0.001, versus untreated Rho0 cells) treated with or without lysosomal inhibitors (NL), 3-methyladenine (3-MA) or rapamycin (Rap) for 4 h; and in MPP^+-treated NT2 Rho+ cells treated with or without 3-MA for 4 h (**C**) (*n*= 6-8; *p<0.001, versus untreated cells; $^{\#\#\#}$p<0.001, versus MPP^+-treated cells; $^{\&\&}$p<0.01, versus 3-MA-treated cells) or Rap for 6 h (**D**) as indicated (*n*= 6-8; ***p<0.001, versus untreated cells; $^{\#}$p<0.01, versus Rap-treated cells; $^{\&\&\&}$p<0.001, versus MPP^+-treated cells).

Rapamycin-induced autophagy did not prevent caspase-3 activation in sPD cybrids, which indicates that the autophagy-lysosomal pathway is impaired in this model as described previously (**Figure V.24A)**. However, rapamycin *per se* was able to further activate caspase-3 in Rho0 cells. **(Figure V.24B**). In MPP^+-treated cells, rapamycin counteracted the deleterious effects of MPP^+ on caspase-3 activation (**Figure V.24D**). Perhaps surprisingly, these results indicate different apoptotic

outcomes upon modulation of authophagy in the different paradigms of mitochondrial dysfunction.

In an acute model, such as MPP^+-treated cells, activation of autophagy by rapamycin can still protect cells. In chronic models with great compromise of mitochondrial function (Rho0 cells), both activation of autophagy by rapamycin or inhibition by 3-MA could be harmful to cells. Additionally, in an intermediate chronic stage, such as cybrids, cells may eventually succumb to biochemical processes typically associated with apoptosis when autophagy is inhibited by 3-MA, in accordance with NT2 cells, but has no additive effect on sPD cybrids. Moreover, when autophagy is stimulated by rapamycin, sPD cybrids are unable to efficiently proceed with the pathway probably due to vesicular traffic impairment, and still activate apoptosis. The mechanisms underlying these differences in cellular responses are unclear but might be related with different capacities of the cell models to compensate for autophagic dysfunction.

5.4 Discussion

In this study, we have demonstrated that a prolonged metabolic failure due to mitochondrial dysfunction, either in cellular models harboring sPD subjects mtDNA (sPD cybrids) or knock-down of all mtDNA (Rho0 cells) or in MPP^+-treated cortical neurons, causes a functional decline in the activity of the autophagic system. Consistently, in our models, autophagosomes are actively formed but some of their structural components and autophagic substrates are unable to be efficiently degraded within lysosomes. We propose that these alterations in autophagosome clearance can originate from a decreased efficiency in the mobilization of autophagosomes from their site of formation toward lysosomal compartments along the microtubule network, thereby impeding the assumed neuroprotective functions of autophagy.

Progress in the understanding of autophagy has emphasized its importance in cellular homeostasis, with significant consequences for the development of new therapeutic strategies for neurodegenerative disorders such as PD. In fact, ultrastructural examination has revealed an abnormal presence of autophagic vacuoles in myelinized neurons of the SNpc in PD patients, in contrast to the rare detection of autophagosomes in normal brains during ageing (Anglade et al., 1997).

Although the presence of accumulating autophagosomes could represent an aberrant activation of autophagy, we provide evidence that autophagy is not over-stimulated in our models and, instead, defective clearance of the autophagic vacuoles might account for those observations. In our study, the rapid accumulation of autophagosomes within a few hours after blocking of lysosomal proteolysis, even in primary cortical neurons, evidences a proper basal level of autophagic activity. However, and of significant relevance to PD pathology, the data on autophagic flux indicate that formed autophagosomes are not efficiently eliminated by lysosomal degradation. The situation in cortical neuron cultures treated with MPP^+ was somewhat different than in other cellular models, but essential features of the effects of PD-related mitochondrial impairment in the lysosomal pathway were confirmed in this primary neuron setting.

The aforementioned results raise the possibility that alterations in mitochondrial energy metabolism play a role in the modulation of autophagy and, therefore, multiple defects in mitochondria-dependent metabolism might be the initial events in sPD-related autophagy pathology.

Mitochondria are the site of many biochemical reactions fundamental for normal cellular functioning, particularly cellular energy production. Our data further confirm and extend prior studies demonstrating sPD cybrids ATP levels are reduced in sPD cybrids

relative to those of CT cybrids (Esteves et al., 2008; Esteves et al., 2009). In addition, mitochondrial respiration and pathways influenced by aerobic metabolism are also altered in sPD cybrids. sPD cybrids show reduced SIRT1 phosphorylation, reduced PGC-1α levels and increased NF-*k*B activation (Esteves et al., 2010c). In this context, although our findings indicate that ATP may be required to the autophagic response, especially during serum starvation, the lack of effect of the pyruvate/uridine deprivation on the autophagic response in Rho0 cells leads us to hypothesize that an imbalance in glycolytic ATP production is unlikely to represent a primary signal for autophagy deregulation, reinforcing the concept that mitochondrial dysfunction has a main role on the control of the autophagic response. In fact, it is well established that autophagy is an energy-sensitive process (Plomp et al., 1987; Schellens et al., 1988; Plomp et al., 1989). Although the various steps of the autophagic process may differ in their response to the energy status of the cell, early evidence indicated that all steps of this pathway are responsive to relatively small changes of intracellular ATP (Schellens and Meijer, 1991). Whether or not autophagosomes accumulate under ATP-depleted conditions would depend on the relative effects of energy depletion on sequestration and post-sequestrational steps of the autophagic pathway. In view of that, it was described that rapid mitochondrial depolarization with ATP loss did not induce mitochondrial degradation by autophagy, implying that additional mechanisms may regulate mitophagy in neurons (Van Laar et al., 2011).

Our results clearly support the idea that autophagy failure stemming from mitochondrial dysfunction is not translated into defects in autophagosome formation but mainly in the autophagosomes trafficking along the microtubule network toward the lysosomal compartment. Accordingly, in all of our paradigms, LC3B was observed in punctuated structures in both basal or serum deprivation conditions, supporting that the recruitment to the pre-autophagosomal structure is not affected. In addition, we did not find significant differences in the total cellular levels and subcompartimentalization of Beclin-1, a principal regulator in autophagosome formation. However, sPD cybrids exhibited increased basal levels of Bcl-2 mainly associated with increased targeting to mitochondria. Thus, the anti-autophagic activity of Bcl-2 was not verified as the mild changes observed in the binding and sequestration of Beclin-1 by Bcl-2 were not expected to disturb the formation of the class III PI3-kinase complex that is critical to the induction of autophagy. Even under serum starvation conditions, Bcl-2/Beclin-1 association in sPD cybrids was similar to that in CT cybrids allowing Beclin-1 to proceed with autophagy.

Autophagosome and lysosome movement relies on microtubules as tracks and dynein as a motor (Fass et al., 2006; Kimura et al., 2008). Thus, tubulin cytoskeleton is

fundamental to maintain the spatial organization of autophagy-lysosome pathway by conducting the trafficking of organelles and vesicles involved in different interactions during this process. We have previously described that sPD cybrids have mitochondria-dependent cytoskeletal changes, which manifest as microtubule depolymerization and increase in free tubulin levels (Esteves et al., 2010a). In this study, our results using modulators of microtubules assembly and intracellular traffic point to the fundamental requirement of an efficient microtubule network for the transport and so the clearance of autophagic cargos.

We confirm that autophagic flux is microtubule-dependent as depolymerization of microtubules with nocodazole inhibited the degradation of autophagosomes within lysosomes and microtubule stabilization with taxol potentiated autophagosome clearance and cargos motility. In addition, our results on live-cell imageing of autophagic vacuoles and mitochondrial transport clearly demonstrate that mitochondrial deficits as the ones described in our sPD cybrids (Esteves et al., 2008; Esteves et al., 2009; Esteves et al., 2010c) significantly impair autophagic vacuoles and mitochondrial motility, which alter autophagic and mitochondrial dynamics due to disruption of microtubule network trafficking. Moreover, these findings are in accordance with previous observations involving dyneins as essential motors (Jahreiss et al., 2008; Kimura et al., 2008), as starvation induced a slight decrease in the autophagosome flux in CT cybrids and a substantial decline in mitochondria motility. However, it is well established in the literature that starvation induces “bulk” autophagy. A possibility is that those findings could be associated with an intracellular redistribution and specific alterations in the membrane binding ability of cytoplasmic dyneins to organelles (Lin and Collins, 1993; Lin et al., 1994), contributing to their defective transport, but further studies are needed to clarify this point.

Thus, the key role of mitochondria as ATP fuel suppliers for microtubule turnover and microtubule-based motor proteins implies that inherent mitochondrial dysfunction and/or related defects in their distribution in sPD cybrids will have a profound effect on the autophagy-related vesicular trafficking and, as a consequence, autophagy turnover maintenance and function. Interestingly, alterations in microtubules associated with deficient axoplasmic flow, altered mitochondrial turnover and loss of synaptic connectivity, was observed in vulnerable neurons in AD (Cash et al., 2003).

In conjunction with altered mitochondrial function and motility, tubulin cytoskeleton alterations may contribute to the accumulation of protein aggregates and autophagic vesicles, and/or associated substrates, as observed in our sPD cybrid model. The levels of p62 and α-synuclein oligomerization profiles were concomitantly altered in these cells. These findings strongly support the hypothesis that aggregate-

prone proteins, such as α-synuclein, initially interact with p62, and then aggregation of the protein complex occurs in a p62-dependent manner but the aggregates are not efficiently degraded by autophagy. Our data show that the levels of autophagic activity and its efficiency in the clearance of specific substrates and/or aggregated α-synuclein are dependent on the metabolic status of the cell.

Under these circumstances, the resulting accumulation of α-synuclein oligomers, other toxic protein products, and/or damaged organelles, such as dysfunctional mitochondria, will obviously be detrimental for cell functioning and survival. Intracellular accumulation of toxic protein oligomers might in turn contribute to further failure of the autophagic system in cells, as aggregates might physically block vesicular trafficking by secondarily interacting with or sequestrating key elements involved in this process. Interestingly, when neuronal cybrids are differentiated, the resultant neurites exhibit several characteristics of blocked axons, such as α-synuclein aggregates reminiscent of LBs (Trimmer et al., 2009) and accumulation of vesicles resembling nonfused autophagic structures. Moreover, an inefficient degradation of dysfunctional mitochondria due to a decreased autophagic activity will uphold a positive feedback loop that will further propagate the neurodegenerative pathway in PD (Chu, 2012). Accordingly, long-term accumulation of autophagic compartments within cytosol can also be harmful as autophagosomes can became leaky, and if enzyme leakage occurs after fusion, it can lead to lysosomal breakdown and release of lysosomal hydrolases, which frequently activates cell death (Wong and Cuervo, 2010).

In summary, data reported in this work support our hypothesis that a mitochondrial dysfunction induces an alteration in microtubules assembly that unable autophagy turnover which, in turn, potentiates the accumulation of α-synuclein oligomers and, finally, prompts apoptosis.

Although it is predictable that autophagy may be a new therapeutic target in PD, the results obtained in this study indicate that therapeutic modulation in the context of sPD should be aimed at improving autophagy intermediates “backing up”. For example, targeting trafficking proteins (Pandey et al., 2007) and proteins involved in promoting autophagosomes-lysosomes fusion, such as those regulating endosomal fusion and multivesicular bodies (Jager et al., 2004; Filimonenko et al., 2007), will likely improve the efficiency of autophagosome maturation into autolysosomes for subsequent substrate degradation.

CHAPTER VI

Mitochondrial down regulation of tubulin acetylation-dependent intracellular trafficking blight macroautophagy

6.1 Summary

Sporadic Parkinson's disease (sPD) is characterized by mitochondrial dysfunction and abnormal accumulation of protein aggregates in a specific subset of neurons. We have previously shown that defects in microtubule (MT)-based transport associated to an altered mitochondrial metabolism contribute to autophagic pathology and neuronal toxicity observed in this devastating disorder. However, the molecular mechanism(s) underlying how these various events are connected remains elusive.

In this study we demonstrate that SIRT2, a NAD^+ dependent protein deacetylase, controls the functional ability of the autophagic system by modulating MT network acetylation dynamics and provide insights into the association between intracellular metabolism and proteotoxicity in sPD.

We used transmitochondrial cybrids that recapitulate pathogenic alterations observed in sPD patient brains. We observed that NAD^+ metabolism is altered in sPD cybrids contributing to sirtuin 2 (SIRT2) deacetylase activation and subsequent decreased tubulin acetylation. Pharmacological inhibition of SIRT2 deacetylase activity selectively enhanced acetylation at Lys40 of α-tubulin, stabilized MTs and facilitated the clearance of misfolded proteins and autophagic substrates through the MT network, preventing the alterations observed in sPD cybrids cells. This increase in intracellular traffic improved the flux of autophagy cargos and promoted their lysosomal degradation.

Our data provide a strong evidence for a functional role of tubulin acetylation on autophagic vesicular traffic and cargos clearance. Moreover, we identify MTs and SIRT2 mediated-MT acetylation as therapeutic targets in disorders such as sPD in which intracellular transport is altered.

6.2 Introduction

Parkinson's disease (PD) is a devastating neurodegenerative disorder of unknown origin mainly characterized by the loss of dopaminergic neurons from the substantia nigra pars compacta (SNpc) and the presence, in the affected brain regions, of intraneuronal proteinacious cytoplasmic inclusions termed Lewy Bodies (LBs) (Forno, 1996). The presence of LBs in vulnerable neurons affected by PD suggests that defective management of misfolded and aggregated protein may contribute to the pathogenesis of the disease. Cytoplasmic protein aggregates are carried by dynein motors and transported along the microtubule (MT) network to the microtubule-organizing center (MTOC) in the pericentriolar region, where they are concentrated (Johnston et al., 1998; Kopito, 2000). These MT-dependent deposits of protein aggregates are called aggresomes and share with LBs some striking biochemical and molecular characteristics (McNaught et al., 2002), which may explain the biogenesis of these structures found in PD. Therefore, the impairment of the MT system has been increasingly associated with abnormal accumulation of α-synuclein, the major component of LBs (Lee et al., 2006).

Although the mechanism whereby α-synuclein accumulates in LBs is not fully understood, evidence suggests that defective axonal transport of α-synuclein may itself contribute to the process. Supporting this observation, we have previously shown, in cellular models of sporadic PD (sPD) harboring mitochondrial dysfunction (sPD cybrids), cytoskeleton alterations which manifest as MT depolymerization and increased formation of α-synuclein oligomers (Esteves et al., 2009, 2010a). In addition, altered α-synuclein oligomerization pattern was further associated with decreased proteolytic flux through autophagy, resulting from a deficient mobilization of autophagosome cargos toward the lysosomal system due to disruption of MT-dependent trafficking (Arduíno et al., unpublished data).

The discovery that chemical inhibitors of SIRT2 change the characteristics of protein inclusion body and are protective against α-synuclein-induced cytotoxicity (Outeiro et al., 2007) support the association between α-synuclein aggregation and MT stability. In fact, SIRT2 is a cytoplasmic class III histone deacetylase that interacts with and deacetylates MTs *in vitro* and *in vivo* (North et al., 2003; North and Verdin, 2007). Acetylation has been associated with stable MTs, although this relationship is not clear-cut. Some studies have shown that acetylation enhances MT stability (Hubbert et al., 2002; Matsuyama et al., 2002), whereas others have suggested that acetylation occurs only on stable and not dynamic MTs, but the acetylation itself does not stabilize MTs

(Haggarty et al., 2003). Interestingly, recent evidence indicates that α-tubulin acetylation promotes the recruitment of both cytoplasmic dynein and kinesin-1 molecular motors to MTs, stimulating motor processivity on the cytoskeleton and anterograde and retrograde vesicle flux in neurons (Reed et al., 2006; Dompierre et al., 2007), which suggests a possible mechanistic association between inhibition of deacetylase activity and the enhancement of MT-dependent trafficking.

Since MT-dependent intracellular trafficking is altered in sPD (Arduíno et al., unpublished data) and that SIRT2 inhibitors demonstrate a neuroprotective effect (Outeiro et al., 2007), we investigated whether MT acetylation could regulate intracellular transport and compensate for the observed autophagic deficits observed in our models of sPD.

We found that both SIRT2 and HDAC6 inhibitors enhance tubulin acetylation and prevent alterations in MT network stability and functional integrity observed in sPD cybrids. However, inhibition of SIRT2 and HDAC6 deacetylase activity differentially affects autophagic activity and cargos degradation through the autophagy-lysosomal pathway. We show that increased autophagy turnover and associated transport is determined exclusively by SIRT2 inhibition in our models.

Our data demonstrate that SIRT2 selectively controls MT acetylation and establish a functional mechanistic link between intracellular metabolism and proteotoxicity in sPD, by influencing both the formation and catabolism of altered proteins.

6.3 Results

6.3.1 SIRT2 deacetylase activity is increased in the cytosol of hybrid cells harboring sPD patient mitochondria

To gain insight into the metabolic status and mitochondrial function in sPD cybrid cells, we have previously performed a deep characterization of the mitochondrial oxidative phosphorylation system and mitochondrial respiration by using high resolution respirometry (Esteves et al., 2008; Esteves et al., 2010c). In these analyses, we have observed several defects in energy metabolism-dependent processes, including a decline in ATP synthesis capacity and a sustained reduction in mitochondrial complex I and IV activities in sPD cybrid cells relative to control (CT) cells. In addition, we have also found that although the whole cell basal oxygen consumption was comparable between sPD and CT cybrids, the mitochondrial maximum respiratory capacity was decreased in sPD cybrids. These observations on mitochondrial function and ATP production predict alterations on the steady state levels and redox state of pyridine nucleotides, such as NADt (NAD^+ plus NADH), which constitute important indicators and regulators for cell state and metabolic signaling activity (Pollak et al., 2007).

As shown in the **Figure VI.1,** we observed that the total NAD^+/NADt ratio was significantly increased in PD cybrids when compared to CT cybrids.

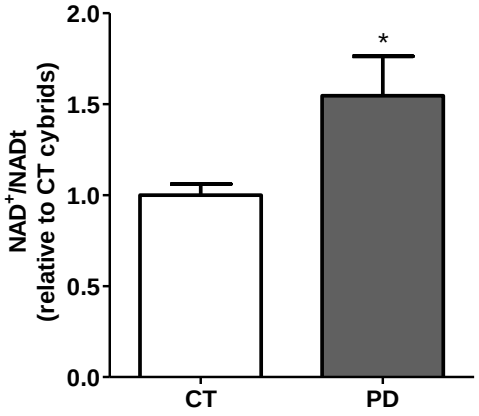

Figure VI.1. NAD^+ metabolism is altered in sPD cybrid cells.

Total nicotinamide adenine dinucleotide (NADt, NADH plus NAD^+) levels were determined as described in Chapter II and NAD^+ levels were obtained subtracting NADH to NADt levels. NAD^+/NADt ratios were then corrected for total protein levels. Values are mean±S.E.M (*n*=4, *p<0.05 versus CT cybrids).

SIRT2 is activated by elevated NAD^+ levels. In addition, NAD^+/NADH intracellular pools (cytosolic, mitochondrial and nuclear) are distinct and not entirely interdependent, suggesting that NAD^+ biosynthesis is compartmentalized and that NAD^+ levels may be differentially regulated within each compartment (Magni et al., 2008). In line with this, we next assessed the cellular subcompartmentalization of SIRT2 in cytosol-, mitochondria-, nuclei and cytoskeleton-enriched fractions. We have observed that the content of SIRT2 was increased in the cytosolic fraction of sPD cybrids relative to CT cybrids (**Figure VI.2A and B**).

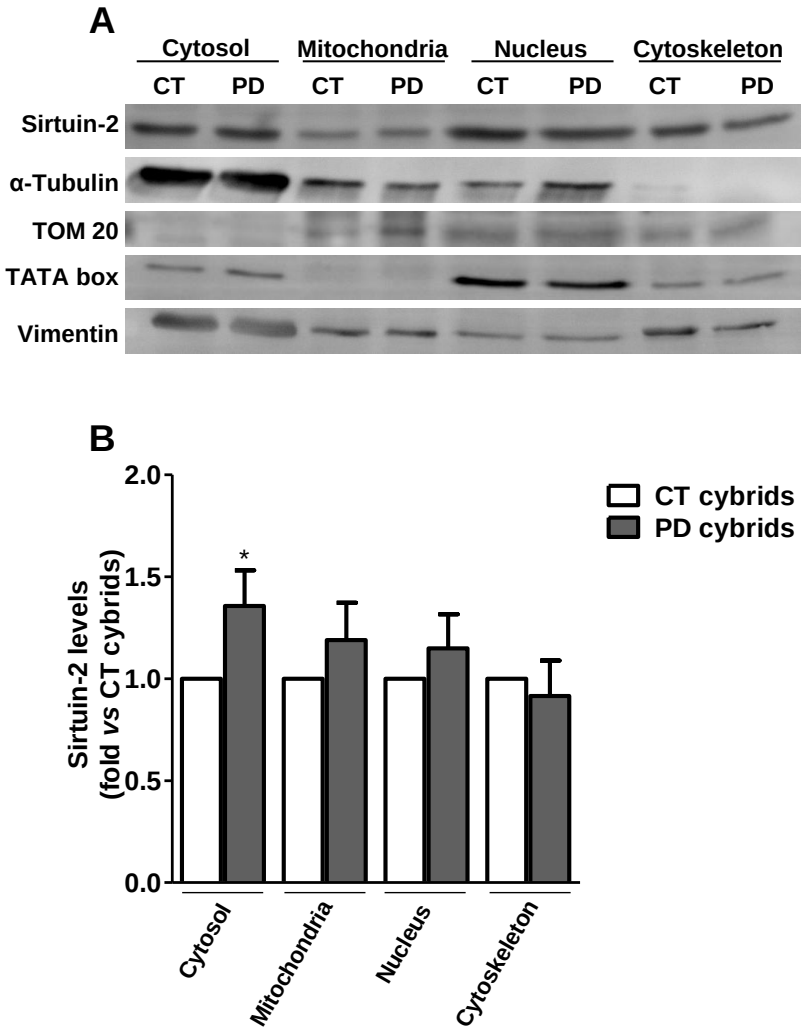

Figure VI.2. SIRT2 is preferentially localized in the cytosolic pool in sPD cybrid cells.

A. Cell lysates of cytosol-, mitochondria-, nuclei- and cystoskeleton-enriched fractions from CT and sPD cybrids were examined by immunoblotting using the anti-SIRT2, anti-α-tubulin, anti-TOM20, anti-TATA box, and anti-vimentin antibodies. Representative immunoblot for SIRT2 cellular subcompartmentalization in cytosol-, mitochondria-, nuclei- and cystoskeleton-enriched fractions. **B.** Densitometric analysis of the levels of SIRT2 normalized against to each fraction corresponding loading control. Values are mean±S.E.M. (*n*=6, *p<0.05 versus CT cybrids).

These results further confirm and extend prior observations demonstrating that SIRT2 levels are, among the cellular subcompartments, higher in the cytosolic pool as well as in the nuclear pool where it can be located, regulating cell cycle as well (Afshar and Murnane, 1999; North et al., 2003; North and Verdin, 2007).

The increased total NAD^+/NADt ratio in conjunction with high SIRT2 levels in sPD cybrids cytosolic pool led us to hypothesize that SIRT2 deacetylase activity may be enhanced in sPD cybrids. Indeed, we have observed a decrease in the cystosolic levels of acetylated α-tubulin in sPD cybrids when compared to CTs (**Figure VI.3A and B)**, which constitutes an indirect evidence for an increased SIRT2 deacetylase activity over the tubulin cytoskeleton in those cells.

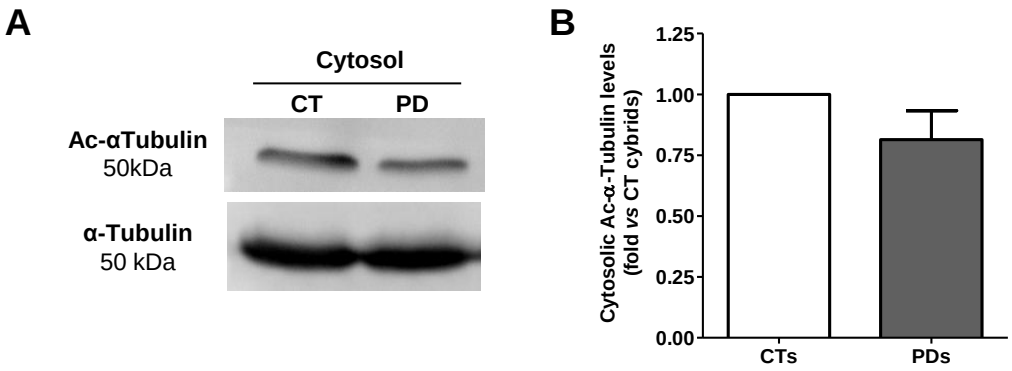

Figure VI.3. Altered NAD^+ metabolism regulates SIRT2 activation in the cytosolic pool of sPD cybrid cells.

A. Cell lysates of cytosol-enriched fractions from CT and sPD cybrids were examined by immunoblotting using the anti-acetyl-α-tubulin and anti-α-tubulin antibodies. Representative immunoblot for SIRT2 levels in cytosol-enriched fractions. **B.** Densitometric analysis of the levels of SIRT2. Values are mean±S.E.M. (*n*=3).

Together, these data suggest that mitochondrial metabolism may regulate SIRT2 deacetylase activity in a NAD^+-dependent manner in our cybrid cell models and can physiologically correlate MT dynamics to energy status in PD milieu.

6.3.2 Promotion of tubulin acetylation levels by specific inhibition of SIRT2 and HDAC6 prevents MT network impairments in sPD cybrid cells

We then decided to directly explore the actual role of SIRT2 deacetylase on the α-tubulin cytoskeleton integrity in our cybrid cell models.

SIRT2 colocalizes with the MT network and deacetylates Lys40 of α-tubulin (North et al., 2003). The same residue of α-tubulin is also deacetylated by HDAC6, a class II HDAC, and deacetylation by HDAC6 leads to changes in cellular motility (Hubbert et al., 2002). SIRT2 and HDAC6 are found along MTs in a complex structure (SIRT2/HDAC6/α-tubulin complex), suggesting that the two proteins coordinately regulate the level of tubulin acetylation (North et al., 2003). In addition, tubulin only binds the SIRT2/HDAC6 complex and not individual HDAC6 or SIRT2 proteins (Nahhas et al., 2007).

Thus, we firstly determined the acetylation state of α-tubulin in our models by analyzing the effects of two deacetylase inhibitors, AK-1 and Tubastatin A, which specifically inhibit SIRT2 and HDAC6, respectively. Under basal conditions, sPD cybrids showed decreased acetylation levels at Lys40 of α-tubulin relative to CT cybrids (**Figure VI.4A and B**). Treatment with both AK-1 and Tubastatin A significantly restored the acetylation of α-tubulin in a dose-dependent manner. This effect was more obvious for Tubastatin A, which significantly enhanced the acetylation levels in both CT and sPD cybrid cells (**Figure VI.4C and D).** The total levels of α-tubulin in CT and sPD cybrids is not different (Esteves et al., 2009, 2010a), further supporting a specific decrease of tubulin acetylation in sPD cybrids.

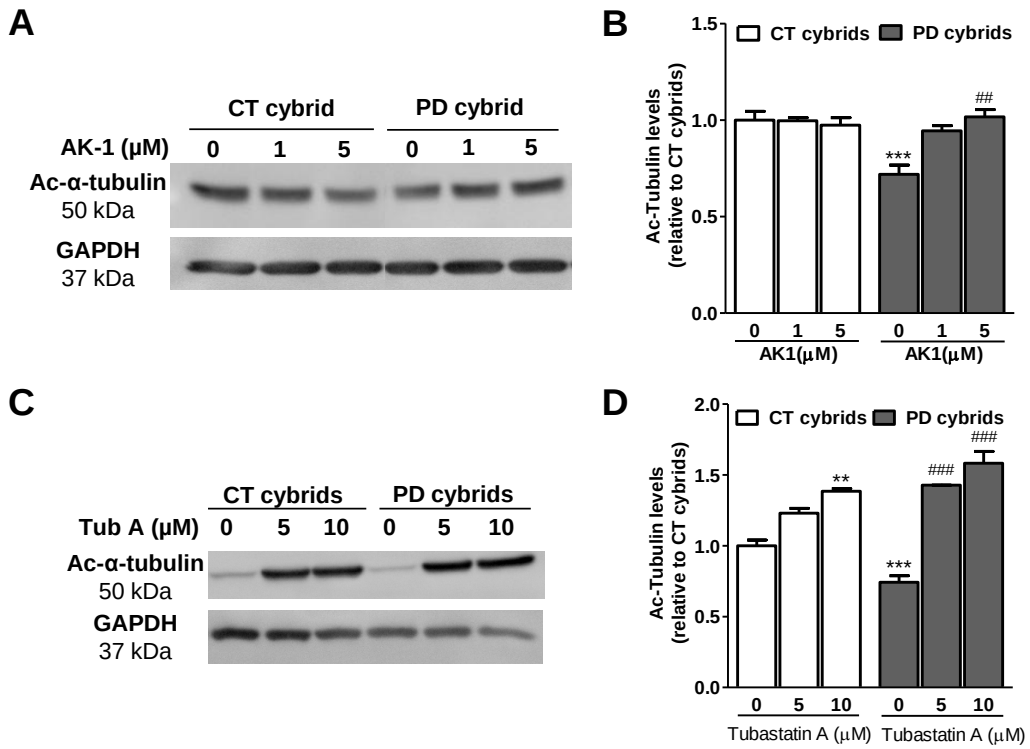

Figure VI.4. Tubulin acetylation is selectively modulated by specific inhibition of SIRT2 and HDAC6 tubulin deacetylases.

A. Cell lysates from CT and sPD cybrids treated with or without AK-1 (1 μM and 5 μM, 24 h) were examined by immunoblotting using the anti-acetyl-α-tubulin and anti-GAPDH antibodies. Representative immunoblot for acetylated α-tubulin levels. **B.** Densitometric analysis of the levels of acetylated α-tubulin. Values are mean±S.E.M. (*n*=5, ***p<0.001, versus untreated CT cybrids; $^{\#\#}$p<0.01, versus untreated sPD cybrids). **C.** Cell lysates from CT and sPD cybrids treated with or without Tubastatin A (Tub A, 5 μM and 10 μM, 24 h) were examined by immunoblotting using the anti-acetyl-α-tubulin and anti-GAPDH antibodies. Representative immunoblot for acetylated α-tubulin levels. **D.** Densitometric analysis of the levels of acetylated α-tubulin. Values are mean±S.E.M. (*n*=5, **p<0.01, ***p<0.001, versus untreated CT cybrids; $^{\#\#\#}$p<0.001, versus untreated sPD cybrids).

Acetylation has been shown to increase MT stability. Therefore, we next considered how AK-1 and Tubastatin (SIRT2 and HDAC6 inhibition, respectively) could contribute to increased MT stability and structural integrity.

We have evaluated MT morphology at steady-state in CTs and AK-1- or Tubastatin A-treated cells by indirect immunofluorescence. We have found that similar to CT cybrids, MTs in sPD cybrids also emanated from MTOC, but appeared shorter and more gnarled than in CT cells. Inhibition of SIRT2 and HDAC6 deacetylase activity further improved MT network in both CT and sPD cybrid cells. Interestingly, Tubastatin

A induced a more extensive MT bundling (**Figure VI.5**) visualized as bright fluorescent foci appearing in MTOC and cell periphery.

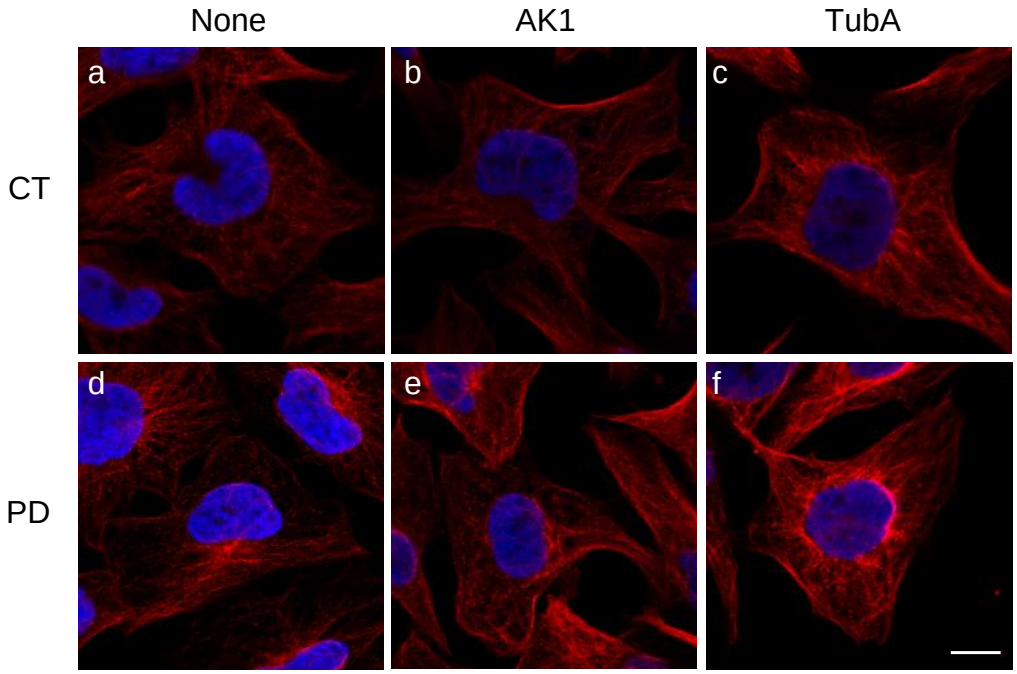

Figure VI.5. Inhibition of SIRT2- and HDAC6–dependent tubulin deacetylation improves MT network morphology.

Cells from CT and sPD cybrids were treated with or without AK-1 (5 µM, 24 h) or Tubastatin A (Tub A, 10 µM, 24 h) and the MTs were visualized by indirect immunofluorescence using an anti-α-tubulin antibody (red). Hoechst 33342-stained nuclei are in blue. Scale bar, 10 µm.

In support, quantitative immunobloting of soluble (free) and cytoskeleton/microtubule bound (polymerized) tubulin confirmed an increased MT destabilization in sPD cybrids in comparison to CT cybrids. This was reflected by a higher free/polimeryzed tubulin ratio, as previously reported in another set of cybrid cells (Esteves et al., 2009). Notably, the proportion of total α-tubulin that is assembled significantly increased after both AK-1 and Tubastatin A treatments, evidenced by a decrease in the ratio free/polimeryzed tubulin ratio in sPD cybrids to values similar to CT cybrids (**Figure VI.6 A-D)**.

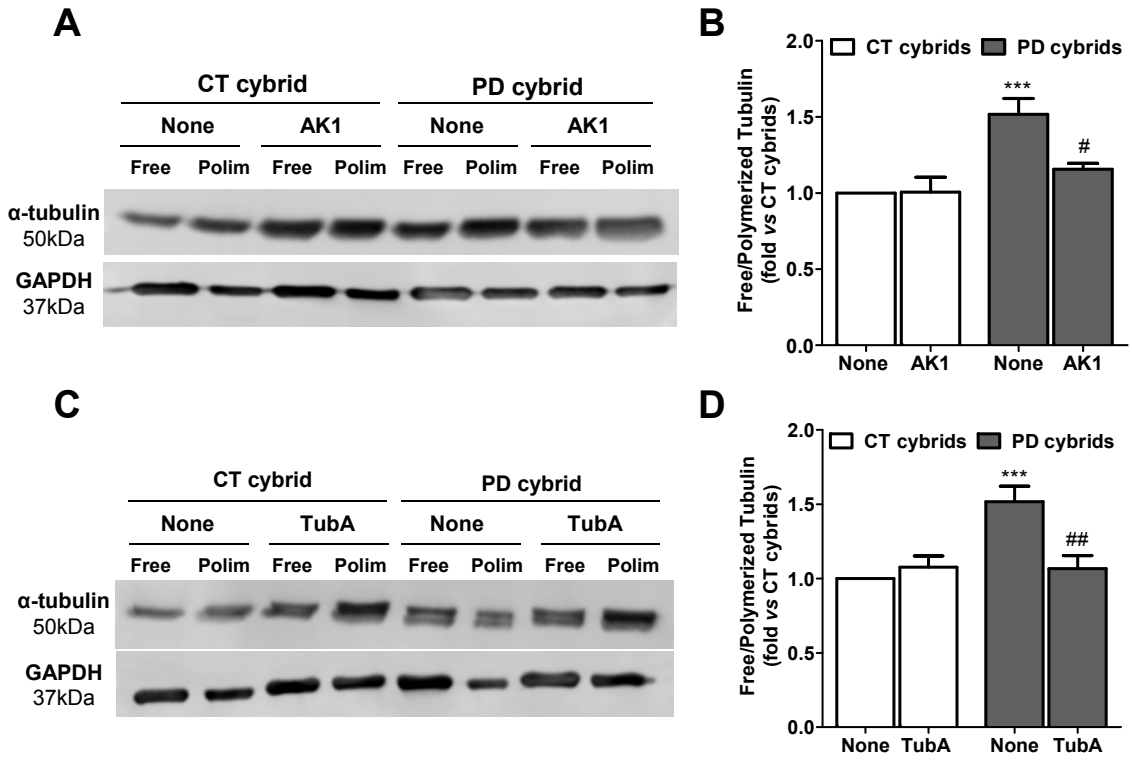

Figure VI.6. Inhibition of SIRT2- and HDAC6-dependent tubulin deacetylation improves MT network structural integrity.

A. Cell lysates containing soluble (free) and MT-bound (polymerized, polim) tubulin from CT and sPD cybrids treated with or without AK-1 (5 μM, 24 h) were examined by immunoblotting using the anti-α-tubulin and anti-GAPDH antibodies. Representative immunoblot for α-tubulin levels. **B.** Densitometric analysis of the levels of free and polymerized α-tubulin. Values represent the ratio free/polymerized tubulin calculated as the ratio of free α-tubulin densitometric value over the corresponding polymerized α-tubulin value. Values are mean±S.E.M. (*n*=4-8, ***p<0.001, versus untreated CT cybrids; $^{\#}$p<0.05, versus untreated sPD cybrids). **C.** Cell lysates containing soluble (free) and MT-bound (polymerized, polim) tubulin from CT and sPD cybrids treated with or without Tubastatin A (Tub A, 5 μM, 24 h) were examined by immunoblotting using the anti-α-tubulin and anti-GAPDH antibodies. Representative immunoblot for α-tubulin levels. **D.** Densitometric analysis of the levels of free and polymerized α-tubulin. Values represent the ratio free/polymerized tubulin calculated as the ratio of free α-tubulin densitometric value over the corresponding polymerized α-tubulin value. Values are mean±S.E.M. (*n*=4-8, ***p<0.001, versus untreated CT cybrids; $^{\#\#}$p<0.01, versus untreated sPD cybrids).

Together, these results show that the structural and functional defects related to MT depolimerization observed in sPD cybrids may be associated with reduced acetylation levels of their tubulin cytoskeleton. In addition, the MT network impairments observed in sPD cybrids can be overcome by enrichment in tubulin acetylation via inhibition of SIRT2 and HDAC6 catalytic activities.

6.3.3 Specific inhibition of SIRT2 catalytic activity improves the autophagic turnover in sPD cybrid cells

Autophagosome formation, sorting, and subsequent cargo transport towards lysosomes are regulated by MTs (Matteoni and Kreis, 1987; Fass et al., 2006; Kochl et al., 2006). Specifically, hyperacetylation of tubulin results in higher affinity of motor proteins to MTs (Reed et al., 2006; Dompierre et al., 2007), which lead to extended motor attachment and enhanced motor processivity on the cytoskeleton.

We have previously shown that in our sPD cybrid model autophagosomes are actively formed but not efficiently eliminated by lysosomal degradation. Defective autophagic clearance ability was associated with impairments in MT trafficking stemming from mitochondrial dysfunction (Arduíno et al., unpublished data). As SIRT2 and HDAC6 regulate tubulin acetylation and MT assembling, we considered the possibility that the decreased autophagic degradation associated to the deregulation of MT-dependent vesicle trafficking may involve SIRT2 and HDAC6 deacetylase activity. To test this hypothesis, we evaluated autophagosome formation by directly measuring the cellular distribution of endogenous LC3B and the turnover of the lipid-conjugated form of the autophagosome marker light chain 3, LC3B-II, (autophagic flux), as determined by comparing the accumulation of autophagosomes after inhibition of lysosomal proteolysis with NH_4Cl/leupeptin (NL) relative to the steady-state levels of autophagosomes (Rubinsztein et al., 2009).

As previously shown**,** under basal conditions, sPD cybrids demonstrate an increase in both the number and size of endogenous LC3B puncta relative to CT cybrids (**Figure VI.7Aa** versus **c**), but when lysosomal degradation was inhibited this number increased more markedly in CT cybrids (**Figure VI.7Ab** versus **d**). Treatment with AK-1 further activated autophagy in a higher extent in sPD cybrids than in CT cybrids, as depicted by the higher increase in the number of bright puncta (**Figure VI.7e** versus **f,** compared with **g** versus **h**). In contrast to the effects of SIRT2 inhibition, no effects were observed upon Tubastatin A treatment on autophagosome formation and autophagic activity (**Figure VI.7i** versus **j,** compared with **a** versus **b,** and **k** versus **l,** compared with **c** versus **d**).

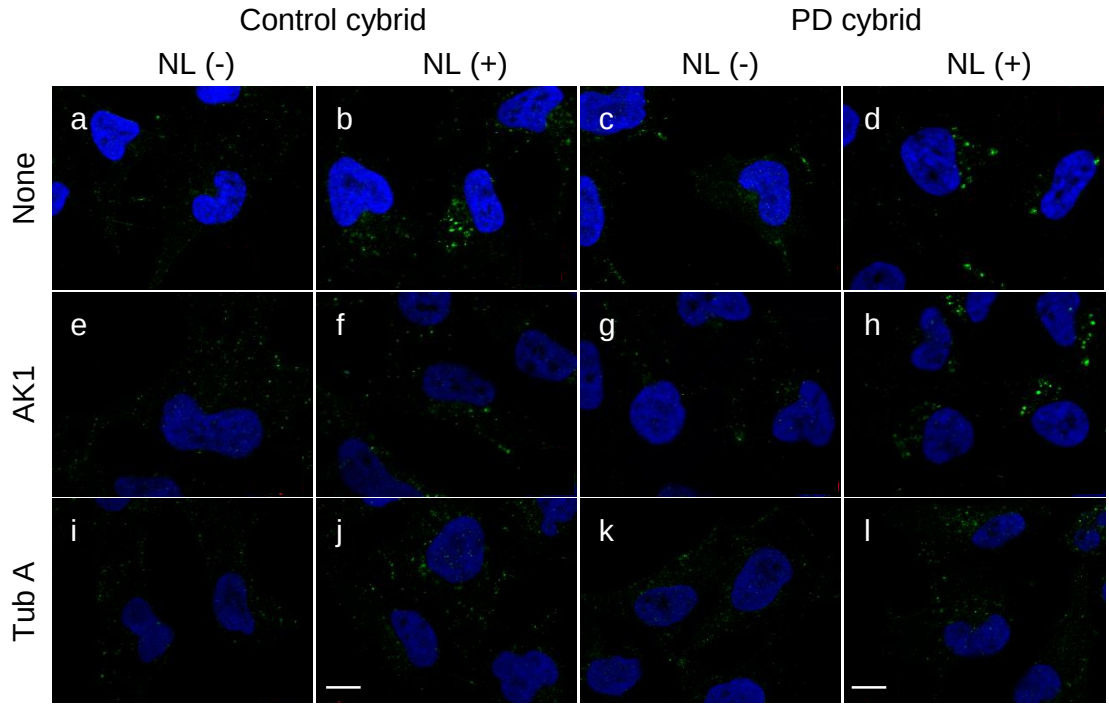

Figure VI.7. Inhibition of SIRT2- and HDAC6-dependent tubulin deacetylation differentially regulates the autophagic turnover.

Cells from CT and sPD cybrids were treated with or without AK-1 (5 µM, 24 h) or Tubastatin A (Tub A, 10 µM, 24 h), following culture in the presence or absence of lysosomal inhibitors (NL) for the last 4 h. LC3B (green)-positive vesicles were visualized by indirect imunofluorescence. Hoechst 33342-stained nuclei are in blue. Scale bars, 10 µm.

The induction of autophagy was also evaluated by examining the levels of LC3B-II. Consistent with the LC3B puncta staining data, when compared with CTs, AK-1 treatment led to a decreased autophagosome content (decreased LC3-II levels) associated to improved autophagic flux in sPD cybrid cells **(Figure VI.8)**.

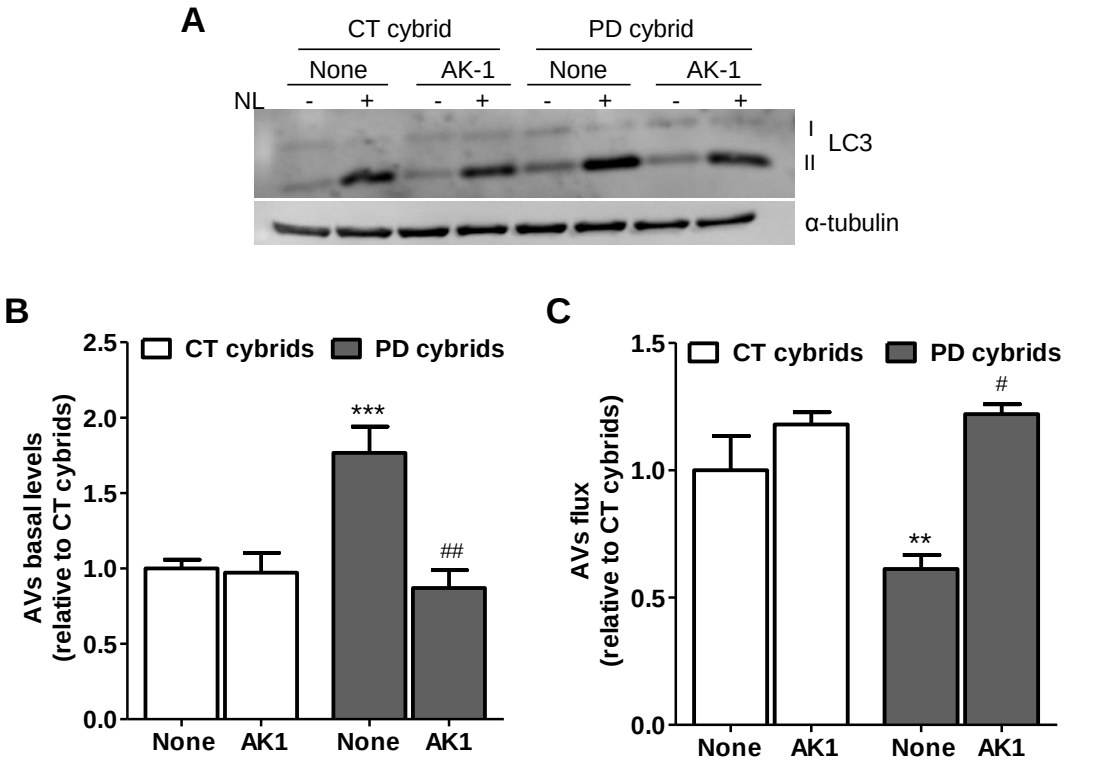

Figure VI.8. Inhibition of SIRT2-dependent tubulin deacetylation improves the autophagic turnover.

A. Cell lysates from CT and sPD cybrid cells treated with or without AK-1 (5 μM, 24 h) in the presence or absence of lysosomal inhibitors (NL, last 4 h) were examined by immunoblotting using the anti-LC3B and anti-α-tubulin antibodies. **B.** Determination of autophagic vacuole (AVs) basal levels. Values of LC3-II in the absence of NL represent the steady-state AV content. Values are mean±S.E.M. (*n*=3-6, ***p<0.001, versus untreated CT cybrids; $^{\#\#}$p<0.01, versus untreated sPD cybrids). **C.** Assessment of autophagic flux, determined as the ratio of LC3-II densitometric value of NL treated samples over the corresponding untreated samples. Values are mean±S.E.M. (*n*=3-6, **p<0.01, versus untreated CT cybrids; $^{\#}$p<0.05, versus untreated sPD cybrids).

Conversely, inhibition of HDAC6 by Tubastatin A induced a dramatic reduction on the autophagic flux in CT cybrids and no positive effects were observed for sPD cybrid cells **(Figure VI.9)**, indicating that this effect may be related with the direct involvement of HDAC6 in the autophagic pathway (Kawaguchi et al., 2003).

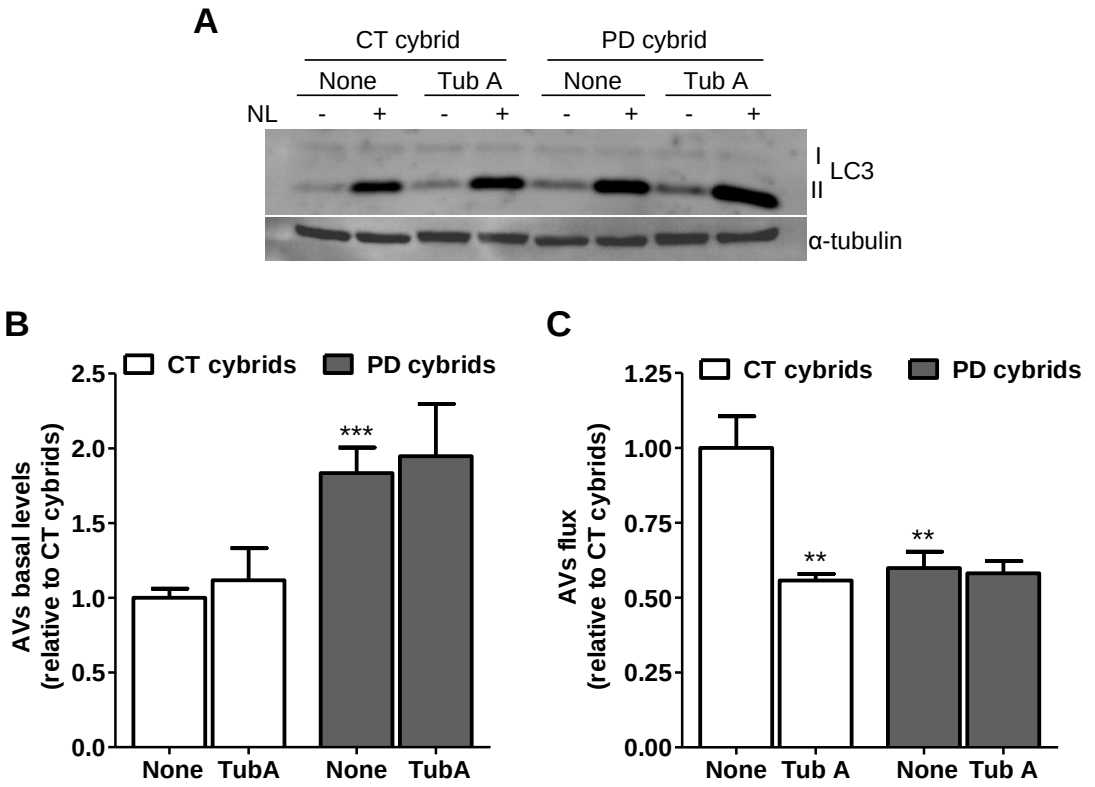

Figure VI.9. Inhibition of HDAC6 catalytic activity declines the autophagic turnover.

A. Cell lysates from CT and sPD cybrid cells treated with or without Tubastatin A (Tub A, 10 µM, 24 h) in the presence or absence of lysosomal inhibitors (NL, last 4 h) were examined by immunoblotting using the anti-LC3B and anti-α-tubulin antibodies. Representative immunoblot for LC3B-I and II levels. **B.** Determination of autophagic vacuole (AVs) basal levels. Values of LC3-II in the absence of NL represent the steady-state AV content. Values are mean±S.E.M. (*n*=3-6, ***p<0.001, versus untreated CT cybrids). **C.** Assessment of autophagic flux, determined as the ratio of LC3-II densitometric value of NL treated samples over the corresponding untreated samples. Values are mean±S.E.M. (*n*=3-6, **p<0.01, versus untreated CT cybrids).

Collectively, these data suggest that SIRT2-mediated tubulin acetylation is a major determinant for an efficient autophagic activity.

6.3.4 SIRT2-dependent tubulin deacetylation regulates α-synuclein protein inclusion clearance

There is evidence that SIRT2 inhibitors ameliorate the neurodegenerative phenotypes of cell and animal models of PD by dramatically modulating the formation of α-synuclein protein inclusion (Outeiro et al., 2007). Additionally, α-synuclein has been shown to interact with MTs (Iseki et al., 2000; Payton et al., 2001; Alim et al., 2004; Zhou et al., 2010), which prompted us to ask whether SIRT2 and HDAC6 inhibition might also modify the oligomerization pattern of α-synuclein previously observed in our sPD cybrid cells [(Esteves et al., 2009, 2010a) and Arduíno et al., unpublished data)].

Treatment with AK-1 significantly reduced the presence of both soluble and insoluble high molecular weight oligomeric species of α-synuclein in both CT and sPD cybrids **(Figure VI.10)**.

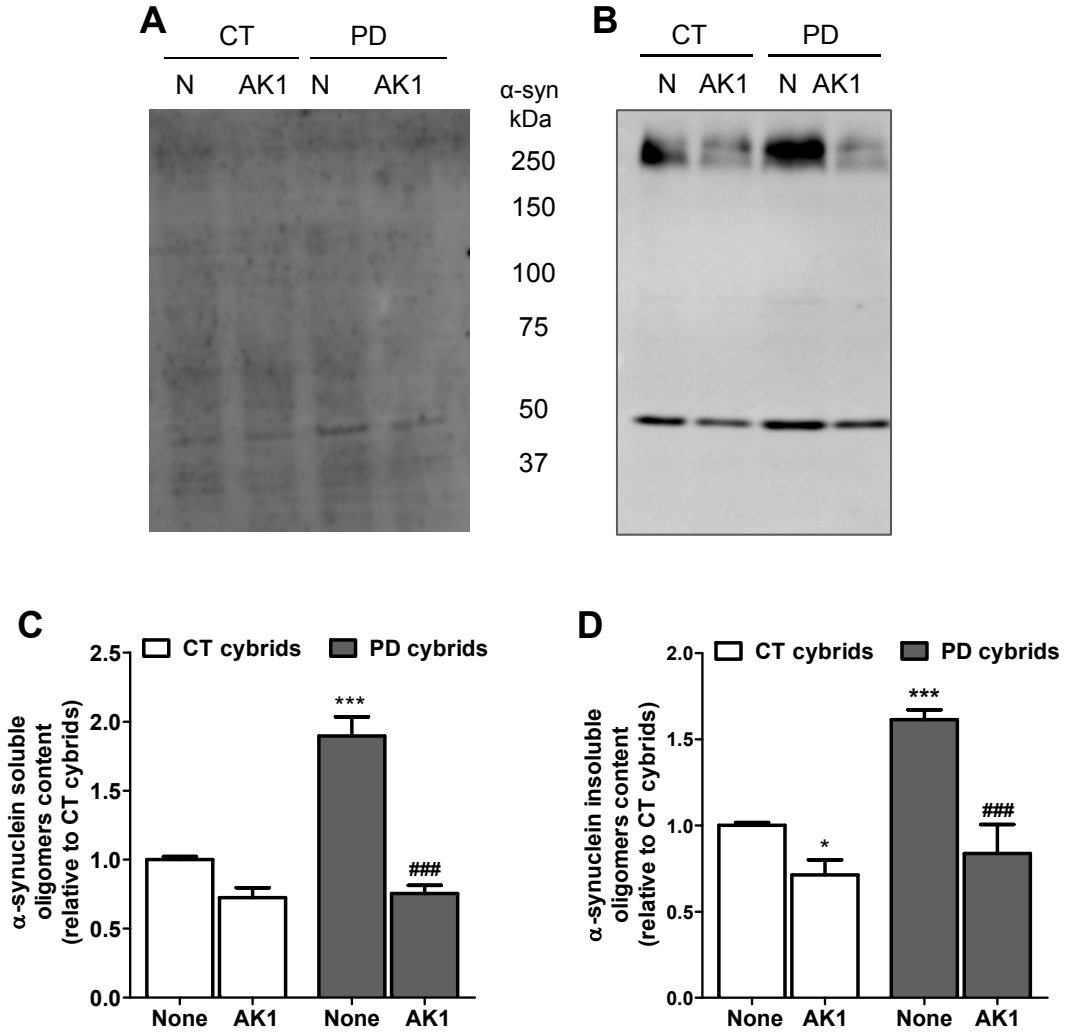

Figure VI.10. Inhibition of SIRT2-dependent tubulin deacetylation improves α-synuclein clearance.

A. and **B.** Cell lysates from CT and sPD cybrid cells treated with or without AK-1 (5 μM, 24 h) in the presence or absence of lysosomal inhibitors (NL, last 4 h) were examined by immunoblotting using the anti-α-synuclein (LB509) and anti-α-tubulin antibodies to assess the α-synuclein oligomeric form content. Representative blots of Triton X-100-soluble oligomeric species (**A**) and Triton X-100-insoluble, and SDS-resistant oligomeric species (**B**). **C.** and **D.** Densitometric analysis of α-synuclein-soluble oligomers content (**C**) (*n*=6-12, ***p<0.001, versus untreated CT cybrids $^{###}$p<0.001, versus untreated sPD cybrids) and α-synuclein-insoluble oligomers content (**D**) (*n*=6-12, *p<0.05, ***p<0.001, versus untreated CT cybrids; $^{###}$p<0.001, versus untreated sPD cybrids). Values are mean±S.E.M.

However, in contrast to the effects of SIRT2 inhibition, no effects were observed on α-synuclein inclusion size in both soluble and insoluble fractions for Tubastatin A treatment in our cybrid cells **(Figure VI.11)**.

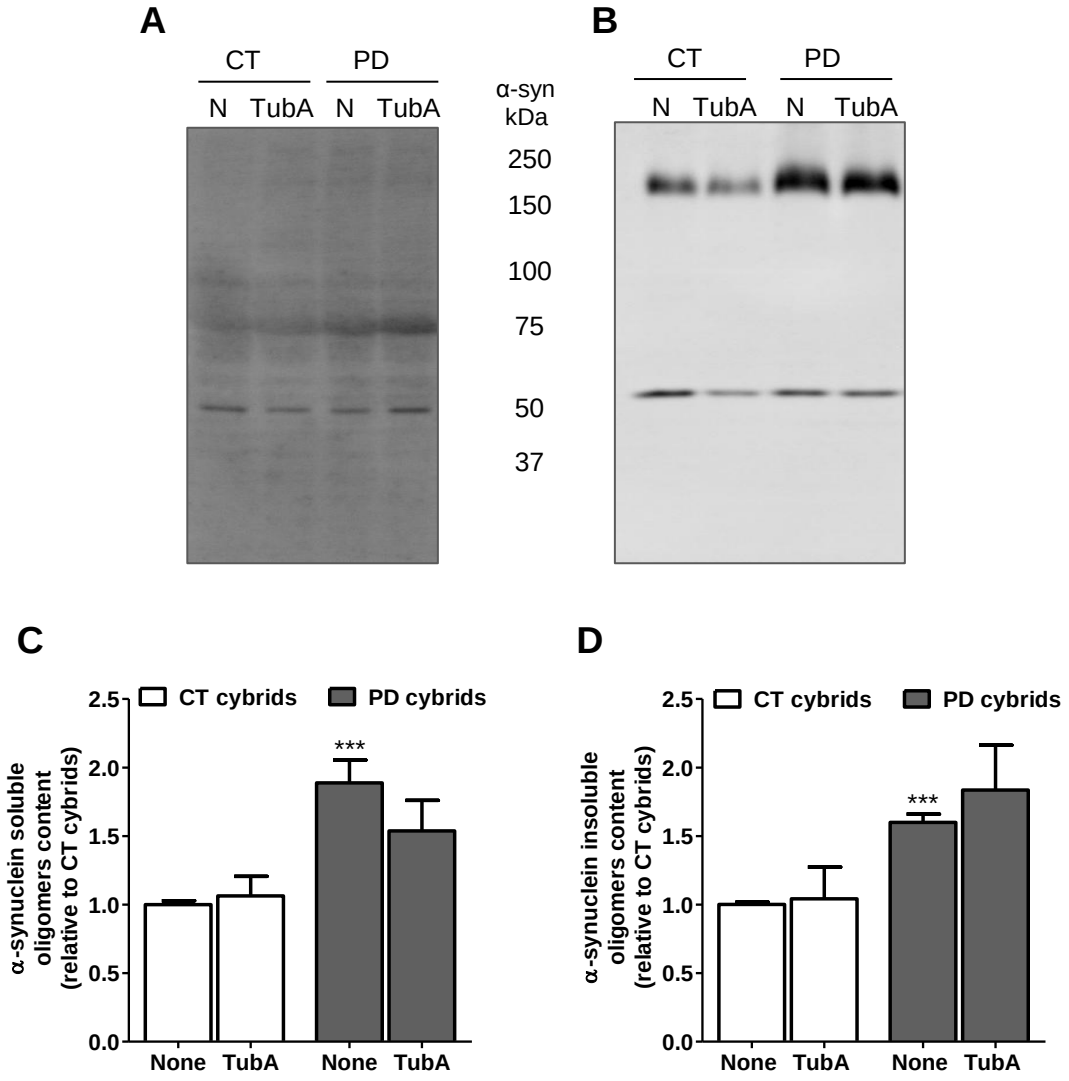

Figure VI.11. Inhibition of HDAC6-dependent tubulin deacetylation fails to promote α-synuclein cleaning up.

A. and **B.** Cell lysates from CT and sPD cybrid cells treated with or without Tubastatin A (10 µM, 24 h) in the presence or absence of lysosomal inhibitors (NL, last 4 h) were examined by immunoblotting using the anti-α-synuclein (LB509) and anti-α-tubulin antibodies to assess the α-synuclein-oligomeric form content. Representative blots of Triton X-100-soluble oligomeric species (**A**) and Triton X-100-insoluble, SDS resistant oligomeric species (**B**). **C.** and **D.** Densitometric analysis of α-synuclein-soluble oligomers content (**C**) (*n*=8-12, ***p<0.001, versus untreated CT cybrids) and α-synuclein-insoluble oligomers content (**D**) (*n*=8-12, ***p<0.001, versus untreated CT cybrids). Values are mean±S.E.M.

The differential efficacy of these two distinct inhibitors against α-synuclein oligomerization in these cells is consistent with their differential effect on the autophagic flux. Thus, these data show that specific deacetylation by SIRT2 on Lys40 of tubulin improves autophagy and thereby enhances α-synuclein clearance, preventing α-synuclein toxicity and consequently PD-related neurodegeneration.

6.4 Discussion

In this study, we have demonstrated a role for deacetylation at Lys40 of α-tubulin in the impairment of the autophagic activity and protein cargo clearance in cellular models harboring sPD subject mtDNA (sPD cybrids). We show here that specific inhibition of SIRT2 deacetylase activity rescues MT-dependent autophagic transport alterations previously observed in sPD cybrids, thus providing a novel insight into how, molecularly, autophagic activity and inherent autophagic clearance are impacted by mitochondrial function.

Our previous work has raised the possibility that alterations in mitochondrial energy metabolism play a role in the modulation of autophagy and, therefore, multiple defects in mitochondria-dependent metabolism might be the initial events in sPD-related autophagic pathology. Mitochondrial dysfunction and oxidative stress have been extensively associated with the majority of neurodegenerative diseases as well with sPD (Henchcliffe and Beal, 2008). In fact, we have previously reported that pathways influenced by aerobic metabolism are altered in sPD cybrids. sPD cybrids showed reduced SIRT1 phosphorylation, reduced peroxisome proliferator-activated receptor-gamma coactivator-1alpha (PGC-1α) levels and increased NF-kB activation (Esteves et al., 2010c). In addition, cellular ATP levels in sPD cybrids are reduced relatively to those of CT cybrids (Esteves et al., 2008; Esteves et al., 2009). Some of these redox-dependent changes may occur in part as a downstream consequence of increased oxidative stress, as sPD cybrids show enhanced generation of reactive oxygen species (ROS) and other free radicals, increased protein oxidation, and decreased glutathione pool, despite the presence of a presumably compensatory increase in the activities of the major antioxidant enzymes relative to CT cybrids (Swerdlow et al., 1996; Cassarino et al., 1997; Esteves et al., 2009). All of these defects result in a deregulation of mitochondrial energy metabolism, as revealed by a decreased mitochondrial respiratory capacity (Esteves et al., 2010c). Although basal oxygen consumption rate between sPD and CT cybrids was comparable, when mitochondria were challenged via chemical-induced uncoupling into a state of maximum oxygen consumption, sPD cybrids revealed increased proton leak in conjunction with a reduced respiratory reserve capacity and ATP production, when compared with CT cells. This means that under basal respiratory conditions sPD cybrids are respiring closely to their maximum respiratory capacity and that oxygen consumption is greatly due to proton leak (Esteves et al., 2010c). Given the decrease in the activity of complex I in sPD cybrids one could expect a decrease in the

NAD^+/NADt ratio (Vemuri et al., 2007; Vinogradov, 2008). However, our results showed the inverse situation suggesting that other pathways dependent on mitochondrial function, but not directly associated to complex I activity, play a role. A possible explanation might be changes in glycolitic flux. A slow decline in glycolytic metabolism may occur, as persistent mitochondrial overfeeding possibly causes system overflow metabolism, and consequently a bioenergetic collapse under these conditions. In addition, because ATP is the principal carrier of energy in cells, this reduction is likely to interfere with many important ATP-dependent cellular processes. These hypotheses were confirmed by our findings that cellular levels of NADt (NAD^+ plus NADH), whose generation is dependent on the levels of ATP (Magni et al., 1999), were significantly decreased and that the ratio NAD^+/NADt was increased in sPD cybrid cells.

Cellular energy status, reflected in NAD^+ levels and NAD^+/NADH ratios, are thought to influence stress-protein synthesis (Westerheide et al., 2009), autophagic activity (Lee et al., 2008; Salminen and Kaarniranta, 2009), sirtuin-mediated protein deacetylation (Bordone and Guarente, 2005; Rodgers et al., 2008) and increased mitogenesis (Bonawitz et al., 2007; Cunningham et al., 2007), all of which impact upon the processes influencing proteostasis and related neurodegeneration. In this study, we report a new finding regarding the interplay between mitochondrial metabolism and SIRT2 and HDAC6 activities in the context of sPD with important consequences for the modulation of the autophagic system and MT-dependent intracellular trafficking. We confirm that both SIRT2 and HDAC6 are MT-associated proteins and active tubulin deacetylases whose inactivation leads to a dramatic accumulation of acetylated MTs (Hubbert et al., 2002; North et al., 2003) in our sPD cybrid cells.

Although α-tubulin acetylation is one of the most common post-translational modifications (Janke and Bulinski, 2011), its biological relevance remains uncertain. Here, we provide evidence that tubulin acetylation is functionally associated with intracellular trafficking and consequently with autophagic turnover maintenance. Elevation of MT acetylation resulting from the selective inhibition of SIRT2 catalytic activity enhanced MT-directed transport of autophagic vacuoles as evidenced by increased proteolytic flux through the autophagy-lysosome pathway. These data are consistent with previous reports demonstrating that α-synuclein-mediated neurotoxicity in several models of PD is due in part to deacetylation of α-tubulin by SIRT2 (Outeiro et al., 2007). Also, hyperacetylation of α-tubulin was found to trigger resistance to axonal degeneration in slow Wallerian degeneration mice, and this was overcome by SIRT2 overexpression (Suzuki and Koike, 2007).

It is well established that α-tubulin is a substrate of both SIRT2 and its cytoplasmic interacting protein HDAC6 and, thus, one would expect a similar effect

from inhibition of HDAC6. However, we found that inhibition of HDAC6 by Tubastatin A induces a dramatic reduction on the autophagic flux in CT cybrids and no positive effects were observed for sPD cybrid cells. Consistently, no significant effects were observed regarding the altered oligomeryzation pattern of α-synuclein observed in sPD cybrids. These results suggest that deacetylation of other substrates by HDAC6 may be essencial to the autophagic dependent protein degradation. In fact, HDAC6 tubulin deacetylase activity has been shown to be required for HDAC6 dependent aggresome formation and autophagic clearance of protein aggregates (Kawaguchi et al., 2003; Pandey et al., 2007). HDAC6 is involved in the transport process as an adaptor protein by binding to p150, a component of the dynein motor complex, and acts as a bridge between the dynein motors and the ubiquitinated proteins leading to aggresome formation (Hubbert et al., 2002). Nevertheless, given that MT stabilization and motor dependent transport is enhanced when MTs are acetylated one would expect that the deacetylase activity of HDAC6 is inhibited during these transport processes and that deacetylase deficient forms of HDAC6 should be able to rescue agressome formation and enhance autophagic turnover. Corroborating this assumption, HDAC6 inhibition in primary cultures of neurons resulted in an effective MT acetylation and stimulated axonal transport, compensating for the BDNF vesicle transport- and release-defect phenotypes that are observed Hungtinton's disease (Dompierre et al., 2007).

However, despite the beneficial effects observed in some vesicular transport systems upon inhibition of HDAC6, in our study we have found a remarkable decrease in autophagic flux following the inhibition of this deacetylase. This apparently contradictory effect might be explained by the role of HDAC6 in the autophagy-lysosome pathway, playing an essential role in the fusion between autophagosomes and lysosomes by recruiting and deacetylating cortactin, which in turn recruits actin filaments to tether the two vesicle populations (Lee et al., 2010b; Lee and Yao, 2010). In addition, it was found that protein aggregates and impaired mitochondria are processed by a common pathway involving HDAC6- and parkin-dependent ubiquitin-selective autophagy and aggresomal machinery (Lee et al., 2010a), thus providing a unifying model toward understanding the two most common pathological features of PD: mitochondrial dysfunction and protein aggregation.

In summary, in this study we dissected the molecular mechanisms by which mitochondrial metabolism in sPD can affect MT-directed autophagic turnover that in turn regulates intracellular protein homeostasis by modulating aggresome formation and protein aggregates degradation. Our findings demonstrate the pathogenic role of α-tubulin deacetylation mediated by SIRT2 in sPD cybrid cell models and highlight the neuroprotective effects of HDAC6 in PD. This observation implies that the ability to

regulate α-tubulin deacetylase activity to modulate protein homeostasis may have important implications for the development of new therapeutic strategies for pathological conditions such as sPD.

CHAPTER VII

Final Remarks

Parkinson's disease (PD) is a disabling neurodegenerative disorder that is strongly associated with ageing, increasing exponentially in incidence above the age of 65 (de Lau et al., 2004). The incidence of PD is expected to rise dramatically worldwide in the next 25 years with the extension of life expectancy by improved health care. Although there are signs of distributed neuropathology, as judged by Lewy bodies (LBs) formation (Braak et al., 2004), the motor symptoms of PD, including bradykinesia, rigidity and resting tremor, are clearly associated to the degeneration and death of SNpc dopaminergic neurons (Obeso et al., 2010). The determination that those cardinal manifestations are primarily due to a profound depletion of dopamine in the striatum led to the development of rational therapies aimed at correcting this deficiency (Calne et al., 1974; Gopinathan et al., 1981; Lieberman et al., 1981). However, despite several breakthrough discoveries in the symptomatic PD therapy, the current therapies are palliative at best and just provide effective control of symptoms, particularly in the early stages of the disease (Thomas, 2009). This is due to the development of motor complications including wearing-off (the return of PD symptoms too soon after a given levodopa dose), the presence of involuntary abnormal movements (dyskinesias and dystonia), and the emergence of treatment-resistant symptoms such as gait impairment, cognitive decline, autonomic dysfunction and medication-induced psychosis (Savitt et al., 2006). Clearly, the current symptomatic therapies cannot completely improve later-stage symptoms and fail to halt the degeneration process in the dopaminergic and nondopaminergic systems. This indeed emphasizes the urgency of developing a more effective therapeutic for PD patients. However, a major hurdle for the development of neuroprotective therapies is the restricted understanding of disease causes and mechanisms leading to death of dopaminergic neurons.

While the etiological factors involved in the development of PD are still uncertain, a combination of genetic susceptibilities and environmental factors seems to play a critical role. Nevertheless, over the course of the past decade, remarkable advances have been made in the identification of genes associated with familial forms of PD. Although familial PD is relatively rare compared with idiopathic disease, the associated genes provide an opportunity to gain important insights into molecular pathways that lead to Parkinsonism and that may be important in the sporadic forms of this disease (sPD) as well. Recent evidences seem to converge on mitochondria as a primary target in the process of dopaminergic neuronal loss observed in PD. Mitochondrial metabolism and energy production impairment are certainly two of important causes and the study of the protein products involved in genetic forms of PD profoundly contributed to extend our knowledge in this topic.

Another organelle that has been widely linked to the pathogenesis of PD is the endoplasmic reticulum (ER). The ER is an integral component of the cellular machinery that coordinates protein synthesis, folding, degradation and transport to ensure accurate and efficient delivery of proteins to the compartments of the secretory pathway, a process generally known as proteostasis (Balch et al., 2008). One of the hallmarks of PD is the formation of LBs, which reflects a deficiency in proteostasis that is accompanied by signs of ER stress and an attempt to sequester cytotoxic proteins (Ryu et al., 2002). Indeed, in this work we demonstrated that in particular stressful conditions mimicking sPD, any alteration in the mitochondrial functionality seems to deeply affect the ability to support cellular stresses, thus making the cells more susceptible to additional insults. We observed that mitochondrial dysfunction induced by an acute stimulus of the neurotoxin MPP^+ renders cells more susceptible to develop an ER stress response, which was mainly translated into a sustained flux of Ca^{2+} from the ER to mitochondria accompanied by the activation of ER- and mitochondria-dependent apoptotic pathways **(Chapter III)**.

Moreover, we also provide evidence that ER stress response may participate in mitochondrial stress-induced abnormalities. We demonstrated that sustained ER stress caused by accumulation of unfolded or misfolded proteins potentiates Ca^{2+}-overload and impairment of mitochondrial function primarily characterized by dissipation of mitochondrial membrane potential and substantial decline in the mitochondrial respiratory chain complex I activity. These cumulative events also coursed in apoptotic cell death induction **(Chapter IV)**. Our findings add on to the exciting concept that mitochondria and ER are actively networking which is fundamental for the maintenance of cellular homeostasis. However, they emphasize that in the context of sPD the close physical and functional association between ER and mitochondria may provide the opportunity for stress or dysfunction in one organelle to potentially disrupt homeostasis in the other organelle, triggering a cascade of deleterious events that culminate in neuronal degeneration. We propose that Ca^{2+} is the main intervenient in the ER and mitochondria crosstalk, functioning as a key modulator of cell death signals triggered by the ER and mitochondria. Ca^{2+}-mediated cellular stress has long been thought to be important in neurodegeneration, but it usually is envisioned as a late stage consequence of organelle damage imposed by some other challenge (Surmeier, 2007). Relevant to sPD pathology, the unusual reliance of SNpc dopaminergic neurons on voltage-dependent L-type Ca^{2+} channels in autonomous pacemaking suggests that the mitochondrial stress created by sustained Ca^{2+} entry could be responsible for their selective vulnerability, rather than simply a late stage consequence. This hypothesis is consistent with the central role of mitochondria in the pathogenesis of sPD.

Despite the unequivocal evidence for the involvement of mitochondria and ER in the sPD pathogenesis, it seems that sPD is distinctively characterized by an additional proteostasis burden that causes SNpc dopaminergic neurons to fail massively. Actually, LBs and other types of protein deposits found in PD patient brains are not merely neuropathological hallmarks of the disease, but rather putative effectors of sPD pathogenesis. A strict policy of quality control mechanisms acts to coordinate the rates of protein synthesis with degradation, preventing such intracellular aggregates from forming (Balch et al., 2008; Powers et al., 2009). Besides ER, cellular proteolytic systems, such as the autophagic-lysosomal pathway, are actively dedicated to protein quality control and their failures have severe negative consequences for cellular homeostasis and cellular functioning, which ultimately result in proteotoxicity.

We demonstrated that a prolonged metabolic failure due to mitochondrial dysfunction, either in cellular models harboring sPD subject mtDNA (sPD cybrids) or knock-down of all mtDNA (Rho0 cells), or in MPP^+-treated rat cortical neurons causes a functional decline in the activity of the autophagic system. Consistently, in all of our paradigms, autophagosomes are actively formed but some of their structural components and autophagic substrates are unable to be efficiently degraded within lysosomes **(Chapter V)**. Although the presence of accumulating autophagosomes could represent an aberrant activation of autophagy, we provided evidence that autophagy is not over stimulated in our models but, instead, defective clearance of the autophagic vacuoles might account for those observations. In addition, we established the proof of concept that autophagy failure stemming from mitochondrial dysfunction is a consequence of alterations in microtubules (MT) assembly that hamper mitochondria and autophagosomes transport along the MT network toward the lysosomal compartment. Consequently, deficient autophagy turnover potentiates the accumulation of α-synuclein oligomers and, ultimately, promotes apoptosis. These findings describe novel and important features in the neuropathological cascade of PD, connecting three important features of sPD: mitochondrial, autophagy and MT dysfunctions.

We further dissected the molecular mechanisms by which mitochondrial metabolism in sPD can affect MT-directed autophagic turnover that in turn regulates intracellular protein homeostasis. We demonstrated a role for the acetylation at Lys40 of α-tubulin in the regulation of the autophagic activity and protein cargo clearance in cellular models harboring sPD subject mtDNA (sPD cybrids). In addition, we showed that specific inhibition of SIRT2 deacetylase activity rescues MT-dependent autophagic transport alterations previously observed in sPD cybrids, thus providing a novel insight

into how, molecularly, autophagic activity and inherent autophagic clearance are impacted by mitochondrial function **(Chapter VI)**.

Collectively this thesis proposes a new conceptual foundation as to how mitochondrial dysfunction can affect intracellular protein quality control systems, the ER and the autophagy-lysosomal system, that in turn regulate cellular protein homeostasis (**Figure VII.1**).

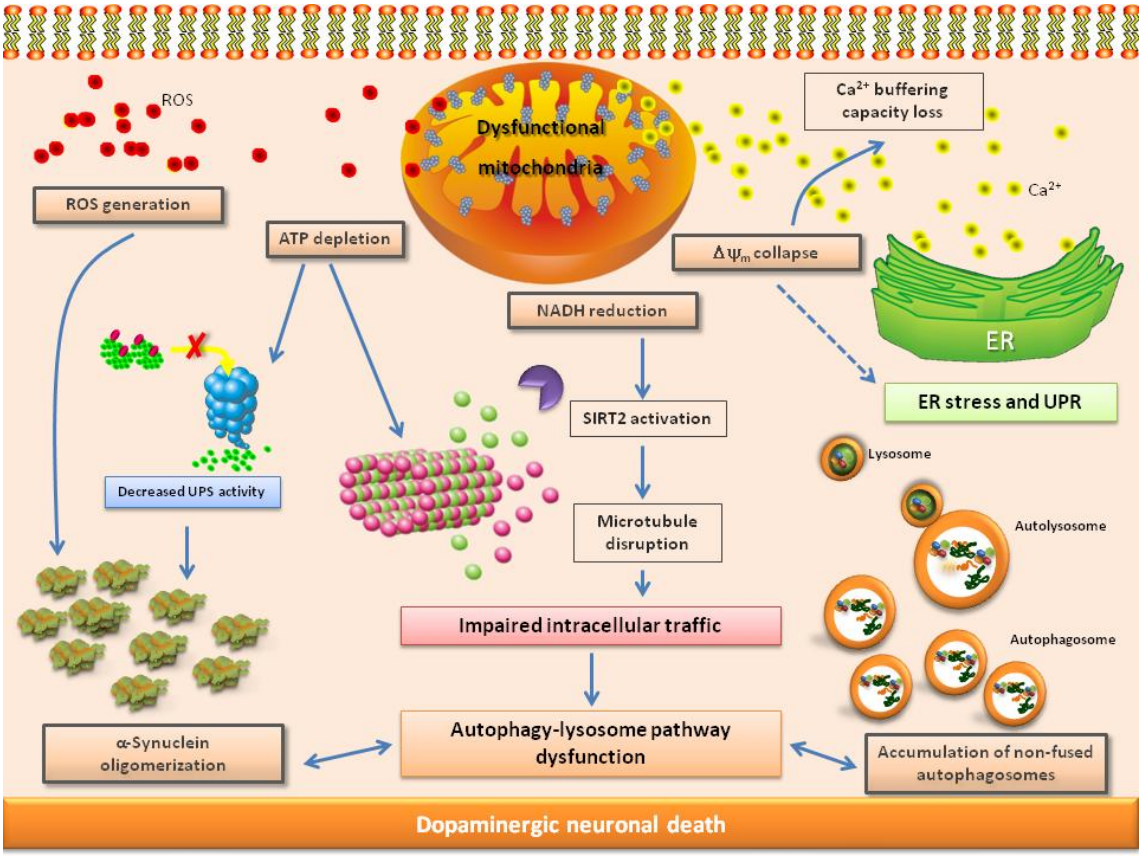

Figure VII.1. Intracellular pathways altered by mitochondrial dysfunction.
Our rationale correlates intracellular events triggered by dysfunctional mitochondria, due to inherited mtDNA, with an accumulation of dysfunctional mitochondria and protein aggregates, leading to dopaminergic cell death.

While it may be difficult to decipher the individual contribution of the different molecular pathways affected by mitochondrial dysfunction, our findings reinforce the concept that restoration of Ca^{2+} homeostasis and of MT network function is indeed able to provide neuroprotection against PD-related dopaminergic neurodegeneration and may thus represent a potentially beneficial new therapeutic strategy for PD.

CHAPTER VIII

References

Afshar G, Murnane JP (1999) Characterization of a human gene with sequence homology to Saccharomyces cerevisiae SIR2. Gene 234:161-168.

Agostinho P, Oliveira CR (2003) Involvement of calcineurin in the neurotoxic effects induced by amyloid-beta and prion peptides. Eur J Neurosci 17:1189-1196.

Ahlqvist G, Landin S, Wroblewski R (1975) Ultrastructure of skeletal muscle in patients with Parkinson's disease and upper motor lesions. Lab Invest 32:673-679.

Akundi RS, Huang Z, Eason J, Pandya JD, Zhi L, Cass WA, Sullivan PG, Bueler H (2011) Increased mitochondrial calcium sensitivity and abnormal expression of innate immunity genes precede dopaminergic defects in Pink1-deficient mice. PLoS One 6:e16038.

Alegre-Abarrategui J, Christian H, Lufino MM, Mutihac R, Venda LL, Ansorge O, Wade-Martins R (2009) LRRK2 regulates autophagic activity and localizes to specific membrane microdomains in a novel human genomic reporter cellular model. Hum Mol Genet 18:4022-4034.

Alim MA, Hossain MS, Arima K, Takeda K, Izumiyama Y, Nakamura M, Kaji H, Shinoda T, Hisanaga S, Ueda K (2002) Tubulin seeds alpha-synuclein fibril formation. J Biol Chem 277:2112-2117.

Alim MA, Ma QL, Takeda K, Aizawa T, Matsubara M, Nakamura M, Asada A, Saito T, Kaji H, Yoshii M, Hisanaga S, Ueda K (2004) Demonstration of a role for alpha-synuclein as a functional microtubule-associated protein. J Alzheimers Dis 6:435-442; discussion 443-439.

Anglade P, Vyas S, Javoy-Agid F, Herrero MT, Michel PP, Marquez J, Mouatt-Prigent A, Ruberg M, Hirsch EC, Agid Y (1997) Apoptosis and autophagy in nigral neurons of patients with Parkinson's disease. Histol Histopathol 12:25-31.

Aplin A, Jasionowski T, Tuttle DL, Lenk SE, Dunn WA, Jr. (1992) Cytoskeletal elements are required for the formation and maturation of autophagic vacuoles. J Cell Physiol 152:458-466.

Arduino D, Silva D, Cardoso SM, Chaves S, Oliveira CR, Santos MA (2008) New hydroxypyridinone iron-chelators as potential anti-neurodegenerative drugs. Front Biosci 13:6763-6774.

Arduino DM, Esteves AR, Cardoso SM (2011a) Mitochondrial fusion/fission, transport and autophagy in Parkinson's disease: when mitochondria get nasty. Parkinsons Dis 2011:767230.

Arduino DM, Esteves AR, Cardoso SM, Oliveira CR (2009a) Endoplasmic reticulum and mitochondria interplay mediates apoptotic cell death: relevance to Parkinson's disease. Neurochem Int 55:341-348.

Arduino DM, Esteves AR, Oliveira CR, Cardoso SM (2010) Mitochondrial metabolism modulation: a new therapeutic approach for Parkinson's disease. CNS Neurol Disord Drug Targets 9:105-119.

Arduino DM, Esteves AR, Domingues AF, Pereira CM, Cardoso SM, Oliveira CR (2009b) ER-mediated stress induces mitochondrial-dependent caspases activation in NT2 neuron-like cells. BMB Rep 42:719-724.

Arduino DM, Esteves AR, Silva DF, Martins-Branco D, Santos D, Pimentel DF, Cardoso SM (2011b) Therapeutic Intervention at Cellular Quality Control Systems in Alzheimer's and Parkinson's Diseases. Curr Pharm Des.

Aridor M, Guzik AK, Bielli A, Fish KN (2004) Endoplasmic reticulum export site formation and function in dendrites. J Neurosci 24:3770-3776.

Arstila AU, Trump BF (1968) Studies on cellular autophagocytosis. The formation of autophagic vacuoles in the liver after glucagon administration. Am J Pathol 53:687-733.

Baas PW (2002) Microtubule transport in the axon. Int Rev Cytol 212:41-62.

Backer JM (2008) The regulation and function of Class III PI3Ks: novel roles for Vps34. Biochem J 410:1-17.

Backman L, Ginovart N, Dixon RA, Wahlin TB, Wahlin A, Halldin C, Farde L (2000) Age-related cognitive deficits mediated by changes in the striatal dopamine system. Am J Psychiatry 157:635-637.

Bains M, Heidenreich KA (2009) Live-cell imaging of autophagy induction and autophagosome-lysosome fusion in primary cultured neurons. Methods Enzymol 453:145-158.

Balch WE, Morimoto RI, Dillin A, Kelly JW (2008) Adapting proteostasis for disease intervention. Science 319:916-919.

Bali P, Pranpat M, Bradner J, Balasis M, Fiskus W, Guo F, Rocha K, Kumaraswamy S, Boyapalle S, Atadja P, Seto E, Bhalla K (2005) Inhibition of histone deacetylase 6 acetylates and disrupts the chaperone function of heat shock protein 90: a novel basis for antileukemia activity of histone deacetylase inhibitors. J Biol Chem 280:26729-26734.

Bando Y, Katayama T, Taniguchi M, Ishibashi T, Matsuo N, Ogawa S, Tohyama M (2005) RA410/Sly1 suppresses MPP+ and 6-hydroxydopamine-induced cell death in SH-SY5Y cells. Neurobiol Dis 18:143-151.

Barroso N, Campos Y, Huertas R, Esteban J, Molina JA, Alonso A, Gutierrez-Rivas E, Arenas J (1993) Respiratory chain enzyme activities in lymphocytes from untreated patients with Parkinson disease. Clin Chem 39:667-669.

Bartels T, Choi JG, Selkoe DJ (2011) alpha-Synuclein occurs physiologically as a helically folded tetramer that resists aggregation. Nature 477:107-110.

Beal MF (2001) Experimental models of Parkinson's disease. Nat Rev Neurosci 2:325-334.

Belmadani S, Pous C, Fischmeister R, Mery PF (2004) Post-translational modifications of tubulin and microtubule stability in adult rat ventricular myocytes and immortalized HL-1 cardiomyocytes. Mol Cell Biochem 258:35-48.

Bender A, Krishnan KJ, Morris CM, Taylor GA, Reeve AK, Perry RH, Jaros E, Hersheson JS, Betts J, Klopstock T, Taylor RW, Turnbull DM (2006) High levels of mitochondrial DNA deletions in substantia nigra neurons in aging and Parkinson disease. Nat Genet 38:515-517.

Berridge MJ (2002) The endoplasmic reticulum: a multifunctional signaling organelle. Cell Calcium 32:235-249.

Berridge MJ, Lipp P, Bootman MD (2000) The versatility and universality of calcium signalling. Nat Rev Mol Cell Biol 1:11-21.

Berridge MJ, Bootman MD, Roderick HL (2003) Calcium signalling: dynamics, homeostasis and remodelling. Nat Rev Mol Cell Biol 4:517-529.

Bertos NR, Gilquin B, Chan GK, Yen TJ, Khochbin S, Yang XJ (2004) Role of the tetradecapeptide repeat domain of human histone deacetylase 6 in cytoplasmic retention. J Biol Chem 279:48246-48254.

Bjorkoy G, Lamark T, Brech A, Outzen H, Perander M, Overvatn A, Stenmark H, Johansen T (2005) p62/SQSTM1 forms protein aggregates degraded by autophagy and has a protective effect on huntingtin-induced cell death. J Cell Biol 171:603-614.

Black JC, Mosley A, Kitada T, Washburn M, Carey M (2008) The SIRT2 deacetylase regulates autoacetylation of p300. Mol Cell 32:449-455.

Bodemann BO, Orvedahl A, Cheng T, Ram RR, Ou YH, Formstecher E, Maiti M, Hazelett CC, Wauson EM, Balakireva M, Camonis JH, Yeaman C, Levine B, White MA (2011) RalB and the exocyst mediate the cellular starvation response by direct activation of autophagosome assembly. Cell 144:253-267.

Bolte S, Cordelieres FP (2006) A guided tour into subcellular colocalization analysis in light microscopy. J Microsc 224:213-232.

Bonawitz ND, Chatenay-Lapointe M, Pan Y, Shadel GS (2007) Reduced TOR signaling extends chronological life span via increased respiration and upregulation of mitochondrial gene expression. Cell Metab 5:265-277.

Bordone L, Guarente L (2005) Calorie restriction, SIRT1 and metabolism: understanding longevity. Nat Rev Mol Cell Biol 6:298-305.

Borgese N, Francolini M, Snapp E (2006) Endoplasmic reticulum architecture: structures in flux. Curr Opin Cell Biol 18:358-364.

Bosco DA, LaVoie MJ, Petsko GA, Ringe D (2011) Proteostasis and movement disorders: Parkinson's disease and amyotrophic lateral sclerosis. Cold Spring Harb Perspect Biol 3:a007500.

Boyce M, Yuan J (2006) Cellular response to endoplasmic reticulum stress: a matter of life or death. Cell Death Differ 13:363-373.

Braak H, Ghebremedhin E, Rub U, Bratzke H, Del Tredici K (2004) Stages in the development of Parkinson's disease-related pathology. Cell Tissue Res 318:121-134.

Braak H, Del Tredici K, Rub U, de Vos RA, Jansen Steur EN, Braak E (2003) Staging of brain pathology related to sporadic Parkinson's disease. Neurobiol Aging 24:197-211.

Braakman I, Helenius J, Helenius A (1992) Role of ATP and disulphide bonds during protein folding in the endoplasmic reticulum. Nature 356:260-262.

Breckenridge DG, Stojanovic M, Marcellus RC, Shore GC (2003a) Caspase cleavage product of BAP31 induces mitochondrial fission through endoplasmic reticulum calcium signals, enhancing cytochrome c release to the cytosol. J Cell Biol 160:1115-1127.

Breckenridge DG, Germain M, Mathai JP, Nguyen M, Shore GC (2003b) Regulation of apoptosis by endoplasmic reticulum pathways. Oncogene 22:8608-8618.

Bridgman PC (2004) Myosin-dependent transport in neurons. J Neurobiol 58:164-174.

Brodsky JL, Skach WR (2011) Protein folding and quality control in the endoplasmic reticulum: Recent lessons from yeast and mammalian cell systems. Curr Opin Cell Biol 23:464-475.

Bunting JR (1992) Influx and efflux kinetics of cationic dye binding to respiring mitochondria. Biophys Chem 42:163-175.

Burns RS, LeWitt PA, Ebert MH, Pakkenberg H, Kopin IJ (1985) The clinical syndrome of striatal dopamine deficiency. Parkinsonism induced by 1-methyl-4-phenyl-1,2,3,6-tetrahydropyridine (MPTP). N Engl J Med 312:1418-1421.

Butow RA, Avadhani NG (2004) Mitochondrial signaling: the retrograde response. Mol Cell 14:1-15.

Calne DB, Teychenne PF, Leigh PN, Bamji AN, Greenacre JK (1974) Treatment of parkinsonism with bromocriptine. Lancet 2:1355-1356.

Calvaruso MA, Willems P, van den Brand M, Valsecchi F, Kruse S, Palmiter R, Smeitink J, Nijtmans L (2012) Mitochondrial complex III stabilizes complex I in the absence of NDUFS4 to provide partial activity. Hum Mol Genet 21:115-120.

Cappelletti G, Surrey T, Maci R (2005) The parkinsonism producing neurotoxin MPP+ affects microtubule dynamics by acting as a destabilising factor. FEBS Lett 579:4781-4786.

Cardoso SM (2011) The Mitochondrial Cascade Hypothesis for Parkinson's Disease. Curr Pharm Des.

Cardoso SM, Santos S, Swerdlow RH, Oliveira CR (2001) Functional mitochondria are required for amyloid beta-mediated neurotoxicity. Faseb J 15:1439-1441.

Cardoso SM, Moreira PI, Agostinho P, Pereira C, Oliveira CR (2005) Neurodegenerative pathways in Parkinson's disease: therapeutic strategies. Curr Drug Targets CNS Neurol Disord 4:405-419.

Cash AD, Aliev G, Siedlak SL, Nunomura A, Fujioka H, Zhu X, Raina AK, Vinters HV, Tabaton M, Johnson AB, Paula-Barbosa M, Avila J, Jones PK, Castellani RJ, Smith MA, Perry G (2003) Microtubule reduction in Alzheimer's disease and aging is independent of tau filament formation. Am J Pathol 162:1623-1627.

Cassarino DS, Fall CP, Swerdlow RH, Smith TS, Halvorsen EM, Miller SW, Parks JP, Parker WD, Jr., Bennett JP, Jr. (1997) Elevated reactive oxygen species and antioxidant enzyme activities in animal and cellular models of Parkinson's disease. Biochim Biophys Acta 1362:77-86.

Chan CS, Gertler TS, Surmeier DJ (2009a) Calcium homeostasis, selective vulnerability and Parkinson's disease. Trends Neurosci 32:249-256.

Chan CS, Guzman JN, Ilijic E, Mercer JN, Rick C, Tkatch T, Meredith GE, Surmeier DJ (2007) 'Rejuvenation' protects neurons in mouse models of Parkinson's disease. Nature 447:1081-1086.

Chan EY, Longatti A, McKnight NC, Tooze SA (2009b) Kinase-inactivated ULK proteins inhibit autophagy via their conserved C-terminal domains using an Atg13-independent mechanism. Mol Cell Biol 29:157-171.

Chan NC, Salazar AM, Pham AH, Sweredoski MJ, Kolawa NJ, Graham RL, Hess S, Chan DC (2011) Broad activation of the ubiquitin-proteasome system by Parkin is critical for mitophagy. Hum Mol Genet 20:1726-1737.

Chandra NC, Spiro MJ, Spiro RG (1998) Identification of a glycoprotein from rat liver mitochondrial inner membrane and demonstration of its origin in the endoplasmic reticulum. J Biol Chem 273:19715-19721.

Chen Y, McMillan-Ward E, Kong J, Israels SJ, Gibson SB (2007) Mitochondrial electron-transport-chain inhibitors of complexes I and II induce autophagic cell death mediated by reactive oxygen species. J Cell Sci 120:4155-4166.

Cheung HH, Lynn Kelly N, Liston P, Korneluk RG (2006) Involvement of caspase-2 and caspase-9 in endoplasmic reticulum stress-induced apoptosis: a role for the IAPs. Exp Cell Res 312:2347-2357.

Chiang HL, Terlecky SR, Plant CP, Dice JF (1989) A role for a 70-kilodalton heat shock protein in lysosomal degradation of intracellular proteins. Science 246:382-385.

Choi WS, Palmiter RD, Xia Z (2011) Loss of mitochondrial complex I activity potentiates dopamine neuron death induced by microtubule dysfunction in a Parkinson's disease model. J Cell Biol 192:873-882.

Choi WS, Kruse SE, Palmiter RD, Xia Z (2008) Mitochondrial complex I inhibition is not required for dopaminergic neuron death induced by rotenone, MPP+, or paraquat. Proc Natl Acad Sci U S A 105:15136-15141.

Choi YM, Kim SH, Chung S, Uhm DY, Park MK (2006) Regional interaction of endoplasmic reticulum Ca2+ signals between soma and dendrites through rapid luminal Ca2+ diffusion. J Neurosci 26:12127-12136.

Choubey V, Safiulina D, Vaarmann A, Cagalinec M, Wareski P, Kuum M, Zharkovsky A, Kaasik A (2011) Mutant A53T alpha-synuclein induces neuronal death by increasing mitochondrial autophagy. J Biol Chem 286:10814-10824.

Chu CT (2012) Introduction. Autophagy dysregulation in neuropathology. Brain Pathol 22:80-81.

Claessen JH, Kundrat L, Ploegh HL (2012) Protein quality control in the ER: balancing the ubiquitin checkbook. Trends Cell Biol 22:22-32.

Conn KJ, Gao W, McKee A, Lan MS, Ullman MD, Eisenhauer PB, Fine RE, Wells JM (2004) Identification of the protein disulfide isomerase family member PDIp in experimental Parkinson's disease and Lewy body pathology. Brain Res 1022:164-172.

Cooper AA, Gitler AD, Cashikar A, Haynes CM, Hill KJ, Bhullar B, Liu K, Xu K, Strathearn KE, Liu F, Cao S, Caldwell KA, Caldwell GA, Marsischky G, Kolodner RD, Labaer J, Rochet JC, Bonini NM, Lindquist S (2006) Alpha-synuclein blocks ER-Golgi traffic and Rab1 rescues neuron loss in Parkinson's models. Science 313:324-328.

Cregan SP, MacLaurin JG, Craig CG, Robertson GS, Nicholson DW, Park DS, Slack RS (1999) Bax-dependent caspase-3 activation is a key determinant in p53-induced apoptosis in neurons. J Neurosci 19:7860-7869.

Crocker SJ, Smith PD, Jackson-Lewis V, Lamba WR, Hayley SP, Grimm E, Callaghan SM, Slack RS, Melloni E, Przedborski S, Robertson GS, Anisman H, Merali Z, Park DS (2003) Inhibition of calpains prevents neuronal and behavioral deficits in an MPTP mouse model of Parkinson's disease. J Neurosci 23:4081-4091.

Csordas G, Renken C, Varnai P, Walter L, Weaver D, Buttle KF, Balla T, Mannella CA, Hajnoczky G (2006) Structural and functional features and significance of the physical linkage between ER and mitochondria. J Cell Biol 174:915-921.

Cuervo AM, Dice JF (1996) A receptor for the selective uptake and degradation of proteins by lysosomes. Science 273:501-503.

Cuervo AM, Stefanis L, Fredenburg R, Lansbury PT, Sulzer D (2004) Impaired degradation of mutant alpha-synuclein by chaperone-mediated autophagy. Science 305:1292-1295.

Cunningham JT, Rodgers JT, Arlow DH, Vazquez F, Mootha VK, Puigserver P (2007) mTOR controls mitochondrial oxidative function through a YY1-PGC-1alpha transcriptional complex. Nature 450:736-740.

Dagda RK, Zhu J, Kulich SM, Chu CT (2008) Mitochondrially localized ERK2 regulates mitophagy and autophagic cell stress: implications for Parkinson's disease. Autophagy 4:770-782.

Dagda RK, Cherra SJ, 3rd, Kulich SM, Tandon A, Park D, Chu CT (2009) Loss of PINK1 function promotes mitophagy through effects on oxidative stress and mitochondrial fission. J Biol Chem 284:13843-13855.

Danzer KM, Haasen D, Karow AR, Moussaud S, Habeck M, Giese A, Kretzschmar H, Hengerer B, Kostka M (2007) Different species of alpha-synuclein oligomers induce calcium influx and seeding. J Neurosci 27:9220-9232.

Darios F, Corti O, Lucking CB, Hampe C, Muriel MP, Abbas N, Gu WJ, Hirsch EC, Rooney T, Ruberg M, Brice A (2003) Parkin prevents mitochondrial swelling and cytochrome c release in mitochondria-dependent cell death. Hum Mol Genet 12:517-526.

Dauer W, Przedborski S (2003) Parkinson's disease: mechanisms and models. Neuron 39:889-909.

De Duve C (1963) The lysosome. Sci Am 208:64-72.

de Lau LM, Giesbergen PC, de Rijk MC, Hofman A, Koudstaal PJ, Breteler MM (2004) Incidence of parkinsonism and Parkinson disease in a general population: the Rotterdam Study. Neurology 63:1240-1244.

Deniaud A, Sharaf el dein O, Maillier E, Poncet D, Kroemer G, Lemaire C, Brenner C (2008) Endoplasmic reticulum stress induces calcium-dependent permeability transition, mitochondrial outer membrane permeabilization and apoptosis. Oncogene 27:285-299.

Dice JF (1990) Peptide sequences that target cytosolic proteins for lysosomal proteolysis. Trends Biochem Sci 15:305-309.

Ding WX, Yin XM (2008) Sorting, recognition and activation of the misfolded protein degradation pathways through macroautophagy and the proteasome. Autophagy 4:141-150.

Domingues AF, Esteves AR, Swerdlow RH, Oliveira CR, Cardoso SM (2008a) Calpain-mediated MPP+ toxicity in mitochondrial DNA depleted cells. Neurotox Res 13:31-38.

Domingues AF, Arduino DM, Esteves AR, Swerdlow RH, Oliveira CR, Cardoso SM (2008b) Mitochondria and ubiquitin-proteasomal system interplay: relevance to Parkinson's disease. Free Radic Biol Med 45:820-825.

Dompierre JP, Godin JD, Charrin BC, Cordelieres FP, King SJ, Humbert S, Saudou F (2007) Histone deacetylase 6 inhibition compensates for the transport deficit in Huntington's disease by increasing tubulin acetylation. J Neurosci 27:3571-3583.

Dorner AJ, Wasley LC, Raney P, Haugejorden S, Green M, Kaufman RJ (1990) The stress response in Chinese hamster ovary cells. Regulation of ERp72 and protein disulfide isomerase expression and secretion. J Biol Chem 265:22029-22034.

Draberova E, Viklicky V, Draber P (2000) Exposure of lumenal microtubule sites after mild fixation. Eur J Cell Biol 79:982-985.

Du H, Guo L, Yan S, Sosunov AA, McKhann GM, Yan SS (2010) Early deficits in synaptic mitochondria in an Alzheimer's disease mouse model. Proc Natl Acad Sci U S A 107:18670-18675.

Duchen MR (1992) Ca(2+)-dependent changes in the mitochondrial energetics in single dissociated mouse sensory neurons. Biochem J 283 (Pt 1):41-50.

Duchen MR, Biscoe TJ (1992) Relative mitochondrial membrane potential and [Ca2+]i in type I cells isolated from the rabbit carotid body. J Physiol 450:33-61.

Duszynski J, Koziel R, Brutkowski W, Szczepanowska J, Zablocki K (2006) The regulatory role of mitochondria in capacitative calcium entry. Biochim Biophys Acta 1757:380-387.

Edde B, Rossier J, Le Caer JP, Berwald-Netter Y, Koulakoff A, Gros F, Denoulet P (1991) A combination of posttranslational modifications is responsible for the production of neuronal alpha-tubulin heterogeneity. J Cell Biochem 46:134-142.

Ekstrand MI, Terzioglu M, Galter D, Zhu S, Hofstetter C, Lindqvist E, Thams S, Bergstrand A, Hansson FS, Trifunovic A, Hoffer B, Cullheim S, Mohammed AH, Olson L, Larsson NG (2007) Progressive parkinsonism in mice with respiratory-chain-deficient dopamine neurons. Proc Natl Acad Sci U S A 104:1325-1330.

Ellgaard L, Helenius A (2003) Quality control in the endoplasmic reticulum. Nat Rev Mol Cell Biol 4:181-191.

Elyaman W, Terro F, Suen KC, Yardin C, Chang RC, Hugon J (2002) BAD and Bcl-2 regulation are early events linking neuronal endoplasmic reticulum stress to mitochondria-mediated apoptosis. Brain Res Mol Brain Res 109:233-238.

Emaus RK, Grunwald R, Lemasters JJ (1986) Rhodamine 123 as a probe of transmembrane potential in isolated rat-liver mitochondria: spectral and metabolic properties. Biochim Biophys Acta 850:436-448.

Engelender S (2008) Ubiquitination of alpha-synuclein and autophagy in Parkinson's disease. Autophagy 4:372-374.

Esteves AR, Arduino DM, Swerdlow RH, Oliveira CR, Cardoso SM (2009) Oxidative Stress involvement in alpha-synuclein oligomerization in Parkinsons disease cybrids. Antioxid Redox Signal 11:439-448.

Esteves AR, Arduino DM, Swerdlow RH, Oliveira CR, Cardoso SM (2010a) Microtubule depolymerization potentiates alpha-synuclein oligomerization. Front Aging Neurosci 1:5.

Esteves AR, Arduino DM, Swerdlow RH, Oliveira CR, Cardoso SM (2010b) Dysfunctional mitochondria uphold calpain activation: contribution to Parkinson's disease pathology. Neurobiol Dis 37:723-730.

Esteves AR, Domingues AF, Ferreira IL, Januario C, Swerdlow RH, Oliveira CR, Cardoso SM (2008) Mitochondrial function in Parkinson's disease cybrids containing an nt2 neuron-like nuclear background. Mitochondrion 8:219-228.

Esteves AR, Lu J, Rodova M, Onyango I, Lezi E, Dubinsky R, Lyons KE, Pahwa R, Burns JM, Cardoso SM, Swerdlow RH (2010c) Mitochondrial respiration and respiration-associated proteins in cell lines created through Parkinson's subject mitochondrial transfer. J Neurochem 113:674-682.

Fahim MA, Lasek RJ, Brady ST, Hodge AJ (1985) AVEC-DIC and electron microscopic analyses of axonally transported particles in cold-blocked squid giant axons. J Neurocytol 14:689-704.

Fass E, Shvets E, Degani I, Hirschberg K, Elazar Z (2006) Microtubules support production of starvation-induced autophagosomes but not their targeting and fusion with lysosomes. J Biol Chem 281:36303-36316.

Ferreiro E, Resende R, Costa R, Oliveira CR, Pereira CM (2006) An endoplasmic-reticulum-specific apoptotic pathway is involved in prion and amyloid-beta peptides neurotoxicity. Neurobiol Dis 23:669-678.

Ferri KF, Kroemer G (2001) Organelle-specific initiation of cell death pathways. Nat Cell Biol 3:E255-263.

Filimonenko M, Stuffers S, Raiborg C, Yamamoto A, Malerod L, Fisher EM, Isaacs A, Brech A, Stenmark H, Simonsen A (2007) Functional multivesicular bodies are required for autophagic clearance of protein aggregates associated with neurodegenerative disease. J Cell Biol 179:485-500.

Flower TR, Chesnokova LS, Froelich CA, Dixon C, Witt SN (2005) Heat shock prevents alpha-synuclein-induced apoptosis in a yeast model of Parkinson's disease. J Mol Biol 351:1081-1100.

Forno LS (1996) Neuropathology of Parkinson's disease. J Neuropathol Exp Neurol 55:259-272.

Foyouzi-Youssefi R, Arnaudeau S, Borner C, Kelley WL, Tschopp J, Lew DP, Demaurex N, Krause KH (2000) Bcl-2 decreases the free Ca2+ concentration within the endoplasmic reticulum. Proc Natl Acad Sci U S A 97:5723-5728.

Frei B, Richter C (1986) N-methyl-4-phenylpyridine (MMP+) together with 6-hydroxydopamine or dopamine stimulates Ca2+ release from mitochondria. FEBS Lett 198:99-102.

Friedlander R, Jarosch E, Urban J, Volkwein C, Sommer T (2000) A regulatory link between ER-associated protein degradation and the unfolded-protein response. Nat Cell Biol 2:379-384.

Funderburk SF, Wang QJ, Yue Z (2010) The Beclin 1-VPS34 complex--at the crossroads of autophagy and beyond. Trends Cell Biol 20:355-362.

Gandhi S, Wood-Kaczmar A, Yao Z, Plun-Favreau H, Deas E, Klupsch K, Downward J, Latchman DS, Tabrizi SJ, Wood NW, Duchen MR, Abramov AY (2009) PINK1-associated Parkinson's disease is caused by neuronal vulnerability to calcium-induced cell death. Mol Cell 33:627-638.

Garnier C, Barbier P, Gilli R, Lopez C, Peyrot V, Briand C (1998) Heat-shock protein 90 (hsp90) binds in vitro to tubulin dimer and inhibits microtubule formation. Biochem Biophys Res Commun 250:414-419.

Gegg ME, Cooper JM, Chau KY, Rojo M, Schapira AH, Taanman JW (2010) Mitofusin 1 and mitofusin 2 are ubiquitinated in a PINK1/parkin-dependent manner upon induction of mitophagy. Hum Mol Genet 19:4861-4870.

Geisler S, Holmstrom KM, Skujat D, Fiesel FC, Rothfuss OC, Kahle PJ, Springer W (2010a) PINK1/Parkin-mediated mitophagy is dependent on VDAC1 and p62/SQSTM1. Nat Cell Biol 12:119-131.

Geisler S, Holmstrom KM, Treis A, Skujat D, Weber SS, Fiesel FC, Kahle PJ, Springer W (2010b) The PINK1/Parkin-mediated mitophagy is compromised by PD-associated mutations. Autophagy 6:871-878.

Geng J, Klionsky DJ (2008) The Atg8 and Atg12 ubiquitin-like conjugation systems in macroautophagy. 'Protein modifications: beyond the usual suspects' review series. EMBO Rep 9:859-864.

Geng J, Nair U, Yasumura-Yorimitsu K, Klionsky DJ (2010) Post-Golgi Sec proteins are required for autophagy in Saccharomyces cerevisiae. Mol Biol Cell 21:2257-2269.

Germain M, Shore GC (2003) Cellular distribution of Bcl-2 family proteins. Sci STKE 2003:pe10.

Germain M, Mathai JP, Shore GC (2002) BH-3-only BIK functions at the endoplasmic reticulum to stimulate cytochrome c release from mitochondria. J Biol Chem 277:18053-18060.

German DC, Manaye KF, Sonsalla PK, Brooks BA (1992) Midbrain dopaminergic cell loss in Parkinson's disease and MPTP-induced parkinsonism: sparing of calbindin-D28k-containing cells. Ann N Y Acad Sci 648:42-62.

Ghadially FN (2001) As you like it, Part 3: A critique and historical review of calcification as seen with the electron microscope. Ultrastruct Pathol 25:243-267.

Ghezzi D et al. (2005) Mitochondrial DNA haplogroup K is associated with a lower risk of Parkinson's disease in Italians. Eur J Hum Genet 13:748-752.

Giacomello M, Drago I, Pizzo P, Pozzan T (2007) Mitochondrial Ca2+ as a key regulator of cell life and death. Cell Death Differ 14:1267-1274.

Giorgi C, De Stefani D, Bononi A, Rizzuto R, Pinton P (2009) Structural and functional link between the mitochondrial network and the endoplasmic reticulum. Int J Biochem Cell Biol 41:1817-1827.

Gitler AD, Bevis BJ, Shorter J, Strathearn KE, Hamamichi S, Su LJ, Caldwell KA, Caldwell GA, Rochet JC, McCaffery JM, Barlowe C, Lindquist S (2008) The Parkinson's disease protein alpha-synuclein disrupts cellular Rab homeostasis. Proc Natl Acad Sci U S A 105:145-150.

Giustiniani J, Daire V, Cantaloube I, Durand G, Pous C, Perdiz D, Baillet A (2009) Tubulin acetylation favors Hsp90 recruitment to microtubules and stimulates the signaling function of the Hsp90 clients Akt/PKB and p53. Cell Signal 21:529-539.

Gopinathan G, Teravainen H, Dambrosia JM, Ward CD, Sanes JN, Stuart WK, Evarts EV, Calne DB (1981) Lisuride in parkinsonism. Neurology 31:371-376.

Gorlach A, Klappa P, Kietzmann T (2006) The endoplasmic reticulum: folding, calcium homeostasis, signaling, and redox control. Antioxid Redox Signal 8:1391-1418.

Grace AA, Bunney BS (1983) Intracellular and extracellular electrophysiology of nigral dopaminergic neurons--1. Identification and characterization. Neuroscience 10:301-315.

Green DR, Kroemer G (2004) The pathophysiology of mitochondrial cell death. Science 305:626-629.

Guo Y, Srinivasula SM, Druilhe A, Fernandes-Alnemri T, Alnemri ES (2002) Caspase-2 induces apoptosis by releasing proapoptotic proteins from mitochondria. J Biol Chem 277:13430-13437.

Guzman JN, Sanchez-Padilla J, Wokosin D, Kondapalli J, Ilijic E, Schumacker PT, Surmeier DJ (2010) Oxidant stress evoked by pacemaking in dopaminergic neurons is attenuated by DJ-1. Nature 468:696-700.

Haas RH, Nasirian F, Nakano K, Ward D, Pay M, Hill R, Shults CW (1995) Low platelet mitochondrial complex I and complex II/III activity in early untreated Parkinson's disease. Ann Neurol 37:714-722.

Haggarty SJ, Koeller KM, Wong JC, Grozinger CM, Schreiber SL (2003) Domain-selective small-molecule inhibitor of histone deacetylase 6 (HDAC6)-mediated tubulin deacetylation. Proc Natl Acad Sci U S A 100:4389-4394.

Hailey DW, Rambold AS, Satpute-Krishnan P, Mitra K, Sougrat R, Kim PK, Lippincott-Schwartz J (2010) Mitochondria supply membranes for autophagosome biogenesis during starvation. Cell 141:656-667.

Hajnoczky G, Hager R, Thomas AP (1999) Mitochondria suppress local feedback activation of inositol 1,4, 5-trisphosphate receptors by Ca2+. J Biol Chem 274:14157-14162.

Halliday GM, Ophof A, Broe M, Jensen PH, Kettle E, Fedorow H, Cartwright MI, Griffiths FM, Shepherd CE, Double KL (2005) Alpha-synuclein redistributes to neuromelanin lipid in the substantia nigra early in Parkinson's disease. Brain 128:2654-2664.

Han Y, Jin YH, Kim YJ, Kang BY, Choi HJ, Kim DW, Yeo CY, Lee KY (2008) Acetylation of Sirt2 by p300 attenuates its deacetylase activity. Biochem Biophys Res Commun 375:576-580.

Hanagasi HA, Ayribas D, Baysal K, Emre M (2005) Mitochondrial complex I, II/III, and IV activities in familial and sporadic Parkinson's disease. Int J Neurosci 115:479-493.

Hara T, Nakamura K, Matsui M, Yamamoto A, Nakahara Y, Suzuki-Migishima R, Yokoyama M, Mishima K, Saito I, Okano H, Mizushima N (2006) Suppression of basal autophagy in neural cells causes neurodegenerative disease in mice. Nature 441:885-889.

Harding HP, Calfon M, Urano F, Novoa I, Ron D (2002) Transcriptional and translational control in the Mammalian unfolded protein response. Annu Rev Cell Dev Biol 18:575-599.

Hartmann A, Hunot S, Michel PP, Muriel MP, Vyas S, Faucheux BA, Mouatt-Prigent A, Turmel H, Srinivasan A, Ruberg M, Evan GI, Agid Y, Hirsch EC (2000) Caspase-3: A vulnerability factor and final effector in apoptotic death of dopaminergic neurons in Parkinson's disease. Proc Natl Acad Sci U S A 97:2875-2880.

He C, Klionsky DJ (2009) Regulation mechanisms and signaling pathways of autophagy. Annu Rev Genet 43:67-93.

Heeman B, Van den Haute C, Aelvoet SA, Valsecchi F, Rodenburg RJ, Reumers V, Debyser Z, Callewaert G, Koopman WJ, Willems PH, Baekelandt V (2011) Depletion of PINK1 affects mitochondrial metabolism, calcium homeostasis and energy maintenance. J Cell Sci 124:1115-1125.

Heidemann SR (1996) Cytoplasmic mechanisms of axonal and dendritic growth in neurons. Int Rev Cytol 165:235-296.

Henchcliffe C, Beal MF (2008) Mitochondrial biology and oxidative stress in Parkinson disease pathogenesis. Nat Clin Pract Neurol 4:600-609.

Hettiarachchi NT, Parker A, Dallas ML, Pennington K, Hung CC, Pearson HA, Boyle JP, Robinson P, Peers C (2009) alpha-Synuclein modulation of Ca2+ signaling in human neuroblastoma (SH-SY5Y) cells. J Neurochem 111:1192-1201.

Hirsch EC, Perier C, Orieux G, Francois C, Feger J, Yelnik J, Vila M, Levy R, Tolosa ES, Marin C, Trinidad Herrero M, Obeso JA, Agid Y (2000) Metabolic effects of nigrostriatal denervation in basal ganglia. Trends Neurosci 23:S78-85.

Hitomi J, Katayama T, Eguchi Y, Kudo T, Taniguchi M, Koyama Y, Manabe T, Yamagishi S, Bando Y, Imaizumi K, Tsujimoto Y, Tohyama M (2004) Involvement of caspase-4 in endoplasmic reticulum stress-induced apoptosis and Abeta-induced cell death. J Cell Biol 165:347-356.

Hollenbeck PJ (1996) The pattern and mechanism of mitochondrial transport in axons. Front Biosci 1:d91-102.

Hollenbeck PJ, Saxton WM (2005) The axonal transport of mitochondria. J Cell Sci 118:5411-5419.

Holtz WA, O'Malley KL (2003) Parkinsonian mimetics induce aspects of unfolded protein response in death of dopaminergic neurons. J Biol Chem 278:19367-19377.

Hoozemans JJ, van Haastert ES, Eikelenboom P, de Vos RA, Rozemuller JM, Scheper W (2007) Activation of the unfolded protein response in Parkinson's disease. Biochem Biophys Res Commun 354:707-711.

Hosokawa N, Hara T, Kaizuka T, Kishi C, Takamura A, Miura Y, Iemura S, Natsume T, Takehana K, Yamada N, Guan JL, Oshiro N, Mizushima N (2009) Nutrient-dependent mTORC1 association with the ULK1-Atg13-FIP200 complex required for autophagy. Mol Biol Cell 20:1981-1991.

Hoth M, Fanger CM, Lewis RS (1997) Mitochondrial regulation of store-operated calcium signaling in T lymphocytes. J Cell Biol 137:633-648.

Hoth M, Button DC, Lewis RS (2000) Mitochondrial control of calcium-channel gating: a mechanism for sustained signaling and transcriptional activation in T lymphocytes. Proc Natl Acad Sci U S A 97:10607-10612.

Hubbert C, Guardiola A, Shao R, Kawaguchi Y, Ito A, Nixon A, Yoshida M, Wang XF, Yao TP (2002) HDAC6 is a microtubule-associated deacetylase. Nature 417:455-458.

Huerta C, Castro MG, Coto E, Blazquez M, Ribacoba R, Guisasola LM, Salvador C, Martinez C, Lahoz CH, Alvarez V (2005) Mitochondrial DNA polymorphisms and risk of Parkinson's disease in Spanish population. J Neurol Sci 236:49-54.

Iaccarino C, Crosio C, Vitale C, Sanna G, Carri MT, Barone P (2007) Apoptotic mechanisms in mutant LRRK2-mediated cell death. Hum Mol Genet 16:1319-1326.

Iacopino AM, Christakos S (1990) Specific reduction of calcium-binding protein (28-kilodalton calbindin-D) gene expression in aging and neurodegenerative diseases. Proc Natl Acad Sci U S A 87:4078-4082.

Ilieva H, Polymenidou M, Cleveland DW (2009) Non-cell autonomous toxicity in neurodegenerative disorders: ALS and beyond. J Cell Biol 187:761-772.

Ilijic E, Guzman JN, Surmeier DJ (2011) The L-type channel antagonist isradipine is neuroprotective in a mouse model of Parkinson's disease. Neurobiol Dis 43:364-371.

Imai Y, Soda M, Takahashi R (2000) Parkin suppresses unfolded protein stress-induced cell death through its E3 ubiquitin-protein ligase activity. J Biol Chem 275:35661-35664.

Imai Y, Soda M, Inoue H, Hattori N, Mizuno Y, Takahashi R (2001) An unfolded putative transmembrane polypeptide, which can lead to endoplasmic reticulum stress, is a substrate of Parkin. Cell 105:891-902.

Iseki E, Marui W, Sawada H, Ueda K, Kosaka K (2000) Accumulation of human alpha-synuclein in different cytoskeletons in Lewy bodies in brains of dementia with Lewy bodies. Neurosci Lett 290:41-44.

Ishii K, Hirose K, Iino M (2006) Ca2+ shuttling between endoplasmic reticulum and mitochondria underlying Ca2+ oscillations. EMBO Rep 7:390-396.

Itakura E, Kishi C, Inoue K, Mizushima N (2008) Beclin 1 forms two distinct phosphatidylinositol 3-kinase complexes with mammalian Atg14 and UVRAG. Mol Biol Cell 19:5360-5372.

Izuta H, Shimazawa M, Tazawa S, Araki Y, Mishima S, Hara H (2008) Protective effects of Chinese propolis and its component, chrysin, against neuronal cell death via inhibition of mitochondrial apoptosis pathway in SH-SY5Y cells. J Agric Food Chem 56:8944-8953.

Jager S, Bucci C, Tanida I, Ueno T, Kominami E, Saftig P, Eskelinen EL (2004) Role for Rab7 in maturation of late autophagic vacuoles. J Cell Sci 117:4837-4848.

Jahreiss L, Menzies FM, Rubinsztein DC (2008) The itinerary of autophagosomes: from peripheral formation to kiss-and-run fusion with lysosomes. Traffic 9:574-587.

Janke C, Bulinski JC (2011) Post-translational regulation of the microtubule cytoskeleton: mechanisms and functions. Nat Rev Mol Cell Biol 12:773-786.

Jenner P (2003) Oxidative stress in Parkinson's disease. Ann Neurol 53 Suppl 3:S26-36; discussion S36-28.

Jiang Q, Ren Y, Feng J (2008) Direct binding with histone deacetylase 6 mediates the reversible recruitment of parkin to the centrosome. J Neurosci 28:12993-13002.

Jin SM, Lazarou M, Wang C, Kane LA, Narendra DP, Youle RJ (2010) Mitochondrial membrane potential regulates PINK1 import and proteolytic destabilization by PARL. J Cell Biol 191:933-942.

Jing E, Gesta S, Kahn CR (2007) SIRT2 regulates adipocyte differentiation through FoxO1 acetylation/deacetylation. Cell Metab 6:105-114.

Johnson KA (1983) The pathway of ATP hydrolysis by dynein. Kinetics of a presteady state phosphate burst. J Biol Chem 258:13825-13832.

Johnston JA, Ward CL, Kopito RR (1998) Aggresomes: a cellular response to misfolded proteins. J Cell Biol 143:1883-1898.

Jonikas MC, Collins SR, Denic V, Oh E, Quan EM, Schmid V, Weibezahn J, Schwappach B, Walter P, Weissman JS, Schuldiner M (2009) Comprehensive characterization of genes required for protein folding in the endoplasmic reticulum. Science 323:1693-1697.

Joshi HC, Cleveland DW (1989) Differential utilization of beta-tubulin isotypes in differentiating neurites. J Cell Biol 109:663-673.

Jung CH, Jun CB, Ro SH, Kim YM, Otto NM, Cao J, Kundu M, Kim DH (2009) ULK-Atg13-FIP200 complexes mediate mTOR signaling to the autophagy machinery. Mol Biol Cell 20:1992-2003.

Kamada Y, Sekito T, Ohsumi Y (2004) Autophagy in yeast: a TOR-mediated response to nutrient starvation. Curr Top Microbiol Immunol 279:73-84.

Kamada Y, Funakoshi T, Shintani T, Nagano K, Ohsumi M, Ohsumi Y (2000) Tor-mediated induction of autophagy via an Apg1 protein kinase complex. J Cell Biol 150:1507-1513.

Kamp F, Exner N, Lutz AK, Wender N, Hegermann J, Brunner B, Nuscher B, Bartels T, Giese A, Beyer K, Eimer S, Winklhofer KF, Haass C (2010) Inhibition of mitochondrial fusion by alpha-synuclein is rescued by PINK1, Parkin and DJ-1. EMBO J 29:3571-3589.

Katayama M, Zhong Z, Lai L, Sutovsky P, Prather RS, Schatten H (2006) Mitochondrial distribution and microtubule organization in fertilized and cloned porcine embryos: implications for developmental potential. Dev Biol 299:206-220.

Kaufman RJ (1999a) Molecular chaperones and the heat shock response. Sponsored by Cold Spring Harbor Laboratory, 6-10 May 1998. Biochim Biophys Acta 1423:R13-27.

Kaufman RJ (1999b) Stress signaling from the lumen of the endoplasmic reticulum: coordination of gene transcriptional and translational controls. Genes Dev 13:1211-1233.

Kawaguchi Y, Kovacs JJ, McLaurin A, Vance JM, Ito A, Yao TP (2003) The deacetylase HDAC6 regulates aggresome formation and cell viability in response to misfolded protein stress. Cell 115:727-738.

Kawajiri S, Saiki S, Sato S, Sato F, Hatano T, Eguchi H, Hattori N (2010) PINK1 is recruited to mitochondria with parkin and associates with LC3 in mitophagy. FEBS Lett 584:1073-1079.

Kazuno AA, Munakata K, Nagai T, Shimozono S, Tanaka M, Yoneda M, Kato N, Miyawaki A, Kato T (2006) Identification of mitochondrial DNA polymorphisms that alter mitochondrial matrix pH and intracellular calcium dynamics. PLoS Genet 2:e128.

Kim-Han JS, Antenor-Dorsey JA, O'Malley KL (2011) The Parkinsonian mimetic, MPP+, specifically impairs mitochondrial transport in dopamine axons. J Neurosci 31:7212-7221.

Kim I, Rodriguez-Enriquez S, Lemasters JJ (2007) Selective degradation of mitochondria by mitophagy. Arch Biochem Biophys 462:245-253.

Kim M, Jung W, Lee IH, Bhak G, Paik SR, Hahn JS (2008a) Impairment of microtubule system increases alpha-synuclein aggregation and toxicity. Biochem Biophys Res Commun 365:628-635.

Kim PK, Hailey DW, Mullen RT, Lippincott-Schwartz J (2008b) Ubiquitin signals autophagic degradation of cytosolic proteins and peroxisomes. Proc Natl Acad Sci U S A 105:20567-20574.

Kim S, Jeon BS, Heo C, Im PS, Ahn TB, Seo JH, Kim HS, Park CH, Choi SH, Cho SH, Lee WJ, Suh YH (2004) Alpha-synuclein induces apoptosis by altered expression in human peripheral lymphocyte in Parkinson's disease. FASEB J 18:1615-1617.

Kimura S, Noda T, Yoshimori T (2008) Dynein-dependent movement of autophagosomes mediates efficient encounters with lysosomes. Cell Struct Funct 33:109-122.

Kirisako T, Ichimura Y, Okada H, Kabeya Y, Mizushima N, Yoshimori T, Ohsumi M, Takao T, Noda T, Ohsumi Y (2000) The reversible modification regulates the membrane-binding state of Apg8/Aut7 essential for autophagy and the cytoplasm to vacuole targeting pathway. J Cell Biol 151:263-276.

Kish SJ, Shannak K, Hornykiewicz O (1988) Uneven pattern of dopamine loss in the striatum of patients with idiopathic Parkinson's disease. Pathophysiologic and clinical implications. N Engl J Med 318:876-880.

Klionsky DJ, Cregg JM, Dunn WA, Jr., Emr SD, Sakai Y, Sandoval IV, Sibirny A, Subramani S, Thumm M, Veenhuis M, Ohsumi Y (2003) A unified nomenclature for yeast autophagy-related genes. Dev Cell 5:539-545.

Kochl R, Hu XW, Chan EY, Tooze SA (2006) Microtubules facilitate autophagosome formation and fusion of autophagosomes with endosomes. Traffic 7:129-145.

Komatsu M, Waguri S, Chiba T, Murata S, Iwata J, Tanida I, Ueno T, Koike M, Uchiyama Y, Kominami E, Tanaka K (2006) Loss of autophagy in the central nervous system causes neurodegeneration in mice. Nature 441:880-884.

Komatsu M, Waguri S, Ueno T, Iwata J, Murata S, Tanida I, Ezaki J, Mizushima N, Ohsumi Y, Uchiyama Y, Kominami E, Tanaka K, Chiba T (2005) Impairment of starvation-induced and constitutive autophagy in Atg7-deficient mice. J Cell Biol 169:425-434.

Koopman WJ, Visch HJ, Verkaart S, van den Heuvel LW, Smeitink JA, Willems PH (2005a) Mitochondrial network complexity and pathological decrease in complex I activity are tightly correlated in isolated human complex I deficiency. Am J Physiol Cell Physiol 289:C881-890.

Koopman WJ, Verkaart S, Visch HJ, van der Westhuizen FH, Murphy MP, van den Heuvel LW, Smeitink JA, Willems PH (2005b) Inhibition of complex I of the electron transport chain causes O2-. -mediated mitochondrial outgrowth. Am J Physiol Cell Physiol 288:C1440-1450.

Kopito RR (2000) Aggresomes, inclusion bodies and protein aggregation. Trends Cell Biol 10:524-530.

Korsmeyer SJ, Shutter JR, Veis DJ, Merry DE, Oltvai ZN (1993) Bcl-2/Bax: a rheostat that regulates an anti-oxidant pathway and cell death. Semin Cancer Biol 4:327-332.

Kovari E, Gold G, Herrmann FR, Canuto A, Hof PR, Bouras C, Giannakopoulos P (2003) Lewy body densities in the entorhinal and anterior cingulate cortex predict cognitive deficits in Parkinson's disease. Acta Neuropathol 106:83-88.

Kraytsberg Y, Kudryavtseva E, McKee AC, Geula C, Kowall NW, Khrapko K (2006) Mitochondrial DNA deletions are abundant and cause functional impairment in aged human substantia nigra neurons. Nat Genet 38:518-520.

Kroemer G, Galluzzi L, Brenner C (2007) Mitochondrial membrane permeabilization in cell death. Physiol Rev 87:99-163.

Kujoth GC, Hiona A, Pugh TD, Someya S, Panzer K, Wohlgemuth SE, Hofer T, Seo AY, Sullivan R, Jobling WA, Morrow JD, Van Remmen H, Sedivy JM, Yamasoba T,

Tanokura M, Weindruch R, Leeuwenburgh C, Prolla TA (2005) Mitochondrial DNA mutations, oxidative stress, and apoptosis in mammalian aging. Science 309:481-484.

Kuznetsov SA, Langford GM, Weiss DG (1992) Actin-dependent organelle movement in squid axoplasm. Nature 356:722-725.

L'Hernault SW, Rosenbaum JL (1985) Chlamydomonas alpha-tubulin is posttranslationally modified by acetylation on the epsilon-amino group of a lysine. Biochemistry 24:473-478.

Lamark T, Kirkin V, Dikic I, Johansen T (2009) NBR1 and p62 as cargo receptors for selective autophagy of ubiquitinated targets. Cell Cycle 8:1986-1990.

Lang AE, Lozano AM (1998a) Parkinson's disease. First of two parts. N Engl J Med 339:1044-1053.

Lang AE, Lozano AM (1998b) Parkinson's disease. Second of two parts. N Engl J Med 339:1130-1143.

Langford GM (2002) Myosin-V, a versatile motor for short-range vesicle transport. Traffic 3:859-865.

Langston JW, Ballard P, Tetrud JW, Irwin I (1983) Chronic Parkinsonism in humans due to a product of meperidine-analog synthesis. Science 219:979-980.

Larm JA, Vaillant F, Linnane AW, Lawen A (1994) Up-regulation of the plasma membrane oxidoreductase as a prerequisite for the viability of human Namalwa rho 0 cells. J Biol Chem 269:30097-30100.

Larsson NG (2010) Somatic mitochondrial DNA mutations in mammalian aging. Annu Rev Biochem 79:683-706.

Lassus P, Opitz-Araya X, Lazebnik Y (2002) Requirement for caspase-2 in stress-induced apoptosis before mitochondrial permeabilization. Science 297:1352-1354.

Laurent M, Fleury A (1996) Hysteretic behavior and differential apparent stability properties of microtubule species emerge from the regulation of post-translational modifications of microtubules. J Cell Sci 109 (Pt 2):419-428.

LeDizet M, Piperno G (1987) Identification of an acetylation site of Chlamydomonas alpha-tubulin. Proc Natl Acad Sci U S A 84:5720-5724.

Lee AS (1992) Mammalian stress response: induction of the glucose-regulated protein family. Curr Opin Cell Biol 4:267-273.

Lee AS (2001) The glucose-regulated proteins: stress induction and clinical applications. Trends Biochem Sci 26:504-510.

Lee AS (2005) The ER chaperone and signaling regulator GRP78/BiP as a monitor of endoplasmic reticulum stress. Methods 35:373-381.

Lee HJ, Khoshaghideh F, Lee S, Lee SJ (2006) Impairment of microtubule-dependent trafficking by overexpression of alpha-synuclein. Eur J Neurosci 24:3153-3162.

Lee IH, Cao L, Mostoslavsky R, Lombard DB, Liu J, Bruns NE, Tsokos M, Alt FW, Finkel T (2008) A role for the NAD-dependent deacetylase Sirt1 in the regulation of autophagy. Proc Natl Acad Sci U S A 105:3374-3379.

Lee JY, Yao TP (2010) Quality control autophagy: A joint effort of ubiquitin, protein deacetylase and actin cytoskeleton. Autophagy 6.

Lee JY, Nagano Y, Taylor JP, Lim KL, Yao TP (2010a) Disease-causing mutations in parkin impair mitochondrial ubiquitination, aggregation, and HDAC6-dependent mitophagy. J Cell Biol 189:671-679.

Lee JY, Koga H, Kawaguchi Y, Tang W, Wong E, Gao YS, Pandey UB, Kaushik S, Tresse E, Lu J, Taylor JP, Cuervo AM, Yao TP (2010b) HDAC6 controls autophagosome maturation essential for ubiquitin-selective quality-control autophagy. EMBO J 29:969-980.

Lee S, Sato Y, Nixon RA (2011) Lysosomal proteolysis inhibition selectively disrupts axonal transport of degradative organelles and causes an Alzheimer's-like axonal dystrophy. J Neurosci 31:7817-7830.

Lemasters JJ, Nieminen AL, Qian T, Trost LC, Elmore SP, Nishimura Y, Crowe RA, Cascio WE, Bradham CA, Brenner DA, Herman B (1998) The mitochondrial permeability transition in cell death: a common mechanism in necrosis, apoptosis and autophagy. Biochim Biophys Acta 1366:177-196.

Levine B, Klionsky DJ (2004) Development by self-digestion: molecular mechanisms and biological functions of autophagy. Dev Cell 6:463-477.

Levine T, Rabouille C (2005) Endoplasmic reticulum: one continuous network compartmentalized by extrinsic cues. Curr Opin Cell Biol 17:362-368.

Liang CL, Wang TT, Luby-Phelps K, German DC (2007) Mitochondria mass is low in mouse substantia nigra dopamine neurons: implications for Parkinson's disease. Exp Neurol 203:370-380.

Lieberman AN, Goldstein M, Leibowitz M, Neophytides A, Gopinathan G, Walker R, Pact V (1981) Lisuride combined with levodopa in advanced Parkinson disease. Neurology 31:1466-1469.

Lievremont JP, Rizzuto R, Hendershot L, Meldolesi J (1997) BiP, a major chaperone protein of the endoplasmic reticulum lumen, plays a direct and important role in the storage of the rapidly exchanging pool of Ca2+. J Biol Chem 272:30873-30879.

Ligon LA, Steward O (2000a) Movement of mitochondria in the axons and dendrites of cultured hippocampal neurons. J Comp Neurol 427:340-350.

Ligon LA, Steward O (2000b) Role of microtubules and actin filaments in the movement of mitochondria in the axons and dendrites of cultured hippocampal neurons. J Comp Neurol 427:351-361.

Lin SX, Collins CA (1993) Regulation of the intracellular distribution of cytoplasmic dynein by serum factors and calcium. J Cell Sci 105 (Pt 2):579-588.

Lin SX, Ferro KL, Collins CA (1994) Cytoplasmic dynein undergoes intracellular redistribution concomitant with phosphorylation of the heavy chain in response to serum starvation and okadaic acid. J Cell Biol 127:1009-1019.

Little E, Ramakrishnan M, Roy B, Gazit G, Lee AS (1994) The glucose-regulated proteins (GRP78 and GRP94): functions, gene regulation, and applications. Crit Rev Eukaryot Gene Expr 4:1-18.

Litvan I, Bhatia KP, Burn DJ, Goetz CG, Lang AE, McKeith I, Quinn N, Sethi KD, Shults C, Wenning GK (2003) Movement Disorders Society Scientific Issues Committee report: SIC Task Force appraisal of clinical diagnostic criteria for Parkinsonian disorders. Mov Disord 18:467-486.

Liu H, Bowes RC, 3rd, van de Water B, Sillence C, Nagelkerke JF, Stevens JL (1997) Endoplasmic reticulum chaperones GRP78 and calreticulin prevent oxidative stress, Ca2+ disturbances, and cell death in renal epithelial cells. J Biol Chem 272:21751-21759.

Lloreta-Trull J, Serrano S (1998) Biology and pathology of the mitochondrion. Ultrastruct Pathol 22:357-367.

Macaskill AF, Rinholm JE, Twelvetrees AE, Arancibia-Carcamo IL, Muir J, Fransson A, Aspenstrom P, Attwell D, Kittler JT (2009) Miro1 is a calcium sensor for glutamate receptor-dependent localization of mitochondria at synapses. Neuron 61:541-555.

Magni G, Orsomando G, Raffelli N, Ruggieri S (2008) Enzymology of mammalian NAD metabolism in health and disease. Front Biosci 13:6135-6154.

Magni G, Amici A, Emanuelli M, Raffaelli N, Ruggieri S (1999) Enzymology of NAD+ synthesis. Adv Enzymol Relat Areas Mol Biol 73:135-182, xi.

Maguire-Zeiss KA, Short DW, Federoff HJ (2005) Synuclein, dopamine and oxidative stress: co-conspirators in Parkinson's disease? Brain Res Mol Brain Res 134:18-23.

Maiuri MC, Le Toumelin G, Criollo A, Rain JC, Gautier F, Juin P, Tasdemir E, Pierron G, Troulinaki K, Tavernarakis N, Hickman JA, Geneste O, Kroemer G (2007) Functional and physical interaction between Bcl-X(L) and a BH3-like domain in Beclin-1. Embo J 26:2527-2539.

Makioka K, Yamazaki T, Fujita Y, Takatama M, Nakazato Y, Okamoto K (2010) Involvement of endoplasmic reticulum stress defined by activated unfolded protein response in multiple system atrophy. J Neurol Sci 297:60-65.

Malhotra JD, Kaufman RJ (2007) The endoplasmic reticulum and the unfolded protein response. Semin Cell Dev Biol 18:716-731.

Mann VM, Cooper JM, Krige D, Daniel SE, Schapira AH, Marsden CD (1992) Brain, skeletal muscle and platelet homogenate mitochondrial function in Parkinson's disease. Brain 115 (Pt 2):333-342.

Mann VM, Cooper JM, Daniel SE, Srai K, Jenner P, Marsden CD, Schapira AH (1994) Complex I, iron, and ferritin in Parkinson's disease substantia nigra. Ann Neurol 36:876-881.

Marella M, Seo BB, Nakamaru-Ogiso E, Greenamyre JT, Matsuno-Yagi A, Yagi T (2008) Protection by the NDI1 gene against neurodegeneration in a rotenone rat model of Parkinson's disease. PLoS One 3:e1433.

Mari M, Griffith J, Rieter E, Krishnappa L, Klionsky DJ, Reggiori F (2010) An Atg9-containing compartment that functions in the early steps of autophagosome biogenesis. J Cell Biol 190:1005-1022.

Martin LJ, Pan Y, Price AC, Sterling W, Copeland NG, Jenkins NA, Price DL, Lee MK (2006) Parkinson's disease alpha-synuclein transgenic mice develop neuronal mitochondrial degeneration and cell death. J Neurosci 26:41-50.

Martinez-Vicente M, Talloczy Z, Kaushik S, Massey AC, Mazzulli J, Mosharov EV, Hodara R, Fredenburg R, Wu DC, Follenzi A, Dauer W, Przedborski S, Ischiropoulos H, Lansbury PT, Sulzer D, Cuervo AM (2008) Dopamine-modified alpha-synuclein blocks chaperone-mediated autophagy. J Clin Invest 118:777-788.

Martinez TN, Greenamyre JT (2011) Toxin Models of Mitochondrial Dysfunction in Parkinson's Disease. Antioxid Redox Signal.

Massey A, Kiffin R, Cuervo AM (2004) Pathophysiology of chaperone-mediated autophagy. Int J Biochem Cell Biol 36:2420-2434.

Matsuyama A, Shimazu T, Sumida Y, Saito A, Yoshimatsu Y, Seigneurin-Berny D, Osada H, Komatsu Y, Nishino N, Khochbin S, Horinouchi S, Yoshida M (2002) In vivo destabilization of dynamic microtubules by HDAC6-mediated deacetylation. EMBO J 21:6820-6831.

Matteoni R, Kreis TE (1987) Translocation and clustering of endosomes and lysosomes depends on microtubules. J Cell Biol 105:1253-1265.

Mattson MP (2007) Calcium and neurodegeneration. Aging Cell 6:337-350.

McMahon A, Wong BS, Iacopino AM, Ng MC, Chi S, German DC (1998) Calbindin-D28k buffers intracellular calcium and promotes resistance to degeneration in PC12 cells. Brain Res Mol Brain Res 54:56-63.

McNaught KS, Shashidharan P, Perl DP, Jenner P, Olanow CW (2002) Aggresome-related biogenesis of Lewy bodies. Eur J Neurosci 16:2136-2148.

Mizushima N, Levine B, Cuervo AM, Klionsky DJ (2008) Autophagy fights disease through cellular self-digestion. Nature 451:1069-1075.

Mizushima N, Yamamoto A, Matsui M, Yoshimori T, Ohsumi Y (2004) In vivo analysis of autophagy in response to nutrient starvation using transgenic mice expressing a fluorescent autophagosome marker. Mol Biol Cell 15:1101-1111.

Mochizuki H, Hayakawa H, Migita M, Shibata M, Tanaka R, Suzuki A, Shimo-Nakanishi Y, Urabe T, Yamada M, Tamayose K, Shimada T, Miura M, Mizuno Y (2001) An AAV-derived Apaf-1 dominant negative inhibitor prevents MPTP toxicity as antiapoptotic gene therapy for Parkinson's disease. Proc Natl Acad Sci U S A 98:10918-10923.

Mogami H, Nakano K, Tepikin AV, Petersen OH (1997) Ca2+ flow via tunnels in polarized cells: recharging of apical Ca2+ stores by focal Ca2+ entry through basal membrane patch. Cell 88:49-55.

Morfini G, Pigino G, Opalach K, Serulle Y, Moreira JE, Sugimori M, Llinas RR, Brady ST (2007) 1-Methyl-4-phenylpyridinium affects fast axonal transport by activation of caspase and protein kinase C. Proc Natl Acad Sci U S A 104:2442-2447.

Mori K (2000) Tripartite management of unfolded proteins in the endoplasmic reticulum. Cell 101:451-454.

Morre DM, Lenaz G, Morre DJ (2000) Surface oxidase and oxidative stress propagation in aging. J Exp Biol 203:1513-1521.

Morris RL, Hollenbeck PJ (1993) The regulation of bidirectional mitochondrial transport is coordinated with axonal outgrowth. J Cell Sci 104 (Pt 3):917-927.

Morris RL, Hollenbeck PJ (1995) Axonal transport of mitochondria along microtubules and F-actin in living vertebrate neurons. J Cell Biol 131:1315-1326.

Mortimore GE, Lardeux BR, Adams CE (1988) Regulation of microautophagy and basal protein turnover in rat liver. Effects of short-term starvation. J Biol Chem 263:2506-2512.

Mouatt-Prigent A, Agid Y, Hirsch EC (1994) Does the calcium binding protein calretinin protect dopaminergic neurons against degeneration in Parkinson's disease? Brain Res 668:62-70.

Nahhas F, Dryden SC, Abrams J, Tainsky MA (2007) Mutations in SIRT2 deacetylase which regulate enzymatic activity but not its interaction with HDAC6 and tubulin. Mol Cell Biochem 303:221-230.

Nakagawa T, Zhu H, Morishima N, Li E, Xu J, Yankner BA, Yuan J (2000) Caspase-12 mediates endoplasmic-reticulum-specific apoptosis and cytotoxicity by amyloid-beta. Nature 403:98-103.

Nakatogawa H, Suzuki K, Kamada Y, Ohsumi Y (2009) Dynamics and diversity in autophagy mechanisms: lessons from yeast. Nat Rev Mol Cell Biol 10:458-467.

Narendra D, Tanaka A, Suen DF, Youle RJ (2008) Parkin is recruited selectively to impaired mitochondria and promotes their autophagy. J Cell Biol 183:795-803.

Narendra DP, Jin SM, Tanaka A, Suen DF, Gautier CA, Shen J, Cookson MR, Youle RJ (2010) PINK1 is selectively stabilized on impaired mitochondria to activate Parkin. PLoS Biol 8:e1000298.

Neufeld TP (2010) TOR-dependent control of autophagy: biting the hand that feeds. Curr Opin Cell Biol 22:157-168.

Nicotra A, Parvez S (2002) Apoptotic molecules and MPTP-induced cell death. Neurotoxicol Teratol 24:599-605.

Nigam SK, Goldberg AL, Ho S, Rohde MF, Bush KT, Sherman M (1994) A set of endoplasmic reticulum proteins possessing properties of molecular chaperones includes Ca(2+)-binding proteins and members of the thioredoxin superfamily. J Biol Chem 269:1744-1749.

Nixon RA, Wegiel J, Kumar A, Yu WH, Peterhoff C, Cataldo A, Cuervo AM (2005) Extensive involvement of autophagy in Alzheimer disease: an immuno-electron microscopy study. J Neuropathol Exp Neurol 64:113-122.

Noda T, Suzuki K, Ohsumi Y (2002) Yeast autophagosomes: de novo formation of a membrane structure. Trends Cell Biol 12:231-235.

Nogales E (1999) A structural view of microtubule dynamics. Cell Mol Life Sci 56:133-142.

Norris EH, Giasson BI, Hodara R, Xu S, Trojanowski JQ, Ischiropoulos H, Lee VM (2005) Reversible inhibition of alpha-synuclein fibrillization by dopaminochrome-mediated conformational alterations. J Biol Chem 280:21212-21219.

North BJ, Verdin E (2007) Interphase nucleo-cytoplasmic shuttling and localization of SIRT2 during mitosis. PLoS One 2:e784.

North BJ, Marshall BL, Borra MT, Denu JM, Verdin E (2003) The human Sir2 ortholog, SIRT2, is an NAD+-dependent tubulin deacetylase. Mol Cell 11:437-444.

Nutt LK, Chandra J, Pataer A, Fang B, Roth JA, Swisher SG, O'Neil RG, McConkey DJ (2002) Bax-mediated Ca2+ mobilization promotes cytochrome c release during apoptosis. J Biol Chem 277:20301-20308.

Oakes SA, Lin SS, Bassik MC (2006) The control of endoplasmic reticulum-initiated apoptosis by the BCL-2 family of proteins. Curr Mol Med 6:99-109.

Oakes SA, Scorrano L, Opferman JT, Bassik MC, Nishino M, Pozzan T, Korsmeyer SJ (2005) Proapoptotic BAX and BAK regulate the type 1 inositol trisphosphate receptor and calcium leak from the endoplasmic reticulum. Proc Natl Acad Sci U S A 102:105-110.

Obeng EA, Boise LH (2005) Caspase-12 and caspase-4 are not required for caspase-dependent endoplasmic reticulum stress-induced apoptosis. J Biol Chem 280:29578-29587.

Obeso JA, Rodriguez-Oroz MC, Rodriguez M, Lanciego JL, Artieda J, Gonzalo N, Olanow CW (2000) Pathophysiology of the basal ganglia in Parkinson's disease. Trends Neurosci 23:S8-19.

Obeso JA, Rodriguez-Oroz MC, Goetz CG, Marin C, Kordower JH, Rodriguez M, Hirsch EC, Farrer M, Schapira AH, Halliday G (2010) Missing pieces in the Parkinson's disease puzzle. Nat Med 16:653-661.

Offen D, Beart PM, Cheung NS, Pascoe CJ, Hochman A, Gorodin S, Melamed E, Bernard R, Bernard O (1998) Transgenic mice expressing human Bcl-2 in their neurons are resistant to 6-hydroxydopamine and 1-methyl-4-phenyl-1,2,3,6-tetrahydropyridine neurotoxicity. Proc Natl Acad Sci U S A 95:5789-5794.

Olzmann JA, Li L, Chudaev MV, Chen J, Perez FA, Palmiter RD, Chin LS (2007) Parkin-mediated K63-linked polyubiquitination targets misfolded DJ-1 to aggresomes via binding to HDAC6. J Cell Biol 178:1025-1038.

Orsucci D, Caldarazzo Ienco E, Mancuso M, Siciliano G (2011) POLG1-related and other "mitochondrial Parkinsonisms": an overview. J Mol Neurosci 44:17-24.

Outeiro TF, Kontopoulos E, Altmann SM, Kufareva I, Strathearn KE, Amore AM, Volk CB, Maxwell MM, Rochet JC, McLean PJ, Young AB, Abagyan R, Feany MB, Hyman BT, Kazantsev AG (2007) Sirtuin 2 inhibitors rescue alpha-synuclein-mediated toxicity in models of Parkinson's disease. Science 317:516-519.

Ozawa K, Kuwabara K, Tamatani M, Takatsuji K, Tsukamoto Y, Kaneda S, Yanagi H, Stern DM, Eguchi Y, Tsujimoto Y, Ogawa S, Tohyama M (1999) 150-kDa oxygen-regulated protein (ORP150) suppresses hypoxia-induced apoptotic cell death. J Biol Chem 274:6397-6404.

Palmer AE, Jin C, Reed JC, Tsien RY (2004) Bcl-2-mediated alterations in endoplasmic reticulum Ca2+ analyzed with an improved genetically encoded fluorescent sensor. Proc Natl Acad Sci U S A 101:17404-17409.

Pandey UB, Nie Z, Batlevi Y, McCray BA, Ritson GP, Nedelsky NB, Schwartz SL, DiProspero NA, Knight MA, Schuldiner O, Padmanabhan R, Hild M, Berry DL, Garza D, Hubbert CC, Yao TP, Baehrecke EH, Taylor JP (2007) HDAC6 rescues neurodegeneration and provides an essential link between autophagy and the UPS. Nature 447:859-863.

Paquet-Durand F, Tan S, Bicker G (2003) Turning teratocarcinoma cells into neurons: rapid differentiation of NT-2 cells in floating spheres. Brain Res Dev Brain Res 142:161-167.

Parekh AB (2003) Mitochondrial regulation of intracellular Ca2+ signaling: more than just simple Ca2+ buffers. News Physiol Sci 18:252-256.

Parihar A, Parihar MS, Ghafourifar P (2008) Significance of mitochondrial calcium and nitric oxide for apoptosis of human breast cancer cells induced by tamoxifen and etoposide. Int J Mol Med 21:317-324.

Parihar MS, Parihar A, Fujita M, Hashimoto M, Ghafourifar P (2009) Alpha-synuclein overexpression and aggregation exacerbates impairment of mitochondrial functions by augmenting oxidative stress in human neuroblastoma cells. Int J Biochem Cell Biol 41:2015-2024.

Park MK, Petersen OH, Tepikin AV (2000) The endoplasmic reticulum as one continuous Ca(2+) pool: visualization of rapid Ca(2+) movements and equilibration. EMBO J 19:5729-5739.

Park MK, Choi YM, Kang YK, Petersen OH (2008) The endoplasmic reticulum as an integrator of multiple dendritic events. Neuroscientist 14:68-77.

Parker WD, Jr., Parks JK (2005) Mitochondrial ND5 mutations in idiopathic Parkinson's disease. Biochem Biophys Res Commun 326:667-669.

Parker WD, Jr., Boyson SJ, Parks JK (1989) Abnormalities of the electron transport chain in idiopathic Parkinson's disease. Ann Neurol 26:719-723.

Parkinson J (2002) An essay on the shaking palsy. 1817. J Neuropsychiatry Clin Neurosci 14:223-236; discussion 222.

Paschen W, Mengesdorf T, Althausen S, Hotop S (2001) Peroxidative stress selectively down-regulates the neuronal stress response activated under conditions of endoplasmic reticulum dysfunction. J Neurochem 76:1916-1924.

Patil C, Walter P (2001) Intracellular signaling from the endoplasmic reticulum to the nucleus: the unfolded protein response in yeast and mammals. Curr Opin Cell Biol 13:349-355.

Pattingre S, Tassa A, Qu X, Garuti R, Liang XH, Mizushima N, Packer M, Schneider MD, Levine B (2005) Bcl-2 antiapoptotic proteins inhibit Beclin 1-dependent autophagy. Cell 122:927-939.

Payton JE, Perrin RJ, Clayton DF, George JM (2001) Protein-protein interactions of alpha-synuclein in brain homogenates and transfected cells. Brain Res Mol Brain Res 95:138-145.

Peck B, Chen CY, Ho KK, Di Fruscia P, Myatt SS, Coombes RC, Fuchter MJ, Hsiao CD, Lam EW (2010) SIRT inhibitors induce cell death and p53 acetylation through targeting both SIRT1 and SIRT2. Mol Cancer Ther 9:844-855.

Penn AM, Roberts T, Hodder J, Allen PS, Zhu G, Martin WR (1995) Generalized mitochondrial dysfunction in Parkinson's disease detected by magnetic resonance spectroscopy of muscle. Neurology 45:2097-2099.

Perier C, Vila M (2012) Mitochondrial biology and Parkinson's disease. Cold Spring Harb Perspect Med 2:a009332.

Perier C, Bove J, Wu DC, Dehay B, Choi DK, Jackson-Lewis V, Rathke-Hartlieb S, Bouillet P, Strasser A, Schulz JB, Przedborski S, Vila M (2007) Two molecular pathways initiate mitochondria-dependent dopaminergic neurodegeneration in experimental Parkinson's disease. Proc Natl Acad Sci U S A 104:8161-8166.

Petit A, Kawarai T, Paitel E, Sanjo N, Maj M, Scheid M, Chen F, Gu Y, Hasegawa H, Salehi-Rad S, Wang L, Rogaeva E, Fraser P, Robinson B, St George-Hyslop P, Tandon A (2005) Wild-type PINK1 prevents basal and induced neuronal apoptosis, a protective effect abrogated by Parkinson disease-related mutations. J Biol Chem 280:34025-34032.

Pickrell AM, Pinto M, Hida A, Moraes CT (2011) Striatal dysfunctions associated with mitochondrial DNA damage in dopaminergic neurons in a mouse model of Parkinson's disease. J Neurosci 31:17649-17658.

Pinton P, Rizzuto R (2006) Bcl-2 and Ca2+ homeostasis in the endoplasmic reticulum. Cell Death Differ 13:1409-1418.

Pinton P, Ferrari D, Magalhaes P, Schulze-Osthoff K, Di Virgilio F, Pozzan T, Rizzuto R (2000) Reduced loading of intracellular Ca(2+) stores and downregulation of capacitative Ca(2+) influx in Bcl-2-overexpressing cells. J Cell Biol 148:857-862.

Pizzo P, Pozzan T (2007) Mitochondria-endoplasmic reticulum choreography: structure and signaling dynamics. Trends Cell Biol 17:511-517.

Pleasure SJ, Lee VM (1993) NTera 2 cells: a human cell line which displays characteristics expected of a human committed neuronal progenitor cell. J Neurosci Res 35:585-602.

Plomp PJ, Gordon PB, Meijer AJ, Hoyvik H, Seglen PO (1989) Energy dependence of different steps in the autophagic-lysosomal pathway. J Biol Chem 264:6699-6704.

Plomp PJ, Wolvetang EJ, Groen AK, Meijer AJ, Gordon PB, Seglen PO (1987) Energy dependence of autophagic protein degradation in isolated rat hepatocytes. Eur J Biochem 164:197-203.

Plowey ED, Cherra SJ, 3rd, Liu YJ, Chu CT (2008) Role of autophagy in G2019S-LRRK2-associated neurite shortening in differentiated SH-SY5Y cells. J Neurochem 105:1048-1056.

Poewe W (2008) Non-motor symptoms in Parkinson's disease. Eur J Neurol 15 Suppl 1:14-20.

Pollak N, Dolle C, Ziegler M (2007) The power to reduce: pyridine nucleotides--small molecules with a multitude of functions. Biochem J 402:205-218.

Powers ET, Morimoto RI, Dillin A, Kelly JW, Balch WE (2009) Biological and chemical approaches to diseases of proteostasis deficiency. Annu Rev Biochem 78:959-991.

Pyle A, Foltynie T, Tiangyou W, Lambert C, Keers SM, Allcock LM, Davison J, Lewis SJ, Perry RH, Barker R, Burn DJ, Chinnery PF (2005) Mitochondrial DNA haplogroup cluster UKJT reduces the risk of PD. Ann Neurol 57:564-567.

Ragan CI, Wilson, M.T., Darley-Usmar, V.M., Lowe, P.N. (1987) Subfractionation of mitochondria, and isolation of the proteins of oxidative phosphorylation. Mitochondria, a practical approach. In. London: IRL Press.

Ramirez A, Heimbach A, Grundemann J, Stiller B, Hampshire D, Cid LP, Goebel I, Mubaidin AF, Wriekat AL, Roeper J, Al-Din A, Hillmer AM, Karsak M, Liss B, Woods CG, Behrens MI, Kubisch C (2006) Hereditary parkinsonism with dementia is caused by mutations in ATP13A2, encoding a lysosomal type 5 P-type ATPase. Nat Genet 38:1184-1191.

Rao RV, Ellerby HM, Bredesen DE (2004) Coupling endoplasmic reticulum stress to the cell death program. Cell Death Differ 11:372-380.

Rao RV, Hermel E, Castro-Obregon S, del Rio G, Ellerby LM, Ellerby HM, Bredesen DE (2001) Coupling endoplasmic reticulum stress to the cell death program. Mechanism of caspase activation. J Biol Chem 276:33869-33874.

Rao RV, Peel A, Logvinova A, del Rio G, Hermel E, Yokota T, Goldsmith PC, Ellerby LM, Ellerby HM, Bredesen DE (2002) Coupling endoplasmic reticulum stress to the cell death program: role of the ER chaperone GRP78. FEBS Lett 514:122-128.

Rautou PE, Mansouri A, Lebrec D, Durand F, Valla D, Moreau R (2010) Autophagy in liver diseases. J Hepatol 53:1123-1134.

Ravikumar B, Moreau K, Jahreiss L, Puri C, Rubinsztein DC (2010) Plasma membrane contributes to the formation of pre-autophagosomal structures. Nat Cell Biol 12:747-757.

Ravikumar B, Acevedo-Arozena A, Imarisio S, Berger Z, Vacher C, O'Kane CJ, Brown SD, Rubinsztein DC (2005) Dynein mutations impair autophagic clearance of aggregate-prone proteins. Nat Genet 37:771-776.

Reddy RK, Mao C, Baumeister P, Austin RC, Kaufman RJ, Lee AS (2003) Endoplasmic reticulum chaperone protein GRP78 protects cells from apoptosis induced by topoisomerase inhibitors: role of ATP binding site in suppression of caspase-7 activation. J Biol Chem 278:20915-20924.

Redmond T, Sanchez ER, Bresnick EH, Schlesinger MJ, Toft DO, Pratt WB, Welsh MJ (1989) Immunofluorescence colocalization of the 90-kDa heat-shock protein and microtubules in interphase and mitotic mammalian cells. Eur J Cell Biol 50:66-75.

Reed NA, Cai D, Blasius TL, Jih GT, Meyhofer E, Gaertig J, Verhey KJ (2006) Microtubule acetylation promotes kinesin-1 binding and transport. Curr Biol 16:2166-2172.

Ren Y, Feng J (2007) Rotenone selectively kills serotonergic neurons through a microtubule-dependent mechanism. J Neurochem 103:303-311.

Ren Y, Liu W, Jiang H, Jiang Q, Feng J (2005) Selective vulnerability of dopaminergic neurons to microtubule depolymerization. J Biol Chem 280:34105-34112.

Richardson JR, Shalat SL, Buckley B, Winnik B, O'Suilleabhain P, Diaz-Arrastia R, Reisch J, German DC (2009) Elevated serum pesticide levels and risk of Parkinson disease. Arch Neurol 66:870-875.

Richardson JR, Caudle WM, Guillot TS, Watson JL, Nakamaru-Ogiso E, Seo BB, Sherer TB, Greenamyre JT, Yagi T, Matsuno-Yagi A, Miller GW (2007) Obligatory role for complex I inhibition in the dopaminergic neurotoxicity of 1-methyl-4-phenyl-1,2,3,6-tetrahydropyridine (MPTP). Toxicol Sci 95:196-204.

Riva A, Tandler B, Lesnefsky EJ, Conti G, Loffredo F, Vazquez E, Hoppel CL (2006) Structure of cristae in cardiac mitochondria of aged rat. Mech Ageing Dev 127:917-921.

Rizzuto R (2001) Intracellular Ca(2+) pools in neuronal signalling. Curr Opin Neurobiol 11:306-311.

Rizzuto R, Pozzan T (2006) Microdomains of intracellular Ca2+: molecular determinants and functional consequences. Physiol Rev 86:369-408.

Rizzuto R, Pinton P, Carrington W, Fay FS, Fogarty KE, Lifshitz LM, Tuft RA, Pozzan T (1998) Close contacts with the endoplasmic reticulum as determinants of mitochondrial Ca2+ responses. Science 280:1763-1766.

Rodgers JT, Lerin C, Gerhart-Hines Z, Puigserver P (2008) Metabolic adaptations through the PGC-1 alpha and SIRT1 pathways. FEBS Lett 582:46-53.

Rose CR, Konnerth A (2001) Stores not just for storage. intracellular calcium release and synaptic plasticity. Neuron 31:519-522.

Rubinsztein DC, Cuervo AM, Ravikumar B, Sarkar S, Korolchuk V, Kaushik S, Klionsky DJ (2009) In search of an "autophagomometer". Autophagy 5:585-589.

Ryu EJ, Harding HP, Angelastro JM, Vitolo OV, Ron D, Greene LA (2002) Endoplasmic reticulum stress and the unfolded protein response in cellular models of Parkinson's disease. J Neurosci 22:10690-10698.

Sadek HA, Szweda PA, Szweda LI (2004) Modulation of mitochondrial complex I activity by reversible Ca2+ and NADH mediated superoxide anion dependent inhibition. Biochemistry 43:8494-8502.

Saha AR, Ninkina NN, Hanger DP, Anderton BH, Davies AM, Buchman VL (2000) Induction of neuronal death by alpha-synuclein. Eur J Neurosci 12:3073-3077.

Saha AR, Hill J, Utton MA, Asuni AA, Ackerley S, Grierson AJ, Miller CC, Davies AM, Buchman VL, Anderton BH, Hanger DP (2004) Parkinson's disease alpha-synuclein mutations exhibit defective axonal transport in cultured neurons. J Cell Sci 117:1017-1024.

Salminen A, Kaarniranta K (2009) SIRT1: regulation of longevity via autophagy. Cell Signal 21:1356-1360.

Samann J, Hegermann J, von Gromoff E, Eimer S, Baumeister R, Schmidt E (2009) Caenorhabditits elegans LRK-1 and PINK-1 act antagonistically in stress response and neurite outgrowth. J Biol Chem 284:16482-16491.

Savitt JM, Dawson VL, Dawson TM (2006) Diagnosis and treatment of Parkinson disease: molecules to medicine. J Clin Invest 116:1744-1754.

Schapira AH, Cooper JM, Dexter D, Jenner P, Clark JB, Marsden CD (1989) Mitochondrial complex I deficiency in Parkinson's disease. Lancet 1:1269.

Schellens JP, Meijer AJ (1991) Energy depletion and autophagy. Cytochemical and biochemical studies in isolated rat hepatocytes. Histochem J 23:460-466.

Schellens JP, Vreeling-Sindelarova H, Plomp PJ, Meijer AJ (1988) Hepatic autophagy and intracellular ATP. A morphometric study. Exp Cell Res 177:103-108.

Schon EA, Przedborski S (2011) Mitochondria: the next (neurode)generation. Neuron 70:1033-1053.

Schroder M, Kaufman RJ (2005) ER stress and the unfolded protein response. Mutat Res 569:29-63.

Schuh RA, Kristian T, Gupta RK, Flaws JA, Fiskum G (2005) Methoxychlor inhibits brain mitochondrial respiration and increases hydrogen peroxide production and CREB phosphorylation. Toxicol Sci 88:495-504.

Schuh RA, Richardson JR, Gupta RK, Flaws JA, Fiskum G (2009) Effects of the organochlorine pesticide methoxychlor on dopamine metabolites and transporters in the mouse brain. Neurotoxicology 30:274-280.

Scorrano L, Oakes SA, Opferman JT, Cheng EH, Sorcinelli MD, Pozzan T, Korsmeyer SJ (2003) BAX and BAK regulation of endoplasmic reticulum Ca2+: a control point for apoptosis. Science 300:135-139.

Seglen PO, Berg TO, Blankson H, Fengsrud M, Holen I, Stromhaug PE (1996) Structural aspects of autophagy. Adv Exp Med Biol 389:103-111.

Seo BB, Nakamaru-Ogiso E, Flotte TR, Matsuno-Yagi A, Yagi T (2006a) In vivo complementation of complex I by the yeast Ndi1 enzyme. Possible application for treatment of Parkinson disease. J Biol Chem 281:14250-14255.

Seo YW, Park SY, Yun CW, Kim TH (2006b) Differential efflux of mitochondrial endonuclease G by hNoxa and tBid. J Biochem Mol Biol 39:556-559.

Sha D, Chin LS, Li L (2010) Phosphorylation of parkin by Parkinson disease-linked kinase PINK1 activates parkin E3 ligase function and NF-kappaB signaling. Hum Mol Genet 19:352-363.

Sheehan JP, Swerdlow RH, Parker WD, Miller SW, Davis RE, Tuttle JB (1997) Altered calcium homeostasis in cells transformed by mitochondria from individuals with Parkinson's disease. J Neurochem 68:1221-1233.

Sherer TB, Betarbet R, Greenamyre JT (2002) Environment, mitochondria, and Parkinson's disease. Neuroscientist 8:192-197.

Shibata M, Lu T, Furuya T, Degterev A, Mizushima N, Yoshimori T, MacDonald M, Yankner B, Yuan J (2006) Regulation of intracellular accumulation of mutant Huntingtin by Beclin 1. J Biol Chem 281:14474-14485.

Shimazawa M, Tanaka H, Ito Y, Morimoto N, Tsuruma K, Kadokura M, Tamura S, Inoue T, Yamada M, Takahashi H, Warita H, Aoki M, Hara H (2010) An inducer of VGF protects cells against ER stress-induced cell death and prolongs survival in the mutant SOD1 animal models of familial ALS. PLoS One 5:e15307.

Shimura H, Hattori N, Kubo S, Mizuno Y, Asakawa S, Minoshima S, Shimizu N, Iwai K, Chiba T, Tanaka K, Suzuki T (2000) Familial Parkinson disease gene product, parkin, is a ubiquitin-protein ligase. Nat Genet 25:302-305.

Slee EA, Harte MT, Kluck RM, Wolf BB, Casiano CA, Newmeyer DD, Wang HG, Reed JC, Nicholson DW, Alnemri ES, Green DR, Martin SJ (1999) Ordering the cytochrome c-initiated caspase cascade: hierarchical activation of caspases-2, -3, -6, -7, -8, and -10 in a caspase-9-dependent manner. J Cell Biol 144:281-292.

Slodzinski H, Moran LB, Michael GJ, Wang B, Novoselov S, Cheetham ME, Pearce RK, Graeber MB (2009) Homocysteine-induced endoplasmic reticulum protein (herp) is up-regulated in parkinsonian substantia nigra and present in the core of Lewy bodies. Clin Neuropathol 28:333-343.

Smith PD, Mount MP, Shree R, Callaghan S, Slack RS, Anisman H, Vincent I, Wang X, Mao Z, Park DS (2006) Calpain-regulated p35/cdk5 plays a central role in

dopaminergic neuron death through modulation of the transcription factor myocyte enhancer factor 2. J Neurosci 26:440-447.

Smith WW, Jiang H, Pei Z, Tanaka Y, Morita H, Sawa A, Dawson VL, Dawson TM, Ross CA (2005) Endoplasmic reticulum stress and mitochondrial cell death pathways mediate A53T mutant alpha-synuclein-induced toxicity. Hum Mol Genet 14:3801-3811.

Sodja C, Fang H, Dasgupta T, Ribecco M, Walker PR, Sikorska M (2002) Identification of functional dopamine receptors in human teratocarcinoma NT2 cells. Brain Res Mol Brain Res 99:83-91.

Sou YS, Waguri S, Iwata J, Ueno T, Fujimura T, Hara T, Sawada N, Yamada A, Mizushima N, Uchiyama Y, Kominami E, Tanaka K, Komatsu M (2008) The Atg8 conjugation system is indispensable for proper development of autophagic isolation membranes in mice. Mol Biol Cell 19:4762-4775.

Sousa SC, Maciel EN, Vercesi AE, Castilho RF (2003) Ca2+-induced oxidative stress in brain mitochondria treated with the respiratory chain inhibitor rotenone. FEBS Lett 543:179-183.

St Martin JL, Klucken J, Outeiro TF, Nguyen P, Keller-McGandy C, Cantuti-Castelvetri I, Grammatopoulos TN, Standaert DG, Hyman BT, McLean PJ (2007) Dopaminergic neuron loss and up-regulation of chaperone protein mRNA induced by targeted over-expression of alpha-synuclein in mouse substantia nigra. J Neurochem 100:1449-1457.

Stark AK, Pakkenberg B (2004) Histological changes of the dopaminergic nigrostriatal system in aging. Cell Tissue Res 318:81-92.

Stefanova N, Klimaschewski L, Poewe W, Wenning GK, Reindl M (2001) Glial cell death induced by overexpression of alpha-synuclein. J Neurosci Res 65:432-438.

Sterky FH, Hoffman AF, Milenkovic D, Bao B, Paganelli A, Edgar D, Wibom R, Lupica CR, Olson L, Larsson NG (2012) Altered dopamine metabolism and increased vulnerability to MPTP in mice with partial deficiency of mitochondrial complex I in dopamine neurons. Hum Mol Genet 21:1078-1089.

Strous GJ, Du Maine A, Zijderhand-Bleekemolen JE, Slot JW, Schwartz AL (1985) Effect of lysosomotropic amines on the secretory pathway and on the recycling of the asialoglycoprotein receptor in human hepatoma cells. J Cell Biol 101:531-539.

Sugeno N, Takeda A, Hasegawa T, Kobayashi M, Kikuchi A, Mori F, Wakabayashi K, Itoyama Y (2008) Serine 129 phosphorylation of alpha-synuclein induces unfolded protein response-mediated cell death. J Biol Chem 283:23179-23188.

Sulzer D (2007) Multiple hit hypotheses for dopamine neuron loss in Parkinson's disease. Trends Neurosci 30:244-250.

Surmeier DJ (2007) Calcium, ageing, and neuronal vulnerability in Parkinson's disease. Lancet Neurol 6:933-938.

Susin SA, Lorenzo HK, Zamzami N, Marzo I, Brenner C, Larochette N, Prevost MC, Alzari PM, Kroemer G (1999) Mitochondrial release of caspase-2 and -9 during the apoptotic process. J Exp Med 189:381-394.

Suzuki K, Koike T (2007) Mammalian Sir2-related protein (SIRT) 2-mediated modulation of resistance to axonal degeneration in slow Wallerian degeneration mice: a crucial role of tubulin deacetylation. Neuroscience 147:599-612.

Suzuki K, Kubota Y, Sekito T, Ohsumi Y (2007) Hierarchy of Atg proteins in pre-autophagosomal structure organization. Genes Cells 12:209-218.

Swerdlow RH (2011) Does Mitochondrial DNA Play a Role in Parkinson's Disease? A Review of Cybrid and Other Supportive Evidence. Antioxid Redox Signal.

Swerdlow RH, Parker WD, Currie LJ, Bennett JP, Harrison MB, Trugman JM, Wooten GF (2001) Gender ratio differences between Parkinson's disease patients and their affected relatives. Parkinsonism Relat Disord 7:129-133.

Swerdlow RH, Parks JK, Miller SW, Tuttle JB, Trimmer PA, Sheehan JP, Bennett JP, Jr., Davis RE, Parker WD, Jr. (1996) Origin and functional consequences of the complex I defect in Parkinson's disease. Ann Neurol 40:663-671.

Swerdlow RH, Parks JK, Davis JN, 2nd, Cassarino DS, Trimmer PA, Currie LJ, Dougherty J, Bridges WS, Bennett JP, Jr., Wooten GF, Parker WD (1998) Matrilineal inheritance of complex I dysfunction in a multigenerational Parkinson's disease family. Ann Neurol 44:873-881.

Tanaka S, Uehara T, Nomura Y (2000) Up-regulation of protein-disulfide isomerase in response to hypoxia/brain ischemia and its protective effect against apoptotic cell death. J Biol Chem 275:10388-10393.

Tanida I, Minematsu-Ikeguchi N, Ueno T, Kominami E (2005) Lysosomal turnover, but not a cellular level, of endogenous LC3 is a marker for autophagy. Autophagy 1:84-91.

Tatton NA (2000) Increased caspase 3 and Bax immunoreactivity accompany nuclear GAPDH translocation and neuronal apoptosis in Parkinson's disease. Exp Neurol 166:29-43.

Taylor DJ, Kemp GJ, Radda GK (1994) Bioenergetics of skeletal muscle in mitochondrial myopathy. J Neurol Sci 127:198-206.

Terman A, Kurz T, Navratil M, Arriaga EA, Brunk UT (2010) Mitochondrial turnover and aging of long-lived postmitotic cells: the mitochondrial-lysosomal axis theory of aging. Antioxid Redox Signal 12:503-535.

Thomas B (2009) Parkinson's disease: from molecular pathways in disease to therapeutic approaches. Antioxid Redox Signal 11:2077-2082.

Thomas B, Beal MF (2007) Parkinson's disease. Hum Mol Genet 16 Spec No. 2:R183-194.

Tieu K, Perier C, Caspersen C, Teismann P, Wu DC, Yan SD, Naini A, Vila M, Jackson-Lewis V, Ramasamy R, Przedborski S (2003) D-beta-hydroxybutyrate rescues mitochondrial respiration and mitigates features of Parkinson disease. J Clin Invest 112:892-901.

Trifunovic A, Wredenberg A, Falkenberg M, Spelbrink JN, Rovio AT, Bruder CE, Bohlooly YM, Gidlof S, Oldfors A, Wibom R, Tornell J, Jacobs HT, Larsson NG (2004) Premature ageing in mice expressing defective mitochondrial DNA polymerase. Nature 429:417-423.

Trimmer PA, Borland MK, Keeney PM, Bennett JP, Jr., Parker WD, Jr. (2004a) Parkinson's disease transgenic mitochondrial cybrids generate Lewy inclusion bodies. J Neurochem 88:800-812.

Trimmer PA, Schwartz KM, Borland MK, De Taboada L, Streeter J, Oron U (2009) Reduced axonal transport in Parkinson's disease cybrid neurites is restored by light therapy. Mol Neurodegener 4:26.

Trimmer PA, Keeney PM, Borland MK, Simon FA, Almeida J, Swerdlow RH, Parks JP, Parker WD, Jr., Bennett JP, Jr. (2004b) Mitochondrial abnormalities in cybrid cell models of sporadic Alzheimer's disease worsen with passage in culture. Neurobiol Dis 15:29-39.

Uehara T, Nakamura T, Yao D, Shi ZQ, Gu Z, Ma Y, Masliah E, Nomura Y, Lipton SA (2006) S-nitrosylated protein-disulphide isomerase links protein misfolding to neurodegeneration. Nature 441:513-517.

Uryu K, Richter-Landsberg C, Welch W, Sun E, Goldbaum O, Norris EH, Pham CT, Yazawa I, Hilburger K, Micsenyi M, Giasson BI, Bonini NM, Lee VM, Trojanowski JQ (2006) Convergence of heat shock protein 90 with ubiquitin in filamentous alpha-synuclein inclusions of alpha-synucleinopathies. Am J Pathol 168:947-961.

Uversky VN (2007) Neuropathology, biochemistry, and biophysics of alpha-synuclein aggregation. J Neurochem 103:17-37.

Van Humbeeck C, Cornelissen T, Hofkens H, Mandemakers W, Gevaert K, De Strooper B, Vandenberghe W (2011) Parkin interacts with Ambra1 to induce mitophagy. J Neurosci 31:10249-10261.

Van Laar VS, Arnold B, Cassady SJ, Chu CT, Burton EA, Berman SB (2011) Bioenergetics of neurons inhibit the translocation response of Parkin following rapid mitochondrial depolarization. Hum Mol Genet 20:927-940.

Vay L, Hernandez-Sanmiguel E, Santo-Domingo J, Lobaton CD, Moreno A, Montero M, Alvarez J (2007) Modulation of Ca(2+) release and Ca(2+) oscillations in HeLa cells and fibroblasts by mitochondrial Ca(2+) uniporter stimulation. J Physiol 580:39-49.

Veech GA, Dennis J, Keeney PM, Fall CP, Swerdlow RH, Parker WD, Jr., Bennett JP, Jr. (2000) Disrupted mitochondrial electron transport function increases expression of anti-apoptotic bcl-2 and bcl-X(L) proteins in SH-SY5Y neuroblastoma and in Parkinson disease cybrid cells through oxidative stress. J Neurosci Res 61:693-700.

Vemuri GN, Eiteman MA, McEwen JE, Olsson L, Nielsen J (2007) Increasing NADH oxidation reduces overflow metabolism in Saccharomyces cerevisiae. Proc Natl Acad Sci U S A 104:2402-2407.

Verkhratsky A (2005) Physiology and pathophysiology of the calcium store in the endoplasmic reticulum of neurons. Physiol Rev 85:201-279.

Vila M, Wu DC, Przedborski S (2001) Engineered modeling and the secrets of Parkinson's disease. Trends Neurosci 24:S49-55.

Vinogradov AD (2008) NADH/NAD+ interaction with NADH: ubiquinone oxidoreductase (complex I). Biochim Biophys Acta 1777:729-734.

Viswanath V, Wu Y, Boonplueang R, Chen S, Stevenson FF, Yantiri F, Yang L, Beal MF, Andersen JK (2001) Caspase-9 activation results in downstream caspase-8 activation and bid cleavage in 1-methyl-4-phenyl-1,2,3,6-tetrahydropyridine-induced Parkinson's disease. J Neurosci 21:9519-9528.

Vives-Bauza C, Zhou C, Huang Y, Cui M, de Vries RL, Kim J, May J, Tocilescu MA, Liu W, Ko HS, Magrane J, Moore DJ, Dawson VL, Grailhe R, Dawson TM, Li C, Tieu K, Przedborski S (2010) PINK1-dependent recruitment of Parkin to mitochondria in mitophagy. Proc Natl Acad Sci U S A 107:378-383.

Vogiatzi T, Xilouri M, Vekrellis K, Stefanis L (2008) Wild type alpha-synuclein is degraded by chaperone-mediated autophagy and macroautophagy in neuronal cells. J Biol Chem 283:23542-23556.

Wang F, Tong Q (2009) SIRT2 suppresses adipocyte differentiation by deacetylating FOXO1 and enhancing FOXO1's repressive interaction with PPARgamma. Mol Biol Cell 20:801-808.

Wang HQ, Imai Y, Kataoka A, Takahashi R (2007) Cell type-specific upregulation of Parkin in response to ER stress. Antioxid Redox Signal 9:533-542.

Wang XJ, Xu JX (2005) Possible involvement of Ca2+ signaling in rotenone-induced apoptosis in human neuroblastoma SH-SY5Y cells. Neurosci Lett 376:127-132.

Webb JL, Ravikumar B, Rubinsztein DC (2004) Microtubule disruption inhibits autophagosome-lysosome fusion: implications for studying the roles of aggresomes in polyglutamine diseases. Int J Biochem Cell Biol 36:2541-2550.

Webb JL, Ravikumar B, Atkins J, Skepper JN, Rubinsztein DC (2003) Alpha-Synuclein is degraded by both autophagy and the proteasome. J Biol Chem 278:25009-25013.

Webster DR, Borisy GG (1989) Microtubules are acetylated in domains that turn over slowly. J Cell Sci 92 (Pt 1):57-65.

Wei MC, Zong WX, Cheng EH, Lindsten T, Panoutsakopoulou V, Ross AJ, Roth KA, MacGregor GR, Thompson CB, Korsmeyer SJ (2001) Proapoptotic BAX and BAK: a requisite gateway to mitochondrial dysfunction and death. Science 292:727-730.

Wei Y, Pattingre S, Sinha S, Bassik M, Levine B (2008) JNK1-mediated phosphorylation of Bcl-2 regulates starvation-induced autophagy. Mol Cell 30:678-688.

Wen Y, Li W, Poteet EC, Xie L, Tan C, Yan LJ, Ju X, Liu R, Qian H, Marvin MA, Goldberg MS, She H, Mao Z, Simpkins JW, Yang SH (2011) Alternative mitochondrial electron transfer as a novel strategy for neuroprotection. J Biol Chem 286:16504-16515.

Westerheide SD, Anckar J, Stevens SM, Jr., Sistonen L, Morimoto RI (2009) Stress-inducible regulation of heat shock factor 1 by the deacetylase SIRT1. Science 323:1063-1066.

White C, Li C, Yang J, Petrenko NB, Madesh M, Thompson CB, Foskett JK (2005) The endoplasmic reticulum gateway to apoptosis by Bcl-X(L) modulation of the InsP3R. Nat Cell Biol 7:1021-1028.

Wilson CJ, Callaway JC (2000) Coupled oscillator model of the dopaminergic neuron of the substantia nigra. J Neurophysiol 83:3084-3100.

Winkler-Stuck K, Kirches E, Mawrin C, Dietzmann K, Lins H, Wallesch CW, Kunz WS, Wiedemann FR (2005) Re-evaluation of the dysfunction of mitochondrial respiratory chain in skeletal muscle of patients with Parkinson's disease. J Neural Transm 112:499-518.

Winslow AR, Chen CW, Corrochano S, Acevedo-Arozena A, Gordon DE, Peden AA, Lichtenberg M, Menzies FM, Ravikumar B, Imarisio S, Brown S, O'Kane CJ, Rubinsztein DC (2010) alpha-Synuclein impairs macroautophagy: implications for Parkinson's disease. J Cell Biol 190:1023-1037.

Wong E, Cuervo AM (2010) Autophagy gone awry in neurodegenerative diseases. Nat Neurosci 13:805-811.

Wood-Kaczmar A, Gandhi S, Yao Z, Abramov AY, Miljan EA, Keen G, Stanyer L, Hargreaves I, Klupsch K, Deas E, Downward J, Mansfield L, Jat P, Taylor J, Heales S, Duchen MR, Latchman D, Tabrizi SJ, Wood NW (2008) PINK1 is necessary for long term survival and mitochondrial function in human dopaminergic neurons. PLoS One 3:e2455.

Xilouri M, Vogiatzi T, Vekrellis K, Park D, Stefanis L (2009) Abberant alpha-synuclein confers toxicity to neurons in part through inhibition of chaperone-mediated autophagy. PLoS One 4:e5515.

Xu C, Bailly-Maitre B, Reed JC (2005) Endoplasmic reticulum stress: cell life and death decisions. J Clin Invest 115:2656-2664.

Yamada M, Iwatsubo T, Mizuno Y, Mochizuki H (2004) Overexpression of alpha-synuclein in rat substantia nigra results in loss of dopaminergic neurons, phosphorylation of alpha-synuclein and activation of caspase-9: resemblance to pathogenetic changes in Parkinson's disease. J Neurochem 91:451-461.

Yamada T, McGeer PL, Baimbridge KG, McGeer EG (1990) Relative sparing in Parkinson's disease of substantia nigra dopamine neurons containing calbindin-D28K. Brain Res 526:303-307.

Yang L, Matthews RT, Schulz JB, Klockgether T, Liao AW, Martinou JC, Penney JB, Jr., Hyman BT, Beal MF (1998) 1-Methyl-4-phenyl-1,2,3,6-tetrahydropyride neurotoxicity is attenuated in mice overexpressing Bcl-2. J Neurosci 18:8145-8152.

Yang Q, She H, Gearing M, Colla E, Lee M, Shacka JJ, Mao Z (2009) Regulation of neuronal survival factor MEF2D by chaperone-mediated autophagy. Science 323:124-127.

Yang Z, Klionsky DJ (2010) Mammalian autophagy: core molecular machinery and signaling regulation. Curr Opin Cell Biol 22:124-131.

Yokota T, Sugawara K, Ito K, Takahashi R, Ariga H, Mizusawa H (2003) Down regulation of DJ-1 enhances cell death by oxidative stress, ER stress, and proteasome inhibition. Biochem Biophys Res Commun 312:1342-1348.

Yoshino H, Nakagawa-Hattori Y, Kondo T, Mizuno Y (1992) Mitochondrial complex I and II activities of lymphocytes and platelets in Parkinson's disease. J Neural Transm Park Dis Dement Sect 4:27-34.

Zhang X, Yuan Z, Zhang Y, Yong S, Salas-Burgos A, Koomen J, Olashaw N, Parsons JT, Yang XJ, Dent SR, Yao TP, Lane WS, Seto E (2007) HDAC6 modulates cell motility by altering the acetylation level of cortactin. Mol Cell 27:197-213.

Zhang Y, Li N, Caron C, Matthias G, Hess D, Khochbin S, Matthias P (2003) HDAC-6 interacts with and deacetylates tubulin and microtubules in vivo. EMBO J 22:1168-1179.

Zhou RM, Huang YX, Li XL, Chen C, Shi Q, Wang GR, Tian C, Wang ZY, Jing YY, Gao C, Dong XP (2010) Molecular interaction of alpha-synuclein with tubulin influences on the polymerization of microtubule in vitro and structure of microtubule in cells. Mol Biol Rep 37:3183-3192.

Zigmond MJ, Abercrombie ED, Berger TW, Grace AA, Stricker EM (1990) Compensations after lesions of central dopaminergic neurons: some clinical and basic implications. Trends Neurosci 13:290-296.

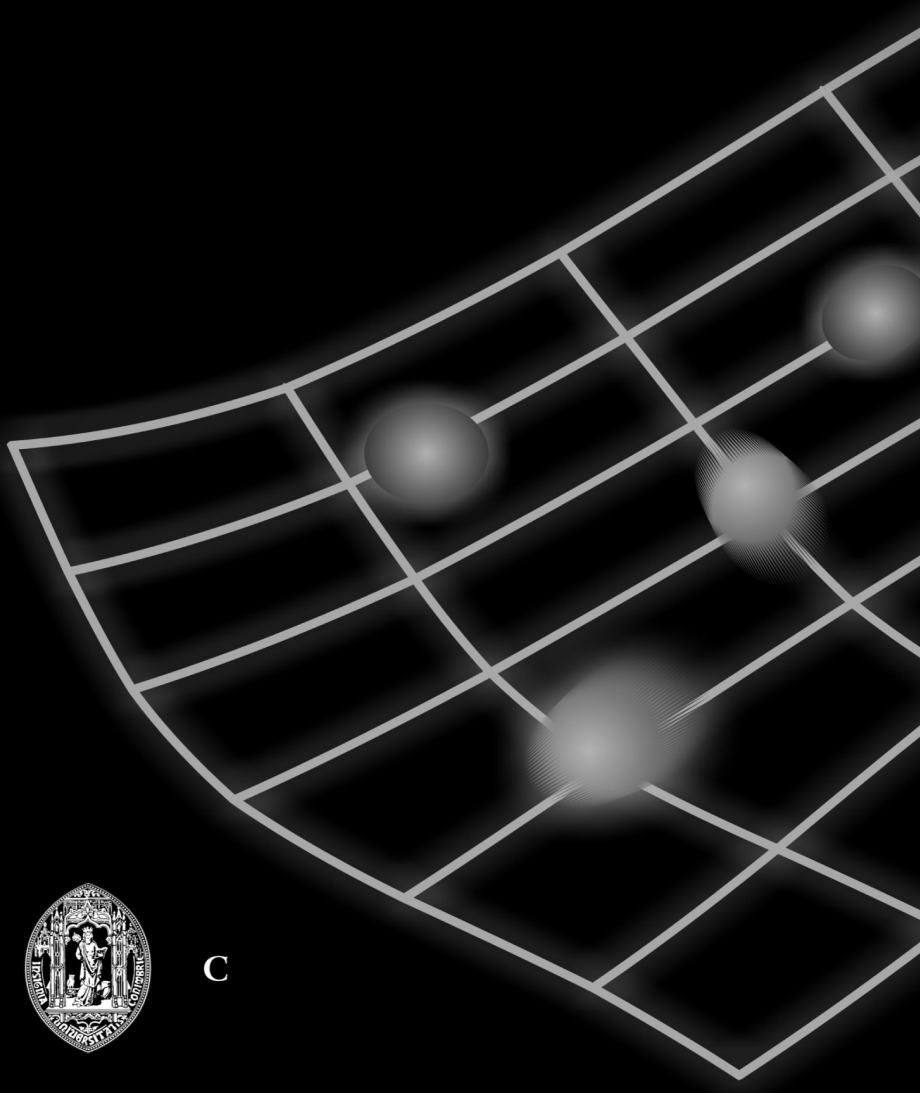

U C